SECOND INTERNATIONAL SYMPOSIUM ON

ELECTROCHEMICAL IMPEDANCE SPECTROSCOPY

UNIVERSITY OF CALIFORNIA, SANTA BARBARA

JULY 12-17, 1992

EXTENDED ABSTRACTS

REPORT DOCUMENTATION PAGE

Form Approved
OMB No. 0704-0188

1. AGENCY USE ONLY (Leave blank)	2. REPORT DATE	3. REPORT TYPE AND DATES COVERED
	1992	Final Report 1/6/92 - 12/31/92

4. TITLE AND SUBTITLE
Extended Abstracts from Second International Symposium on Electrochemical Impedance Spectroscopy, University of California, Santa Barbara

5. FUNDING NUMBERS
Department of the Navy
Grant No. N00014-92-J-1705

6. AUTHOR(S)
Extended abstracts in attached document are organized in alphabetical order according to the name of the first author. (Compiler - Dr. Digby D. Macdonald)

7. PERFORMING ORGANIZATION NAME(S) AND ADDRESS(ES)
Center for Advanced Materials
Pennsylvania State University
517 Deike Building
University Park, PA 16802

8. PERFORMING ORGANIZATION REPORT NUMBER

9. SPONSORING/MONITORING AGENCY NAME(S) AND ADDRESS(ES)
Mr. Douglas E. Heaton
(614) 292-4144

10. SPONSORING/MONITORING AGENCY REPORT NUMBER

11. SUPPLEMENTARY NOTES

12a. DISTRIBUTION/AVAILABILITY STATEMENT

DISTRIBUTION STATEMENT A
Approved for public release;
Distribution Unlimited

12b. DISTRIBUTION CODE

13. ABSTRACT *(Maximum 200 words)* This grant was made available to partially support a workshop on electrochemical impedance spectroscopy. The Symposium provided a forum for recent advances and applications of electrochemical impedance spectroscopy to a variety of problems related to general electrochemical mechanisms and models, passivity, electrochemistry in non-aqueous environments, batteries and fuel cells, mass transport, photoelectrochemistry and semi-conducductors, and membranes and biological systems..
The extended abstracts provided in this document are for talks and posters presented at the workshop.

14. SUBJECT TERMS			15. NUMBER OF PAGES
			16. PRICE CODE
17. SECURITY CLASSIFICATION OF REPORT	18. SECURITY CLASSIFICATION OF THIS PAGE	19. SECURITY CLASSIFICATION OF ABSTRACT	20. LIMITATION OF ABSTRACT
			Unlimited

Preface

The extended abstracts in this document are for talks and posters presented at the Second International Symposium on Electrochemical Impedance Spectroscopy. The Symposium provides a forum for recent advances and applications of electrochemical impedance spectroscopy to a variety of problems related to general electrochemistry, coatings, corrosion, solid state electrochemistry, electrochemical mechanisms and models, passivity, electrochemistry in non-aqueous environments, batteries and fuel cells, mass transport, photoelectrochemistry and semiconductors, and membranes and biological systems. The abstracts have been organized in alphabetical order according to the name of the first author.

The organizers gratefully acknowledge support from the staff of the Center for Advanced Materials at The Pennsylvania State University and the Information Processing Services Department of Rockwell International Science Center for their roles in preparing and printing these extended abstracts.

July 1992

GENERAL ELECTROCHEMISTRY

Session Chairman: D.D. Macdonald

Some New Directions in Impedance Spectroscopy Data Analysis	J. Ross Macdonald *(Plenary)*
Impedance Spectroscopy of Ramified Electrodeposits	E. Chassaing, M. Rosso, B. Sapoval, J.-N. Chazalviel
Calculation of Complex Impedances by Laplace Transformation of Voltage Transients Generated by Current Step Excitation	Michael Neumann-Spallart and Mohamed Etman
Impedance Measurement at Electrodes of Continuously Changing State	H. Goehr, H. Bode, A. Burghart and C.-A. Schiller
The Double Layer Impedance at a Rough Electrode: A Random Walk Approach	Thomas C. Halsey and Michael Leibig
Impedance Analysis of Layers on Iron	U. Rammelt and G. Reinhard
Electrochemical Characterization of Hydrogen Evolution Reaction on Nickel-Sulfur Electrodes	M. Ferreira and G. Tremiliosi-Filho
An Inexpensive Low Frequency Impedance Analyzer Based on Direct Sampling	E. Skou
The Problem of the Identity of the EIS Measured Electrode Capacity and Thermodynamical One in the Solutions with the Constant Ionic Strength	B.M. Grafov and B.B. Damaskin

COATINGS

Session Chairman: M. Kendig

Polymer Protective Coatings — The Distinction Between Coating Porosity and the Wetted Metal Area	R.D. Armstrong *(Plenary)* and J.D. Wright
Coating Inspection by a Scanning Electrochemical Impedance Spectroscopy Technique	R.S. Lillard, J. Kruger, P.J. Moran and, W.S. Tait
Relation Between Adherence of a Paint Film and Corrosion Protection	E. Spengler, I.C.P. Margarit, and O.R. Mattos
Study of the Electrical Anisotropy of Polypyrrole Films by Means of Impedance Spectroscopy	M.C. Montemayor, R. Jimenez, and E. Fatas
Evaluation of Painted Steel Under Cathodic Protection	Isabel C.P. Margarit, Oscar Rosa Mattos, and Joaquim Pereira Quintela
Determination of Dielectric Characteristics of Organic Coatings by Alternative Current	G. Rocchini and P. Spinelli
Influence of Particle Size on the Behavior of Zinc Rich Primers by Means of Electrochemical Impedance Spectroscopy	A. Luana, M. Izquierdo, A. Sanchez, X.R. Novoa, and L. Espada
A Discussion on the Molecular Basis for Using Electrochemical Impedance Spectroscopy to Estimate Coating and Corrosion Parameters	W. Stephen Tait
Electrochemical Impedance Spectroscopy of Electrocoated Aluminum Food Cans	E.S. Bovard, T.D. Burleigh, and A.T. Smith

CORROSION

Session Chairman: D. Silverman

AC Probing of the Faradic Non-Linear Response	M.C.H. McKubre *(Plenary)* and F. Tanzella
Use of Electrochemical Noise in the Study of Corrosion Inhibition. 2. gem-Diphosphonates	Stanley T. Hirozawa, David E. Turcotte, and Michael C. Welch
Copper Dissolution in Acidic Sulfate Medium Studied by Electrogravimetric and Electrocoulometric Transmittance Techniques	[illegible] Le Gal La Salle-Morin, A. Hardy, R. Rossen, M. Keddam, M. Takenouti
Application of the AC Impedance Mapping Technique to the Corrosion Detection of Steel Pipes in Concrete	M. Shibata, H. Adachi, A. Sakakura, and K. Kasahara
Rapid Corrosion Estimation in Poorly Characterized Fluids by Electrochemical Impedance Spectroscopy (EIS)	David C. Silverman
The Detection and Analysis of Chemical and Electrochemical Damage in BMI/Graphite Fiber Composites Using Electrochemical Impedance Spectroscopy	S.R. Taylor, D.F. Wall, and G.L. Cahen, Jr.
Corrosion of Steel in Concrete Studied by Electrochemical Impedance Spectroscopy. Model and Applications	F. Wenger and J. Galland
Impedance Spectra for Corroding Aluminum and Zinc	Joseph Hazan
Inhibition of Aluminum Corrosion in Chloride Media	C.M.A. Brett, I.A.R. Gomes, J.P.S. Martins
Study by AC Impedance of Macrocell Activity of Concrete Rebars	M. Keddam, R. Novoa, L. Soler, and C. Andrade

SOLID STATE

Session Chairman: J. Kennedy

Impedance of Composites Media	Micha Tomkiewicz *(Plenary)*
Impedance of Potassium Beta"Alumina Ceramic at High Temperature	R.M. Williams, B. Jeffries-Nakamura, M.L. Underwood, M.A. Ryan, D. O'Connor, and S. Kikkert
The Constant Phase Impedance in Solid Electrolytes	A. Ukshe
Electrochemical Impedance Spectroscopy of a Yttria-Stabilized Zirconia Cell at High Oxygen Pressures	M.L. Underwood, R.M. Williams, D.J. Clark, and R. Losey
Model for Impedance of an Ionic Conductor Sandwiched Between Blocking Electrodes	J.C. Wang
Immittance Spectra for Thin Film Solid Electrolyte Cells	A.K. Ivanov-Shitz and L.A. Tsvetnova
Ion Mobility Into Sepiolite	D. Gonzalez-Roman, R. Pozas-Tormo, M.D. Ruiz-Cruz, L. Moreno-Real, J.R. Ramos-Barrado, and C. Criado
Impedance Spectroscopy Study with $NH_4UO_2PO_4 \cdot 3H_2O$ (NHUP) Self-Supported Membranes	J. Benavente, J. Ramos-Barrado, S. Bruque, M. Martinez-Lara
Impedance Spectroscopy Study of Superplasticity in 0.3 Mole CuO Modified 3YTZP Oxygen Sensor Material	J. Vangrunderbeek, J. Luyten, S. Kupers, W. Hendrix, and F. DeSchutter

MECHANISMS AND MODELS

Session Chairman: R. Armstrong

Three-Dimensional Impedance Spectroscopy Diagrams for Processes Involving Electrosorbed Intermediates, Introducing the Third Electrode-Potential Variable—Examination of Conditions Leading to Pseudo-Inductive Behavior	L. Bai *(Plenary)* and B.E. Conway
AC ImpedanceStudy of Dendritic 3D Silver Electrodeposits	A. Hernandez Creus, A.E. Bolzan, P. Carro, S. Gonzalez, R.C. Salvarezza, and A.J. Arvia
Mechanism of Cadmium Underpotential Absorption on Platinum as Obtained From Quartz Electrogravimetry and Potential Step Relaxation Data	V. Daujotis and R. Raudonis
Electrode Kinetics of Oxygen Reduction on Porous Nickel in Carbonate Melt	L. Giorgi, E. Simonetti, F. Croce, and A. Pozio
Applications of the AC Impedance Spectroscopy to Study the Hydrogen Evolution Reaction	A. Lasia
EIS Investigations of Charge Transfer Kinetics in Photoelectrochemistry	Ingo Uhlendorf, Rolf Reineke, and Dieter Meissner
Microscopic, Self-Oscillating Domains at the Silicon Surface During Its Anodic Dissolution in a Fluoride Electrolyte	F. Ozanam, N. Blanchard, and J.-N. Chazalviel
Impulse Charge (Coulostatic) Relaxation Method Applied to the Kinetic Study of a T40 Titanium Electrode in Acidic Media	F. Del Rey, J. P. Frayret, T. Jaszay, and A. Capranu
The Impedance Study of the Oxidation of Acid at a Platinum Electrode	H. Matsui, M. Yasuzawa, and A. Kunugi

GENERAL ELECTROCHEMISTRY

Session Chairman: M. Keddam

Attempts for Describing the Rough Solid Electrode Surfaces Through STM, SEM, and EIS	A.J. Arvia *(Plenary)* and Dr. R. Salvarezza
AC Impedance and Voltammetry Study on the Kinetics of Roughness Relaxation of Gold Electrodes	M.P. Garcia, M.M. Gomez, R.C. Salvarezza, and A.J. Arvia
Analysis of Impedance Spectroscopy for Porous Silica Gels	Rosario Gerhardt, Guangqun Zhang, and Wanqing Cao
Electrochemical Impedance Spectroscopy on Metal Hydride Electrodes	Nobuhiro Kuriyama, Tetsuo Sakai, Hiroshi Miyamura, Itsuki Uehara, and Hiroshi Ishikawa
Electrochemical Impedance Measurements in the Pd/D2O System	S.I. Smedley, M.C.H. McKubre, R.C. Rocha-Filho, F.L. Tanzella
The Effect of Surface Inhomogeneities on the Electrochemical Impedance Response of Aluminum	Gayle R.T. Schueller and S. Ray Taylor
A New Approach to Calculation of the Frequency Response of Space Charge-Containing Interfaces	I. Jamnik, S. Pejovnik and J. Maier
The Relation Between Kramers-Kronig Transforms and Stability Analysis of Faradaic Admittance	Jianqing Zhang and Chu-nan Cao
Theory of Missing Data in EIS	M. Urquidi-Macdonald

PASSIVITY

Session Chairman: S. Smedley

Electrogravimetric Transmittance Investigation of the Oxide Formation Processes on Gold in Acidic Medium	S. Bourkane, C. Gabrielli *(Plenary)*, and M. Keddam
Anodic Behavior of Ni-P Alloys Studied by Impedance Spectroscopy	A. Krolikowski and P. Butkiewicz
Kinetic Models of Passivation of Metals Based on AC Impedance Measurements	M. Bojinov
Impedance Studies of the Oxide Layer on Zircaloy After Previous Oxidation in Water at 400°C	H. Goehr, H. Schaller, and C.-A. Schiller
Anodic Dissolution and Passivation of Iron Analyzed in Frequency and Time Domains with Channel Flow Double Electrode	Masayuki Itagaki and Tooru Tsuru
Analysis of the Passive Film on Iron Chromium Alloys by Potential Modulated Ellipsometry	L.C. Jacobs, Ph. Habing, J.H.W. de Wit
Investigation of Passive Layers on Iron and Iron-Chromium Alloys by Electrochemical Impedance Spectroscopy	E.B. Castro and J.R. Vilche
Frequency- and Time-Domain Investigations of Modified Aluminum Oxide Layers	K. Kluger, M.M. Lohrengel
Electrochemical Impedance Spectroscopy of Tungsten Implanted Aluminum Surfaces	C.M. Rangel and M.A. Travassos
A Generalizable Approach for the Electric Behavior in the Presence of Conducting Films with an Example of Growing Film with Nernstian Reactions	Daniel Schuhmann

NON-AQUEOUS SYSTEMS

Session Chairman: I. Uchida

Electrochemical Impedance for Large Structure in Soil	Shiro Haruyama *(Plenary)* and Shirohi Sudo
Constant Phase Angle Behavior of SnO_2/WO_3 Thin Film Electrodes in Anhydrous $LiClO_4$-Propylene Carbonate Electrolyte	Cl. Bohnke, O. Bohnke, B. Vuillemin
Impedance Measurements in Silica Melts	P. Claes, J.Y. Tilquin, and J. Glibert
Impedance Diagrams of Concentrated Solutions of Ammonium Polysulfides in Liquid Ammonia: An Illustration of the Gerischer Impedance	A. Demortier, E. Levillain, J.P. Lelieur
Investigation of the Electrochemical Oxidation of Copper in Molten NH_4HF_2-HF	Denis J.-F. Filliaudeau and Gérard S. Picard
The Determination of the Double Layer Capacitance of Reversible Electrodes in Pure Molten Salts	Adolf Kisza and Jerzy Kazmierczak
Electrochemical Impedance and Potential Scanning Voltammetry of Passivated Aluminum Electrodes in Molten Carbonates	V.I. Sannikov
Kinetic Study of Porous Electrodes in Molten Carbonate Fuel Cell System by Polarization Measurements and AC Impedance Spectroscopy	Isamu Uchida, Goran Lindbergh and Tatsuo Nishina
Analysis of Immittance Data for O/Li3M2 (PO4)3/O (M-Sc,Fe) Electrochemical Cells	A.K. Ivanov-Shitz
Stone Impact Damage of Automotive Paint Finishes - Applications of EIS and Neural Net Analysis	A. C. Ramamurthy, W. Lorenzen, and M. Urquidi-Macdonald

SOLID STATE

Session Chairman: I. Raistrick

The Oxygen Transfer Process on Solid Oxide/Noble Metal Electrodes, Studied with Impedance Spectroscopy, dc-Polarization and Isotope Exchange	Bernard A. Boukamp *(Plenary)*, B.A. van Hassel, I.C. Vinke, K.J. de Vries, and A.J. Burggraaf
Study of the Conduction Mechanism of $MgAl_2O_4$ at Different Environmental Humidities	G. Gusmano, G. Montesperelli, P. Nunziante, E. Traversa
Microstructure and EIS Correlation Studies in the Y_2O_3-ZrO_2/Mullite and Y_2O_3-ZrO_2/Alumina Solid Electrolyte Composites	M.I. Osendi, M.T. Hernandez and J.R. Jurado
AC Impedance Spectroscopy Measurements on Y-Ba-Cu-O and Y-Ba-Cu-O/Ag Bulk and Thick Films	E. Safz, J.R. Jurado, and J.S. Moya
Impedance Studies of the Interphase Electrode/Zn-Montmorillonite	Wang Wenlou, Liu Wanyu, Lin Fengliang, Yu Wenhai
The Influence of Crystallography Orientation of Solid Electrolyte on Properties of Au/YSZ Inteface	E.M. Novitskiy and I.D. Remez
AC-Impedance Study of the Oxygen Reduction Mechanism on $La_{1-x}Sr_xMnO_3$ in Solid Oxide Fuel Cells	M.J.L. Ostergard, M. Mogensen, C. Bagger, and L. Christensen
Surface Process on Na^+ Ion Selective NASICON Based Membrane	O. Damasceno, E. Siebert, and P. Fabry
The Method of Potentiodynamic Impedancemetre	I.V. Murygin, A.N. Ezin, I.D. Remez

COATINGS

Session Chairman: F. Mansfeld

The Coating/Metal/Electrolyte Interfacial Impedance and Its Global Fractal Model	J. Hubrecht *(Plenary)*, M. Embrechts, W. Bogaerts
The Corrosion of Aluminum and the Role of Chromate Conversion Coatings on Aluminum in Acid and Neutral Solutions	H.J.W. Lenderink, M.A. van der Linden, J.H.W. de Wit
EIS As A Means of Evaluating Electroless Nickel Deposits	E.T. van der Kouwe
Characterization of Aluminum Surface Treatments with Electrochemical Impedance Spectroscopy and Spectroscopic and Ellipsometry	J. de Laet, J. Scheers, H. Terryn, J. Vereecken
An Electrochemical Impedance Spectroscopy Study of Zinc Rich Paints on Steels in Artificial Sea Water by a Transmission Line Model	S.G. Real, A.C. Elias, C.A. Gervasi, A. Di Sarli and J.R. Vilche
Application of Impedance Analysis Method, Z.Calc, to Painted and Unpainted Metals	G.W. Walter, D.N. Nguyen and M.A.D. Madurasinghe
The Determination of Coating Performance Using Electrochemical Impedance Spectroscopy	E.P.M. van Westing, G.M. Ferrari, and J.H.W. de Wit
The Effect of Coating Thickness on Corrosion Behavior of Ion Plated Films	Richard Brown and Mohd N. Alias
Electrochemical Impedance Spectroscopy of Electrochemically Polmerized Polyphenylene Films on Platinum Electrode	Ari Ivaska, Carita Kvarnström and Zhiqiang Gao

GENERAL ELECTROCHEMISTRY

Session Chairman: J. Vilche

Nonstationary Impedance Spectroscopy: Theory and Application	Z. Stoynov *(Plenary)*
Impedance Spectroscopy at Very Low Frequencies	Stefan Lanyi
Low Frequency Measurements in Impedance Spectroscopy: Correlation of the Warburg Impedance	R. Jimenez, M.C. Montemayor, and E. Faraś
Open Circuit Voltages on Humid Insulators	Enapu F. Owede
The Effect of Surface Roughness on the AC Impedance of Palladium in Sulfuric Acid	B.G. Pound
Time Domain Responses of Constant Phase Electrodes	A. Sadkowski
A New Approach to the Problem of "Good" and "Bad" Impedance Data in Electrochemical Impedance Spectroscopy	G.S. Popkirov and R.N. Schindler
On Interpretation of Results of Impedance Measurements	S. Shkerin
A Comparative Study of the Impedance Characteristics of Thin Redox-Polymer Films on Electrodes	Michael Sharp and Åsa Genborg
Impedance Measurements with Real Potentiostats: Corrections for Potentiostat Response	Robert S. Rodgers
Determination of Mechanisms Through Impedance Spectroscopy	S.K. Rangarajan *(Guest Lecture)*

BATTERIES AND FUEL CELLS

Session Chairman: M. McKubre

AC Impedance Characteristics of Fuel Cell Porous Electrodes	J. Robert Selman *(Plenary)*
Study on (Y, Ce)-TZP-Al2O3 Ceramics by AC Impedance Spectroscopy Technique	Meng Guangyao, Wei Zhenghui, Liu Xingqin, Peng Dingkun, and Takao Hakata
Electrochemical Impedance Spectroscopy of Intercalated Electrodes	Andre Métrot and A. Harrach
Impedance Analysis of Electropolymerized Conducting Polymers for Polymer Battery Cathodes	Tetsuya Osaka and Toshiyuki Momma
Impedance of Polymer Electrolyte Fuel Cell Electrodes	T.E. Springer, I.D. Raistrick, S. Gottesfeld, M. Wilson, and T. Zawodzinski
Cation Mobility in Poly (Ethylene Oxide) Solid Electrolytes	M.J. Plancha, C.M. Rangel, C.A.C. Sequeira
Changes in Impedances of Ni/Cd Cells with Voltage and Cycle Life	Margaret A. Reid
AMTEC Electrode Studies Using Electrochemical Impedance Spectroscopy	M.A. Ryan, M.L. Underwood, R.M. Williams, D. O'Connor and B. Jeffries-Nakamura
An AC Impedance Study of the Ni/NiCl2 Electrode of Sodium/Metal Chloride Cells	B.J. Dougherty, M.C.H. McKubre, S.I. Smedley, and F.L. Tanzella
Impedance Spectroscopy -- A Method for In-Situ Characterization of Experimental Fuel Cells	W. Jenseit, O. Böhme, F.U. Leidich, and H. Wendt

THURSDAY, JULY 16 - MORNING SESSION

CORROSION

Session Chairman: *C. Gabrielli*

Models for the Impedance Behavior of Common Corrosion Systems	Flonan Mansfeld *(Plenary)*
Electrochemical Evaluation of Corrosion Inhibitors for Sour Gas and Oil Production and Water Injection	Nguyen N. Bich
The Interpretation of EIS at Corrosion Potential	Chu-nan Cao
Effect of Phosphorus on Anodic Behavior of Iron in Carbonate/Bicarbonate Solution	E. Sikora, A. Sadkowski, and J. Flis
Acetylenic Derivatives as Inhibitors of Armco Iron Acid Corrosion	A. Frignani, C. Monticelli, G. Trabanelli
AC Impedance Analysis for Atmospheric Corrosion	Atsushi Nishikata and Tooru Tsuru
Polarization Current Distribution and Electrochemical Impedance Response of Reinforced Concrete when Using Guard Ring Electrodes	S.C. Kranc and A.A. Sagues
EIS Studies of Molybdate and Some Organic Inhibitors	M. Saremi and J.P.G. Farr

MASS TRANSPORT

Session Chairman: *Z. Stoynov*

Frequency Response of Small Electrodes to Hydrodynamic or to Potential Perturbations	B. Tribollet *(Plenary)*, O. Gil, and , C Deslouis
Analysis of Charge Transfer and Mass Transport Processes for the Redox Containing Modified Poe Electrolyte - SnO2 System	B. Marsan and H. Cachet
Turbulent Noise Measurements: A New Possibility in Electrochemical Impedance Technique	S.A. Martemyanov
Iron Dissolution Under Mass Transport Control: The Effect of Viscosity	J.R.R.M. Ferreira, O.E. Barcia, O.R. Mattos, and B. Tribollet
Thermoelectrical Impedances: A New Device and Some Results on Mass Transport	A. Aaboubi, A. Olivier, E. Merienne, J.P. Chopart, C. Gabrielli, and B. Tribollet
Zinc Deposition and Dissolution in a Flow-Through Porous Electrode	C. Cachet, R. Wiart, J. Zoppas-Ferreira
Diffusion Impedance in Planar, Cylindrical and Spherical Symmetry	T. Jacobsen and K. West
Convective Warburg Impedance at an Impinging Jet Electrode	W.H. Smyrl and B.T. Bell
Diffusive Mass Transport and Impedance Measurements in Corrosion Systems	W.H. Smyrl and B.T. Bell

THURSDAY, JULY 16 - AFTERNOON SESSION

COATINGS

Session Chairman: A. Sagues

The Past and Future of Electrochemical Impedance Analysis of Organic Coatings on Metals	Martin Kendig *(Plenary)*
Testing of Corrosion Resistant Fluoropolymer Coatings	F. Deflorian, L. Fedrizzi, A. Locaspi, P.L. Bonora
Prediction of Coating Performance by Rapid Electrical Impedance Measurements	Angela M. Ross and Earl L. Diamond
The Influence of Extender Pigments on the Performance of Ethyl Silicate Zinc Rich Paints	I. P. Margaru, O. R. Mattos, F. L. Fragata, C.R.S. Mussoi
Investigation of Ion Exchange at Mixed Conductor Electrodes by Electrogravimetric Transmittance	P. Bernard, C. Gabrielli, M. Keddam, and H. Takenouti
Electrochemical Impedance in Electroless Plating	Izumi Ohno and Shiro Haruyama
Impedance Analysis of Polymer Film Electrodes	G. Láng, J. Bácskai, and G. Inzelt
Electrical Characterization of Polymer-Metal Composites by Impedance Spectroscopy	J.R. Jurado, M. Rodriguez and J.L. Acosta
An Impedance Study of Polypyrrole Films Doped with Tetrathiomolybdate Anions	Siyu Ye, Francois Girard, and Daniel Belanger
Interface Phenomena: Characterization of Lithium/Composite Electrolyte Polymers Interface by Impedance Spectroscopy	F. Croce

MECHANISMS AND MODELS

Session Chairman: P. Searson

Development of Physico-Chemical Models for Electrochemical Impedance Spectroscopy	Mark E. Orazem *(Plenary)*
Theoretical Investigation of the Electrochemical Deposition of Metal Involving Absorption and Desorption Steps	Sylvie Rouquette-Sanchez, Pierre Cowache, Pascale Boncorps, Jacques Vedel
The Study of Medium Effects on the Electrochemical Reduction of Nitromethane by the Impedance Analysis	M. Rueda, F. Prieto, and I. Navarro
Nonstationary Modelling of the Basic Electrochemical Impedances	B. Savova-Stoynov and Z.B. Stoynov
Kinetic Study of the Hydrogen Evolution Reaction by Impedance Spectroscopy: Structural Effects	E.L. de Sa, A.A. Tanaka, G. Tremiliosi-Filho
Impedance Analysis of the Kinetics of Electrochemical Processes Mediated by Polymer Layers	C. Deslouis, M.M. Musiani, and B. Tribollet
Time Resolved Impedance Spectroscopy of Electrocatalytic Active Surfaces	Markus Weidenauer, Michael Wanner, and Konrad G. Weil
A Kinetic Model for the Dissolution Mechanism of Copper in Acidic Sulfate Solutions	Danny K.Y. Wong, Bruce A.W. Coller, and Douglas R. MacFarlane
The Capacity of Monocrystalline Nickel Electrode in Potassium Hydroxide Solution at Low Hydrogen Overpotentials	P. Zoltowski
Characterization of Some III-V Semiconductor/Electrolyte Interfaces Utilizing Electrochemical Impedance Spectroscopy	Shyam S. Kocha and Bruce E. Liebert

PHOTO-EFFECTS AND SEMICONDUCTORS

Session Chairman: W. Smyrl

Frequency Domain Analysis of the Relaxation of Photoprocesses at Illuminated Semiconductor Electrodes	Peter C. Searson *(Plenary)* and Digby D. Macdonald
Low Temperature Impedance of Semiconducting n-RuS2/HClO4-5.5H2O Interface	H. Colell and N. Alonso-Vante
Impedance Spectroscopic Studies on High Tc Superconductors	M. Mohammad, A.Y. Khan, U. Akhtar, S. Malik, M.S. Subhani, and R. Wahab
Combination of Impedance and Intensity Modulated Photocurrent Spectroscopy for the Characterization of Semiconductor-Photoelectrodes	J. Schefold and F. Philipps
Recombination in Semiconductor-Electrodes: Investigation by the Electrical and the Opto-electrical Impedance Methods	D. Vanmaekelbergh, A.R. de Wit, and F. Cardon
Study on SnO2-Fe2O3 Gas Sensing System by AC Complex Impedance Technique	Liu Xingqin, Chen Chunhua, Xu Wendong, Shen Yusheng, and Meng Guangyao
The Photoimpedance of Passive Metal Electrodes	Albert Goossens and Digby D. Macdonald
An Electrochemical Study of Copper Sulphide Minerals by AC Impedance Spectroscopy	C. Hecker, S.H. Castro, J.P. Diard, and B. Le Gorrec
Electrochemical Impedance Spectroscopy of Galena/Xanthate System	J. Genesca and J.M. Valverde

MEMBRANES AND BIOLOGICAL SYSTEMS

Session Chairman: D.D. Macdonald

Current-Time Responses and Impedances of Model Thin Layer and Membrane Cells with Steady State Current	Richard P. Buck *(Plenary)* and Tal M. Nahir
A Study on Toad Bladder Membranes by Electrochemical Impedance Spectroscopy	Li Jialing, Cui Yanfang, Xiong Yan, Liu Jie, and Long Guangdou
Impedance Study on Titanium Nitride Coatings	J. Piippo, B. Elsener, and H. Böhni
Electrochemical Impedance Spectroscopy Characteristics of Poly- O- Aminophenol Modified Electrodes	C. Barbero, R.I. Tucceri, and D. Posadas
The Use of EIS to Study Membrane Transport in Nicotinic Acetylcholine Receptor	H. Arias, F. Barrantes, S. Alonso-Romanowski and J.R. Vilche
Impendance Spectroscopy of Artificial Membranes Deposited on Metal Surfaces with Langmuir-Blodgett Technique	Britta Lindholm and Per-Åke Ohlsson
Impedance Spectral Studies of Herbicide Challenge to Plant Cell Monolayers	J.B. Lee, H. Coombs, J.P.G. Farr
A Comparative Study by Impedance Spectroscopy of Differently Treated Tomato Cuticular Membranes	J.R. Ramos-Barrado, J. Benavente, and A. Heredia

POSTERS

A Study of Photoanodic Dissolution of CdS with the Opto-Electrical Impedance Method	A.R. de Wit and D. Vanmaekelbergh and J J. Kelley
AC-Superimposed-On-DC Characteristics of Fuel Cell Electrodes	Gwo-lin Lee and J. Robert Selman
An Impedance Investigation of Thin Oxide Layers on Pure Aluminum and of Their Water Content	A. Frichet, P. Gimenez, and M. Keddam
Application of Electrochemical Impedance Spectroscopy and Rotating Ring-Disc Measurements on Fe-Cr Binary Alloys	A. Annergren, M. Keddam, H. Takenouti, and D. Thierry
Application of Measurement Models to Electrochemical Impedance Spectroscopy	Pankaj Agarwal, Mark Orazem, and Luis H. Garcia-Rubio
Assessment of the Efficiency of Different Inhibitors on Rusted Steel by Impedance Spectroscopy	J.C. Galvan, M. Morcillo, S. Feliu Jr., J.M. Bastidas, J. Simancas, E.M. Almeida, and S. Feliu
Characterization of Chromate Conversion Layers of Al-alloys by Electrochemical Impedance Spectroscopy (EIS) and Optical Spectroscopy	D. Ende, R.W. Kessler, D. Oelkrug, and R. Fuchs
Characterization of Lead Corrosion Films by EIS	F.E. Varela, L.M. Gassa and J.R. Vilche
Comparison of AC Impedance and Cyclic Voltammetry for Estimating the Faradaic Capacitance of a Redox Material: Influence of a Steep Insulator-Conductor Transition	P. Bernard, M. Keddam, and H. Takenouti
Corrosion Inhibition Study of Pure Iron in Neutral Solutions by an Organic Compound Using Electrochemical Methods	M.C. Lafont, N. Pebere, C. Deslouis, and F. Dabosi
CPA - Phenomenon in the Electrode System	S. Shkerin and U. Vlasova
Dielectic Properties and Mesomorphism of the Second Organic Phase	V. V. Korolev, M. A. Afonin, V. A. Scherbako, E. V. Komarov and L. B. Shpunt
Differential Surface Tension of Solid Metals/Molten Alkali Halides Interfaces	Yurij Pastukhov
E.H.D. Impedance Study for the Electrodissolution of Copper in Acidic Chloride Solutions	E. D'elia, O.E. Barcia, O.R. Mattos, N. Pebere, and B. Tribollet
EIS Application: Influence of the Mechanical Forming on the Quality of Protection Coating in the Case of Lacquered Tinplate	C. Bugnard, L. Billen, P. Jnges, J. Morreale
EIS Characterization of Candidate Coating Materials for Aerospace Applications	H.L. Novak and J.F. McIntyre
EIS Study on the Solubility and Diffusivity of O_2 and CO_2 in Molten Carbonates	Isamu Uchida and Tatsuo Nishina
Electrochemical Characterization of Organosilicic Membranes Doped with Crown Ethers	P. Aranda, J.M. Amarilla, J.C. Galvan, B. Casal, E. Ruiz-Hitzky

POSTERS

A Study of Photoanodic Dissolution of CdS with the Opto-Electrical Impedance Method	A.R. de Wit and D. Vanmaekelbergh and J J. Kelley
AC-Superimposed-On-DC Characteristics of Fuel Cell Electrodes	Gwo-lin Lee and J. Robert Selman
An Impedance Investigation of Thin Oxide Layers on Pure Aluminum and of Their Water Content	A. Frichet, P. Gimenez, and M. Keddam
Application of Electrochemical Impedance Spectroscopy and Rotating Ring-Disc Measurements on Fe-Cr Binary Alloys	A. Annergren, M. Keddam, H. Takenouti, and D. Thierry
Application of Measurement Models to Electrochemical Impedance Spectroscopy	Pankaj Agarwal, Mark Orazem, and Luis H. Garcia-Rubio
Assessment of the Efficiency of Different Inhibitors on Rusted Steel by Impedance Spectroscopy	J.C. Galvan, M. Morcillo, S. Feliu Jr., J.M. Bastidas, J. Simancas, E.M. Almeida, and S. Feliu
Characterization of Chromate Conversion Layers of Al-alloys by Electrochemical Impedance Spectroscopy (EIS) and Optical Spectroscopy	D. Ende, R.W. Kessler, D. Oelkrug, and R. Fuchs
Characterization of Lead Corrosion Films by EIS	F.E. Varela, L.M. Gassa and J.R. Vilche
Comparison of AC Impedance and Cyclic Voltammetry for Estimating the Faradaic Capacitance of a Redox Material: Influence of a Steep Insulator-Conductor Transition	P. Bernard, M. Keddam, and H. Takenouti
Corrosion Inhibition Study of Pure Iron in Neutral Solutions by an Organic Compound Using Electrochemical Methods	M.C. Lafont, N. Pebere, C. Deslouis, and F. Dabosi
CPA - Phenomenon in the Electrode System	S. Shkerin and U. Vlasova
Dielectic Properties and Mesomorphism of the Second Organic Phase	V. V. Korolev, M. A. Afonin, V. A. Scherbako, E. V. Komarov and L. B. Shpunt
Differential Surface Tension of Solid Metals/Molten Alkali Halides Interfaces	Yurij Pastukhov
E.H.D. Impedance Study for the Electrodissolution of Copper in Acidic Chloride Solutions	E. D'elia, O.E. Barcia, O.R. Mattos, N. Pebere, and B. Tribollet
EIS Application: Influence of the Mechanical Forming on the Quality of Protection Coating in the Case of Lacquered Tinplate	C. Bugnard, L. Billen, P. Jnges, J. Morreale
EIS Characterization of Candidate Coating Materials for Aerospace Applications	H.L. Novak and J.F. McIntyre
EIS Study on the Solubility and Diffusivity of O_2 and CO_2 in Molten Carbonates	Isamu Uchida and Tatsuo Nishina
Electrochemical Characterization of Organosilicic Membranes Doped with Crown Ethers	P. Aranda, J.M. Amarilla, J.C. Galvan, B. Casal, E. Ruiz-Hitzky

POSTERS

Electrochemical Impedance for Passive Iron in Organic Solvents Containing Sulfuric Acid and Water	V.A. Safonov and Shiro Haruyama
Electrochemical Impedance Studies of Polymer Electrolyte Membrane Fuel Cell and Electrolyzer	F. Mahlendorf, V. Peinecke, A. Heinzel, K. Ledjeff
Frequency Dependence of Modulated Surface Tension of Solid Metals	Gintaras Valincius
Frequency Dependence of the Conductivity for a Cu+--Conducting Glass Determined by the Impedance Spectroscopy	Yuan Yang, Jianguo Hou, and Wenhai Yu
Frequency Resolved Faradaic Processes in Polypyrrole Films Observed by Electrochemical Impedance, Color Admittance and Mass Admittance Spectroscopies	T. Amemiya
Impedance of Stainless Steel During Pitting Repassivation	Shenghan Zhang and Shizhong Huo
Impedance Spectroscopy Under Steady-State Currents of Plasticized PVC Membranes Containing Valinomycin and Mobile Sites	Tal M. Nahir and Richard P. Buck
Impedance Studies of Steel-Mortar System	E. Czechowska, P. Persidok, A. Krolikowski, and J. Przyluski
Impedance Studies of Thin Films of Nickel Hydroxide	P. Bernard, M. Keddam, and H. Takenouti
In-Situ Real-Area Determination in the Evaluation of Porous, Gas-Evolving Electrocatalysts by Means of Potential Relaxation and Impedance Measurements	L. Bai, L. Gao, and B.E. Conway
Influence of Magnetic Field on Mass Transport: MHD Impedance	O. Aaboubi, J.P. Chopart, A. Olivier, C. Gabrielli, and B. Tribollet
Influence of Surface Roughness and Electrolyte Concentration on the Pt/$HClO_4$ Interface CPE	E.D. Bidóia, L.O.S. Bulhoes, and R.C. Rocha-Filho
Microscopic and Electrochemical Impedance Analysis of the Degradation of Polymide-Coated Al Metalization	M. Kendig, S. Jeanjaquet, J. Lumsden, and R. Addison
Monitoring of Localized Corrosion and Methods of Corrosion Protection with EIS	Florian Mansfeld
Partially Blocked Surface Studied by Electrohydrodynamic Impedance	C.R. Souza, O.E. Barcia, O.R. Mattos, C. Deslouis
Properties of Gold-related Surface States at p-Gas/Electrolyte Interfaces	G. Oskam, D. Vanmaekelbergh and J.J. Kelly
Relative Reactivity of Various Copper Oxide and Fulleride High Temperature Superconductor Phases	David R. Riley, Ji-Ping Zhou, A. Manthiram, David Jurbergs, Jianai Zhao, and John T. McDevitt
Studies on Film Formed on Copper Electrode by Cyclic Voltammetry, AC-Impedance Spectroscopy and IR-Reflection Spectroscopy	Qiguang Yin and Jiujun Zhang

POSTERS

Electrochemical Impedance for Passive Iron in Organic Solvents Containing Sulfuric Acid and Water	V.A. Safonov and Shiro Haruyama
Electrochemical Impedance Studies of Polymer Electrolyte Membrane Fuel Cell and Electrolyzer	F. Mahlendorf, V. Peinecke, A. Heinzel, K. Ledjeff
Frequency Dependence of Modulated Surface Tension of Solid Metals	Gintaras Valincius
Frequency Dependence of the Conductivity for a Cu+--Conducting Glass Determined by the Impedance Spectroscopy	Yuan Yang, Jianguo Hou, and Wenhai Yu
Frequency Resolved Faradaic Processes in Polypyrrole Films Observed by Electrochemical Impedance, Color Admittance and Mass Admittance Spectroscopies	T. Amemiya
Impedance of Stainless Steel During Pitting Repassivation	Shenghan Zhang and Shizhong Huo
Impedance Spectroscopy Under Steady-State Currents of Plasticized PVC Membranes Containing Valinomycin and Mobile Sites	Tal M. Nahir and Richard P. Buck
Impedance Studies of Steel-Mortar System	E. Czechowska, P. Persidok, A. Krolikowski, and J. Przyluski
Impedance Studies of Thin Films of Nickel Hydroxide	P. Bernard, M. Keddam, and H. Takenouti
In-Situ Real-Area Determination in the Evaluation of Porous, Gas-Evolving Electrocatalysts by Means of Potential Relaxation and Impedance Measurements	L. Bai, L. Gao, and B.E. Conway
Influence of Magnetic Field on Mass Transport: MHD Impedance	O. Aaboubi, J.P. Chopart, A. Olivier, C. Gabrielli, and B. Tribollet
Influence of Surface Roughness and Electrolyte Concentration on the Pt/HClO4 Interface CPE	E.D. Bidóia, L.O.S. Bulhoes, and R.C. Rocha-Filho
Microscopic and Electrochemical Impedance Analysis of the Degradation of Polymide-Coated Al Metalization	M. Kendig, S. Jeanjaquet, J. Lumsden, and R. Addison
Monitoring of Localized Corrosion and Methods of Corrosion Protection with EIS	Florian Mansfeld
Partially Blocked Surface Studied by Electrohydrodynamic Impedance	C.R. Souza, O.E. Barcia, O.R. Mattos, C. Deslouis
Properties of Gold-related Surface States at p-Gas/Electrolyte Interfaces	G. Oskam, D. Vanmaekelbergh and J.J. Kelly
Relative Reactivity of Various Copper Oxide and Fulleride High Temperature Superconductor Phases	David R. Riley, Ji-Ping Zhou, A. Manthiram, David Jurbergs, Jianai Zhao, and John T. McDevitt
Studies on Film Formed on Copper Electrode by Cyclic Voltammetry, AC-Impedance Spectroscopy and IR-Reflection Spectroscopy	Qiguang Yin and Jiujun Zhang

POSTERS

Study of the Electrochemical Grafting and the Growth of Polymers on Metallic Surface by Impedance Spectroscopy	J. Tanguy, A. Servais, and G. Lécayon
Study of the Oxygen Transfer Process at the YSZ and Fe-Implanted YSZ/Au, O2 Gas Electrode	B.A. Boukamp, B.A. van Hassel and A.J. Burggraaf
The Application of the Electrochemical Impedance Spectroscopy in Porous Electrode Studies for Hydrogen Evolution	A.H. Fakeeha., F.A. Abdelaleem, T.F. Al-Fariss, and A.S. Al-Mutaz
The Corrosion of Aluminum Alloys by Chlorinated Hydrocarbons	Schalk W. Vorster and Ockert J. Van Der Schijff
The Effect of Parasitic Conduction Pathways on EIS Measurements in Low Conductivity Media	D.G. Kolman, K.C. Stewart, S.R. Taylor
The Effects of Nongomoheneous Structure and Diffusion Coefficients on the Impedance of Solid Electrolyte-Gas-Electrode Interface	I.V. Murygin, R.U. Atangulov
The Impedance Response of Sodium Sulfur Cells	M.C.H. McKubre, S.I. Smedley, and F.L. Tanzella
The Role of Phosphate, Perchlorate and Chloride Anions on Copper Electrodissolution	J.D. Cardoso, E. D'Elia, O.E. Barcia, and O.R. Mattos
Transient Impedance Study of Time Behaviour of Ag Surface Passivation by Cyanide Ions Under Potentiostatic Conditions	Vytautas Daujotis, Virgaudas Kubilius, and Darius Jasaitis
Use of Electronically Blocking Oxygen Electrodes in Impedance Measurements on Mixed Conducting Oxides	L.G.J. de Haart, B.A. Boukamp, K.J. de Vries and A.J. Burggraaf

POSTERS

Study of the Electrochemical Grafting and the Growth of Polymers on Metallic Surface by Impedance Spectroscopy	J. Tanguy, A. Servais, and G. Lécayon
Study of the Oxygen Transfer Process at the YSZ and Fe-Implanted YSZ/Au, O2 Gas Electrode	B.A. Boukamp, B.A. van Hassel and A.J. Burggraaf
The Application of the Electrochemical Impedance Spectroscopy in Porous Electrode Studies for Hydrogen Evolution	A.H. Fakeeha., F.A. Abdelaleem, T.F. Al-Fariss, and A.S. Al-Mutaz
The Corrosion of Aluminum Alloys by Chlorinated Hydrocarbons	Schalk W. Vorster and Ockert J. Van Der Schijff
The Effect of Parasitic Conduction Pathways on EIS Measurements in Low Conductivity Media	D.G. Kolman, K.C. Stewart, S.R. Taylor
The Effects of Nongomoheneous Structure and Diffusion Coefficients on the Impedance of Solid Electrolyte-Gas-Electrode Interface	I.V. Murygin, R.U. Atangulov
The Impedance Response of Sodium Sulfur Cells	M.C.H. McKubre, S.I. Smedley, and F.L. Tanzella
The Role of Phosphate, Perchlorate and Chloride Anions on Copper Electrodissolution	J.D. Cardoso, E. D'Elia, O.E. Barcia, and O.R. Mattos
Transient Impedance Study of Time Behaviour of Ag Surface Passivation by Cyanide Ions Under Potentiostatic Conditions	Vytautas Daujotis, Virgaudas Kubilius, and Darius Jasaitis
Use of Electronically Blocking Oxygen Electrodes in Impedance Measurements on Mixed Conducting Oxides	L.G.J. de Haart, B.A. Boukamp, K.J. de Vries and A.J. Burggraaf

INFLUENCE OF MAGNETIC FIELD ON MASS TRANSPORT : MHD IMPEDANCES

O. AABOUBI, J.P. CHOPART, A. OLIVIER
Laboratoire d'Electrochimie et Chimie du Solide, UFR Sciences
51062 Reims Cedex - FRANCE

C. GABRIELLI, B. TRIBOLLET
UPR15 du CNRS, Physique des Liquides et Electrochimie,
Université P. et M. Curie, 4 place Jussieu, 75252 Paris Cedex 05 - FRANCE

INTRODUCTION

In an electrochemical cell an external magnetic field generates a forced convection in the vicinity of an electrode. This leads to electrolysis stable and reproducible currents [1-7] whose values are in accordance with theory.

The dynamic analysis of the convective diffusion impedance performed by classical electrochemical impedance measurements confirm that the observed current changes can be interpreted by the velocity gradient generated by the magnetic field [6,7].

A new technique based on the frequency analysis of the potential (or current) response to a low amplitude sine wave perturbation of the magnetic field leads to the magnetohydrodynamic (MHD) impedance [7,8].

STEADY STATE CURRENTS

The application of a magnetic field B perpendicular to the electrode plane imposes a forced convection. In these conditions the limiting current is equal to

$$I_L = 0.678\, n\, F\, D^{2/3}\, C^*\, \alpha^{1/3}\, d^{5/3} \qquad (1)$$

where F is the Faraday, D the diffusion coefficient, C* the concentration of the reactive species in the bulk of the solution, α the velocity gradient and d the electrode diameter. In eq(1) α is proportional to C* and to the magnetic field B, and can be written as $\alpha = kC^*B$ where k is a constant depending of the set-up geometry.

ELECTROCHEMICAL IMPEDANCE

The measurement of the electrochemical impedance brings informations on the mass transport. For a redox reaction of reaction rate, $k_o \exp bV$, the impedance of the convective diffusion is equal to

$$Z_D = \frac{-1}{b\, C(o)\, n\, F} \cdot \frac{\Delta C(o)}{\left.\frac{\partial \Delta C}{\partial y}\right|_{y=0}} \qquad (2)$$

The convective diffusion on a non uniformly accessible small electrode had been recently calculated.

In the high frequency range it can be shown that this impedance is independent upon α and hence upon the magnetic field. These theoretical predictions are experimentally confirmed.

MHD IMPEDANCE

The perturbation of the magnetic field by a low amplitude sine wave $\Delta B \sin \omega t$ leads to the following modifications :

$$\Delta B \rightarrow \Delta v = \Delta\alpha\, y \rightarrow \left|\frac{\partial C}{\partial y}\right|_{y=0} \rightarrow \Delta I$$

magnetic field — convective diffusion — kinetics

where

$$\frac{\Delta I}{\Delta B} = n F C^* \left(D^2 \frac{d^5}{\alpha^2}\right)^{1/3} H(\sigma) \cdot \frac{\Delta\alpha}{\Delta B} \qquad (3)$$

$H(\sigma)$ is the frequency response of a small electrode to a velocity perturbation [11,12].

From (1) at zero frequency the amplitude of the $\Delta I/\Delta B$ transfer function is equal to :

$$A_0 = 0.226\, n F D^{2/3} C^{*4/3} d^{5/3} k^{1/3} B^{-2/3}$$

This technique allows the investigation of the mass transport as shown by the experimental results obtained on the $Fe(CN)_6^{3-}/Fe(CN)_6^{4-}$ system.

REFERENCES

[1] E.Z. GAK, E.K. ROKHINSON, N.F. BONDARENKO, Elektrokhimiya, 11 (1975) 528, 535

[2] Y.G. MIKHALEV, L.A. ISAEVA, P.V. POLYAKOV, Elektrokhimiya, 21 (1985) 519

[3] Z.H. GU, T.Z. FAHIDY, J. Electrochem. Soc., 134 (1987) 2241

[4] C. IWAKURA, T. EDAMOTO, H. TAMURA, Denki Kagaku, 52 (1984) 596, 654

[5] R. AOGAKI, K. FUEKI, T. MUKAIBO, Denki Kagaku, 43 (1975) 504, 509

[6] A. OLIVIER, J.P. CHOPART, J. DOUGLADE, C. GABRIELLI, J. Electroanal. Chem., 217 (1987) 443

[7] O. AABOUBI, Thèse, Reims (1991)

[8] O. AAOUBI, J.P. CHOPART, J. DOUGLADE, A. OLIVIER, C. GABRIELLI, B. TRIBOLLET, J. Electrochem. Soc., 137 (1990) 1796

[9] A. OLIVIER, J.P. CHOPART, J. DOUGLADE, C. GABRIELLI, B. TRIBOLLET, J. Electroanal. Chem., 227 (1987) 275

[10] C. DESLOUIS, B. TRIBOLLET, M.A. VOROTYNTSEV, J. Electrochem. Soc., 138 (1991) 2651

[11] V.Y. NAKORYAKOV, A.P. BUDUKOV, O.N. KASHINSKY, P.I. GESHEV, "Electrodiffusion Method of Investigation into the Local Structure of Turbulent Flows", Ed. V.G. Gasenko, Novosibirsk (1986)

[12] C. DESLOUIS, O. GIL, B. TRIBOLLET, J. Fluid Mech., 215 (1990) 85

$$j\omega\Delta c - D\frac{\partial^2\Delta c}{\partial y^2} + \alpha y^2 \frac{\partial \Delta c}{\partial y} = -\left(\frac{\Delta D}{\delta^3} + \Delta\alpha\right) y^2 \frac{\partial c}{\partial y} \qquad (3)$$

This equation is similar to the equation obtained for an hydrodynamic perturbation (for example in the case of the EHD impedance [5]) . On the diffusion plateau $\frac{\partial \Delta c}{\partial y}|_o$ is then proportional to the function W(ω) previously calculated [5] :

$$\frac{\partial \Delta c}{\partial y}|_o = W(\omega)\left(\frac{\Delta D}{\delta^3} + \Delta\alpha\right) \qquad (4)$$

In first approximation, if the frequency is low enough, $\beta = F\,D\left(\frac{1}{\delta^3}\frac{\Delta D}{\Delta T} + \frac{\Delta\alpha}{\Delta T}\right)$ can be assumed independant of the frequency, and :

$$\frac{\Delta i_f}{\Delta T} = \beta\, W(\omega) + i_f \frac{1}{D}\frac{\Delta D}{\Delta T} \qquad (5)$$

D can be expressed as an empirical function of the temperature [6] :

$$D = \frac{RT}{|z|F^2}\left(\lambda + A\,(T - 298) + B\,(T - 298)^2 + C\,(T-298)^3\right) \qquad (6)$$

where λ is the ionic equivalent conductance, z the charge number of the electroactive species and A, B, C are some constants depending of the species.

In the high frequency range W(ω) tends towards zero [5] and $\Delta i_f/\Delta T$ tends towards a real number equal to $\frac{i_f}{D}\frac{\Delta D}{\Delta T}$.

Experimentally, the behaviour of $\frac{\Delta i_f}{\Delta T}$ is in agreement with (5) and in the high frequency the impedance tends towards a real number Q . Q/i_f is found between 0.01 K^{-1} and 0.02 K^{-1}. This value is close to the theoretical one calculated from (6) with the usual values for the constants given in [6] .

REFERENCES

[1] V.A. Benderskii and G.I. Velichko, J. Electroanal. Chem., 140, (1982), 1-22
[2] C. Gabrielli, M. Keddam, J.F. Lizee, J. Electroanal. Chem., 148, (1983), 293-297
[3] B. Miller, J. Electrochem. Soc., 130, (1983), 1639-1640
[4] A. Olivier, E. Merienne, J.P. Chopart, O. Aaboubi, Electrochimica Acta, (1992), in press
[5] B.Tribollet and J.Newman, J. Electrocem. Soc., **130**, (1983) , 2016-2026 .
[6] R. Parsons, *Handbook of Electrochemical Constants*, Butterworths, London (1962)

THERMOELECTRICAL IMPEDANCES AT LIMITING DIFFUSION CURRENT

O. AABOUBI , J.P. CHOPART , E. MERIENNE , A. OLIVIER
Laboratoire d'Electrochimie et Chimie du Solide, UFR Sciences, 51062 Reims Cedex, France

C. GABRIELLI , B.TRIBOLLET
UPR 15 du CNRS, "Physique des Liquides et Electrochimie", associé à l'Université P. et M. Curie, 4 Place Jussieu, 75252 Paris Cedex 05, France

INTRODUCTION

The temperature dependance of an electrochemical system arises from a number of possible sources which include equilibrium potential, electron transfer, adsorption of intermediates, rate constants, electrochemical kinetics and mass transport. In the steady state analysis it is difficult to separate clearly the contribution of each source and so some transient techniques had been developped, essentially temperature jump technique obtained with a laser [1] or by Joule effect [2] and temperature modulation at a constant frequency by means of a laser [3] . A sinusoidal perturbation of the temperature in a large frequency range had not been obtained so far due to the thermal inertia of the electrochemical cell.

A new technique is presented where a steady temperature gradient is imposed from the electrode interface to the electrolyte bulk [4]. A modulation of the interface temperature which induces a modulation of the temperature gradient is not frequency limited by the thermal inertia of the cell. This new impedance technique is applied on a wellknown fast redox system in order to improve our knowledge of the corresponding mass transport and kinetic theoretical response.

ANALYSIS

The response of the faradaic current to a temperature perturbation is due to the induced perturbation of the diffusion coefficient and to the induced perturbation of the concentration gradient :

$$\Delta i_f = F\, D \frac{\partial \Delta c}{\partial y}\Big|_o + F \frac{\partial c}{\partial y}\Big|_o \Delta D \qquad (1)$$

The response of the concentration gradient is obtained by the integration of the mass balance equation:

$$j\omega \Delta c - D \frac{\partial^2 \Delta c}{\partial y^2} + \left(\alpha y^2 - \frac{\partial D}{\partial y} \right) \frac{\partial \Delta c}{\partial y} = \Delta D \frac{\partial^2 c}{\partial y^2} + \frac{\partial \Delta D}{\partial y} \frac{\partial c}{\partial y} - \Delta\alpha\, y^2 \frac{\partial c}{\partial y} \qquad (2)$$

where the electrode is supposed uniformly accessible and $V_y = \alpha\, y^2$.

The thickness of the thermal diffusion layer is about 10 times larger than the thickness of the mass diffusion layer δ, so in a first step the gradient of the diffusion coefficient can be neglected . Taking into account the expression of the steady concentration field, equation (2) becomes :

APPLICATION OF MEASUREMENT MODELS TO ELECTROCHEMICAL IMPEDANCE SPECTROSCOPY

Pankaj Agarwal and Mark E. Orazem
Department of Chemical Engineering
University of Florida
Gainesville, Florida 32611-2021

and

Luis H. Garcia-Rubio
Department of Chemical Engineering
University of South Florida
Tampa, Florida 33620

Measurement models have recently been developed as a tool for characterization of electrochemical impedance data.[1,2] Measurement models are distinguished from process models by their physical origin and by their means of application. Process models are used to predict the response of a system from physical phenomena that are hypothesized to be important. Regression of process models to data allows identification of physical parameters based upon the original hypothesis. In contrast, measurement models are built by sequential regression of line shapes to the data. The lineshapes used are derived loosely from a physical model, but no direct correspondence to the physical system is assumed. The measurement model is intended to identify characteristics of the data set that could facilitate selection of an appropriate process model.

Four applications of measurement models will be discussed:

1. *The measurement model can be used to check data for consistency with the Kramers-Kronig relations.* Inconsistency can be associated with non-stationary behavior or with measurement artifacts. The regression of measurement models as a means of determining consistency with the Kramers-Kronig relations is an extension to the use of electrical circuit analogues. Because the model itself is consistent with the Kramers-Kronig relations, successful regression of the model to a given spectrum implies that the data are consistent. Integration over zero to infinity in frequency is not required. The measurement model is composed of a summation of lineshapes that will, with a sufficient number of terms, provide a statistically adequate fit to any consistent data set. Since the model will provide an adequate representation of a consistent spectrum, failure to fit the data can be attributed to inconsistency with the Kramers Kronig relations, thus eliminating ambiguity in the interpretation of a "poor fit" to the data.

2. *The measurement model can be used to provide increased sensitivity to system parameters.* The measurement model can be applied to determine whether

a system parameter (e.g., rotation speed or time) influences the impedance response. The model is regressed to the combined data from experiments run with different parameter values. Examination of residual errors from the fit can show the influence of parameters that might be too subtle to see in the raw data. Standard statistical tools can be employed to determine whether the differences are significant. Such examination may suggest modifications to the experimental design.

3. *The measurement model can be used to provide a means for model identification through examination of residual errors and identification of an upper bound to the number of time constants evident in the spectrum.* For solid-state systems, a one-to-one correspondence has been found between the number of lineshapes employed in the regression and the number of physical processes discernable from the spectrum. While a direct correspondence has not been observed in electrochemical systems, examination of the residual errors can identify the importance of processes (such as diffusion) that must be modeled through distributed elements.

4. *The measurement model can be used to provide a rationale for extrapolation of impedance data to the zero frequency asymptote without selection of an explicit process model.* While extrapolation of impedance data is necessarily uncertain, the measurement model approach will allow estimation of the polarization resistance for a given incomplete impedance spectrum. This may be useful as a tool for the rapid screening of metals so often needed in industrial corrosion applications.

The approach taken here involves a considerable degree of interaction between collection of data, application of measurement models as a data screening, and development of physico-chemical process models. The results of the measurement model are used to suggest changes in the experimental design and to guide development of models based on a more physical description of the system under study.

REFERENCES

1. P. Agarwal, M. E. Orazem, and L. H. Garcia-Rubio, "Measurement Models for Electrochemical Impedance Spectroscopy: 1. Demonstration of Applicability," *Journal of the Electrochemical Society,* in press.

2. P. Agarwal, M. E. Orazem, and L. H. Garcia-Rubio, "Application of the Kramers-Kronig Relations in Electrochemical Impedance Spectroscopy," *Electrochemical Impedance: Analysis and Interpretation,* J. Scully, D. Silverman, M. Kendig, Editors, American Society for Testing and Materials, Philadelphia, in press.

FREQUENCY RESOLVED FARADAIC PROCESSES IN POLYPYRROLE FILMS OBSERVED BY ELECTROCHEMICAL IMPEDANCE, COLOR ADMITTANCE AND MASS ADMITTANCE SPECTROSCOPIES

T. Amemiya, K. Hashimoto and A. Fujishima
Department of Synthetic Chemistry, Faculty of Engineering,
The University of Tokyo, Bunkyo-ku, Tokyo 113, JAPAN.

Two parallel studies (I and II) on dynamics of charge transport processes in polypyrrole (PPy) films deposited on electrodes are presented. One is to investigate the faradaic processes in PPy/PSS^- (PSS^- =polystyrenesulfonate) films immersed in an aqueous electrolyte (1M KCl) containing a redox species $[Fe(CN)_6]^{3-/4-}$ by impedance and color admittance ($\Delta T/\Delta E$) spectroscopies.[1] The other is to make clear ion (anion and cation) transport properties in PPy/Cl^- films by impedance and mass admittance ($\Delta m/\Delta E$) spectroscopies.[2]

(I) Dynamic behavior of faradaic processes in PPy/PSS^- films has been separately monitored from the other redox reaction of the redox species, $[Fe(CN)_6]^{3-/4-}$ by color admittance at 700 nm. The color admittance data of the PPy/PSS^- films (Fig.1) can be reproduced by using an equivalent circuit as shown in Fig. 2. The color admittance plots have been found to follow the modulation of charge ($\Delta Q_1/\Delta E$) in the faradaic impedance branch (Z_{PPy}) of the PPy/PSS^- films connected in parallel with the other faradaic impedance branch (Z_W) of the redox species.

(II) The contributions of anions and cations to the charge transport processes in PPy/Cl^- films have been elucidated by analyzing both the capacitance plots (Fig.3(a)) and the mass admittance plots (Fig.3(b)) with following equations[2]

$$C=(\Delta Q/\Delta E)=(1/i\omega)[z_-(\Delta\phi_-/\Delta E)+z_+(\Delta\phi_+/\Delta E)] \quad (1)$$

$$M=(\Delta m/\Delta E)=(1/i\omega)[m_-(\Delta\phi_-/\Delta E)-m_+(\Delta\phi_+/\Delta E)] \quad (2)$$

where z_- and z_+ are the number of electric charges, m_- and m_+ are the molar masses and $\Delta\phi_-$ and $\Delta\phi_+$ are the fluxes of anions and cations. It has been found that the contribution of cations (K^+) to the charge transport processes is rather important in the PPy/Cl^- films, though they are generally called anion exchange type films.

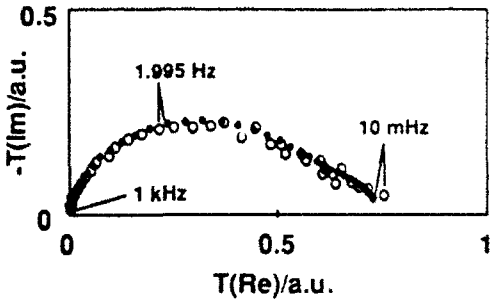

Fig.1

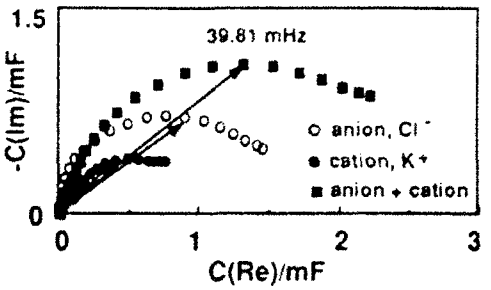

Fig.3 (a)

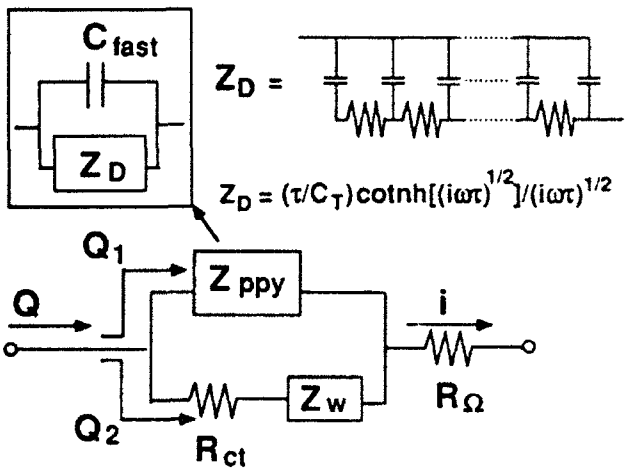

Fig.2

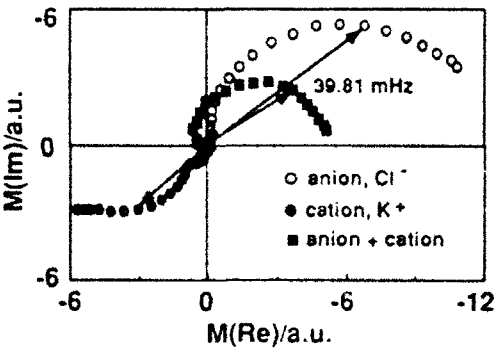

Fig.3 (b)

Fig.1. Color admittance plots of a PPy/PSS^- film at 0.2V in an aqueous solution of 1M KCl + 10mM $K_4[Fe(CN)_6]$. (o):experimental data, (■):simulated plots using an equivalent circuit as shown in Fig. 2 with C_{fast}=3.4mF, R_Ω=21Ω, C_T=0.3mF and τ=1s.

Fig.2. Equivalent circuit for the PPy/PSS^- film immersed in a solution containing the redox species. Z_{PPy} is the impedance of the PPy/PSS^- film, Z_W is the Warburg impedance of the redox species, and R_{ct} is the charge transfer resistance.

Fig.3. Capacitance plots (a) and mass admittance plots (b) for a PPy/Cl^- film at -0.2V in a 1M KCl aqueous solution.

References;(1) (a) Gabrielli, C.; Keddam, M.; Takenouti, H. *Electrochim. Acta.* 1990, *35*, 1553. (b) Hutton, R. S.; Kalaji, M.; Peter. L. M. *J. Electroanal. Chem.* 1989, *270*, 429. (2) Torresı, S. C.; Gabrielli, C.; Keddam, M.; Takenouti, H.; Torresi, R. *J. Electroanal. Chem.* 1990, *290*, 269.

ELECTROCHEMICAL CHARACTERIZATION OF ORGANOSILICIC MEMBRANES DOPED WITH CROWN-ETHERS

P. Aranda, J.M. Amarilla, J.C. Galván* , B. Casal, E. Ruiz-Hitzky

Instituto de Ciencia de Materiales, CSIC, c/Serrano 115 bis, 28006 Madrid (Spain)
(*) CENIM-CSIC, Avda. Gregorio del Amo 8, 28040 Madrid (Spain)

Composite membranes have been prepared as follows: an organo-inorganic matrix is generated via sol-gel by controlled hydrolysis of ethyltriethoxysilane incorporating in the sol phase a selected crown-ether. After gelation, the organosilicic compound is deposited by spin-coating on a borosilicate porous support, the system being slowly dried to allow the formation of a continous network as it is shown by SEM.

The presence of the crown-ether (12-crown-4, 15-crown-5, 18-crown-6) homogeneously distributed into the organosilicic matrix is evidenced by IR and ^{13}C-NMR spectroscopies. As it is well known, crown-ethers are strong complexing agents for alkali-metal ions, even when they are located in inorganic constrained systems[1-3]. These membranes are comparable to those studied by Armstrong where crown-ethers are incorporated in an organic polymer (PVC)[4,5].

Electrochemical characterization of these membranes is realized in typical cells using four electrodes, two CSE (reference electrodes) and two graphite electrodes. The membrane separates two identical electrolytes, which are choiced either by its different ability to form complexes with the selected crown-ethers and by the size of the ionic species in solution.

The resulting impedance diagrams (Cole-Cole) consist in a semicircle which corresponds to a simple equivalent circuit constituted by two elements: an electric resistor associated in parallel with a capacitor. The physical significance of these elements are related with the ionic resistance of the membrane and its geometrical capacitance, respectively. Typical R_i values are in the 50 - 100 kΩ range.

The impedance plots varie with the nature of the doped crown-ether materials as well as with the selected electrolyte. Thus, for alkaline cations, the ionic conductivity through the membrane are in the order:

12-crown-4>18-crown-6>15-crown-5

This result indicates that conductivity, better than the tendency to form complexes, can be controlled by additional factors based in the inner network of the organosilicic matrix (topology & microporosity).

The observed conductivity depends directly on the electrolyte concentration.

Nevertheless, these membranes are only operatives for low concentrated salt solutions (<0.1 M), because high electrolyte concentrations provokes a crown-ether release.

Concerning the nature of the electrolyte we have found the following conductivity sequence for alkali-metal chloride solutions:

$$K^{+} > Na^{+} > Li^{+}$$

indicating that the membrane conductivity diminishes as the hydration energy of those cations increases.

References

1. E. Ruiz-Hitzky, B. Casal, **Nature, 276, 596 (1978)**
2. E. Ruiz-Hitzky, B. Casal, in "Chemical Reactions in Organic and Inorganic Constrained Systems", R. Setton, ed., Reydel publish. Co. Dordrech, 179 (1986)
3. P. Aranda, Ph. D. Thesis, Universidad Complutense, Madrid (1991)
4. R.D. Armstrong, G. Horavai, **Electrochim. Acta, 35, 1 (1990)**
5. R.D. Armstrong, H. Ashassi-Sorkabi, **Electrochim. Acta, 32, 135 (1987)**

POLYMER PROTECTIVE COATINGS - THE DISTINCTION BETWEEN COATING POROSITY AND THE WETTED METAL AREA

R D Armstrong and J D Wright

Chemistry Department
University of Newcastle upon Tyne
Newcastle upon Tyne NE1 7RU
England

Introduction

The perfect polymer protective coating would have:
1. No free ions present in it.
2. No O_2 or H_2O present in it.
3. Zero mobility for ions.
4. Zero diffusion coefficients for O_2 and H_2O.

Such a protective coating would prevent either atmospheric or electrochemical corrosion of the underlying metal. The impedance for such a coated metal when in contact with an aqueous solution would be entirely capacitive with the capacity C_g given by

$$C_g = \varepsilon_o \varepsilon_r A/d$$

Where A is the surface area of the coated metal, d is the polymer thickness and ε_r is the dielectric constant of the film (assumed frequency independent). In this paper we shall consider protective coatings which have defects in them which allow a contacting aqueous solution to penetrate through to the underlying metal and which are not ideal for this reason.

The Coating Porosity

Because of the presence of thin channels of electrolyte running through the coating between the electrolyte and the metal the coating behaves as though it has a finite ionic conductivity equivalent to a resistance R_b which appears to be a bulk property of the film. Where these are of near uniform cross section in nature and run orthoganal to the polymer film we can write

$$R_b = d/aN\kappa$$

where N is the number of defects per unit area, a is the average cross-sectional area of a single defect and κ is the conductivity of the aqueous solution. Therefore one way of characterizing defective coatings of this type is to measure R_b and calculate the apparent value of aN. This is done by calculating the resistance of the layer of electrolyte which would occupy the same space (and hence the same thickness) as the coating can be calculated from the formula

$$R_{bt} = d/\kappa A$$

The ratio

$$R_{bt}/R_b = Na/A = P$$

is the fraction of the coating which consists of voids filled by aqueous solution (ignoring any tortuosity in the defects).

Na/A (a dimensionless quantity) will be called the open porosity of the coating (P) in this paper. This present concept of film porosity has been used recently by Walter [1].

The wetted metal area

In the literature up to the present time it has generally been assumed that the porosity of the coating is the same as the fraction of the metal surface which is wetted by the aqueous solution. This has been most clearly expressed in the paper by Haruyama et al [2]. However we have found that in many cases that the aqueous solution, having penetrated down a fine pore may spread in a thin layer between the coating and the metal. This means that the circuit which is commonly used for such a coating should be modified to take account of this possibility. The interfacial impedance arising from the parts of the metal wetted by the penetrating aqueous solution is represented (for the simplest possible case) by a resistance and capacitance in parallel. These are R_{ct}, the charge transfer resistance of the electrochemical processes occurring at the interface and C_{dl}, the double layer capacity arising from the charge separation which occurs at the metal/solution interface. C_{dl} (measured in Fcm^{-2}) on a coated sample would be expected to be very much smaller than the corresponding C_{dl} value for the bare metal surface (C_{dlo}) in contact with an aqueous solution. This is because of the very much smaller contact area between the metal and the aqueous solution in the film covered case. In fact C_{dl}/C_{dlo} should correspond to the ratio of wetted surfaces in the two cases. Likewise if R_{cto} is the R_{ct} value for the bare metal R_{cto}/R_{ct} should also give the ratio of wetted surfaces, provided that both are measured at an identical potential. Measurements of interfacial impedances are generally made at the open circuit corrosion potential in which case the R_{ct} values will be identical to the corrosion polarisation resistance values, normally designated R_p. However this is not the case if measurements are made at potentials different from the corrosion potential. Thus the wetted metal area (W) expressed as a dimensionless ratio can be evaluated as

$$W = C_{dl}/C_{dl0} = R_{ct0}/R_{ct}$$

We expect W to be often greater than P and in the measurements which we will report to the conference we will show that this is frequently the case.

References

1. G.W.Walter Corr.Science **32**, 1085 (1991)
2. S.Haruyama, M.Asari, T.Tsuru. Corrosion Protection by Organic Coatings. The Electrochem. Soc. Proc. 87-2 p.197

THREE-DIMENSIONAL IMPEDANCE SPECTROSCOPY DIAGRAMS FOR PROCESSES INVOLVING ELECTROSORBED INTERMEDIATES, INTRODUCING THE THIRD ELECTRODE-POTENTIAL VARIABLE -- EXAMINATION OF CONDITIONS LEADING TO PSEUDO-INDUCTIVE BEHAVIOR

L. Bai and B.E. Conway
Department of Chemistry, University of Ottawa, Ottawa K1N 6N5, Canada

The experimental characterization of the behavior of adsorbed intermediates in Faradaic processes proceeding at appreciable current-densities has been little studied, except in recent years by means of analysis of potential-relaxation transients and impedance spectra [1,2]. For a number of multistep reactions, e.g. oxidation of Fe [3,4], anodic dissolution of Al [5,6,7], an important additional feature of the frequency dependence of the impedance is pseudo-inductive behavior. Sometimes the latter arises when a negative Tafel slope for an anodic reaction arises, e.g. in passivation, corresponding formally to a negative reaction resistance. However, even in some processes exhibiting normal positive reaction resistance, pseudo-inductive behavior is still manifested. Possible origins of this effect constitute the main matters examined in the present paper.

In the present paper we examine, by means of the "kinetic" type of approach developed by Armstrong et al. [8], conditions that can give rise to pseudo-inductive behavior in multi-step reactions involving both one and two chemisorbed intermediates. The kinetic approach, involving no arbitrary equivalent circuits, is preferred as the impedance behavior is then formulated in terms of rate-constants of reaction steps and coverages by intermediates, as in steady-state kinetic analyses. This procedure is preferred to the "equivalent-circuit" type of approach which can be arbitrary and empirical, while "components" of such circuits are not always identifiable with the properties of individual reaction steps. Additionally, in the present work, we examine the effects of variation of the important electrode-potential variable and illustrate, in 3-dimensional plots, how the impedance parameters depend not only on frequency but also substantially on potential for various reaction conditions.

For multi-step electrode reactions involving adsorbed intermediates, with positive b_i values (no passivation step(s)), it is found that appearance of inductive behavior in the Faradaic impedance is usually associated with negative slopes of θ_i vs E plots, as for the example considered here. One negative ($d\theta/dE$) gives a single "inductive loop" while two negative slopes give two "inductive loops". However, the potential range over which the impedance is dominated by inductive behavior can be much wider for the reactions involving multi-adsorbed intermediates than that for a reaction involving only one adsorbed intermediate.

The 3-d impedance spectroscopy diagrams in the present work provide a very convenient and clear way to illustrate the dependence of impedance parameters on electrode potential, E, the variable of main importance in electrode kinetics and reaction mechanisms.

The generalized kinetic analysis method was applied to the impedance spectra for Al dissolution in non-aqueous acetonitrile (0.33 mol dm^{-3} $AlCl_3$) solution, which were characterized by one or two overlapping pseudo-inductive loops in the fourth quadrant in the complex-plane at all potentials studied. The major features of the impedance spectra can be simulated by a reaction model involving three intermediates participating in two dissolution paths. The agreement between the experimental and simulated behavior is

reasonably good and can only be achieved (with a set of reasonably-valued parameters) when two of the dependencies of the surface-concentration fractions, θ_i, of the intermediates, on potential are negative and one is positive.

References

1. B.E. Conway and L. Bai, J. Chem. Soc. Faraday Trans. I, 81 (1985) 1841.
2. L. Bai, D.A. Harrington and B.E. Conway, Electrochim. Acta, 32 (1987) 1713.
3. I. Epelboin and M. Keddam, J. Electrochem. Soc., 117 (1970) 1052.
4. M. Keddam, O.R. Mattos and H. Takenouti, J. Electrochem. Soc., 128 (1981) 257 and 266.
5. D.D. Macdonald, S. Real, S.I. Smedley and M. Urquidi-Macdonald, J. Electrochem. Soc., 135 (1988) 2410 and 2397.
6. L. Bai and B.E. Conway, J. Electrochem. Soc., 137 (1990) 3737.
7. L. Bai and B.E. Conway, J. Electrochem. Soc., 138 (1991) 2897.
8. R.D. Armstrong and M. Henderson, J. Electroanal. Chem., 39 (1972) 81.

IN-SITU REAL-AREA DETERMINATION IN THE EVALUATION OF POROUS, GAS-EVOLVING ELECTROCATALYSTS BY MEANS OF POTENTIAL RELAXATION AND IMPEDANCE MEASUREMENTS

L. Bai, L. Gao and B.E. Conway
Chemistry Department, University of Ottawa, Ottawa K1N 6N5, Canada

The experimental determination of the real effective surface area of a porous electrode, especially by *in situ* methods, still remains an unsatisfactorily resolved problem. The measured real surface area, or the roughness factor defined as the ratio of real surface area to apparent geometrical area, is usually found to vary depending on the actual method used. For example, the commonly used BET method gives the real surface area accessible to a gas phase and includes an area fraction which may not be wetted by an electrolyte in a real electrode/electrolyte solution system.

The real electrochemically active area of a rough or porous electrode can be calculated from the experimentally determined value of C_{dl} in the overpotential region if the C_{dl} for the corresponding smooth, flat electrode is known or measurable under the same conditions [1].

As may be expected, the major difficulties for C_{dl} measurement in the overpotential region are associated with three problems: (i) the presence of the usually substantial faradaic current; (ii) the involvement of the pseudocapacitance, C_ϕ, corresponding to the adsorption of (a) reaction intermediate(s) and (iii) the influence of the porosity of the electrode on the distributed double-layer capacitance and resistance, related to the internal current-distribution.

In the present studies, the hydrogen evolution reaction (HER) from KOH solution on a bright smooth Pt electrode and a porous, plated Pt one (platinized Pt) have been examined comparatively. It is believed that this system provides the best example for illustrating treatments designed to overcome the above mentioned difficulties in C_{dl} measurements in the overpotential regions, since the kinetics of the HER and its associated H-adsorption pseudocapacitance at a Pt electrode have been well investigated previously [2]. Moreover, the Pt electrode has a unique characteristic that its real electrochemically accessible surface area can be directly measured *in situ* reliably and accurately by means of cyclic-voltammetry from which the monolayer UPD H charge can be precisely determined.

The problem of evaluation of the electrochemically effective area of porous electrocatalyst materials is treated by examination of kinetics of hydrogen evolution from aq. KOH at a plated porous Pt electrode in relation to *in situ* real area determination by means of SEM, cyclic voltammetry (CV), potential relaxation and impedance measurements. With regard to its electrochemical accessibility, the rough or porous electrode surface can be "unfolded" experimentally by increasing the electrolyte conductivity, i.e. simplifying the transmission line model [3] by diminishing the distributed electrolyte resistance.

It is found in the impedance studies that, for the same porous plated Pt electrode, the exponent α_1 associated with double-layer capacitance varies from 0.56 to 1.0 (corresponding to constant phase angle shift 38° to 0° in the standard "RC" circuit) for the HER in 0.5 and 2.0 mol dm^{-3} KOH solutions, respectively. That is α (or the fractal dimension factor, D, derived from α [4]) is not an intrinsic property of a given porous electrode, but strongly depends on the conductivity of electrolyte solution in the pores.

The determined accessible real surface area (C_{dl} values) for the HER at a plated Pt electrode is increased with increasing electrolyte conductivity. The effective roughness factor is about 20 times larger in 4.0 than in 0.1 mol dm^{-3} KOH solutions for the same plated Pt electrode. In the highly conducting KOH solutions (4.0 M KOH), the measured roughness factor for a plated Pt electrode determined by both impedance and potential-decay methods becomes almost the same as that determined by means of the CV method; that is, the porous plated Pt electrode becomes completely "unfolded" with respect to its electrochemical response.

The developed initial potential-decay rate and impedance methods are shown to be capable of giving reasonably reliable and accurate C_{dl} measurements under conditions where a simultaneous significant faradaic current is passing and where an appreciable adsorption pseudocapacitance arises, e.g. due to adsorbed H in the HER at Pt electrodes.

References

1. S. Trasatti and O.A. Fetrii, Pure & Appl. Chem., Vol. 63, No. 5 (1991) 711.
2. B.E. Conway and L. Bai, J. Electroanal. Chem., 198 (1986) 149.
3. R. deLevie, in Advances in Electrochemistry and Electrochemical Engineering, Vol. 6, Ed. P. Delahay, Interscience Publishers, New York (1964).
4. L. Nyikos and T. Pajkossy, Electrochim. Acta, 30 (1985) 1533.

A COMPARATIVE STUDY BY IMPEDANCE SPECTROSCOPY OF DIFFERENTLY TREATED TOMATO CUTICULAR MEMBRANES

J. R. Ramos-Barrado and J. Benavente, Dpto.Física Aplicada.
A. Heredia, Dpto.Bioquímica y Biología Molecular.
Facultad de Ciencias. Universidad de Málaga. 29071 Málaga (Spain).

The objective of our research is to determine the structure of the plant cuticle, which can be considered as the interface between the environment and the vegetal cells, in the plant and to correlate it with the sorption and uptake of selected chemicals. The plant cuticle is a heterogeneous membrane, consisting of a polyester matrix, cutine, and cuticular lipids [1]. The cuticles have a weak ion exchange capacity [2], and this fact is an important characteristic affecting the sorption and transport of water and ions. In this way, we have recently shown that the incorporation of sodium and calcium ions at the cuticular matrix modifies the water penetration by changes in the arrangement in the polymer matrix [3].

Astomatous cuticles from tomato fruits (Lycopersicon esculentum, Mill.) were studied. The native membranes,T[nat], were previously isolated and two samples were treated in order to put the cuticles in the ionic forms (T[Na] and T[Ca]). Impedance spectroscopy technique was used as a tool to determine some characteristic electrical parameters of these membranes in two different forms: i) as a solid phase (dry cuticles); ii) in contact with NaCl solutions (wet cuticles).

RESULTS AND DISCUSSION

The complex impedance for the three dry membranes were measured and the following resistance values were obtained: Rs(nat)=10.2 $10^7(\Omega)$, Rs(Na)=3.8 $10^7(\Omega)$ and Rs(Ca)=4.7 $10^7(\Omega)$. These results show that the resistance values for both treated cuticles are more similar and lower than that corresponding to the native one.

The influence of the exchangeable cation on the electrical response of the tomato cuticle is clearly shown in the imaginary impedance (Z") versus frequency plot drawn in Fig.1. From this picture the different effect of both membrane and electrolyte on Z" values are evidently shown. In Fig.2 the typical curves for the membrane/electrolyte solution system are drawn. The highest circle (circle m), which appears at the lowest frequencies (that means high relaxation time) corresponds to the membrane, and the small circle (circle s) represents the electrolyte and cell geometry contribution to the impedance of the whole system. Similar pictures were found at the other concentrations studied.

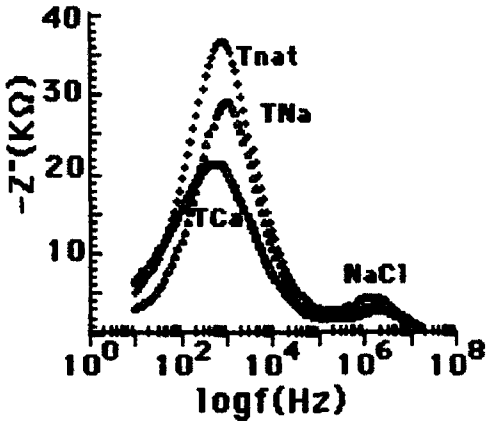

Fig 1. Imaginary impedance (-Z") vs frequency for the membrane/electrolyte solution

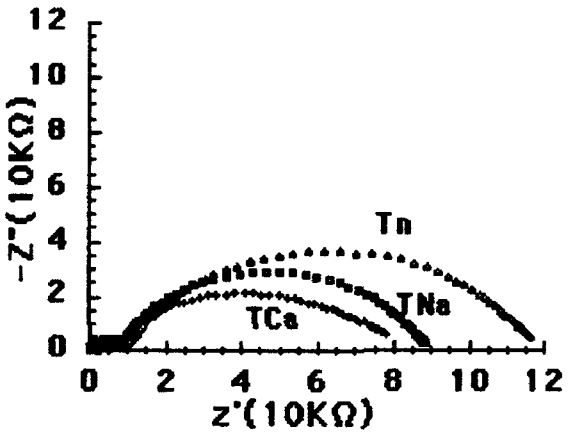

Fig. 2. Complex impedance plot for the membrane/electrolyte solution system

The resistance values determined for both treated membranes are not very different one from the another (about 10%), but they are much lower than those obtained for the native cuticle at the same concentration (about 40%). These results agree with those indicated above for the dry cuticles, and also with those found by X ray diffraction, which show a more open membrane structure as a result of the presence of the exchangeable cations [3]. This fact could be correlated to the more polar parts of the cuticle and with the fractional group located in the phenolic compounds which form a part of the cuticle structure.

REFERENCES

1. P.J. Hollowey, *The Plant Cuticle*, Academic Press, London (1982).
2. A. Heredia and J. Benavente, *Biochim. Biophys. Acta* ,**1062**, 239, (1991).
3. P.Luque, A. Heredia and S. Bruque, SBE91, Madrid (1991)

IMPEDANCE SPECTROSCOPY STUDY WITH $NH_4UO_2PO_4.3H_2O$ (NUP) SELF SUPPORTED MEMBRANES

J.Benavente, J.R.Ramos-Barrado, Departamento de Física Aplicada.
M.Martinez and S.Bruque, Departamento.de Química Inorgánica.
Facultad de Ciencias, Universidad de Málaga, E-29071 Málaga,(SPAIN).

Hydrogen uranyl phosphate, $H_3OUO_2PO_4.3H_2O$ (HUP), and its derivatives are lamellar solids which present intercalation and ion exchange reactions. The HUP is a very well known proton conductor and it is being employed in some microelectronic devices [1]. One of the HUP derivatives, the ammonium uranyl phosphate, $NH_4UO_2PO_4.3H_2O$ (NUP), is studied in this work. It is an insoluble compound ($Ksp = 10^{-6.85}$) and then, it is an optimal material to be used as a current rectifier when it is in contact with two of the generating electrolytes. The propose of this work is the study of the electrical properties of this material as dry and wet membranes.

RESULTS AND DISCUSSION

The experimental points obtained for the NUP dry membrane at different temperatures were fitted to a parallel combination of a constant resistance, R_S, and a (CPE) constant phase element (Q_S). In general, R_S values decrease slightly when the temperature increases, which is due to the partial protonic character of the precipitate, but for the interval $60ºC \leq t \leq 80ºC$ a dramatic change was found, which is attributed to the binder rearangement at these temperatures.

The electrical behavior of the NUP wet membrane, at 25ºC, was also studied. The effect of different ions and electrolyte concentrations is considered. Fig.1 shows the impedance plot for the system NUP-membrane/electrolyte solution, with three different electrolytes, which contain one of the ion forming the NUP precipitate. The total experimental values, for each concentration and electrolyte, were fitted to a circuit which consists of a series association of two parallel RQ elements, corresponding one of them to the NUP membrane and the other one to the electrolyte solution. The effect of both, membrane and electrolyte solution, on the measured impedance is more evident for $UO_2(NO_3)_2$ than for $NH_4H_2PO_4$ solutions, but it hardly appears with H_3PO_4 ones. An explanation of the different behaviour found with the H_3PO_4 solutions can be mainly attributed to the content of HUP phase in the membrane, which present a high proton mobility.

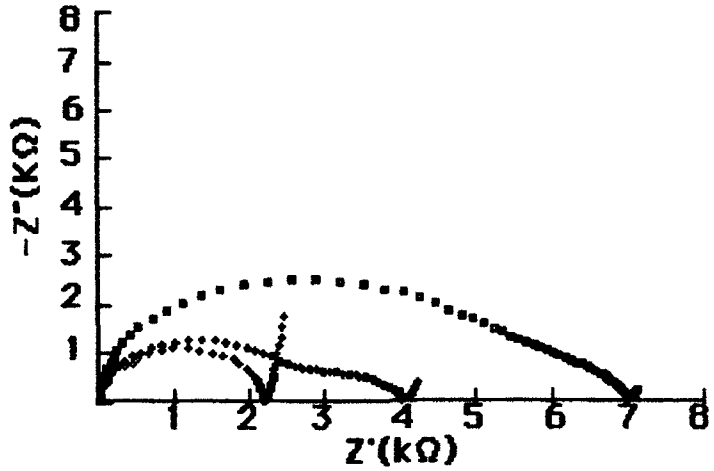

Fig1.Nyquist plot for NUP membrane with different electrolytes
(C=5.10^{-3})$UO_2(NO_3)_2$(°); NH_4PO_4(+); H_3PO_4(•)

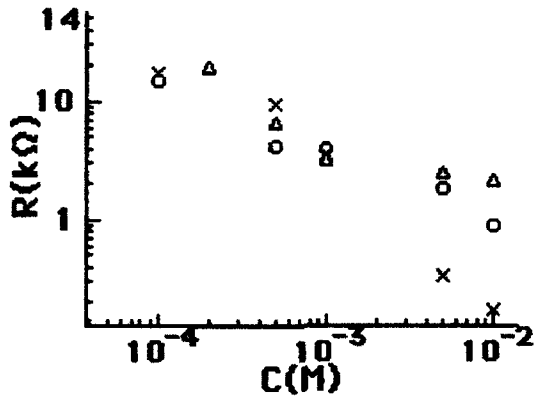

Fig.2 Variation of the resistance with concentration for the different electrolytes
(C=5.10^{-3})$UO_2(NO_3)_2$(°); NH_4PO_4(Δ; H_3PO_4(x)

Variation of R_m with concentration is shown in Fig.2 for the three electrolytes. The decrease of the NUP membrane resistance values when the concentration increases is attributed to the electrolyte invation in the membrane. With respect to the CPE parameters, it is worth noticing that the change of n_m values goes from 0.99 (similar to a capacitor) at low concentrations, to a value more similar to a Warburg impedance at the highest concentration studied.

In short, this paper shows that different electrical parameters for the NUP membrane can be obtained depending on the electrolyte considered. The different behaviuor of the membrane when H_3PO_4 solutions are used, with respect to the other electrolytes, can be due to a different conduction mechanism, which is mainly protonic for H_3PO_4 and ionic for the other electrolytes.

REFERENCES

1. M. Pham-Thi, Rh. Adet and G. Velasco, *Appl. Phys. Lett.* **48**, 1348, (1986).

COMPARISON OF *AC* IMPEDANCE AND CYCLIC VOLTAMMETRY FOR ESTIMATING THE FARADAIC CAPACITANCE OF A REDOX MATERIAL: INFLUENCE OF A STEEP INSULATOR-CONDUCTOR TRANSITION.

P. BERNARD, M. KEDDAM AND H. TAKENOUTI

UPR 15 du CNRS "Physique des Liquides et Electrochimie", Université P. & M. Curie
Tour 22, 4, place Jussieu, 75252 Paris cedex 05, France.

INTRODUCTION

This study concerns $Ni(OH)_2$ electrode used for Ni-Cd battery. The electrode capacitance determined by the charge corresponding to the surface area of voltammogram agrees well with the nominal value determined by a constant discharge current. The electrode impedance measured at the steady state under potential regulation showed a capacitive branch at low frequencies *ie* the blocking electrode behaviour as expected for battery processes. However, the capacitance thus determined is about one tenth's of that evaluated from voltammograms. The aim of this paper is to understand these apparent experimental contradictions.

The impedance measurement showed a steep change of film resistance (R) during the redox transformation [1]. With respect to the discharge percentage (P), we found experimentally the following relationship:

$$R = \frac{R_c}{e} \exp(P - P_c)^{\alpha} + R_0 \qquad (1)$$

where R_c stands for the film resistance in electrolyte (= 1.51 10^{-3} $\Omega.cm^3$), e the film thickness film, P_c the critical discharge state (= 80%), α a constant (= 0.3) and R_0 the resistance at the completely oxidized state.

EXPERIMENTALS

The preparation procedure of $Ni(OH)_2$ film on Ni substrate was briefly written in the reference [1]. The voltammetry as well as EIS measurements were performed with Solartron equipments (EI 1286 and FRA 1254). The mass change due to the redox transformation was determined by a QCM developped in this laboratory and details are given elsewhere [2]. The charge-discharge experiments were performed in 5N KOH aqueous solution at room temperature. To compare the voltammogram data to those of EIS, we registered the current response due to the stepwise voltage change. The mean sweep rate was kept at 2mV/s whereas the voltage step was 10 to 50 mV. The current response was LP filtered at 100Hz then registered by a Digital Audio Tape adapted to DC signal (Biologic DTR 1200).

RESULTS

In the major potential range, the current response agrees well with the impedance data. However, during the anodic sweep, just when the electrode potential becomes more anodic than the peak potential on the voltammograms, a strongly non-linear current response can be seen. At fractions of second, a current plateau can be seen followed by a neat current increase, revealing the maximum, then decreases slowly with an exponential like decay (*cf* Fig 1). This non-linear response can be explained qualitatively by a steep decrease of material resistance: by the anodic current flow, $Ni(OH)_2$ is oxidized and becomes conducting making current flow even easier, then leads to the oxidation of almost of the entire active materials. During the cathodic sweep, such a non linear behaviour can only be seen when the largest potential step (50mV) was apllied. The charge determined by this method is equal to that of voltammogram data under linear potential sweep.

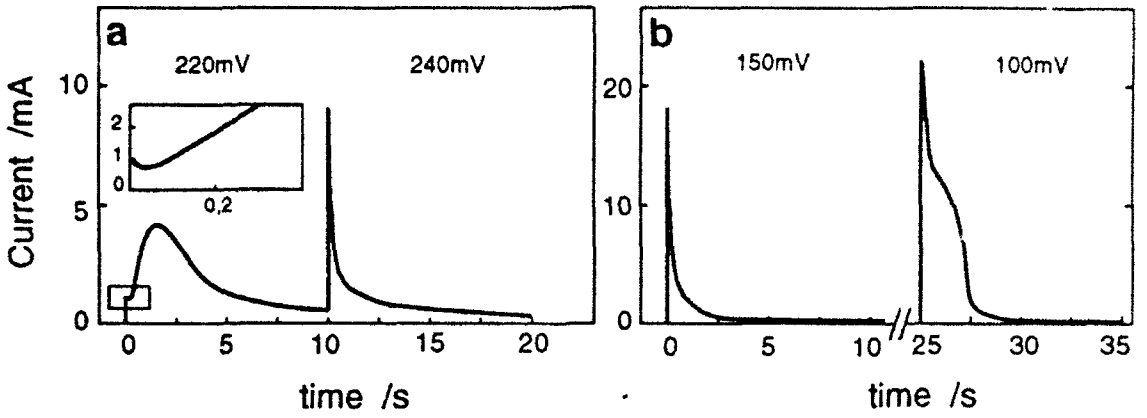

Fig 1. Chronoamperograms of Ni/Ni(OH)2 in 5M KOH:
(a) anodic sweep with 20 mV step. The insert for the short periode current change
(b) cathode sweep with 50mV step. The surface area was 0,2 cm^2

MODELLING

The following hypotheses were made to modelling the electrical behaviour of $Ni(OH)_2$:

- Faraday's law is applied for the transformation of active material, whose total amount is M:

$$I = F\,M\,\frac{d\theta}{dt} \qquad (2)$$

where θ stands for the fraction of electrode material at oxidized state.

- Electrode potential (E) is determined by the Nerst law:

$$E = E_0 + 0.06\,\log\left(\frac{\theta}{1-\theta}\right) \qquad \text{at } 25°C \qquad (3)$$

where E_0 is the standard potential. The elecrode behaviour is therefore considered similar to a monomolecular surface coverage.

- The current flow (I) and applied voltatage (V) are linked to the potential (E) through:

$$V = E + RI \qquad (4)$$

This relationship implicitly imposes that there is an ohmic drop inside the film, *i.e.* no voltage nor current distribution phenomena are taking place.

For the potential sweep experiments the electrode potential V can be expressed by

$$V = V_0 + \nu t \qquad (5)$$

where V_0 stands for the initial sweep potential and ν the sweep rate. Similary, for the potential step of lhe height ΔV, one can write:

$$V = V_0 + \Delta V\,N\,t \qquad (N = 0, 1, 2\,,,,) \qquad (6)$$

Eq 2 is then solved by a digital integration of 4th order Runge-Kutta method with variable increment Δt. We used Eq 1 for R value in Eq 4.

We found a fairly good agreement to experimental data both for the voltage sweep and for the voltage step techniques. The discrepancy observed in the battery capacity between voltammograms and impedance data lies on the fact that this latter are measured only at the steady state.

REFERENCES

(1) P. Bernard, M.Keddam, H. Takenouti, "Impedance sudies of thin films of nickel hydroxide ", This seminor
[2] S.Bourkane, C.Gabrielli, M.Keddam, Electrochim.Acta, 34 (1989) 1081

INVESTIGATION OF ION EXCHANGE AT MIXED CONDUCTOR ELECTRODES BY ELECTROGRAVIMETRIC TRANSMITTANCE.

P. BERNARD, C. GABRIELLI, M. KEDDAM AND H. TAKENOUTI

UPR 15 du CNRS "Physique des Liquides et Electrochimie"
Université P.& M. Curie
Tour 22. 4, place Jussieu, 75252 Paris cedex 05 France.

INTRODUCTION.

Mixed conductor materials in thin films, organic or inorganic, play a major role in many electrochemically related technologies such as devices for energy storage, electrochromic displays, sensors. Charge storage are linked to various physico-chemical phenomena responsible for the flows of electrons and electrolyte species: Red-Ox transfers associated to counter-ions entry, intercalation or insertion...Elucidation of the microscopic transformations implies spectroscopies giving access to molecular and electronic transitions in the material. The kinetics aspects are tentatively investigated by electrochemical response of the electrode and a.c. impedances are intensively applied to this problem. They reveal important features such as the capacitance, reflecting th potential dependence of the charge incorporated in the electrode. However unambiguous models remain out of reach and the situation can be substantially improved by collecting gravimetric information. Frequency resolved measurements of the mass/potential response performed with a EQCM has been associated to electrode impedance for studying the mass exchanges taking place on thin layers of some organic and inorganic materials.

EXPERIMENTAL and DATA PROCESSING.

Electrogravimetric transmittance $\Delta m/\Delta V$ was measured simultaneously to impedance with a Quartz Crystal Microbalance. Frequency resolution was provided by using a frequency/voltage converter. The converted voltage, proportional to the mass response Δm, is supplied to one channel of a Schlumberger 1254 (4-channel FRA) along with potential ΔV and current ΔI. Carefull calibration of the mass channel allows to extend the bandwidth to about 1 kHz.

After computer correction of the ohmic term $R_e\Delta I$ of ΔV and of the double layer current in ΔI the quantities $\Delta m/\Delta E$, $\Delta m/\Delta I$ and $\Delta m/\Delta Q$ are calculated. Parasitic contribution to the quartz response arising from non-gravimetric effects, mainly stresses due to mechanical changes in the layers, have been quantitatively assessed.

Further processing depends on whether the nature of the exchanged species is known or not. The main source of information available is the ratio $\Delta m/\Delta Q = M_w/zF$, where M_w is the molecular weight and z the number of elementary charges exchanged. M_w being known, the partial fluxes of mass associated with every species can be calculated.

RESULTS.

Polyaniline films (PANI): electrochemically deposited by potential cycling of the gold electrode in aniline+HCl. In this case exchanges are due to the contribution of deprotonation and anions entry during anodic oxidation of the polymer. Frequency response of the fluxes of both ions and of their ratio is shown in Fig 1 for PANI oxidation in $HClO_4$.

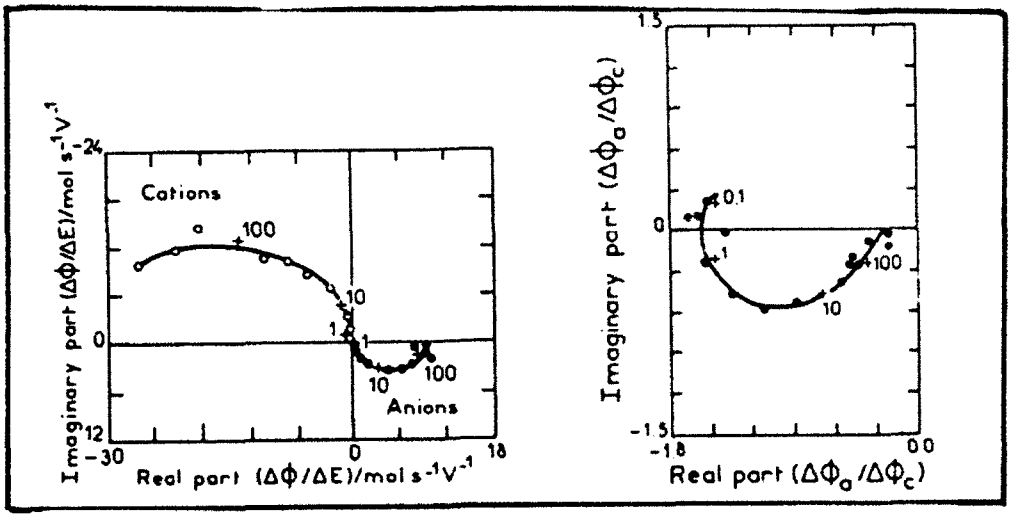

Fig 1: Nyquist plots of fluxes of anions (perchlorates) and cations (H_3O^+) (left) and of their ratio (right) in PANI. $HClO_4$, 0.25 V/SCE.

Comparison of anions and cations fluxes suggests that mass exchange is controlled by both electric field strength and ion size. Potential dependence of these fluxes intensities show a decaying contribution of protons at higher potentials whilst anions flux remains constant.[1]

Tungsten trioxide: evaporated films are submitted to cathodic insertion of Li^+ in PC+Li ClO_4 . As shown in Fig 2 mass/potential transmittance exhibits 2 time constants with a positive real part at high frequencies and a negative real part at low frequencies.(by respecting the IUPAC conventions) $\Delta m/\Delta Q$ transmittance clearly relates the low frequency limit to the insertion of Li^+ (7g/F) and leads one to ascribe a limiting value of about 120 g/F to the high frequency relaxation. A model will be presented interpreting this faster process by the transient desorption-adsorption of ClO_4^- at the surface of WO_3. No experimental thickness dependence of this term is in favour of such an interpretation.

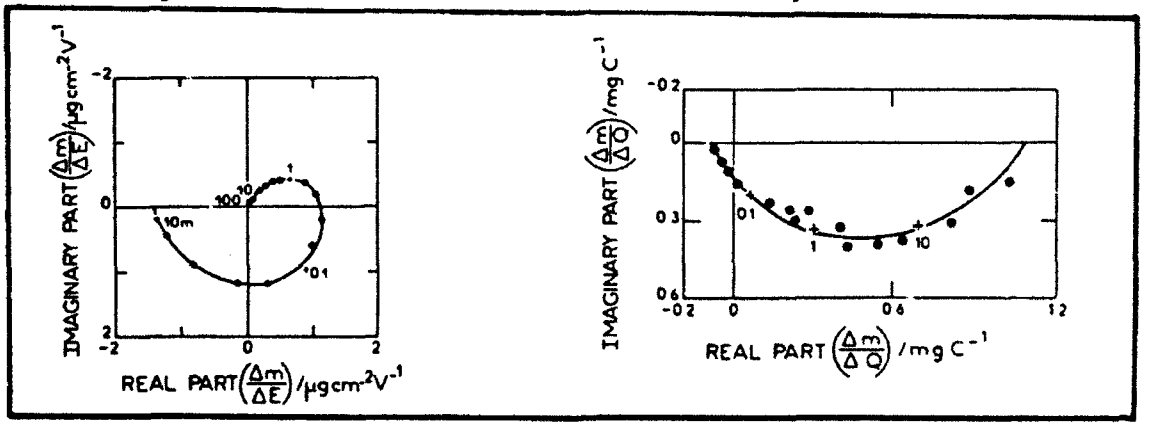

Fig 2: mass/potential (left) and mass/charge (right) transmittances of a WO_3 layer (200nm thick) during Li^+ insertion in PC+$LiClO_4$.

REFERENCES

1. S.CORDOBA-TORRESI, C. GABRIELLI, M. KEDDAM, H. TAKENOUTI, R. TORRESI: J. Electroanal. Chem. 290,269,(1990).

IMPEDANCE STUDIES OF THIN FILMS OF NICKEL HYDROXIDE

P. BERNARD, M. KEDDAM and H TAKENOUTI.

UPR 15 du CNRS "Physique des Liquides et Electrochimie". Université P&M Curie.
Tour 22. 4, place Jussieu, 75252 Paris cedex 05 France.

INTRODUCTION.

Mechanism of charge and of discharge at the positive electrode (Ni) of the Ni-Cd battery are obscured by potential and concentration gradients within the bulk porous electrode material. Separation of kinetics and conduction in the electrode behaviour is of primary importance for designing new electrode technologies and improving the electrode performances by addition of foreign elements. A thorough impedance investigation has been performed of $Ni(OH)_2$ layers, ranging up to a few µm thick, prepared by electrochemical precipitation onto a Ni substrate.

EXPERIMENTS

-Films preparation was done by cathodic deposition from a Ni $(NO_3)_2$ bath (Carpenter method [1]). Incorporation of Co and other elements (Cd, Mg,..) was performed by co-precipitation from nitrates mixtures. Film growth was *in-situ* monitored with a EQCM.

-Impedance measurements on films studied in various concentrations of KOH were carried out following 3 different procedures:
i) conventional, at potentials sampling the whole Red-Ox range of the layer.
ii) under constant discharging currents (regimes between 2C/3 and 6C).
iii) electrical impedance on dry layers sandwiched between the Ni base and a mercury pool.

-Electrogravimetric transmittance, $\Delta m/\Delta E$, was also used as a complementary tool for investigating the mass exchanges between layer and electrolyte[2].

RESULTS and DISCUSSION.

An impedance of the blocking-electrode type is found in the whole range of potential either at equilibrium, as illustrated in Fig 1, or under constant current even though the actual values are dependent on the polarisation mode. Steep transitions take place at the voltammetric peaks. Discharged states exhibit a high frequency capacitive loop which vanishes totally when the layer is switched into the charged states and *vice-versa*

By comparison with the resistance measured by mercury contact it is concluded that this loop arises essentially from the ohmic and the dielectric properties of the reduced phase (ß-$Ni(OH)_2$). "On dry" resistances are by about 3 orders of magnitude greater than electrolytic ones at the same potential thus revealing a high microporosity of the material. Similar conclusions are drawn from the important result that the electrochemical impedance is inversely proportional to the layer thickness (or mass) *i.e.* resulting from a **volumic** contact between the electrolyte and the reacting solid phase.

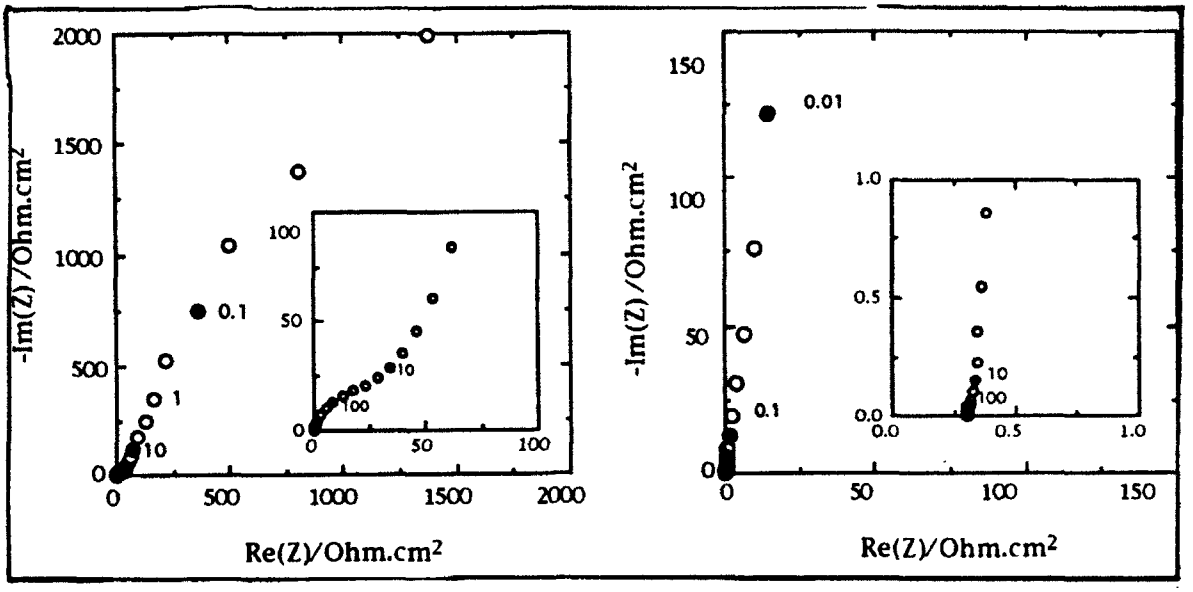

Fig 1: potentiostatic impedances of $Ni(OH)_2$, (0.6 µm thick), in 5M KOH, S=0.2cm². Left: 50mV/ SCE (Discharged state). Right: 280 mV/SCE (Charged state). Inserts are high frequency magnifications.

The low frequency blocking capacitance C_{LF} is related to the charging-discharging Red-Ox process involved in the storage capacity of the electrode. In fact, the C_{LF} behaviour is more complicated than expected from a true reversible Red-Ox transformation.

Integration of the charge stored in C_{LF} between the discharged and the charged potential bounds is only about 10% of the total charge actually computed under the voltammogram. This is quantitatively interpreted by the sharp insulator-conductor transition of the layer material corresponding to the oxidation peak.[2]

Charge dependence of the high frequency capacitance and resistance take place essentially between 80 and 100% of the full discharge.They can be related to the in-depth propagation of the conversion front separating the reduced and the oxidized states.

Addition of Co, co-precipitated with $Ni(OH)_2$, is shown to improve the discharging performances of the electrode by decreasing the resistivity of the reduced phase. This was established by both electrochemical and electrical impedance measurements on mixed-hydroxide layers.

Electrochemistry of thin layers of $Ni(OH)_2$ is substantially simpler than on bulk powdered, pasted or sintered electrode material and give access to more intrisic properties. However at the µm scale its remains seriously influenced by micro-geometric factors.

REFERENCES

1. M.K. CARPENTER, R.S. CONNEL, D.A. CORRIGAN:
Solar Energy Mat. 16, 333, (1987).

2. P. BERNARD, M. KEDDAM, H. TAKENOUTI: This Symposium.

3. P. BERNARD, C. GABRIELLI, M. KEDDAM, H. TAKENOUTI: This Symposium.

ELECTROCHEMICAL EVALUATION OF CORROSION INHIBITORS FOR SOUR GAS AND OIL PRODUCTION AND WATER INJECTION

Nguyen N. Bich
Shell Canada Limited - Waterton Gas Complex

EXTENDED ABSTRACT

The performance of corrosion inhibitors under simulated field conditions including extremely sour and high salinity environments can be evaluated quickly, accurately and economically in the laboratory using electrochemical techniques. Over the past three years, in our test facilities, 73 different batch and continuous injection inhibitors have been evaluated in autoclaves containing solutions of up to 170,000 ppm chloride with up to 2 MPa H_2S and 1.3 MPa CO_2 partial pressures. Over 300 tests have been carried out and nearly 20,000 electrochemical impedance spectroscopy (EIS) plots analyzed.

EIS is a very valuable tool in assessing the performance of a corrosion inhibitor. Different corrosion process components can be identified thanks to the selective frequency response of a paired RC circuit to the applied AC signal. In a sour solution, the frequency where the phase angle is maximized can be estimated by the equation:

$$f \approx \frac{1}{RC}$$

Typical frequency values where a corrosion process component in sour systems can be identified are:

Component	R, ohm.cm²	C, μF/cm²	RC, μs	f, Hz
General dissolution	1000	100	100,000	10
Pitting	100	10	1,000	1,000
Inhibitor Film	10	1	10	100,000
Solution	1	0	0	infinity

Since the frequencies for the phase angle peaks differ by an average of 2 decades, they are usually resolvable in Bode plots. Nyquist plots are often of limited value in process identification.

Polarization resistance, determined from both Linear Polarization (LP) and EIS and correlated to weight losses, level of protection, film persistency, and localized corrosion can be continuously monitored. Behavior patterns for good and poor performers have been consistently observed and characterized according to their RC time constants. Phase angle plots versus frequency for most good performers show a stable peak in the high frequency (HF) region, between 10,000 and 100,000 Hz. Lack of a HF peak for some good performers possibly indicated the formation of either a very thin or conductive film. Poor performance is exhibited by a combination of two or more indicators: instability of the HF peak, shifting of the low-frequency (LF) phase angle peak (below 10 Hz) to a lower frequency, emergence of a mid-frequency (MF) phase angle peak in the 100-1,000 Hz range, and erratic changes in polarization resistance.

Large values of polarization resistance, as measured by LP which might indicate low average corrosion rates often are the results of film breakdown leading to localized corrosion. Other pitfalls of LP technique such as infrequent measurement rates; comparisons of polarization resistances taken of different inhibitors, or for the same inhibitor in different tests, or for the same test at different time are presented. The necessity of correlating electrochemical data to weight loss is also illustrated.

INFLUENCE OF SURFACE ROUGHNESS AND ELECTROLYTE CONCENTRATION ON THE Pt/$HClO_4$ INTERFACE *CPE*

E. D. Bidóia*, L. O. S. Bulhões and R. C. Rocha-Filho

Chemistry Department, Federal University of São Carlos,
C. P. 676, 13560 S. Carlos - SP, Brazil

The impedance of the double-layer region of *polycrystalline Pt/perchloric acid solution* interfaces was measured to determine the influence of electrode surface roughness and solution electrolyte concentration on the exponent n of the constant phase element — *CPE*, as given by the usefull empirical equation (1):

$$Z(\omega) = R + Q(j\omega)^{-n} \qquad (1)$$

where Q is a constant, $j = \sqrt{-1}$, and ω the angular frequency. The value of the exponent n is a measure of how much the electrochemical system deviates from the ideal RC behavior, a consequence from the equivalent circuit elements becoming frequency dependent. Normally, polarized polycrystalline solid electrode/solution interfaces, even under ideal experimental conditions, always present a CPE, its cause being still somewhat controversial (2-5).

All measurements were carried out in the double-layer region. The roughness of the electrode surface was varied by using emery paper, or alumina, of different grades; the electrode roughness factor was determined through the adsorption charge of hydrogen. The different impedance spectra obtained were fitted through least squares linear regression (6) with equation 1 (in the 6 Hz $\leq f \leq$ 10 kHz range).

The impedance data obtained for Pt/$HClO_4$ solution interfaces (for different solution concentrations), polarized at a potential in the double-layer region, showed that the phase angle varies with the concentration of the solution electrolyte only for smaller $HClO_4$ concentrations. As it can be seen in Figure 1, n shows a significant dependence on c only for $HClO_4$ concentrations under 0.5 mol/L, that is, only for the more diluted solutions. This behavior is probably due to the variation of the conductivity of the solution as well as to the thickness of the diffuse part of the double layer. It should be noted that the value of n does not reach unity at high $HClO_4$ concentrations due to other concomitant factors, such as the roughness of the electrode surface.

The Pt/$HClO_4$ interface was chosen for the study here reported because it is possible to determine the values of the surface roughness factor (δ) and n, in the same experimental conditions. Thus, in experiments consisting of cyclic voltammetry followed by impedance spectroscopy, one can determine the relationship between δ and n. A plot of the values of n obtained from impedance spectra for a polycrystalline platinum electrode subjected to different degrees of polishing, using abrasives of different grades, in 0.5 mol/L $HClO_4$, is shown in Fig. 2 as a function of δ. The asymptotic dependence of n on δ clearly shows that the electrode surface roughness has a marked effect on the CPE. Furthermore, a plot of n *vs.* $1/\delta$ displays a linear relationship, allowing the determination of n when δ tends to infinite, that is, 0.84. Assuming that the linear relationship between n and δ still holds for $\delta \rightarrow \infty$, for $HClO_4$ concentrations $\geq$ 0.5 mol/L, the minimum value of the constant phase angle (ϕ) for aqueous systems presenting ideally polarized interfaces would be

---

* Permanent address: Department of Biochemistry and Microbiology, IB - UNESP, 13500 Rio Claro -SP, Brazil

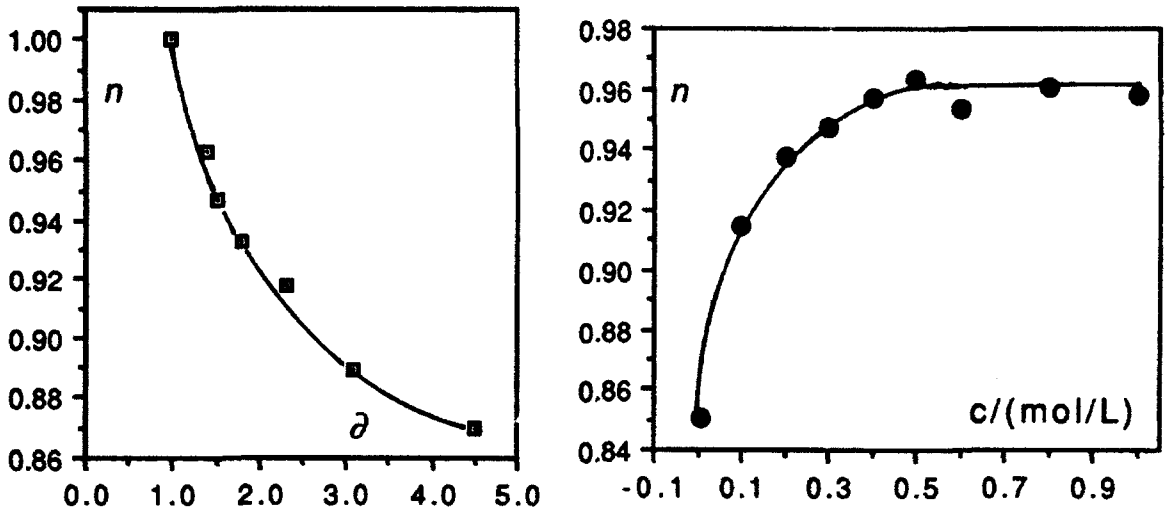

FIGURE 1 – CPE exponent n for Pt/$HClO_4$ as a function of the concentration of the solution electrolyte. $A_{effective} = 0.0030\ cm^2$; $T = 293$ K; $E_a = 0.470$ V (*vs.* HESS).

FIGURE 2 – CPE exponent n as a function of the roughness factor, δ, of the electrode surface for Pt/0.5 mol/L $HClO_4$. $A_g = 0.0020\ cm^2$; $T = 300$ K; (●) experimental points and (□) theoretical point for n and δ equal to 1.

approximately 76°. This result, however, differs from the limit value, $\phi = 45°$, theoretically predicted by De Levie for an ideal porous electrode (3). Two conflicting hypothetical reasons may be proposed to explain this discrepancy:

a) The extrapolation of the value of n for $1/\delta$ tending to zero may not be representative for the behavior of the system, since the maximum value for δ obtained in this work was approximately 6. In another words, for a broader range of values for δ, using additional rougher or more porous electrodes, the relationship between n and $1/\delta$ would deviate from linearity or even have a different slope.

b) The quantitative relationship between n and $1/\delta$ here obtained may represent a general behavior, since impedance measurements for porous Pt electrodes, using solid solutions, carried out by Bauerle (7), led to minimum values of the constant phase angle equal to 72.3°, that is, quite near the limit here obtained for platinum in aqueous $HClO_4$.

Finally, once again using the linear relationship between n and $1/\delta$, using Mandelbrot's equation, it was possible to find a logarithmic relationship between the fractal dimension of the electrode and the exponent n. This relationship contrasts with the linear ones predicted by several models that relate fractal geometry and the CPE, and indicates that the matter of how n depends on the fractal nature of electrode is still open to further investigations.

ACKNOWLEDGEMENTS: The authors thank CNPq, CAPES, FAPESP and FUNDUNESP for the financial support provided.

1. G. J. Brug, A. L. G. Van Den Eeden, M. Sluyters-Rehbach and J. H. Sluyters, *J. Electroanal. Chem.* **176**, 275 (1984).
2. W. Schelder, *J. Phys. Chem.* **79**, 127 (1975).
3. R. De Levie, *Electrochim. Acta.* **10**, 113 (1965).
4. J. B. Bates, Y. T. Chu and W. T. Stribling, *Phys. Rev. Lett.* **60**, 627 (1988).
5. A. Le Mehaute and G. Crepy, *Solid State Ionics* **9&10**, 17 (1983).
6. B. A. Boukamp, *Solid State Ionics* **20**, 31 (1986).
7. J. E. Bauerle, *J. Phys. Chem. Solids* **30**, 2657 (1969).

ELECTROGRAVIMETRIC TRANSFER FUNCTION INVESTIGATION OF THE OXIDE FORMATION PROCESSES ON GOLD IN ACIDIC MEDIUM

S. BOURKANE, C. GABRIELLI, M. KEDDAM

UPR15 du CNRS, Physique des Liquides et Electrochimie,
Université P. et M. Curie, 4 place Jussieu, 75252 Paris Cedex 05 - FRANCE

INTRODUCTION

Investigations on gold oxidation in acidic electrolyte published in the literature were carried out in various media by using cyclic voltammetry. This technique has shown that gold oxidation in aqueous medium proceeds in several steps which lead to an oxide layer obtained through the successive adsorption of OH^- ions coming from the water contained in the electrolytic medium. Once formed, this oxide film isolated the surface and the electrode becomes practically a blocking interface.

In this paper, a model based on a three-step reaction mechanism such as

$$M \rightleftarrows M^+ + e$$

$$M^+ \rightleftarrows M^{2+} + e$$

$$M^{2+} \rightleftarrows M^{3+} + e$$

where M represents the oxidized gold electrode, is analysed by simulating the use of various techniques : namely cyclic voltammetry, electrochemical impedance and electrogravimetric transfer function.

By using the laws of the heterogeneous kinetics, the evolution equations of the surface coverages of the adsorbed reaction intermediates M^+, M^{2+} and M^{3+} and the faradaic current can be obtained. In addition to classical approaches, a new investigation technique based on the use of a quartz microbalance is proposed here. The plots of the voltamassograms and of the electrogravimetric transfer function are obtained.

CYCLIC VOLTAMMETRY

Here, the potential is assumed to slowly change with time in a linear manner. The concomitant changes of the surface coverages and of the faradaic current (voltammograms) are numerically calculated and compared with experiments in various experimental conditions.

ELECTROCHEMICAL IMPEDANCE

After linearization of the evolution equations and of the faradaic current, the electrochemical impedance is calculated. The impedances were measured at various potentials and the experimental results were compared with theory. The components of the equivalent circuits are plotted versus the potential.

ELECTROGRAVIMETRIC TRANSFER FUNCTION

The plots of the mass changes for a sweeping potential is called voltamassograms. The ratio between the response in mass to a potential sine wave perturbation is the electrogravimetric transfer function. These quantities are theoretically derived from the model and compared to the experimental results.

DISCUSSION

The dynamic relationships between current and potential considered here, either the voltammogram or the electrochemical impedances confirm the hypothesis of a three-steps reaction mechanism to explain gold oxidation in sulfuric medium.

Usually, the use of a quartz crystal microbalance in steady-state regime gives information on the total mass gain or loss of the electrode without any distinction or identification of the species. The use of the quartz crystal microbalance in sinusoidal regime allows the response of the mass to a potential perturbation to be analysed. The transfer function between mass and potential, which can be measured in these conditions, should give information on the atomic mass of the adsorbed intermediate species of a multi-steps reaction.

In this study, the new transfer function allows the results obtained from the electrochemical impedance to be confirmed. However, if the kinetics parameters (b_i, K_{io}) can be estimated from a parameter identification procedure by means of a fitting on the experimental impedances, the chemical data are out of range. The electrogravimetric transfer function allows the atomic weight of the adsorbed reaction intermediates and of the final oxide to be evaluated. Therefore, it brings further informations to the measured voltamassogram which leads only to the mass of the final oxide.

REFERENCES

[1] C.M. FERRIO, A.J. CLANDRA, A.J. ARVIA, J. Electroanal. Chem., 50 (1974) 403

[2] A. HAMELIN, P.D. DECHY, C.R. Acad. Sci. Paris, 33 (1971) 276

[3] S. BOURKANE, Thesis, Paris (1989)

[4] S. BOURKANE, C. GABRIELLI, M. KEDDAM, Electrochim. Acta, 34 (1989) 1081

KINETIC MODELS OD PASSIVATION OF METALS BASED ON AC IMPEDANCE MEASUREMENTS - I. THE ANODIC BEHAVIOUR OF BI-SB ALLOYS IN H_2SO_4 SOLUTIONS

M. BOJINOV* and I. KANAZIRSKI**
*Central Laboratory Of Electrochemical Power Sources, Bulgarian Academy Of Sciences, 1113 Sofia, BULGARIA
** Department of Physical Chemistry, Sofia University Of Technology, 1156 Sofia, BULGARIA

INTRODUCTION

In concentrated H_2SO_4 solutions, the impedance of the passivation of Sb[1] is very much similar to the one obtained during investigations of the anodic behaviour of metals in concentrated acid solutions (used in electropolishing, anodic brightening or battery operation) [2-5]. The purpose of the present investigation is to give a complete picture of the impedance behaviour of Sb-Bi alloys in the passivation range in 4,5 M H_2SO_4.

RESULTS

The polarization curves for the alloys present a peculiar combination of the curves obtained for the pure metals. For the Sb-40% Bi and Sb-20% Bi alloys, three distinct peaks are observed, i.e. the combination between the Sb and Bi polarization curves is nearly an algebraic one. Summarizing the polarization results, a suggestion arises that the passivation process of the alloys appears quite intricate.

During oxidation at potentials equal or more anodic than -0,3 V, a stationary current density is reached which is no longer dependent on the potential. An approximately linear decrease of the stationary current density with the increase of the Sb content is observed.

Basically three types of impedance spectra can be distinguished for all the alloys. For the potential range -0,4/-0,25 V, in addition to the high-frequency loop ascribed to charge transfer , a pseudo-inductive loop is observed. This fact is an indication that in this potential region, one stable intermediate is detected. At potentials close to the second anodic current maximum the inductive loop is replaced by a new low-frequency semicircle including a negative resistance. At the low frequency end the spectrum circles the origin through quadrants III and IV. At potentials equal to, or more anodic than -0,1 V, a further low-frequency loop appears including a negative resistance.

The resistance of the high-frequency loop increases linearly with the potential. Following Keddam *et al.* [6], the equation of the high-field assisted film growth can be used to evaluate the field intensity. The obtained values for the field intensity lay in the range $1,4\nu2,0.10^6$ $V.cm^{-1}$ i.e. are close to the typical values for valve metals. The charge transfer resistance at the metal/film boundary do not present any dependence on the potential. This observation

can be tentatively explained suggesting that the main part of the voltage drop is located within the barrier film. The parameters associated to the reactions of activation/passivation at the film/solution interface either do not change with the potential in any logical way. It can be suggested that the local potential at the layer/electrolyte boundary is also negligible in comparison with the voltage drop within the barrier film.

DISCUSSION

The passivation process of the Sb-Bi alloys proceeds via two consecutive stages depending on the anodic potential. In the first potential region, located between -0,40 and -0,25 V, a very thin and highly conductive gel-like layer is assumed to be formed by a dissolution/precipitation mechanism. We shall denote this layer as *conductive layer* (CL). At potentials greater than or equal to -0,25 V a new, hydroxide sublayer is formed. We shall denote the latter as the *insulator layer* (IL). A simplified scheme of the processes is presented:

$Me \Longrightarrow Me(III)_{IL} + V_O^{2+}{}_{Me/IL} + e^-(Me)$ (charge transfer)

$V_O^{2+}{}_{Me/IL} \Longrightarrow V_O^{2+}{}_{IL/CL}$ (migration)

$Me(III)_{IL} + HSO_4^-{}_{aq} + H_2O \Longrightarrow MeOHSO_4 + H^+$ (dissolution)

$OH^-{}_{aq} + V_O^{2+}{}_{IL/CL} \Longrightarrow O_{IL} + H^+$ (film formation)

According to this scheme, at least four time constants have to contribute to the overall impedance response. This fact is in agreement with the experimental results obtained. The time constant detected at highest frequencies is associated with the migration through the barrier film. The capacitive time constant observed at medium frequencies can be ascribed to the charge transfer at the metal/IL boundary. The complex behaviour at low frequencies is physically related to the competitive adsorption of HSO_4^- and OH^- at the IL/CL boundary, the former resulting in a barrier film dissolution and the latter causing film formation.

REFERENCES

1. M. Bojinov and D. Pavlov, *J. Electroanal. Chem.* (submitted)
2. I. Epelboin, Proceedings of "Surface 66", Foster - Verlag, Zurich, 1966, p.161.
3 M. Keddam, Phd Thesis, Paris, 1968, p. 101.
4. S.H. Glarum, J.H. Marshall, *J. Electrochem. Soc.* 132 (1985)2878.
5. C. Clerc and D. Landolt, *Electrochim. Acta* 33(1988)859.
6. M. Keddam, J.-F. Lizee, C. Pallotta and H. Takenouti, *J. Electrochem. Soc.* 131(1984)2016.

ELECTROCHEMICAL IMPEDANCE SPECTROSCOPY OF ELECTROCOATED ALUMINUM FOOD CANS

F.S. Boyard, T.D. Burleigh, and A.T. Smith
Alcoa Technical Center, 100 Technical Drive, Alcoa Center, PA, 15069 USA

Current test methods for evaluating the corrosion resistance of coated aluminum food cans have various shortcomings. The two-year pack-test, which is the industry standard, requires a long time for results and the rating system is subjective because it relies on visual examination. Other methods accelerate corrosion by changing the exposure conditions and are therefore no longer application/product specific. Electrochemical impedance spectroscopy (EIS), however, can provide more quantitative information for evaluating pack test performance and can also be used to predict long-term performance.

We have used EIS to evaluate the corrosion performance of aluminum easy-open end food cans coated with two different proprietary coating formulations, Formula H and Formula P. Cans packed with eight different food products were tested "in situ." Three methods were used to reduce the EIS data to numerical performance indicators:

1.) low frequency (0.04 Hz) impedance [~coating resistance (R_{ct})]
2.) break-point frequency (f_{45})
3.) % Ideal

All three indicators reflect the extent of corrosion and/or coating degradation. The three methods of data reduction are illustrated in Figure 1. The first method assumes a nested, simplified Randles equivalent circuit which has been used extensively in the evaluation of organic coatings on steel.[1-5]. It focuses on the low frequency impedance (in our case log /Z/ at 0.04 Hz) which is approximately equal to the charge transfer resistance (R_{ct}). The second method also implicitly assumes the equivalent circuit but focuses on the breakpoint frequency, f_{bp}, or the frequency at which the phase angle (Θ) is 45°. The breakpoint frequency has been shown, under restricted conditions, to be proportional to the delaminated area of degrading coated steels.[2-6] The third method, % Ideal, is a novel method for reducing EIS data to a single numerical performance indicator. The % Ideal is the ratio of the area under the Bode magnitude curve of the actual data to the area under an ideal (purely capacitive) curve. The advantage of this method is that it incorporates EIS data from the entire spectrum whereas the other two methods use only one data point.

Some differences between the Formula H and Formula P coatings were apparent, but they were food product dependent . These differences are illustrated in Figure 2 using the low frequency impedance data (log /Z/ at 0.04 Hz). Neither Formula H nor Formula P was superior across the board. Formula P performed significantly better than Formula H in the tomato sauce and slightly better in the sauerkraut. Formula H perfomed significantly better in the three bean salad and slightly better in pet food and chicken noodle soup. There is no significant difference between the performance of the two coating formulations in the acidified onions, pasta and sauce, and green beans. The impedance data also indicates the same trends as the standard visual ratings.

All three numerical perfomance indicators were in agreement with all of the above reported differences in coating performance. The low frequency impedance (log /Z/ at 0.04 Hz) is the easiest to determine. The breakpoint frequency, f_{bp} (Θ=45°), in some cases, is proportional to the delaminated or defective area but it is not always accurately obtainable. The % Ideal is relatively easy to calculate and it includes information from the entire range of frequencies.

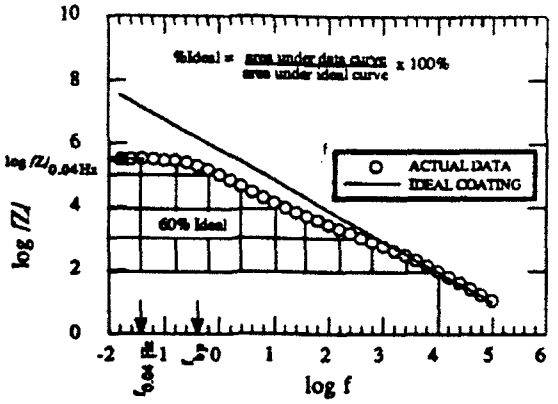

Figure 1. Three methods of reducing EIS data to single numerical indicators; 1. log /Z/ at 0.04 Hz, 2. breakpoint frequency (f_{bp}), and 3. % Ideal using integration limits of log f = -2 to 4 and log /Z/(min) = 2.

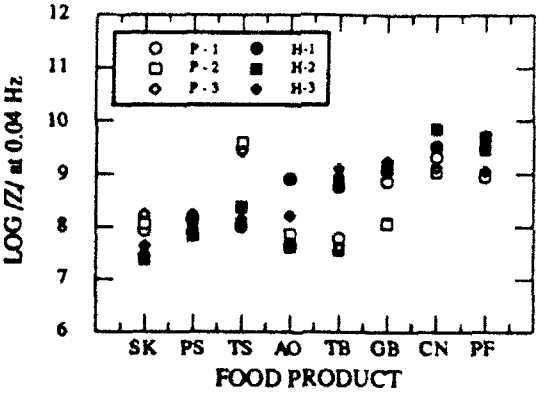

Figure 2. Low frequency impedance (log $/Z/_{0.04\ Hz}$) for Formula H and Formula P in all eight food products; sauerkraut (SK), pasta and sauce (PS), tomato sauce (TS), acidified onions (AO), three bean salad (TB), green beans (GB), chicken noodle soup (CN), and pet food (PF).

REFERENCES

1. W.S. Tait, "Use of Electrochemical Impedance to Evaluate Organic Coatings on Aerosol Containers", in Corrosion Protection by Organic Coatings, ECS Procs. Vol. 87-2, edited by M.W. Kendig and H. Leidheiser, Jr., The Electrochemical Society, Inc., Pennington, NJ (1987) pp. 229.

2. J.R. Scully, "Electrochemical Impedance of Organic Coated Steel: Correlation of Impedance Parameters witth Long-term Coating Deterioration," Journal of Electrochem. Soc., Vol. 136, No.4, (April 1989) pp. 979-990.

3. J.N. Murray and P.J. Moran, "An EIS Study of the Corrosion Behavior of Polyethylene Coating Holidays in Natural Soil Conditions," Corrosion, Vol. 45, No. 11, (Nov. 1989) pp. 885-895.

4. H.P. Hack and J.R. Scully, "Defect Area Determination of Organic Coated Steels in Seawater Using the Breakpoint Frequency Method," Journal of Electrochem. Soc.,Vol 138, No. 1, (Jan. 1991) pp. 33-40.

5. J.N. Murray and H.P. Hack, "Testing Organic Architectural Coatings in ASTM Synthetic Seawater Immersion Conditions Using EIS," Corrosion 91, paper # 131, NACE Meeting, Cincinnati Covention Center. Cincinnati, Ohio (Mar. 11-15, 1991).

6. S. Haruyama, M. Asari, and T. Tsuru, "Impedance Characteristics During Degradation of Coated Steel," in Corrosion Protection by Organic Coatings, ECS Procs. Vol. 87-2, M.W. Kendig and H. Leidheiser, Jr. Editors, Pennington, NJ, (1987) pp. 197-207.

INHIBITION OF ALUMINIUM CORROSION IN CHLORIDE MEDIA

C.M.A. Brett, I.A.R. Gomes, J.P.S. Martins

Departamento de Química, Universidade de Coimbra, 3049 Coimbra Codex, Portugal

Studies of aluminium corrosion in chloride media have been carried out under a variety of experimental conditions in order to understand the effect of chloride ion on the protective oxide film (1) and thence how to prevent pitting corrosion.

In this work the inhibition of the corrosion of aluminium in aqueous neutral chloride solution of constant ionic strength by chromate and nitrite ions has been investigated using electrochemical impedance spectroscopy. Results have been compared to those obtained in the absence of inhibitor and/or absence of chloride ion.

Experiments were performed on pure aluminium (5N) disc electrodes of area 0.2cm^2, using Pt gauze counter and SCE reference electrodes. Solutions contained up to 0.1M potassium chloride, with and without one of the two inhibitors in up to equimolar concentration, the ionic strength being made up to 1.2 mol dm^{-3} with potassium sulphate (the equivalent of 0.4M K_2SO_4 electrolyte) besides 0.4M K_2SO_4 electrolyte alone. The pH was adjusted to be around 7.0. Data were recorded using a Solartron 1250 Frequency Response Analyser, with 5mV rms perturbation, coupled to the electrochemical cell via a Solartron 1286 Electrochemical Interface.

Examples of the impedance spectra, positive of the chloride pitting potential at -0.6V vs. SCE, are shown in Fig.1. The effect of chloride-induced corrosion on the impedance values is clear, as it is from cyclic voltammetry and potential step techniques. These inhibitors are effective in reducing the higher currents obtained with chloride alone to values close to those in its absence. The form of the impedance spectra in the presence of inhibitor alone and inhibitor plus chloride are similar, for both chromate and nitrite ions. However, the mechanism of action is different. Whereas chromate spectra show clear evidence of a redox process, the nitrite spectra suggest adsorption on the electrode surface and inhibition of the surface reaction of chloride.

From the high frequency semicircles, considered as a parallel RC combination, the following deductions can be made:

- there is a decrease in R with more positive applied potential, except for the system inhibitor/K_2SO_4, where it remains approximately constant;
- R decreases significantly in the presence of chloride, but this effect is mitigated by the inhibitor;
- below the pitting potential, the values of C increase in the presence of chloride, whereas above the pitting potential this does not occur, and the higher currents oscillate in value leading to less reproducible spectra.

The low frequency inductive feature, associated with relaxation processes in the oxide film, disappears with inhibitor.

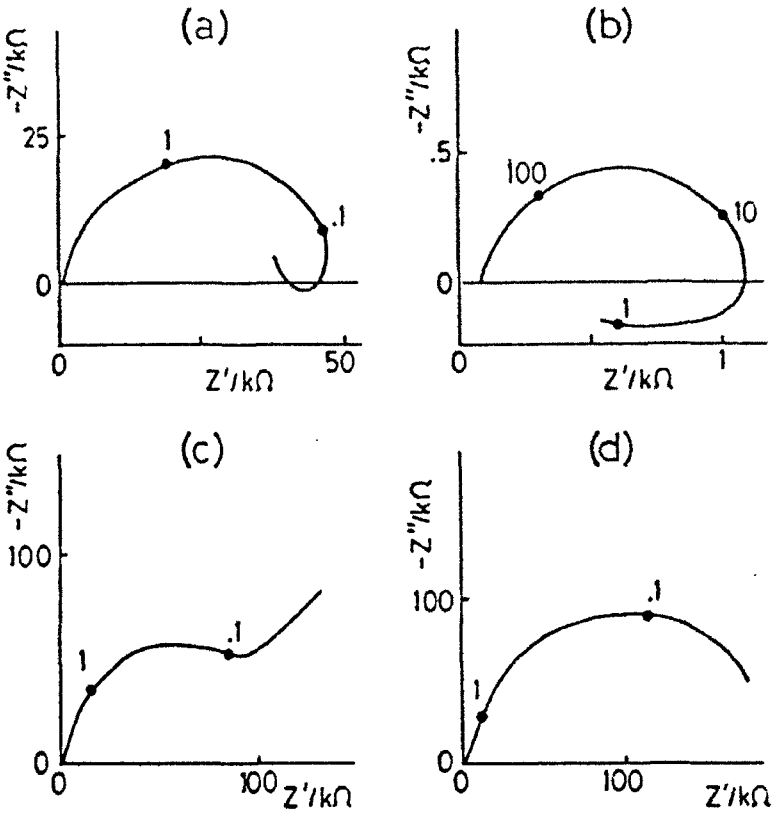

Fig.1 Impedance spectra in the complex plane of Al in:
(a) 0.40M K_2SO_4;
(b) 0.10M KCl + 0.36M K_2SO_4;
(c) 0.10M KCl + 0.10M K_2CrO_4 + 0.27M K_2SO_4;
(d) 0.10M KCl + 0.10M $NaNO_2$ + 0.33M K_2SO_4;
at -0.6V vs. SCE. Frequencies shown in Hz.

Analysis of the full impedance spectra, at different applied potentials, together with results from other types of experiment, enables interpretation in terms of adsorption and elucidation of the mechanism of inhibitor action. Nitrite is shown to be a more effective inhibitor than chromate anion under these experimental conditions, as corroborated by results from other electrochemical techniques.

Reference

1. See C.M.A. Brett, *Corrosion Sci.*, 1992, **33**, 203 and references therein.

THE EFFECT OF COATING THICKNESS ON CORROSION BEHAVIOR OF ION PLATED FILMS

Richard Brown, and Mohd N. Alias

Corrosion Group, Chemical Engineering Dept.
University of Rhode Island,
Crawford Hall, Kingston, RI 02881.

Previous study on the effect of cathodic ion plating on 52100 and 304 stainless steel in 0.5N NaCl solution indicated an inherently protective passive film of ZrN and poor protection by TiN for 5 μm thickness, even with excess Ti ions from ion implantation (1). A further study was conducted in similar environment utilizing cyclic polarization, linear polarization and ac impedance techniques to investigate the effect of multilayers of TiN/Ti/TiN and ZrN/Zr/ZrN coatings and single layers of TiN and ZrN of different thicknesses on corrosion behavior of 304 stainless steel.

Impedance behavior for a perfectly layered single and multilayer coatings on steel is modelled by a solution resistance in series with a parallel circuit of a charge transfer resistance and a constant phase element (CPE) due to the effect of heterogeneity within the depth and in lateral direction of the film (2). For coating with defects, a transmission-line type model simulates the impedance behavior; this consists of two R-CPE parallel subcircuits in series with solution resistance. Changes in behavior at frequencies less than 0.1 Hz with time is suggested as contributed to changes in the surface film.

Calculated charge transfer resistance (R_t), and double layer capacitance (C_{dl}) from the constant phase element shows significant differences between TiN and ZrN coated steels, see figures 1 and 2. In general, ZrN coated steel always has higher Rt and lower Cdl than TiN coated steel. Lower capacitance suggesting of a thicker surface film or a film of a higher dielectric constant. The mechanism to explain these differences has not yet determined, however studies from cyclic polarization shows different ranges and values for passive film formation currents. These could be contributing to different type of surface films on both TiN and ZrN coated steels. Similar relationship is found for the multilayer coatings; higher R_t and lower C_{dl} for ZrN/Zr/ZrN than TiN/Ti/TiN.

References:

1. L. van Leaven, M. N. Alias, and R. Brown, "Corrosion Behavior of Ion Plated and Implanted Films", accepted for publications, Journal of Surface and Coatings Technology, 1992

2. J. A. Bardwell, and M. C. H. McKubre, "AC Impedance Spectroscopy of the Anodic Film on Zirconium in Neutral Solution", Electrochimica Acta, v36 (1991), p.647

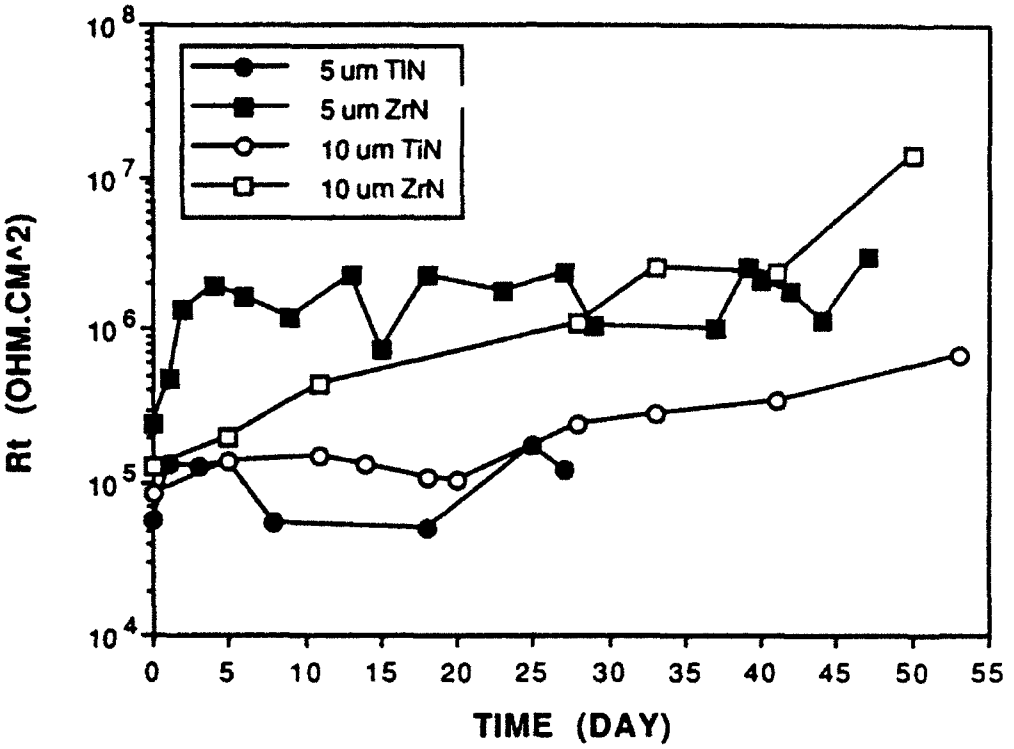

Figure 1. R_t vs time for different coatings on 304 SS exposed to 0.5N NaCl

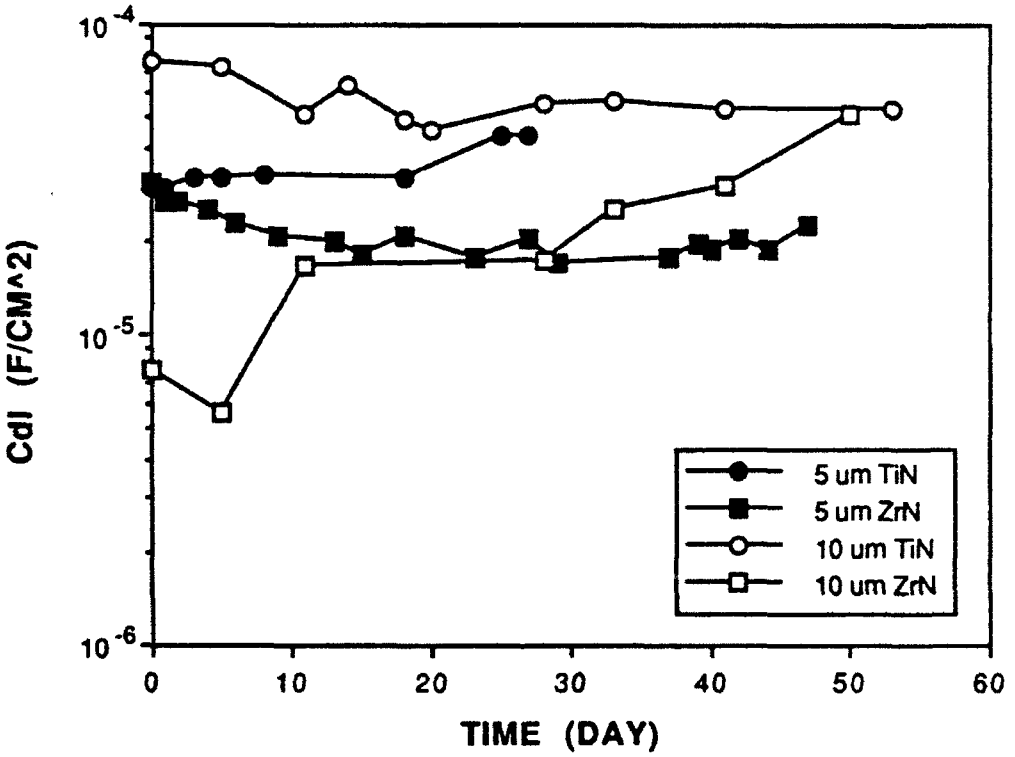

Figure 2. C_{dl} vs time for coatings on 304 SS exposed to 0.5N NaCl

CURRENT-TIME RESPONSES AND IMPEDANCES OF MODEL THIN LAYER AND MEMBRANE CELLS WITH STEADY STATE CURRENT

Richard P. Buck and Tal M. Nahir
Department of Chemistry, University of North Carolina
Chapel Hill, N. C. 27599-3290, USA

Impedance data, e.g. system responses, from perturbing small amplitude applied sinusoid signals of near dc to high kilohertz frequencies, give chemical significance indirectly. It is possible to interpret bulk transport processes, surface kinetic effects, diffusion phenomena, and dependencies on the type of contacts: symmetric ion contact, symmetric metal contact or asymmetric metal-ion interfaces, and cell design: even (battery or sensor) and odd numbered (constrained junction or immiscible liquid) interfaces in a system [1-2]. These analyses cover the chemical origins, locations and meanings of the lumped and distributed resistances, capacitances and transmission lines that are introduced in analog interpretations of the impedance data. Selected cases have been analyzed or reviewed [3-6]

Examples covering simple ohmic, simple diffusive behavior, complex behavior with surface interfacial kinetics or surface resistances, and with finite (nonblocking) or infinite (blocking) dc impedance, systems with Donnan Failure and negative resistances and capacitances were illustrated at the First Congress [2].

Recently, we have studied, in detail, one of the four classes presented previously, e.g. those systems with blocked, but concentration-polarizable sites, and/or concentration-polarizable permeable charge carriers. Theses are systems identified by S-shape, steady-state current-voltage curves characterized by limiting dc currents [7]. They are symmetric thin-layer electrode cell model systems without redox ions and they are closely related to membrane systems.

The cases identified for study, because of their practical importance are: CASE I - $R_{ac} = 0$ High Inert Supporting Electrolyte Thin Layer Cells
CASE II - R_{ac} Constant, Fixed-Site Membranes With Neutral Carriers
CASE III - R Variable In Space And Time - Single Salt Cells And Liquid Ion Exchanger Membranes With No Supporting Electrolyte.

This paper focusses mainly on the analysis of *resistive* system responses for large dc applied voltage (applied voltages greater than RT/F) [7,8]. Only a single z-z salt with permeable cation and blocked anion is considered, and non-Faradaic processes, e.g. double layer charging, are ignored. Items discussed include: 1) concentration profiles in transient and steady state domains; 2) transient I-t responses showing modified-Cottrell behavior; 3) steady state I-V curves and voltage (or current)-dependent resistances; 4) relations of tangent resistances at zero current and at large dc currents, with the small amplitude impedance response quantities; differential vs integral resistances, and steady state resistivity distribution within concentration polarized cells.

Key results include for the unsupported electrolyte (membrane) systems with reversible interfacial processes include the diffusional impedance

$$Z(s) = (R_{dc} - R_{ac})(\Delta VzF/4RT)\coth(\Delta VzF/4RT)\tanh[(s\tau)^{1/2}]/(s\tau)^{1/2} + R_{ac} \quad (1)$$

with $s = j\omega$; $R_{dc(\Delta V=0)} = (4RT/z_iF)/I_L'$ and $I'_L = 2z_iFAD_iC^o/d$ (2a,b,c)

and $\tau = d^2/D = (\text{thickness})^2/4D$; $I_{dc} = -I_L'\tanh[z_iF(\Delta V)/4RT]$ (3,4)

I'_L is the limiting current; z, F, and RT have the usual electrochemical meanings. R subscripted is a resistance. The time constant is expressed in eq. 3 and the I-V curve in eq. 4, so that the explicit dependence of Z on I_L' can be expressed. In supported electrolytes the factor 4 in eqs. 1, 2b and 4 is replaced by 2. The impedance functions intersect the real axis at finite values for both zero and high frequencies as recently pointed out [9]. The high frequency "bulk" semicircle is found by an appropriate, current-perturbed double layer "geometric" capacitance with the steady, perturbed resistance found from

$$R_{dc}(\Delta V \text{ or } I) = \int_{-d}^{d} \frac{RT dx}{(zF)^2 A D_M C(x)} = R_{dc(\Delta V=0)} (I_L'/2I) \ln \frac{[1-I/I_L']}{[1+I/I_L']} \quad (5)$$

and the diffusion-migration impedance follows from linearizing the very non-linear expression

$$Z(s) = \frac{RT}{\Delta IF} \ln \frac{1 - \frac{\Delta I}{I_L'} \tanh[(s\tau)^{1/2}]/(s\tau)^{1/2}(1 - I/I_L')}{1 + \frac{\Delta I}{I_L'} \tanh[(s\tau)^{1/2}]/(s\tau)^{1/2}(1 + I/I_L')} \quad (6)$$

The results are illustrated in Figs. 1 and 2.

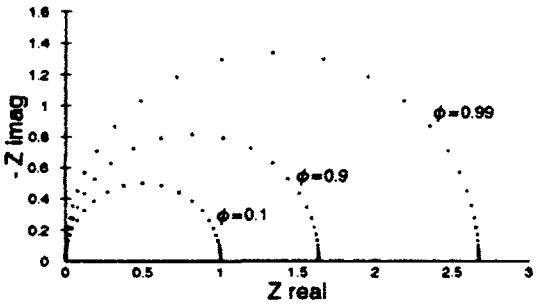

Fig. 1 Geometric Impedance
$\phi = I/I_L'$

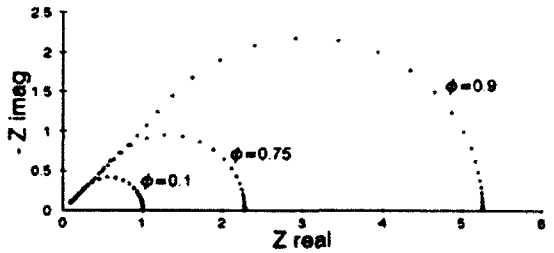

Fig. 2 Diffusional Impedance
$\phi = I/I_L'$

REFERENCES

1. R. P. Buck, *Impedances of Thin and Layered Systems: Cells with Even Odd Numbers of Interfaces*, (Special Issue on Bioelectrodes), R. A. Schmukler and R. P. Buck, eds.), Annals of Biomedical Engineering (H. H. Sun, ed.), Vol. 20, Issue #3, 5/22/92 Pergamon Press.
2. R. P. Buck, Electrochim. Acta 35, 1609-1617 (1990).
3. R. P. Buck, J. Phys. Chem. 92, 4196-4200 (1988).
4. R. P. Buck, J. Electroanal. Chem. 210, 1-19 (1986).
5. R. P. Buck, J. Membrane Sci. 17, 1-62 (1984).
6. R. P. Buck, Ion-Selective Electrode Rev., 4, 3-74 (1982).
7. R. P. Buck, T. M. Nahir, R. Mackel, and H.-D. Liess, J. Electrochem. Soc. 139 1611-1618 (1992).
8. T. M. Nahir and R. P. Buck, "Modified Cottrell Behavior: applied voltage steps under diffusion control for constant resistance systems" J. Electroanal. Chem., (in press 1992).
9. D. R. Franceschetti, J. R. Macdonald, and R. P. Buck, J. Electrochem. Soc., 138, 1368-1371 (1991).

E.I.S. APPLICATION : INFLUENCE OF THE MECHANICAL FORMING ON THE QUALITY OF THE PROTECTIVE COATING IN THE CASE OF LACQUERED TINPLATE

C. BUGNARD, L. BILLEN, P. JUNGES, J. MORREALE

Centre de Recherches du Fer Blanc - Laboratoire de Développement des Produits Plats
SOLLAC
Chaussée d'Europe - BP n°135
57103 Thionville Cedex - FRANCE

INTRODUCTION :

Steel is one of the most widely used materials for food and beverage packaging. Its corrosion resistance is based on a metallic electroplating, generally tin, and on a protective coating. This organic layer is a physical barrier which prevents the foodstuff to come into contact with the metallic base.

For a good protection two kinds of defects in the lacquer must be avoided (Diag.1):

- the coverage defects which allow a direct contact (pore and scratch).
- and the structural defects which induce a penetration through the polymer coating (non-emerging pore, bubble, cross linkage defect).

LACQUER QUALITY CHARACTERIZATION :

E.I.S. is a method used successfully for investigation of the corrosion behaviour of organic coated metals [1]. Using an equivalent circuit with two time constants (Diag. 2), we are able to quantify the lacquer's characteristics in terms of porosity and permeability :

$$\text{porosity} = \frac{S_{pore}}{S_{analysis}} = \frac{\rho_{electrolyte} \cdot d_{lacquer}}{R_{pore} \cdot S_{analysis}} \quad \text{and} \quad \text{permeability} = \varepsilon = \frac{C^{\alpha}_{lacquer} \cdot d_{lacquer}}{\varepsilon_0 \cdot S_{analysis}}$$

where S represents a surface, ρ a resistivity, d a depth of layer, ε the dielectric constant of the coating soaked with electrolyte and ε_0 the vacuum permittivity.

Diagram 1

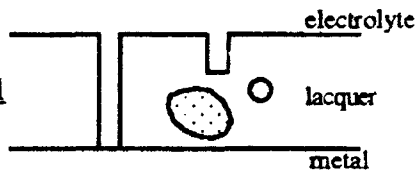

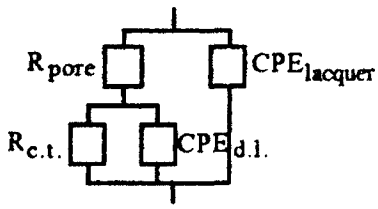

Diagram 2

EXPERIMENTAL :

Impedance measurements are made under galvanostatic control (I = 0) in the frequency range of 10 kHz to 1 mHz, at 25°C in a diluted citric acid solution (foodstuff model) after low energy ultrasonic pretreatment for contact acceleration.

Impedance spectra are measured with Schlumberger devices (electrochemical interface Solartron 1286 and frequency response analyzer Solartron 1250). For their analysis we used the "Equivcrt" software [2].

INFLUENCE OF THE MECHANICAL FORMING :

During manufacturing from coated sheets to cans, the material is submited to forming which can change the quality of the organic coating, initially caracterized on the flat sheets (Fig. 1).

So the porosity and permeability measurements must be made also on the strained material, in order to evaluate the real protective effect of the lacquer and the aggressivity of the mechanical forming process (Fig. 2).

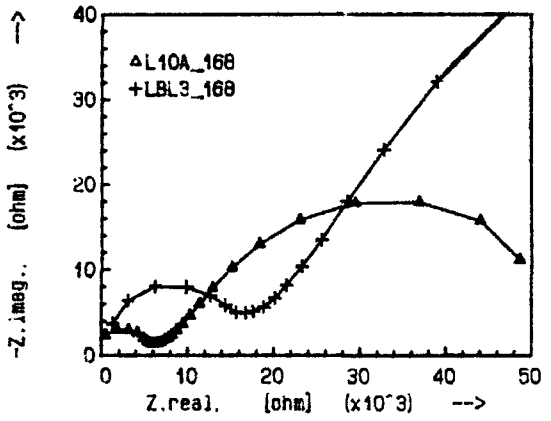

Figure 1 : impedance spectra of a material before (+) and after 10% plane strain (Δ).

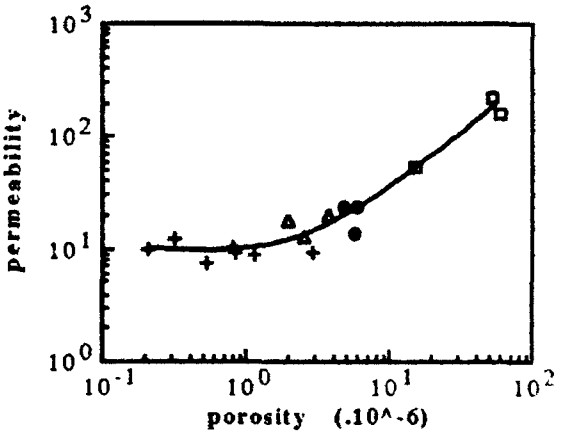

Figure 2 : lacquer characteristics before (+) and after 10% (Δ), 20% (•) and 30% (□) plane strain.

RESULTS :

The can forming is a complex process resulting from a combination of different stress modes which is dependent of the studied can type.

For this reason, at first we characterized the lacquer before and after some different elementary stresses, like the plane strain (Fig. 1 and 2). So we are able to show the effect of each elementary strain on the lacquer quality for the whole mechanical forming for food and beverage cans.

Secondly we will use a stress model of the reals cans in order to assess the protection loss of the lacquer after forming. It will allow us to fit, on one hand the nature and the thickness of the polymer coating and on the other hand the mechanical forming process, to the best behaviour of the can.

REFERENCES :

[1] F. MANSFELD, Electrochimica Acta 35, 10 (1990) 1533 (Special Issue : Proceedings of the First International Symposium on Electrochemical Impedance Spectroscopy)

[2] B.A. BOUKAMP, Proceedings of the First International Symposium on Electrochemical Impedance Spectroscopy, Bombannes (1989) C1.11

ZINC DEPOSITION AND DISSOLUTION IN A FLOW-THROUGH POROUS ELECTRODE

C. CACHET, R. WIART, J. ZOPPAS-FERREIRA*

UPR 15 du CNRS, Physique des Liquides et Electrochimie
Tour 22, 4 Place Jussieu, 75252 Paris Cedex 05 - FRANCE

It is known that the impedance of a porous electrode is closely related to the geometry and size of pores. Various approaches to the application of EIS to the study of porous electrodes have been recently reviewed [1]. The electrode impedance has been extensively modelled on the basis of idealized one-dimensional cylindrical pores [2,3].

The formulation of the electrode impedance of cylindrical pore models has been utilized to estimate the average pore texture of zinc particles of irregular shape used in electrochemical batteries [4,5]. It was shown that zinc electrodes can be described by equivalent cylindrical pore electrodes whose parameters (radius, depth, surface density of pores) have been determined from impedance measurements in a practically non-corrosive electrolyte [4] and also for corroded electrodes in acidic sulphate or chloride electrolytes [5].

In the present study, EIS has been applied to follow the pore texture of a flow-through electrode made of zinc particles during the charge / discharge cycling in a circulating alkaline zincate electrolyte.

From current-potential curves and impedance plots, it is shown that a flow-through porous electrode made of zinc particles behaves similarly to a flat electrode. The electrode is quasi-blocked by a surface layer near the rest potential and is sharply activated at either anodic or cathodic polarizations [6].

Impedance plots also reveal that the powder electrode can be considered as equivalent to a cylindrical pore electrode, obeying the De Levie's theoretical model which can be applied at low current density to characterize the porous texture of charging and discharging electrodes. A least-square fitting procedure of the impedance spectra recorded with the flow-through electrode allows the determination of the parameters of cylindrical pores (length, radius and number) and gives the penetration depth of current. An example of fitted results is exhibited in figure 1.

* Present address: LACOR/DEMAT/UFRGS Av. Osvaldo Aranha 99/706 90210 Porto Alegre -R S- BRAZIL

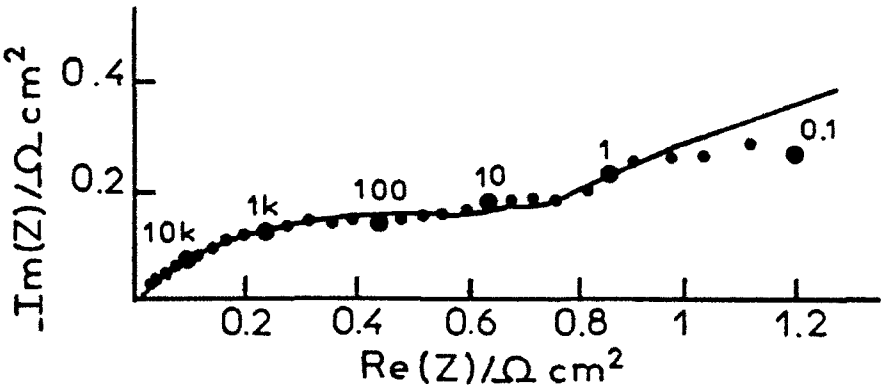

Figure 1:
For η_c = 2 mV, fitting of experimental data (•) to calculated impedance (solid line) from the De Levie's model of cylindrical pores.

At low cathodic overpotentials η_c, the kinetics of zinc deposition are controlled by the ion diffusion through a solid layer formed on the surface of particles in the powder electrode. The zinc deposit remains thin and little modifies the pores geometry, by slightly decreasing the radius of cylindrical pores. With increasing η_c, the length of cylindrical pores and the penetration depth of current shorten significantly and reduce the active surface area.

Whatever the anodic overpotential η_a, the powder electrode behaves as semi-infinite cylindrical pores. The pore radius is again shown to be reduced by the dissolution process, due to the presence of a porous layer of oxidation products on the lateral wall of pores, similarly to the situation evidenced for a flat electrode. Even with a forced convection, the very small penetration depth makes the electrode dissolve only on superficial particles, similarly to a rough electrode.

REFERENCES

[1] I.D. RAISTRICK, Electrochim. Acta **35**, 1579 (1990)
[2] R. de LEVIE in Advances in Electrochemistry and Electrochemical Engineering (Edited by P.Delahay) vol VI p329, Interscience, New York (1967)
[3] J.R. PARK and D.D. MACDONALD, Corros. Sci., **23**, 295 (1983)
[4] C. CACHET and R. WIART, Electrochim. Acta, **29**, 145 (1984)
[5] C. CACHET, C.P. DE PAULI and R. WIART, Electrochim. Acta, **30**, 719
[6] C. CACHET, B. SAIDANI and R. WIART, J. Electrochem. Soc.,**138**, 678 (1991) and **139**, 644 (1992)

THE INTERPRETATION OF EIS AT CORROSION POTENTIAL

Chu-nan CAO
Corrosion Science Laboratory,Institute of Corrosion and Protection
of Metals, The Chinese Academy of Sciences,
Wen-cui Road,Shenyang 110015, CHINA

The Faradaic admittance at mixed potential when two reactions are taking place simultaneously at the electrode can be expressed as:

$$Y_F=(\Delta I_{F1}/\Delta E)ss+(\Delta I_{F2}/\Delta E)ss=Y_{F1}+Y_{F2}$$

It can be deduced that if there is a state variable X other than electrode potential E affecting the rates of the reactions, the Faradaic admittance at the mixed potential can be expressed as

$$Y_F=1/Rt+B/(a+j\omega)$$

where

$$1/Rt=Rt_1+1/Rt_2$$

$$B=(\partial I_{F1}/\partial X)ss(\partial \dot{X}/\partial E)ss+(\partial I_{F2}/\partial X)ss(\partial \dot{X}/\partial E)ss$$

and

$$a=-J=-(\partial \dot{X}/\partial X)ss$$

$$\dot{X}=dX/dt$$

$j=\sqrt{-1}$, ω is the circular frequency. An interesting point is that if X affects the rates of both reactions and $(\partial I_{F1}/\partial X)ss = -(\partial I_{F2}/\partial X)ss$, B equals zero and the EIS display at mixed potential will degenerate to a single capacitive loop generated from the interfacial capacitance Cd and Rt. For a corroding metallic electrode in a solution containing an interface inhibitor, the state variable other than E is the coverage θ of the adsorbed inhibitive species, thus the Faradaic admittance at corrosion potential can be expressed by

$$Y_F=1/Rt+[(\partial Ia/\partial \theta)ss-(\partial |Ic|/\partial \theta)ss]/(a+j\omega)$$

Here Ia and Ic are the current densities of the anodic and cathodic reactions respectively. Ia is positive and Ic is negative. If the inhibition is due to the geometric blocking effect[1], both rates of the anodic and cathodic reactions will be reduced in the same extent and then $(\partial Ia/\partial \theta)ss - (\partial |Ic|/\partial \theta)ss = 0$. In this case, the Faradaic admittance at corrosion potential is

$$Y_F=(1-\theta)Y_{F(b)}+\theta Y_{F(\theta)}$$

where $Y_{F(b)}$ is the Faradaic admittance on the bare surface area and $Y_{F(\theta)}$ is that on the surface area covered by the adsorbed inhibitive species. The latter equals to $1/Rt$ as discussed above. So if the inhibition efficiency is high enough that the first term on the right side in the above equation can be neglected,

$$Y_F\approx Y_{F(\theta)}=1/Rt$$

The EIS will degenerate to a simple capacitive loop as the example shown in

Fig.1(A). If the inhibition is due to the geometric blocking effect but the inhibition efficiency is not so high that $(1-\theta)Y_{F(b)}$ can not be neglected, the Faradaic admittance at corrosion potential will be

$$Y_F = \theta / Rt + (1-\theta)Y_{F(b)}$$

and the feature of the EIS in the inhibitor-containing solution will be similar to that in the blank solution. An example is shown in Fig. 1(B).

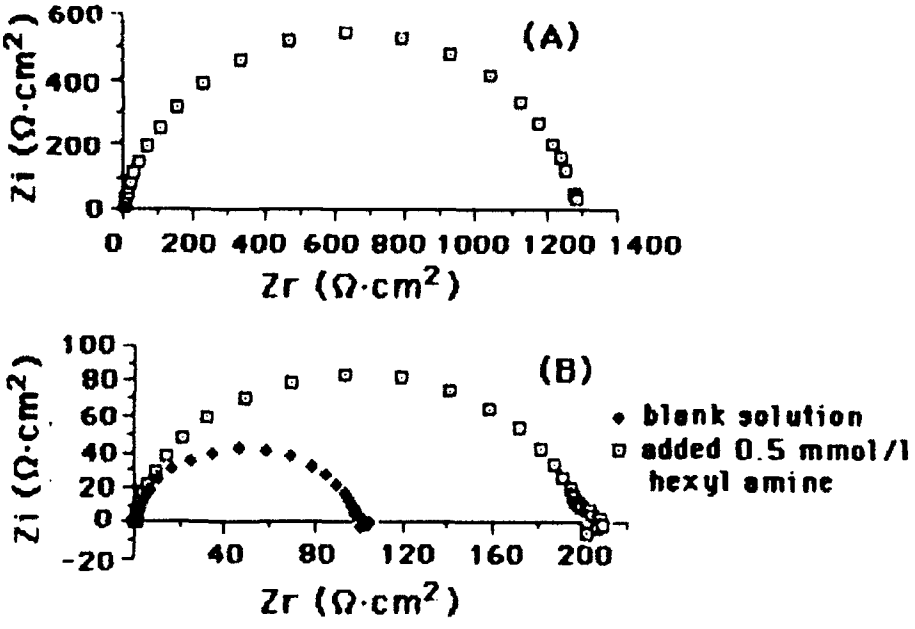

Fig.1 EIS at corrosion potential of Armco Fe in 1N HCl added with 1 mmol / L dodecyl amine (A) and in 1N HCl without and with addition of 0.5 mmol / L hexyl amine (B)

If two state variables X_1 and X_2 affect the rates of the reaction, the Faradaic admittance at mixed potential will be expressed generally as

$$Y_F = 1 / Rt + (A + j\omega B) / (D - \omega^2 + j\omega T)$$

which is formally the same as the equation deduced previously for one electrode reaction with two state variables other than E[2]. The explicit expressions of the parameters A, B, D and T are given for various cases. The possible types of EIS displays are discussed. As an example, the EIS display at the corrosion potential of Armco iron in 1 mol / L HCl is analyzed by the proposed theory.

References

[1] W.J.Lorenz and F.Mansfeld, Proc.6SEIC,Univ.Ferrara, pp.23–40(1985)

[2] Ch.Cao, Electrochim. Acta, 35, 837 (1990)

THE ROLE OF PHOSPHATE, PERCHLORATE AND CHLORIDE ANIONS ON COPPER ELECTRODISSOLUTION

J.C.Cardoso[1], E.D'Elia[1], O.E.Barcia[1,2] and O.R.Mattos[1,3]

1-Laboratório "Prof.Manoel de Castro" - PEMM/COPPE/UFRJ - Caixa Postal 68505, CEP: 21945, RJ, Brazil.
2-Depto. de Físico-Química - IQ/UFRJ - RJ, Brazil.
3-Escola de Engenharia - UFRJ - RJ, Brazil.

INTRODUCTION

Recently, Cordeiro et al [1,2] have proposed a mechanism with two adsorbed species to explain the results obtained in 1M of sulfate, pH=0-5. The mechanism proposed by the authors was able to account for the polarization curves and impedance diagrams in a large range of potential:

$$Cu \underset{K_{-1}}{\overset{K_1}{\rightleftharpoons}} Cu(I)_{ads} + e^-$$

$$Cu + Cu(I)_{ads} \xrightarrow{K_2} Cu^{++} + Cu(I)_{ads} + 2e^-$$

$$Cu(I)_{ads} \underset{K_{-3}}{\overset{K_3}{\rightleftharpoons}} Cu(II)_{ads} + e^-$$

$$Cu + Cu(II)_{ads} \xrightarrow{K_4} Cu^{++} + Cu(II)_{ads} + 2e^-$$

The steps K_2 and K_4 are considered as catalytic processes. The authors [1,2] have considered K_1 and K_{-1} pH function but the ratio K_1/K_{-1} is assumed pH-independent.

In the present paper results for perchlorate, phosphate and chloride anions will be shown and compared with those already presented for sulfate medium. The possibility of maintaining the same model already proposed for sulfate is also analyzed.

EXPERIMENTAL RESULTS AND DISCUSSION

For the perchlorate anion, the inductive loop seen easily in the sulfate medium, is present only at very high current densities (pH=5), and it is not present at pH=0. The capacitive loop at low frequencies diminishes but is maintained in the diagrams even for high current densities ($0.2\ A.cm^{-2}$). To maintain the capacitive loop always present at low frequencies, and to impose that the inductive process, seen only at very high current densities, it is necessary to change the values of K_1 and K_{-1}. The first

step of the above mechanism, will be considered faster in the presence of perchlorate than in sulfate, showing that the anion has a marked role in the structure of $Cu(I)_{ads}$.

For the phosphate medium, pH=0.7, the results are quite equivalent to those already simulated for sulfate [2]. However, for pH=3 and pH=5 the impedance diagrams are not the same as obtained for sulfate medium. To account for the peculiarities involved with phosphate anions a new species adsorbed at the electrode surface is proposed. This new species could be the origin of a film limiting the current in a large potential range. The new reaction could be griffed in the $Cu(II)_{ads}$ species in the above mechanism:

$$Cu(II)_{ads} \underset{K-5}{\overset{Ks}{\rightleftharpoons}} Cu^{*}(II)_{ads}$$

For chloride solution, pH=0, the mass transport plays an important role even at the corrosion potential of this system. At low polarization range, the current flux is through $Cu(I)_{ads}$ species in the above mechanism. This species in the case of chloride needs to be soluble to justify the mass transport control [3].

CONCLUSIONS

The results in this paper show that copper electrodissolution is strongly influenced by the anion present in the solution. In particular the equilibrium $Cu/Cu(I)_{ads}$ and the transition $Cu(I)_{ads}/Cu(II)_{ads}$ are a function of the anions.

In perchlorate and phosphate, as well as sulfate, the copper electrodissolution is via two adsorbed species at the electrode surface. In chloride one faradaic inductive loop is present in the dissolution process and the particular influence of mass transport is a supplementary difficulty to determine the charge transfer mechanism itself.

REFERENCES

1) G.G.O. Cordeiro, E. D'Elia, O.E. Barcia and O.R. Mattos, *Electrochemical Methods in Corrosion Research* , Helsinki - Finland, 1991 in press.
2) G.G.O. Cordeiro, O.E. Barcia and O.R. Mattos, *Electrochim. Acta*, submitted (1992).
3)C.Deslouis, B.Tribollet, G.Mengoli and M.M.Musiani, *J. Appl. Electrochem.*, **18** , 374 (1988).

INVESTIGATION OF PASSIVE LAYERS ON IRON AND IRON-CHROMIUM ALLOYS BY ELECTROCHEMICAL IMPEDANCE SPECTROSCOPY

E.B.Castro and J.R.Vilche

Instituto de Investigaciones Fisicoquimicas Teóricas y Aplicadas (INIFTA)
Casilla de Correo 16, Sucursal 4
(1900) La Plata, Argentina

It is a well known fact that at bare metal electrodes the rate of outer-sphere electron transfer reactions show only a small dependence on the nature of the substrate (1). At film covered electrodes the equilibrium potential of the redox reaction is the same as for bare metals but the exchange current densities are lower by up to 8 or 9 orders of magnitude depending on the nature of the passive film, moreover the anodic and cathodic transfer coefficients may vary in a broad range between 1 and 0.

The aim of this paper is to correlate the kinetic response of the $Fe(CN)_6^{3-}/Fe(CN)_6^{4-}$ redox couple over passive films, corresponding to iron and iron-chromium alloys, with the thickness and electronic properties of these oxides. In this sense Electrochemical Impedance Spectroscopy (EIS) is a powerfull tool to separate contributions due to ionic transport processes in solution or in the film from electron transfer processes.

High purity iron ("Specpure", Johnson Matthey Chemical Ltd) and Fe-12%Cr discs supported on a PTFE holder were used as working electrodes. Before each measurement the potential was held for five minutes at 1.2V vs SCE and then oxide films were anodically formed at different potentials ranging from 1V to 0.6V vs SCE, during 60 min, in a base solution consisting of 0.1M H_3BO_3 + 0.05M $Na_2B_4O_7.10H_2O$ + 1M KNO_3. After the film formation $K_3Fe(CN)_6$ and $K_4Fe(CN)_6$ were added to the base solution up to a concentration of 0.1M of the reduced and oxidised species and then impedance measurements were performed at different potentials in the anodic and cathodic range with respect to the equilibrium potential, the frequency range was $0.01Hz<f<65000Hz$. Impedance measurements in the same frequency range were also obtained with the passivated electrodes in the base solution without the redox couple. Impedance measurements of the system Pt(disc electrode)/redox couple in the same solution were also accomp'ished.

All the experiments were performed at 25 C under purified N_2 saturation. Impedance measurements were conducted using a Solartron 1250 FRA and an 1186 EI, controlled by a personal computer.

The measured equilibrium potential of the system electrode/ 0.1M $Fe(CN)_6^{3-}$ - 0.1M $Fe(CN)_6^{4-}$ was approximatelly E=0.230V vs SCE, this value did not depend on the nature of the electrode. The impedance diagrams corresponding to Pt electrodes exhibit the contribution of mass transport processes in solution being the dynamic response highly affected by the hydrodinamic condition. Transfer coefficients determined from impedance data are close to 0.5. The ETR current densities over Pt are approximatelly 4 orders of magnitud bigger than over Fe oxides formed at 1V vs SCE, and are strongly dependent on the formation potential of the oxides, Fe oxides formed at 0.6V exhibit current densities 2 orders of magnitud bigger than for oxides formed at 1V, very little differences are observed between oxides formed at 0.6V on Fe and Fe-12%Cr.

Under steady state conditions the current density associated with the system oxide/redox couple is the sum of two partial current densities one related to the transport of ions or vacancies through the film and the other to the electron or hole transfer from the oxide to the redox couple(2). If these currents are statistically independent the total admittance at $f \rightarrow 0$ is the sum of two terms, one associated with the electronic transport from the metal/oxide interfase to the redox couple (Ye) and the other related to the ionic transport (Yi).

For thin films (E_f=0.6V) $Y_e >> Y_i$ that means the total impedance $Z_T = Z_e$. This is easily determined comparing impedance diagrams of Fe oxides in the base solution with and without the redox couple.

Impedance plots of thin oxide films (E_f = 0.6), in presence of the redox couple, exhibit mass transport in solution effects only for high overpotentials ,E_c=-0.2V or E_a=0.6V. From impedance data, the transfer coefficients (α) can be easily determined, anodic transfer coefficients (α_a) are close to 0.15 ,being this in accordance with an electron transfer mechanism via the conduction band, while the cathodic transfer coefficients change from α_c = 0.85 at E= 0.230V to α_a= 0.5 at E=-0.2V , this fact may probably be related to a change in the electron transfer mechanism , from a conduction band mechanism to a direct tunneling through the oxide.

The oxide films formed on Fe at 1V in solutions containing the redox couple exhibit more complicated impedance diagrams than those associated with thinner oxide films. The dynamic response of this system is probably related to transport processes in the oxide and transfer coefficients are not easily derived from impedance data ,mass transport processes in solution do not contribute to the total impedance

REFERENCES

1.T. Iwasita, W. Schmikler, J.W.Schultze, Ber. Bunsenges. Phys. Chem. **89**(1985).

2.K.E. Heusler and Kyung Suk Yun, Electrochim. Acta **22**,977(1977).

IMPEDANCE SPECTROSCOPY OF RAMIFIED ELECTRODEPOSITS

E. Chassaing,
Centre d'Etudes de Chimie Métallurgique-CNRS, F94407 VITRY-SUR-SEINE Cedex,
M. Rosso, B. Sapoval, J.-N. Chazalviel,
Laboratoire de Physique de la Matière Condensée, Ecole Polytechnique, F91128 PALAISEAU Cedex, France.

Introduction

Ramified electrodeposits may be obtained in a variety of experimental conditions. In the last decade, much attention has been paid to these deposits in relation to the growing interest on fractal geometry. In particular, many authors have reported that electrodeposition may create aggregates very similar to the Diffusion Limited Aggregation cluster [1].

Several theoretical [2] and experimental [3] studies have shed some light on the basic electrochemistry involved in these electrodeposition processes. In particular, it has been shown recently that in simple binary electrolytes, the combined motion of anions and cations induces the creation of a non-classical space-charge region near the cathode. This was suggested to be responsible for the onset of ramified aggregation.

Impedance Spectroscopy (IS) may provide useful informations on the reaction kinetics and surface states involved in electrochemical processes. It has also been shown to be related to the electrode surface morphology [4]. In some cases, the Constant Phase Angle (CPA) exponent may be calculated as a function of the fractal dimension of the surface.

Kahanda and Tomkiewicz have studied IS of electrodeposited silver aggregates [5]. They found a monotonous relation between the measured CPA exponent η and the fractal dimension of the aggregates, which they attempted to compare with theoretical predictions. However, in these experiments, the electrolyte was changed before measuring the impedance of the deposits. This caused some destruction of the aggregate. The purpose of the present work was to investigate the IS of Cu aggregates with minimum disturbance of the system, i.e. in the cell and electrolyte where these aggregates were grown.

Experimental procedure

The experiments have been carried out in a pseudo 2D-cell with 0.1 M $CuSO_4$ solutions at room temperature. Cathode and anode were parallel copper foils (0.3mm thick, 65 mm long), 12 mm apart. A copper wire close to the cathode was used as a reference electrode. Prior to each experiment the cathode was polished with diamond paste to 1µm. Galvanostatic polarizations have been applied for various time intervals. The time dependency of the cathode potential enables to monitor the deposit growth [3]. Only the onset of the ramifed growth has been investigated. The electrochemical impedance spectra, in the range 50kHz-10mHz, have been measured at the rest potential before and after cathodic polarization, and their time evolution recorded.

Results

In pure copper sulfate solutions, due to passivation, the cathode impedance tends to increase and very slowly stabilizes. The addition of dilute hydrochloric acid (5.10^{-3}N) was shown to impede copper oxidation and stabilization of the impedance occurs rapidly.

Before deposit growth the impedance spectra are not very reproducible. They usually consist in two overlapping loops : the resistance associated with higher frequency loop (r_1) has the magnitude of the charge transfer resistance (ca. 30 ohms), calculated from literature data [6]. The associated capacitance is of the order of the double layer capacitance for our cell

(20μF). A second capacitive feature with a larger resistance, r_2 , is observed at lower frequencies. Both are best fitted using CPA elements, with exponents ranging from 0.2 to 0.4. A very low frequency feature was also observed, but could not be investigated in detail, due to experimental limitations.

After cathodic growth the impedance diagrams are strongly modified. The impedance diagrams exhibit two main capacitive features (Fig.1). The high-frequency resistance, related to electrolyte resistance between working and reference electrodes, is increased as a result of cupric species consumption. It then progressively returns to its previous value due to solution homogeneisation controlled by diffusion. The resistances, r_1 and r_2 , are markedly decreased and the associated capacitances increased because of the much larger electrode surface area. After stopping the polarization, the resistances increase with time due to deposit reorganisation and/or dissolution. A CPA behavior is again observed, with exponents larger than those for the initial electrode.

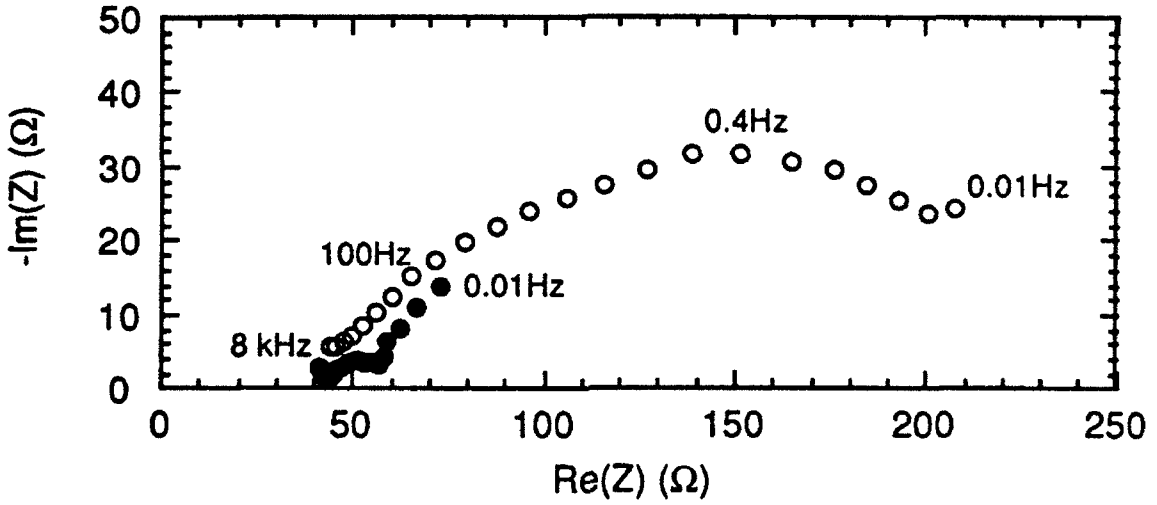

Fig.1 Impedance diagrams before (o) and after (•) electrodeposition of a 200 μm deposit, obtained after polarizing the cell under 7 mA for 185 sec. Note that y-axis has been expanded for a better visualization of the results.

Conclusion

We have performed impedance analysis of ramified electrodeposited copper aggregates. Our results evidence the large increase of the cathode surface area at the early stages of the growth. The observed CPA exponents ask for further interpretation.

REFERENCES

[1] See for example Ben-Jacob E. & Garik P., Nature, 343, 523 (1990) and references therein.
[2] Chazalviel J.-N., Phys. Rev. A42, 7355 (1990).
[3] Fleury V., Rosso M., Chazalviel J.-N. & Sapoval B., Phys. Rev. A44, 6693 (1991).
[4] Sapoval B., in "Fractals and disordered systems", Springer Verlag, 1991, p.207.
[5] Kahanda G.L.M.K.S. & Tomkiewicz M., J. Electrochem. Soc. 137, 3423 (1990).
[6] Cabán R. & Chapman T.W., J. Electrochem. Soc. 124, 1371 (1977).

LOW TEMPERATURE IMPEDANCE OF SEMICONDUCTING n-RuS_2 / $HClO_4 \cdot 5.5H_2O$ INTERFACE

H. Colell and N. Alonso-Vante

Hahn-Meitner-Institut Berlin, Abteilung Solare Energetik
Glienicker Straße 100, D-1000 Berlin 39, Germany

Semiconducting n-RuS_2 is an interesting photoelectrocatalytic material tested for photoevolution of oxygen from water [1]. The examination of this process at low temperature is rather scarce. The electrolyte $HClO_4$ $5.5H_2O$, which freezes at 228K allows such measurements in the liquid and frozen state, due to its high conductivity [2]. Recently, we have obtained (photo)current-voltage characteristics of the oxygen evolution kinetics in the temperature range of 180K to 300K [3]. To get more insight of the interfacial charge transfer kinetics and energetics at this interface, we performed impedance measurements in darkness and under illumination (He-Ne-laser, 633nm, 15mW/cm^2) in the temperature range (216 to 295K) and electrode potential range (0.4 to 1.6V/RHE) using differently doped RuS_2 samples.

The electrochemical set up for low temperature experiments is described elsewhere [3]. Impedance measurements were done using a Solartron Electrochemical interface (SI 1286) coupled to a Solartron HF Frequency Response Analayzer (SI 1255) controlled by a Macintosh (IIcx) computer with software developed in our laboratory.

A NLLS analysis [4] of each impedance spectrum (frequency range 1 to 10^6 Hz) at a constant potential and temperature was obtained using a Voigt-type kinetic electrical circuit [5]. This latter allowed us to find a physical description of our system with a total of five elements fitting: series resistance, R_s, semiconductor resistance, R_{sc}, charge transfer resistance, R_{ct}, space charge capacity, C_{sc} and Helmholtz layer capacity, C_H. Fig. 1a and 1b show the impedance spectra of the less degenerate electrode in $HClO_4$ $5.5H_2O$ presented as Bode plots at an electrode potential of 1.6V/RHE in darkness and under illumination for two temperatures, i.e. 295K and 216 K. At 295 K the magnitude and phase of the impedance show no significant changes when the electrode is illuminated, whereas a drastic change is observed at 216K with illumination. This is again contrasted in the magnitude and maxima displacement of the phase, fig. 1b. Two time constants for all temperatures were also observed. In all cases the applied equivalent circuit fitted the data very nicely as indicated by the solid lines in fig. 1a and 1b. With exception of the series resistance, fig. 2 shows the dependence of $1/R_{ct}$, $1/R_{sc}$, C_{sc} and C_H, as a function of the inverse temperature. The ensemble of results can be summarized as follows: (1), no dependence of the space charge region capacity neither with temperature nor with the applied electrode potential is observed, this latter acounts for unpinned band edges; (2), the charge transfer resistance, proper to the faradaic process, remains activated under illumination (E_A=0.27eV); and (3) a correlation between R_{sc} and C_H is evident. In darkness, the former describes the thermal activation for electron transfer to the conduction band, whereas under illumination this parameter is determined by the photogenerated holes reaching the surface. This creates a charge accumulation at the semicoductor surface (interfacial states?) which is reflected by the capacity change of the Helmholtz layer.

In conlusion, the application of complex impedance measurements revealed interesting features of the photoelectrocatalytic RuS_2/electrolyte interface as a function of temperature. In investigating differently doped materials, it was found that most of the applied potential drops essentially in the Helmholtz layer, which serves as the driving force for the reaction. This would explain that the different catalytic activity is not due to different interfa-

cial states concentration but to an occupation of the interfacial states serving as catalytic sites.

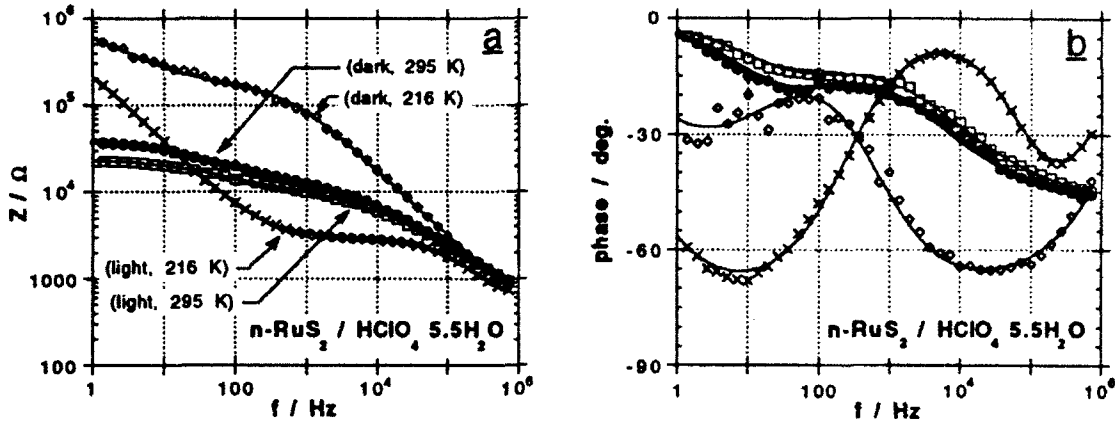

Fig. 1: Magnitude (a) and phase (b) of the complex impedance for n-RuS_2 in darkness and under laser illumination (633 nm) at an electrode potential of 1.6V/RHE for two different temperatures (295K and 216K).

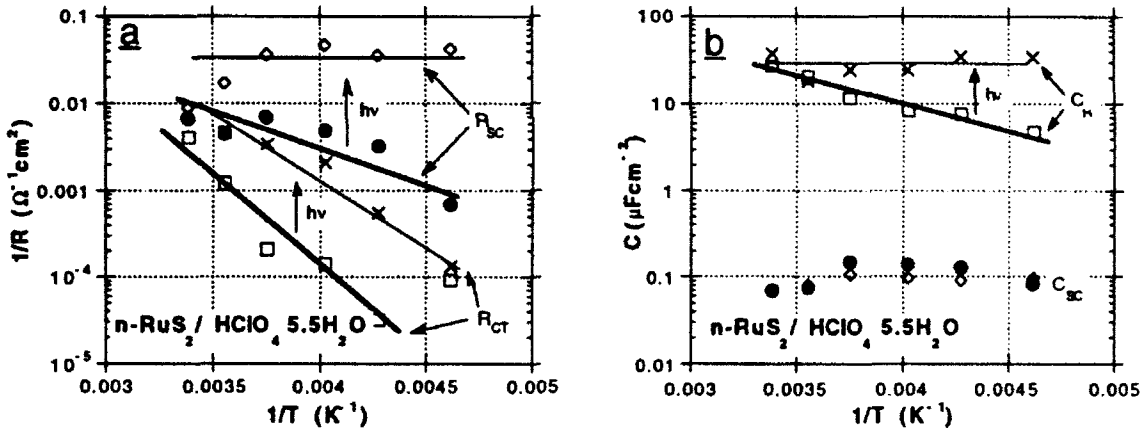

Fig. 2: Dependence of the fitted parameters $1/R_{ct}$, $1/R_{sc}$, C_{sc} and C_H on the reciprocal temperature in darkness and under illumination at an electrode potential of 1.6V/RHE.

Acknowledgement:

This work was supported in part by a grant 'catalytic energy conversion' of the BMFT (Nr. 0329032B).

References:

[1] H.-M. Kühne, H. Tributsch, J. Electroanal. Chem., 201 (1986) 263.
[2] M. Cappadonia and U. Stimming, J. Electroanal. Chem., 300 (1991) 235.
[3] N. Alonso-Vante, H. Colell, U. Stimming and H. Tributsch, submitted.
[4] Software purchased from B. A. Boucamp, Univ. Twente, Netherlands.
[5] J. Ross MacDonald, J. Electroanal. Chem., 223 (1987) 25.

TRANSIENT IMPEDANCE STUDY OF TIME BEHAVIOUR OF Ag SURFACE PASSIVATION BY CYANIDE IONS UNDER POTENTIOSTATIC CONDITIONS

V. DAUJOTIS, V. KUBILIUS and D. JASAITIS

Department of General and Inorganic Chemistry, Vilnius University
Vilnius 2734 - LITHUANIA

The analysis of a kinetics of the electrode reactions at solid surfaces are greatly complicated by that the state of the surface is not constant during the reaction. The variation of the capacitance of the double layer with time can provide data on the time dependence of surface state, although macroscopic in character. Nevertheless, this information can be adequate for the intended purpose, articulated by a researcher. Then the problem is to measure impedance responses for series of frequencies, where every series correspond to the time of interest. For this purpose, the excitation by step waveforms and the measurement of transient impedance serves best.

A potential step technique used in this work involves superimposition of a series of the short (1 ÷ 2 ms) potential steps (≤ 5 mV) on the controlled potential, i.e. on the large potential step (Fig.1A). The responses, which correspond to the small potential perturbations, were partitioned from the resulting current (Fig.1B) by passing it through the high frequency filter. The distortion of the response passed through filter was negligible and always was within the accuracy of measurements. At the same time the perturbing small potential steps were also partitioned from the large potential step and amplified by using differential amplifier. Two ADC modules with built-in memory buffers were used to record every small potential step and the corresponding responses at a sampling rate 20 MHz. The Laplace transforms of every perturbation - response have been carried out as described elswhere [1]. Every perturbing step and current response to it gives one dependence of the operational impedance on the Laplace variable, p. In case of real-axis Laplace transform Nyquist theorem gives the maximum p value equal to 10^7 s^{-1}. The slope of the dependence of the operational impedance on p^{-1} gives $C\ (p^{-1} \Rightarrow 0)$. In that way, double layer capacitance is calculated for every perturbation - response, i.e. starting from the beginning of the large potential step perturbation the variation of the capacitance with time is obtained.

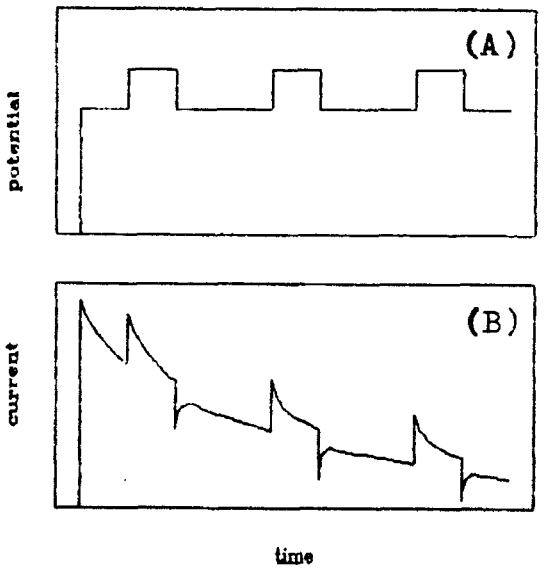

Fig. 1. Schematic diagram of the potential relaxation experiment for evaluation of the variation of the double layer capacitance with time: (A) perturbing potential pulse; (B) response - current.

The above technique has been applied to the study of the reaction at

the electrode silver/(dicyanoargentate solution). The inhibition of the cathodic reaction at this electrode is usually attributed to the passivation of the electrode surface. It was shown that this passivation occurs to be governed mainly by cyanide ions [2]. As it was obtained by us, during this process the adsorbed cyanide ion should loose its charge and the formation of a surface CN polymer like paracyanogen should occur. Fig. 2 shows some examples of the measured current transients and the correspondig variations of the double layer capacitance with time. An unusual profile of current transients has been clearly pronounced for potential steps exceeding 100 mV. In former potentiostatic pulse study [3] this effect has not been taken into account because the pulses applied were too small to observe the distortion of transients clearly. Nevertheless, an analysis of every transient must include this effect. Time behaviour of the double layer capacitance (Fig. 2) gives additional information about the passivation of silver electrode surfa- ce. However, to be accurate, one problem must be solved in advance, i.e. whether the decrease in the initial current transient values depends on the probable electron transfer from the cyanide ion. This problem can be best solved by simultaneous measuring charge and mass at a short time.

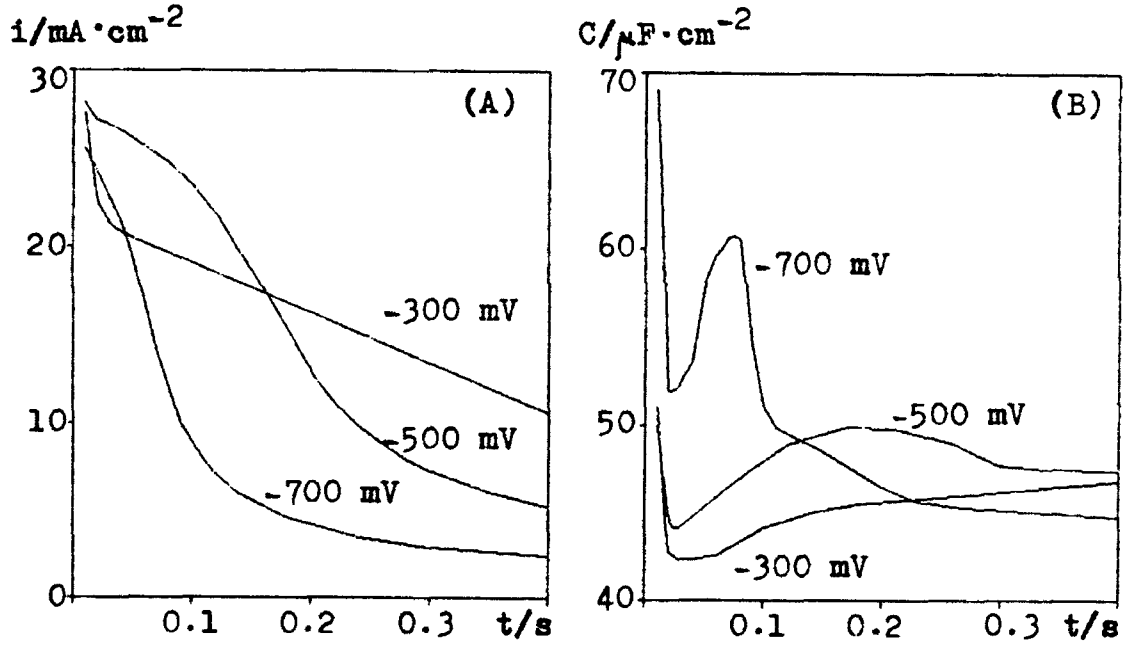

Fig. 2. (A) The measured current-time transients and (B) the corresponding variations of the double layer capacitance with time at different cathodic overpotentials in 0.1 M $KAg(CN)_2$ + 1.0 M K_2CO_3 at 25°C. For transients ΔE=-500 and -700 mV, current values must be multiplied by 2 and 4 respectively.

References

1. D.D. Macdonald and M.C.H. McKubre in J.O'M. Bockris, B.E. Conway and R.E. White (Eds.), Modern Aspects of Electrochemistry, Vol. 14, Plenum Press, New York and London, p.61 (1983).
2. V. Daujotis, G. Baltrunas and V. Kaikaris, Electrochim. Acta, 28, 1319 (1983).
3. H. Baltruschat and W.Vielstich, J.Electroanal.Chem., 154, 141 (1983).

MECHANISM OF CADMIUM UNDERPOTENTIAL ADSORPTION ON PLATINUM AS OBTAINED FROM QUARTZ ELECTROGRAVIMETRY AND POTENTIAL STEP RELAXATION DATA

V. DAUJOTIS and R. RAUDONIS

Department of General and Inorganic Chemistry, Vilnius University
Vilnius 2734 - LITHUANIA

In a relatively small number of the studies of the underpotential adsorption (UPA) kinetics, the classical electochemical methods have been used to a full extent. Ususally, the coupling of a variety of phenomena that characterize the UPA system leads to the opinion that the UPA currents can be best interpreted only with the aid of other techniques. However, the classical electrochemical means of investigation deserve to be accounted for better attitude. An analysis of published kinetic studies shows that a great deal of controversy can be reduced by a proper application of investigation technique. In addition, the treatment of measured data leaves a lot to be desired. As the main evidence in support of the model considered comes from the internal compatibility of the kinetic data obtained, large approximations, though correct, lead unavoidably to a decrease in such an evidence.

The present work has the twofold purpose of: (i) contribution to technical and analytical extension of the potential step relaxation technique, and (ii) mechanism/rate analysis of cadmium underpotential ad sorption on polycrystalline platinum electrode surface from acidic (sulfuric acid) aqueous media.

Using the original computerized potential step technique, the mechanism for the initial stage of cadmium underpotential adsorption (UPA) on platinum electrodes has been determined. The most probable general scheme for the UPA reactions of cadmium(II) on a polycrystalline platinum electrode in the potential region considered (peak I in Fig.1, 530 ÷ 710 mV vs. SHE) is

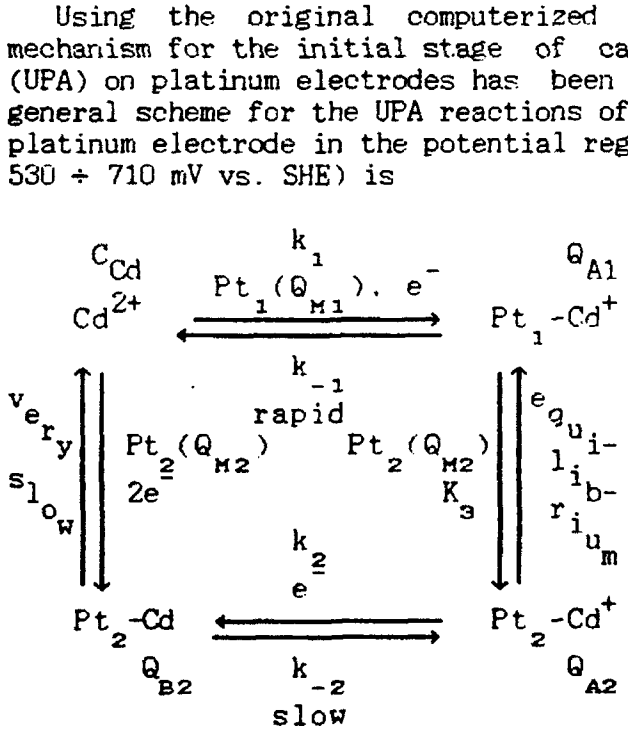

The evidence for this mechanism comes from: (i)within this mechanism, all the potential step relaxation data agree in between; (ii) the potential-dependent formal partial charge number, *l*, calculated on a basis of the above mechanism from the potential-dependent surface coverages (measured in charge units) is in an agreement with that obtained from the quartz electrogravimetry data. In the potential region considered, *l* changes in the range from about 1.1 to almost 2.

To determine the above mechanism an analysis of the small potential step (≤5 mV) relaxation data was carried out in relation with the large signal response. The analytical expression for the current relaxing by

above mechanism can be obtained only for small potential perturbations: (i) the terms containing the functions of higher order can be omitted from the differential equations written for this mechanism; (ii) the rate constants are also coverage-dependent: if the potential step is small enough, then this dependence can be ignored. However, the number of parameters to be established for the above mechanism (rate constants, equilibrium constant and surface fractions) outnumbers the amount of magnitudes obtained by a numerical fitting procedure according to the final transformed expression for the Laplace current ($\Delta E \leq 5$ mV). An examination of this mechanism reveals a way out of this situation. At zero time of the potential perturbation the influence of cadmium surface migration on the occurrence of the charge transfer steps can be ignored. Then it is possible to obtain simplified kinetic equations which are valid for arbitrary potential steps but only at zero and near zero time. The developed equations had shown how the experiments should be arranged and how the experimental data should be analysed. In this way, all the kinetic (rate constants) and equilibrium (equilibrium constant and surface fractions) parameters plotted in the above scheme of cadmium UPA were obtained without any aid of other techniques.

Now, when the potential step relaxation analysis is finished, the independent indication of the "goodness" of this analysis would be strongly desirable. An oscillating quartz crystal microbalanlance has been used to verify the foregoing results. Fig. 1 shows the current and frequency response as the platinum electrode is scanned through the UPA region. Then the formal partial charge number, l, was obtained from the slope of the dependence of the charge passed during cadmium adsorption on the mass change, which was calculated from the frequency shift. l changes from about 1.1 to 2 as the potential varies from 710 to 530 mV.

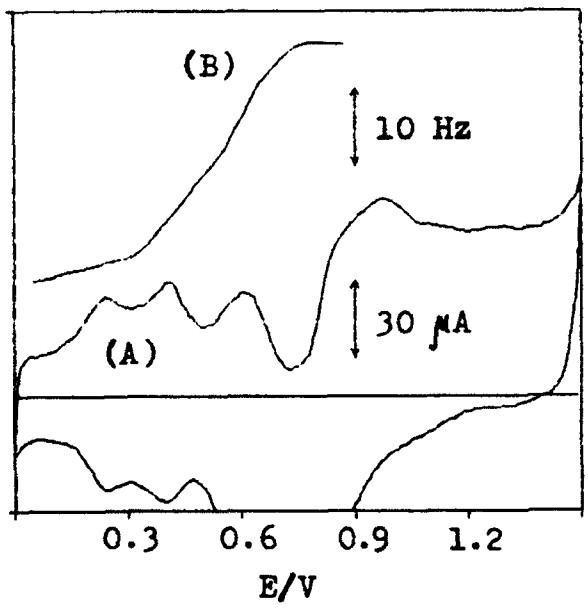

Fig.1. (A) Cyclic voltammogram for polycrystalline platinum and (B) frequency shift of the quartz microbalance during the UPA process in 0.2 M $CdSO_4$ + 0.2 M H_2SO_4 at 25°C.

The formal partial charge number can be also calculated on a basis of suggested mechanism. According to it cadmium electrosorption valency values values are 1 (for cadmium adsorbed in states A1 and A2) and 2 (for cadmium adsorbed in state B2). Using these values together with the coverages of these states gives the variation of calculated l from 1.3 to almost 2 in the potential region from 710 to 530 mV. This agreement serves as a strong independent evidence for the suggested mechanism.

It follows that the UPA of cadmium ions can not be used as a proof of non-integral electron transfer. The data obtained make a contribution to the viewpoint that at least for simple ions the electrosorption valency should be integer.

TESTING OF CORROSION RESISTANT FLUOROPOLYMER COATINGS

F. Deflorian°, L. Fedrizzi°, A. Locaspi*, P.L. Bonora°

° Material Engineering Department, University of Trento
*** Montefluos S.p.A., Research Center, Bollate, Milano, Italy**

Fluoropolymers have attained great importance as coating materials because of their excellent resistance to high temperature, chemicals and organic solvents. Electrochemical Impedance Spectroscopy (EIS) was used to study the electrochemical behaviour properties both of undamaged fluoropolymer coatings and of samples with an artificial defect

The area of the defects in the coatings was determined using the method of break point. For samples with an artificial defect, a good agreement was found between the defect area determined using the break-point method and the defect area measured by light microscope observation. The use of the break-point method to calculate the area of defects was discussed in comparison with other methods for measuring the defect area in polymeric coating. The use of fitting procedures, which allow Rp to be calculated, is also effective in determining the defect area. In this case, too, is possible to calculate the Rct values by which the real active area under the coating can be obtained.

The use of the break-point method on undamaged coatings as well showed a smaller presence of defect in the fluorinated coatings with in comparison to the corresponding hydrogenated coatings

CHARACTERIZATION OF ALUMINIUM SURFACE TREATMENTS WITH ELECTROCHEMICAL IMPEDANCE SPECTROSCOPY AND SPECTROSCOPIC ELLIPSOMETRY

J. De Laet, J. Scheers, H. Terryn and J. Vereecken.

Department of Metallurgy, Electrochemistry and Materials Science
Vrije Universiteit Brussel
Pleinlaan 2, 1050 Brussels, BELGIUM

In virtually all applications of aluminium, the surface finishing plays a major role in providing the aluminium product with the required properties. The morphological and chemical aspects of the applied surface treatments are intensively investigated to optimize the processing conditions of the substrate so that the customers can be met with the best quality products. Most often these investigations are performed with established analysis techniques such as transmission electron microscopy (TEM), Auger electron spectroscopy (AES), X-ray photoelectron spectroscopy (XPS) or secondary ion mass spectroscopy (SIMS). Unfortunately, these complementary techniques can damage the structure under investigation by the radiation or the ultra high vacuum in the analysis chamber or the specimen preparation prior to the analysis. For example, the minute phenomena that take place in the initial stages of the hydration of the porous aluminium oxide film leave no trace after the elaborate thinning procedure required for TEM investigation. In such cases a non destructive technique can supply complementary information.

In the present study two techniques, electrochemical impedance spectroscopy (EIS) and spectroscopic ellipsometry (SE), are used for the characterization of the barrier and porous anodic films and the sealing of the porous film on aluminium. Not only these techniques leave the specimen intact during the characterization, they are also very rapid and offer the potential for in situ application. In this way EIS can be easily superimposed upon treatments in aqueous environments, whereas SE allows to perform the characterization in different environments including the ambient atmosphere, high vacuum, electrolytes, plasma reactors etc.

The interpretation of EIS or SE data is performed by fitting the calculated response of an idealized model of the presumed surface composition and morphology to the experimental data. The approach for SE is very similar to the interpretation of EIS measurements, that are usually interpreted by means of an equivalent network. In the case of ellipsometry data, the model consists of a multilayer structure of several sublayers characterized by their refractive indices and thicknesses. From the available knowledge of the surface properties, determined by the sample preparation procedure and the application of complementary analytical techniques such as TEM and AES it can be checked if the obtained values for thicknesses and compositions are physically realistic.

In the first part of this paper this interpretation procedure is used to determine quantitatively the structural properties of the barrier and the porous anodic film on aluminium. For the barrier film it is concluded that both techniques give similar characterizations of the film thickness and the anodizing ratio. The SE measurements allow to gain supplementary information on the film/substrate roughness by means of a simple two-layer model.
For the characterization of the porous film, SE is superior to EIS, since the latter technique can give only information on the barrier film part from measurements in aqueous solutions. SE however gives quantitative estimations of barrier film thickness, porous film thickness, porosity and interface roughness by means of a two layer

model. All t quantitative characterizations of the film characteristics (film thickness, interface roughness, porosity) are in agreement with TEM observations.

The second part aims at the characterization of the sealing of the porous anodic film. In this case it is shown that EIS is capable to give qualitative and quantitative information as soon as the pores are completely sealed using an equivalent network which takes the barrier film, the porous film and the hydrated film into account.
SE proves to be more sensitive to the minute hydration effects at the beginning of the sealing treatment, but it is concluded that the technique is only capable of a qualitative investigation, as long as the refractive indices of the hydrated oxide are not determined in the visible light spectrum. However, it is clear that the qualitative ellipsometric differences, observed between a dry and a sealed spectrum can be linked with the structural evolution of the film as observed by TEM.

Yet, on of the most important conclusions of this thorough evaluation is that SE and EIS are mutually complementary techniques, that give accurate structural information.

E.H.D. IMPEDANCE STUDY FOR THE ELECTRODISSOLUTION OF COPPER IN ACIDIC CHLORIDE SOLUTIONS

E. D'ELIA [1], O.E. BARCIA [1,2], O.R. MATTOS [1]
N. PEBERE [3] AND B. TRIBOLLET [4]

1. Laboratorio de Corrosao "Prof. Manoel de Castro"
PEMM/COPP/UFRJ - Caixa Postal 68505 - CEP : 21945 - Rio de Janeiro - Brasil

2. Departamento de Fisico-Quimica - Universidade
Federal do Rio de Janeiro - Brasil

3. URA CNRS 445, Equipe de Métallurgie Physique, E.N.S.C.T.
118, Route de Narbonne - 31077 Toulouse Cédex - France

4. UPR 15 du CNRS, Physique des Liquides et Electrochimie
4, Place Jussieu - 75252 Paris Cédex 05 - France

Anodic dissolution of copper in chloride media has prompted numerous studies. It has been found that the dissolution is mass transport controlled and leads to the formation of $CuCl_2^-$. Nevertheless, the diffusion step has been ascribed by different authors either to Cl^- transport to the surface [1] or to the transport of $CuCl_2^-$ to the bulk solution [2-3].

The aim of this paper is to clarify this particular point to know the species involved during the electrodissolution of copper in the mass transport process and in addition, the present study was designed to further understanding of the behavior of the film formed on the copper surface.

The kinetic process of copper dissolution in acidic chloride solution 1M (pH = 0) was studied by steady-state and transient (electrohydrodynamical (EHD) impedance) techniques.

The steady-state current-voltage curves have presented a region of mixed kinetic and another of mass transport control characterized by a current plateau. The limiting current is $\Omega^{1/2}$ function in the whole range of rotation rate.

The EHD impedance diagrams were performed for the region of mixed kinetic, with galvanostatic regulation and, with potentiostatic regulation for the current plateau region. All results were reported in Bode coordinates, amplitude and phase shift versus the dimensionless frequency, p ($p= \omega/\Omega_0$).

As an example, in figure 1, the results were given for 5×10^{-4} A for different rotation rates. The EHD diagrams were reduced to a single curve. Therefore, the interface was uniformly accessible from the viewpoint of mass transport. Data analysis provides a Schmidt number of 2000. The diffusion species was likely to be $CuCl_2^-$. Indeed, the diffusion of Cl^- should lead to a Schmidt number of 500. Thus, the difference in Sc values is sufficiently high in order to conclude that $CuCl_2^-$ is the limiting diffusion species. This result was in agreement with the previous work of Deslouis *et al* [4] obtained only at anodic current lower than 1.5×10^{-4} A.

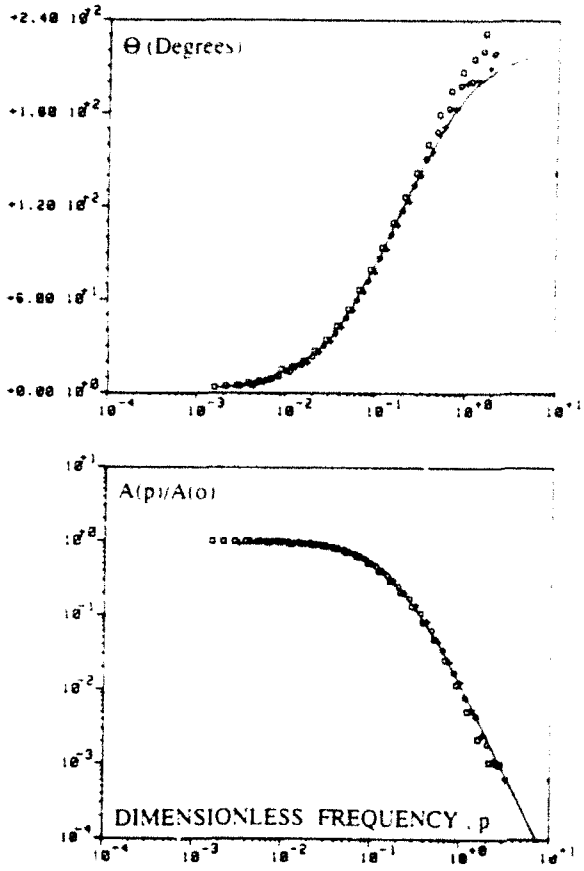

Figure 1 : EHD impedance with galvanostatic regulation below the diffusion plateau for different rotation rates (□) 120 rpm, (+) 240 rpm, (○) 480 rpm (___) theoretical curve for Sc = 2000

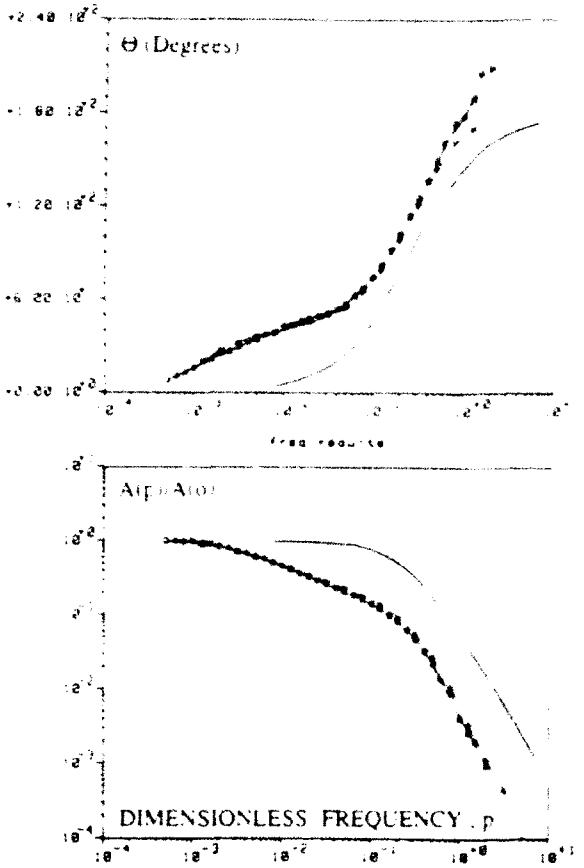

Figure 2 : EHD impedance with potentiostatic regulation on the diffusion plateau for different rotation rates : (+) 120 rpm, (□) 480 rpm, (○) 600 rpm (___) theoretical curve for Sc = 2000

The Schmidt number measured for different anodic currents is always 2000. This result clearly evidence that, below the anodic plateau, the limitation by mass transport is due to $CuCl_2^-$ and the limitation due to Cl^- does not occur.

The EHD impedance diagrams obtained on the current plateau were also reduced to a single curve (figure 2) whatever the potential. The experimental curves are different from the theoretical one obtained on a diffusion plateau with a pure diffusion control.

This result may be accounted for the presence of a salt layer covering the copper surface, the rate of formation of this layer being identical to the rate of dissolution.

REFERENCES

[1] M. Braun and K. Nobe, J. Electrochem. Soc. 126, 1666 (1979) and references cited therein.

[2] H.P. Lee and K Nobe, ibid., 133, 2035 (1986).

[3] A. Moreau, Electrochim. Acta 26, 1609 (1981) ; A. Moreau J P. Frayret, F. Del Rey and R. Pointeau, ibid 27, 1281 (1982).

[4] C. Deslouis, B. Tribollet, G. Mengoli and M.M. Musiani, J. Appl. Electrochem. 18, 384 (1988).

IMPULSE CHARGE (COULOSTATIC) RELAXATION METHOD APPLIED TO THE KINETIC STUDY OF A T40 TITANIUM ELECTRODE IN ACIDIC MEDIA

F. DEL REY*, J.P. FRAYRET*, T. JASZAY* and A. CAPRANI**

* Laboratoire de Mécanique des Fluides
URA 1217 CNRS
ECOLE CENTRALE DE NANTES
1 rue de la Noë, 44072 NANTES Cedex 03
FRANCE

** Laboratoire de Biorhéologie et d' Hydrodynamique Physicochimique
URA 343 CNRS - Université PARIS VII
2 place Jussieu, 75251 PARIS Cedex 05
FRANCE

In order to get the interfacial operational impedance, a full computerized apparatus had been set up, using an impulse charge (coulostatic) perturbation and the Laplace transform with a real parameter s [1].

It is constituted of 3 main elements : an analog module to control the cell and provide the coulostatic perturbation; a data acquisition module to capture the cell response with a variable set sampling; a signal processing module to compute the operational impedance.

The results obtained with a T40 electrode in 8N hydrochloric acid medium are similar when deduced from sinusoidal perturbation or impulse charge measurements. This validates the experimental set up and the coulostatic method for studying corrodible electrodes.

From the steady-state (I,E) curve, a dissolution-passivation mechanism for T40 titanium in 4N H_2SO_4 is proposed. It is similar to the Ti/HCl one [2] and involves 5 electrochemical and 2 chemical steps.

$$Ti(0) \xrightarrow{K_1} Ti(I) \xrightarrow{K_2} Ti(II) \xrightarrow{K_3} Ti(III) \begin{cases} \xrightarrow{k_4} Ti(III)_s \\ \xrightarrow{K_5} Ti(IV) \xrightarrow{k_6} Ti(IV)_s \end{cases}$$

The kinetic parameters associated to this model are calculated from an optimization method using the following relationship between current and potential :

$$I = \mathcal{F}\left(\frac{3k_4 + 4K_5}{1 + \frac{k_4 + K_5}{K_1} + \frac{k_4 + K_5}{K_2} + \frac{k_4 + K_5}{K_3} + \frac{K_5}{k_6}} \right) \qquad (1)$$

Despite the good agreement between the experiment and the computation under steady-state conditions, we may be doubtful about the validity of the model, particularly about the weight of the first two steps and the change in the reaction path.

Our purpose now is, by studying the operational impedance, to verify the validity of the model. Examples of the operational impedance are given on the following figure :

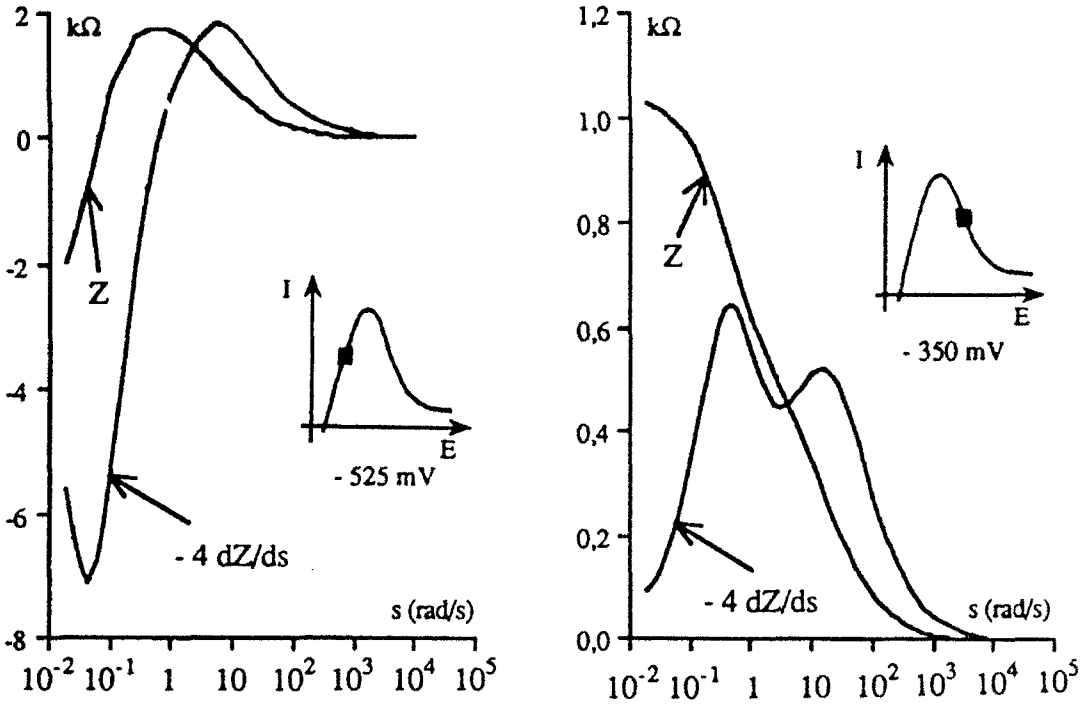

The R_tI product is a reliable information to remove indetermination. It may be calculated according to relation (2) :

$$R_tI = \frac{3\,k_4 + 4\,K_5}{k_4\,(b_1 + b_2 + b_3) + K_5\,(b_1 + b_2 + b_3 + b_5)} \qquad (2)$$

The computed b_5 coefficient has no physical significance for it is too great. Besides, the computed R_tI curve shows two plateaus in contrast to three on the experimental curve. Various assumptions can be made to account for this discrepancy ; the modification of the electrode structure at the most anodic potentials further to the formation of an amorphous titanium oxide is the one with the highest likelihood.

In the passivation range, it is suitable to provide information on phenomena ignored by steady state methods which necessarily leads to consider a new reaction mechanism.

REFERENCES

[1] - F. DEL REY - Thèse d'Etat - Nantes (1981)

[2] - A. CAPRANI and J.P. FRAYRET - J. Less Common Metals, 69, (1980), p. 29

IMPEDANCE DIAGRAMS OF CONCENTRATED SOLUTIONS OF AMMONIUM POLYSULFIDES IN LIQUID AMMONIA : AN ILLUSTRATION OF THE GERISCHER IMPEDANCE.

A. Demortier, E. Levillain, J.P. Lelieur
Laboratoire des Surfaces et Interfaces (URA 253 du CNRS)
H.E.I , 13, rue de Toul
F 59046 LILLE Cedex France

The coupling of an electron transfer reaction with homogeneous, reversible chemical reaction(s) leads to a specific type of impedance derived theoretically by Gerischer in 1951. This work has been extended by Sluyters to the mechanisms studied by Smith for ac polarography. According to a suggestion of Sluyters, we will name hereafter this type of impedance the "Gerischer impedance". The description of the origin of the Gerischer impedance appears in several textbooks, however, no experimental illustration has yet been given.

The purpose of this communication is to show that the solutions of ammonium polysulfides in liquid ammonia offer an experimental illustration of the Gerischer impedance.

The Gerischer impedance.

For a simple first order equilibrium coupled to an electron transfer reaction :

$$A \text{ <===> } O \qquad K = [O]/[R] = k_1/k_2$$
$$O + n\,e^- \text{ <===> } R$$

the faradaic impedance, for a stationnary electrode and in the case of semi-infinite linear diffusion, is given by :

$$Z = R_{ct} + \left(\sigma_R + \sigma_O \frac{K}{1+K}\right).(1-j)\omega^{-1/2} + \sigma_O . \frac{1}{1+K} . G(\omega,k)$$

where R_{ct}, σ_O, σ_R are respectively the charge transfer resistance, the Warburg coefficients associated to the equilibrium concentration of O and R, and $G(\omega,k)$ the function :

$$G(\omega,k) = \frac{2^{1/2}}{(k+j\omega)^{1/2}} = \left(\frac{\left(k^2+\omega^2\right)^{1/2}+k}{k^2+\omega^2}\right)^{1/2} - j \left(\frac{\left(k^2+\omega^2\right)^{1/2}-k}{k^2+\omega^2}\right)^{1/2}$$

with $k = k_1 + k_2$.

If the electroactive species O and R are involved in two, three ... equilibrium reactions, the faradaic impedance is given by :

$$Z_F = R_{ct} + Z_W + A_1.G(\omega,k_{G1}) + A_2.G(\omega,k_{G2}) + ...$$

The parameters A_1 , A_2 ...are function of the concentration of the electroactive species and of the equilibrium constants. The kinetic parmeters k_{G1} , k_{G2} ...are function of the rate constants of the chemical reactions. The experimental diagram will display two, three ... Gerischer impedances if the kinetic parameters k_G are significantly different. Figure 1 shows an example

Impedance diagrams of $(NH_4)_2S_n$-NH_3 solutions.

In a polysulfide ion, S_n^{2-}, the formal oxidation number of sulfur is -2/n. It has been shown that in liquid ammonia solutions the least reduced polysufide ion is S_6^{2-} and all the polysulfides ions are more or less disproportionated in acidic (NH_4^+) solutions. As a consequence, the redox level of the various solutions is always well defined. It has also been shown that, at the equilibrium potential, the electrochemical properties are governed by the monoelectronic transfer between the ion radical S_3^- and S_3^{2-} and that this reaction is strongly influenced by homogeneous equilibrium reactions.

It will be shown in this communication that according to the experimental conditions (temperature, concentration, stoichiometry) the $(NH_4)_2S_n$-NH_3 solutions display one, two, three Gerischer impedances. It will also be shown that a non linear least squares procedure can be used to derive impedance parameters from the experimental data. The discussion of the experimental data from the chemical point of view will be given in another paper.

Conclusion.

The observation of the Gerischer impedance(s) is limited by the double layer capacitance and by the freqency range available in the electrochemical impedance technique. As a consequence, the number of CEC systems which display the Gerischer impedance(s) are limited: the rate constants of the coupled chemical reactions have to be moderately fast.

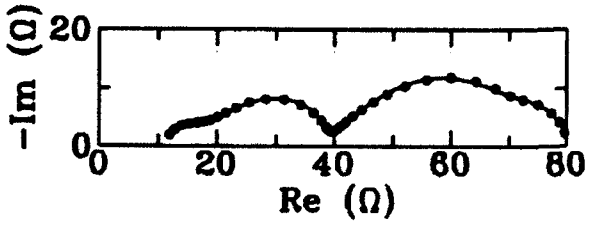

Figure 1. Impedance diagram of a 3.0 M $(NH_4)_2S_2$-NH_3 solution at 0°C. The diagram displays 3 Gerischer impedances.
o : experimental ; ——— best fit

FREQUENCY RESPONSE OF SMALL ELECTRODES TO HYDRODYNAMIC OR TO POTENTIAL PERTURBATIONS

C. Deslouis, O. Gil and B.Tribollet

UPR 15 du CNRS, "Physique des Liquides et Electrochimie", associé à l'Université P. et M. Curie, 4 Place Jussieu, 75252 Paris Cedex 05, France

INTRODUCTION

In order to take into account the mass transport in the analysis of electrochemical and engineering problems, the hydrodynamic electrodes [1,2] are widely used in the recent years.

Hydrodynamic electrodes and impedance techniques, though more complex to analyse theoretically, are very powerful, but only the rotating disk electrode had been extensively studied [3,4].

The present paper is concerned with non accessible electrodes, as channel electrodes, the forced convection being employed as a variable, by moving the solution over a stationary electrode embedded in the wall. These electrodes have been investigated mainly with a view to analytical applications [4] or to hydrodynamic measurements [5]. Impedance techniques corresponding to a perturbation of potential (or current) or of hydrodynamic will be considered.

In this paper, a mathematical treatment is presented on one hand for the diffusion impedance influenced by convection, when diffusion-convection becomes prevailing and on the other hand for the transfer function $H(f)$ between the mass transfer rate and the velocity perturbation. The response of rectangular, circular and bi-circular electrodes will be analyzed, the latter one having a greater practical importance in hydrodynamic.

EXPERIMENTAL VERIFICATION FOR THE CONVECTIVE DIFFUSION IMPEDANCE

The theoretical framework presented does not require a specific flow field but only that the wall velocity gradient α is known, that the electrode is small enough for ensuring a constant α value over its surface and also a negligible influence of a possible velocity component normal to the electrode plane. The chosen system is the flow in a circular pipe with circular platinum small electrodes embedded flush with the wall .The experimental diagrams, obtained at the half limiting current value, follow the theoretical one.

EXPERIMENTAL VERIFICATION FOR THE FREQUENCY RESPONSE TO A FLOW PERTURBATION

A well defined periodic flow is very difficult to obtain in a pipe or a channel, and the previous attempts with those flows were not completely successful [6,7].

The flow generated by a rotating disk, the angular velocity of which is sinusoidally modulated, is accurately known for both amplitude and phase. However, with this flow geometry, the instantaneous direction of the velocity vector being not aligned with the time average one except for very low frequencies, the comparison between theory and experiment was limited to circular microelectrodes [8].

For extending the validity of the theoretical predictions and checking the response of rectangular probes, a similar experimental study with a modulated flow in a cone-and-plate system was carried out [9]. In the absence of secondary flow, this system provides indeed a one-dimensional velocity field in the circumferential direction. First, an analysis of the sinusoidally modulated laminar flow in small oscillations for this system is reported. The resulting effect on mass transfer is then deduced and the relevant variations with frequency further compared to the experimental data relative to circular or rectangular probes.

APPLICATION TO HYDRODYNAMIC

The experiments were conducted on a fully turbulent flow in a two dimensional rectangular channel. The diffusion current in the electrolysis cell was measured by means of a current follower. The spectrum analyzer used (Hewlett Packard 5451 C) allows the signal to be analyzed in a wide frequency range (10^{-4} - 5.10^{4} Hz).

By measuring simultaneously the currents $\tilde{I}_1$ and $\tilde{I}_2$ on each part of the bi-circular microelectrode ,we are able to analyse their sum and their difference .

So, the power spectral density of the longitudinal velocity gradients fluctuations W_α and the power spectral density of the transverse velocity gradient fluctuations W_β can be obtained through the relationships :

$$W_\alpha = \frac{1}{|H_X(f)|^2} W_{I_1 + I_2} \qquad \text{and} \qquad W_\beta = \frac{1}{|H_Z(f)|^2} W_{I_1 - I_2}$$

Where $H_X(f)$ and $H_Z(f)$ are the hydrodynamic transfer functions for the longitudinal and transverse velocity components respectively.

REFERENCES

[1] C.M.A. Brett and A.M.C.F. Oliveira Brett, "*Hydrodynamic electrodes*" in Comprehensive Chemical Kinetics, Vol 26, edited by C.H. Bamford and R.G. Compton pp 355-441 (1986) .

[2] P.R. Unwin and R.G. Compton, "*The use of channel electrodes in the investigation of interfacial reaction mechanisms*" in Comprehensive Chemical Kinetics, Vol 29, edited by R.G. Compton, pp173-296 (1989) .

[3] B.Tribollet and J.Newman, J. Electrocem. Soc., **130**, (1983) , 822 .

[4] C. Deslouis and B. Tribollet, "*Flow modulation techniques in electrochemistry*" in Advances in Electrochemical Science and Engineering, Vol 2, edited by H. Gerischer and C. W. Tobias , pp 205-264 (1991) .

[5] T.J. Hanratty and J.A. Campbell, "*Measurement of wall shear stress*" in Fluid Mechanics Measurments, edited by Goldstein, Hemishere, Washington (1983) .

[6] G. Fortuna and T.J. Hanratty, Int. J. Heat Mass Transfer, **14**, (1971), 1499 .

[7] A. Ambari, C. Deslouis and B.Tribollet, Int. J. Heat Mass Transfer, **29**,(1986), 35 .

[8] C. Deslouis, O. Gil and B. Tribollet , J. Fluid Mech., **215** , (1990), 85 .

[9] C. Deslouis, O. Gil and B. Tribollet , Int. J. Heat Mass Transfer, **33**, (1990), 2525

IMPEDANCE ANALYSIS OF THE KINETICS OF ELECTROCHEMICAL PROCESSES MEDIATED BY POLYMER LAYERS

C.DESLOUIS[1], M. M. MUSIANI[2], B. TRIBOLLET[1]

1-UPR 15 du CNRS, "Physique des Liquides et Electrochimie", Paris, France.

2-Istituto di Polarografia ed Elettrochimica Preparativa, CNR, Padova, Italy.

INTRODUCTION

Several factors complicate the kinetic analysis of electrochemical reactions occurring at polymer modified electrodes :
- the presence of two interfaces (metal/polymer, polymer/electrolyte),
- the occurrence of the electron exchange reaction over a variable depth of the polymer film,
- the yet unclear nature of charge transport in polymer films.

We have earlier presented a calculation of the ac and EHD impedance of a mediated reaction occurring exclusively at the polymer-electrolyte interface, based on the assumption that the electron exchange reaction could be split in two electrochemical half reactions [1]. We examine here the possibility of calculating the ac impedance of the same system by describing electron exchange by a chemical reaction and charge transport by electron hopping. Such an approach has, in principle, the advantage that it may be extended to situations in which electron exchange occurs over any depth from 0 to the whole film thickness ϕ (including direct reaction on the metal).

MODEL

The polymer contains fixed redox centres, either reduced (P) or oxidized (Q), and is permeated by the electrolyte so that, in the absence of any current the substrate Ox/Red is present at all x at its bulk concentration.

At the metal-polymer interface both couples may undergo electrochemical reaction following Butler-Volmer kinetics :

$$i_{P/Q} = C_P(o)\, k_{f1} \exp \frac{\alpha_1 F}{RT}\,\eta \; - \; C_Q(o)\, k_{b1} \exp - \frac{(1-\alpha_1)F}{RT}\,\eta \qquad (1)$$

$$i_{Red/Ox} = C_{Red}(o)\, k_{f2} \exp \frac{\alpha_2 F}{RT}\,\eta \; - \; C_{Ox}(o)\, k_{b2} \exp - \frac{(1-\alpha_2)F}{RT}\,\eta \qquad (2)$$

where η is the electrode potential measured with respect to the equilibrium potential of Ox/Red.

Gradients of both polymer and substrate redox centres are given by :

$$i = i_{P/Q} + i_{Red/Ox} = F\,(D_E \left.\frac{\partial C_P}{\partial x}\right|_o + D_f \left.\frac{\partial C_{Red}}{\partial x}\right|_o) \qquad (3)$$

where D_E is the so-called diffusion coefficient of electrons, and D_f the diffusion coefficient of Red/Ox in the film.

In the polymer film, electron transport by hopping and chemical reaction between P/Q and Red/Ox occurs, so that :

$$\frac{\partial C_P}{\partial t} = - K_F C_P C_{Ox} + K_B C_Q C_{Red} + D_E \frac{\partial^2 C_P}{\partial x^2} \qquad (4)$$

$$\frac{\partial C_{Ox}}{\partial t} = - K_F C_P C_{Ox} + K_B C_Q C_{Red} + D_f \frac{\partial^2 C_{Ox}}{\partial x^2} \quad (5)$$

The stationary concentration profile of C_{Ox} becomes :

$$C_{Ox}(x) = \frac{C_\infty}{\cosh \frac{\phi}{x_r}} \frac{\frac{K_F C_P - K_B C_Q}{K_F C_P + K_B C_Q}}{1 + \frac{D_f \delta}{x_r D_s} \tanh \frac{\phi}{x_r}} \cosh \frac{x}{x_r} + \frac{2 C_\infty K_B C_Q}{K_F C_P + K_B C_Q} \quad (6)$$

where x_r is the depth over which a net exchange reaction occurs, K_B and K_F the backward and forward rate constants of the chemical reaction. The faster is the mediation reaction, the thinner is x_r and the smaller the difference between $C_{Ox}(\phi)$ and $C_{Ox}(o)$.

IMPEDANCE

The ac impedances are calculated by assuming that i and E undergo sinusoidal variations, so that, e.g. :

$$E = \bar{E} + Re\,(\tilde{E} \exp j\omega t) \quad (7)$$

By differentiating Eq. (1) :

$$\tilde{i} = \tilde{i}_{P/Q} = A_1 \tilde{C}_P(o) + R_t^{-1} (\tilde{E} - R_E \tilde{i}) \quad (8)$$

where :

$$A_1 = k_{f1} \exp \frac{\alpha_1 F}{RT} \eta + k_{b1} \exp - \frac{(1-\alpha_1)F}{RT} \eta \quad (9)$$

$$R_t^{-1} = \frac{F}{RT} [\, \alpha_1 k_{f1} C_P(o) \exp(\alpha_1 F \bar{E}/RT) + (1-\alpha_1) k_{b1} C_Q(o) \exp - (1-\alpha_1) F \bar{E}/RT \,] \quad (10)$$

R_E is the uncompensated electrolyte resistance. The ac impedance becomes :

$$\frac{\tilde{E}}{\tilde{i}} = R_E + R_t + \frac{Z_D + \frac{1}{C_{LF}} \frac{\phi^2}{D_E} \frac{\tanh s_1^{1/2}}{s_1^{1/2}}}{1 + Z_D C_{LF} \frac{D_E}{\delta^2} s_1^{1/2} \tanh s_1^{1/2}} \quad (11)$$

where $C_{LF} = F\phi/A_1 R_t$ is the polymer redox capacitance, $s_1 = j\omega\phi^2/D_E$, and Z_D is the convective diffusion impedance for an infinitely fast reaction.

Eq. (11) has the same form as the ac impedance expression given in ref. [1], except that charge transfer resistances relative to the polymer/electrolyte interface cannot appear here. Simulated impedance diagrams reproduce fairly well the diagrams experimentally observed for some redox and conducting polymers [2,3,4].

REFERENCES

1. C. Deslouis, M. M. Musiani, B. Tribollet, J. Electroanal. Chem., 264, 37 (1989).
2. C. Deslouis, M. M. Musiani, B. Tribollet, J. Elec troanal. Chem., 264, 57(1989).
3. C. Deslouis, M. M. Musiani, B. Tribollet, Synth. Met., 38, 195 (1990).
4. C. Deslouis, J.F. Equey, M. M. Musiani, B. Tribollet, 3ème forum Impédances Electrochimiques, Montrouge, France, 1988. Proceedings, Vol. p. 151.

A STUDY OF THE PHOTOANODIC DISSOLUTION OF CdS WITH ELECTRICAL AND OPTO-ELECTRICAL IMPEDANCE SPECTROSCOPY

A. R. de Wit, D. Vanmaekelbergh, and J. J. Kelly
Debye Research Institute, University of Utrecht
P.O. Box 80.000, 3508 TA UTRECHT, The Netherlands

In the present work we used electrical and opto-electrical impedance methods to investigate the competition between anodic decomposition and recombination occurring at the illuminated n-CdS/electrolyte interface. A model is presented to account for this competition. The electrical and optoelectrical impedance results are interpreted on the basis of this model.

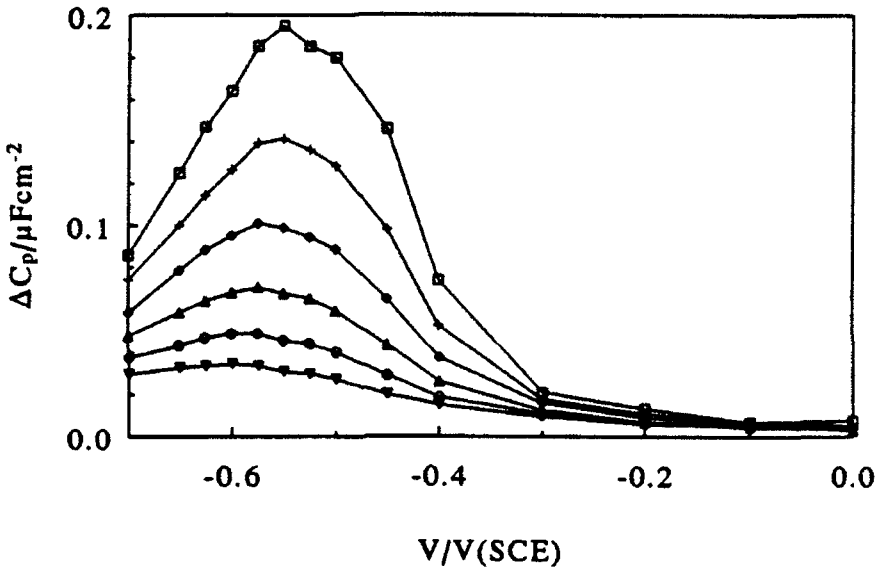

Fig. 1 The potential dependence of ΔCp of a CdS electrode under illumination (i_h = 21.6 $mAcm^{-2}$) - (□) 158 Hz, (+) 251 Hz, (◇) 398 Hz, (△) 631 Hz, (○) 1000 Hz, (▽) 1585 Hz.

In the potential range between -0.4 and -0.7 V(SCE) the measured parallel equivalent capacitance C_p is increased by illumination. Fig. 1 shows the additional capacitance ΔC_p (the difference between the values under illumination and in the dark) as a function of the applied potential. A maximum (ΔC_p^{max}) can be observed at about -0.55 V(SCE). The value of ΔC_p^{max} increases when the measuring frequency ω is decreased. The plot of ΔC_p^{max} versus the limiting photocurrent density (i_h) at a fixed frequency is linear and passes through the origin.

In the case of opto-electrical impedance the intensity of the incident light is modulated with a frequency ω. In fig. 2a real and imaginary components of the resulting photocurrent measured in the limiting photocurrent range are shown in the complex plane; a semicircle in the negative imaginary plane was found, indicating that electron excitation occurs during photo-anodic dissolution. Results are also shown in fig.

2a for three different potentials in the recombination region. Flattened semi-circles are found with a high frequency limit which depends only slightly on the potential. It should be noted that the high frequency limit of the semicircle due to electron excitation is almost the same as that of the flattened semicircles resulting from recombinatio This indicates that at high frequencies, recombination and excitation processes are too slow to follow the light intensity modulation. When the constant light intensity is increased, similar semicircles are found but ω_{max} shifts to higher frequencies. Fig. 2b shows a plot of the ω_{max} versus the hole current density measured at three different potentials in the recombination region. A linear dependence of ω_{max} on i_h is observed, also at potentials where the dc recombination is complete. It is surprising that the slope of the plots increases with decreasing potential.

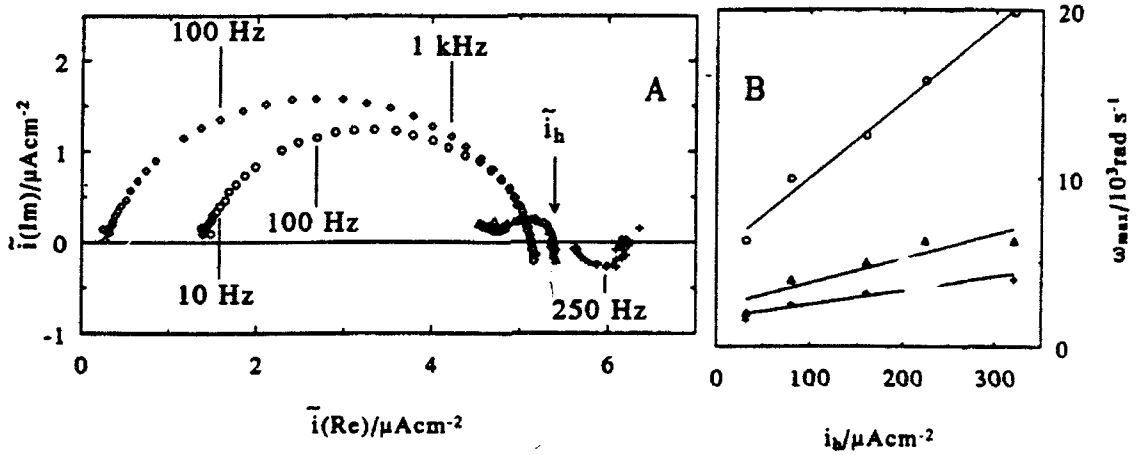

Fig. 2 a: Complex plane plot of i for an illuminated CdS electrode (i_h = 80 mAcm-2) at various potentials - (+) 0.0 V, (△) -0.4 V, (o) -0.5 V, (◇) -0.6 V. b: The dependence of ω_{max} on the hole current density (i_h) in the recombination region, - (+) -0.4 V, (△) -0.6 V, (o) -0.8 V.

Both the electrical and the opto-electrical impedance results indicate that recombination of electrons and holes occurs predominantly at the surface. A model is proposed to account for the observed phenomena. The first step of the dissolution involves the formation of an intermediate X_1 which is formed by hole capture in a surface bond. Dissolution takes place when a second hole is captured or an electron is excited to the conduction band. At cathodic potentials X_1 can capture an electron resulting in a cathodic recombination current. An interesting point concerns the quantitative interpretation of the opto-electrical impedance measured in the recombination region. We found that ω_{max} is only slightly dependent on the electrode potential but increases strongly with increasing light intensity. This effect cannot be explained by assuming that modulation of the incident light intensity leads only to a perturbation of the minority carrier concentration. A perturbation of the surface charge (X_1) and hence of the potential distribution over the semiconductor/electrolyte interface must be taken into account. An unexpected result is that the capacitance of the Helmholtz layer at the CdS/electrolyte interface could be determined from the opto-electrical impedance results.

Characterization of Chromate Conversion Layers on Al-Alloys by Electrochemical Impedance Spectroscopy (EIS) and Optical Measurements

D. Ende and W. Kessler
Institut für Angewandte Forschung, FH Reutlingen, Alteburg-straße 150, D-7410 Reutlingen, Germany

D. Oelkrug
Institut für Physikalische Chemie, Universität Tübingen, Auf der Morgenstelle, D-7410 Reutlingen, Germany

R. Fuchs
Alusuisse Lonza GmbH, Bad. Bahnhofstraße 16, CH-8212 Neu-hausen, Switzerland

Abstract

Chromate conversion layers on Al-alloys of a thickness ranging from 20 - 250 nm are characterized by EIS in 0,1M Na_2SO_4 at Ecorr. Figure 1 represents an EIS-spectrum with two time constants of a chromated AlMn05Mg05 sheet with a layer thickness of 250 nm.

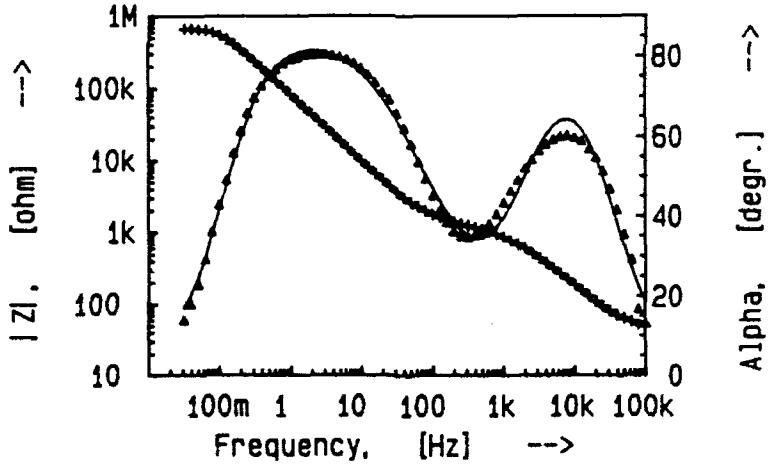

Figure 1: Bode plot of a chromated alumium sheet. Film thickness: 250 nm, solution: 0,1 M Na_2SO_4, open circuit delay: 2000 sec at E_{corr}

A model is derived from these data which describes the mechanism of the corrosion of the samples. Assuming a duplex layer explains the EIS data best. This implies a transititon .palayer between the alloy and the protective layer. The property of this barrier layer depends on the alloy composition and the chemical treatment. In the initial

phase of the chromatation, patches of thin films are spread over the surface. These patches grow to a homogeneous highly protective layer. At longer treatments partial disolution of the chrome phosphate crystals takes place with a simultaneous corrosion of the layer. The result is a porous film showing a higher active metal surface also proposed by Losch in case of phosphated steel [1]. Electrogenerated luminescence confirms this model independently to EIS. In the electrochemical model, the penetration velocity of the corrosive medium may be represented by 1/Rs (Rs = coating resistance) and the active area for the charge transfer may be interpreted by 1/Rp (Rp = polarisation resistance). The corrosion of the alloy is therefore the superposition of these two effects resulting in a "bath tub" function as shown in figure 2.

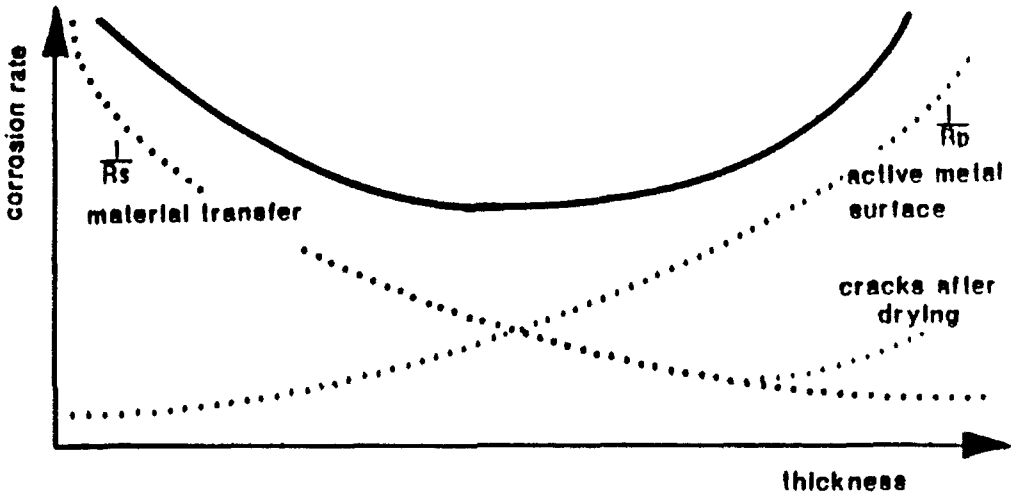

Figure 2: Superposition of the protective effect of coating thickness and the destructive effect of defect sites in a chromated aluminium alloy.

Refereces

[1] A. Losch, technical note in Werkstoffe und Korrosion **42**, 441 (1991)

The EHD impedance diagrams show that the curves obtained at different speeds of rotation, for all solutions, are reduced to one by the dimensionless frequency $p=\omega/\Omega$, where ω is the perturbation frequency. This result corresponds to the kinetic behavior of a uniformly accessible electrode. When the viscosity increases, the curves are more and more translated towards the lower p values, with an increase in the Schmidt number. The Schmidt number obtained with EHD impedance (8000 without glycerol, 15000 for 1M and 25000 for 2M) is higher than the values in the bulk solution (1200 for 0M, 2500 for 1M and 3900 for 2M). This is a clear indication of the existence of a viscosity gradient from the solid interface to the bulk solution. The analysis method for the EHD results are similar with and without glycerol. The simulation of the results for 1M and 2M in glycerol can be performed based in the mathematical model already presented for 0M in glycerol [1].

In agreement with our previous results [1], the steady-state and EHD impedance curves can be explained by the effect of the mass transport by diffusion, convection and migration in the solution. No information about the nature of the interface (bare electrode or electrode covered with a salt film) can be obtained with these techniques, an in-situ optical measurement could be a way to conclude on this last controversial point.

CONCLUSIONS

The mass transport mechanism of iron in sulfate medium is not changed by 1M or 2M glycerol additions. With or without glycerol the iron-sulfate system behaves as a uniformly accessible electrode.

The current instabilities at the beginning of the plateau region are strongly influenced by the medium viscosity and can be eliminated when the viscosity increases. This implies that these instabilities are a process governed by the hydrodynamic conditions near the electrode interface.

ACKNOWLEDGMENTS

This paper was developed by a contract n° 115/90 CAPES (Brazil)-COFECUB (France).

REFERENCES

1. O. E. Barcia, O. R. Mattos and B. Tribollet, J.Electrochem.Soc., 139 , 446 (1992).
2. B.Tribollet and J.Newman, J.Electrochem.Soc., 130 , 2016 (1983).
3. P. Russell and J. Newman, J.Electrochem.Soc., 133, 2093 (1986).
4. J.R.R.M. Ferreira, M. Sc Thesis, PEMM/COPPE/UFRJ.

IRON DISSOLUTION UNDER MASS TRANSPORT CONTROL: THE EFFECT OF VISCOSITY

J.R.R.M. Ferreira[1], O.E. Barcia[1,2], O.R. Mattos[1] and B. Tribollet[3]

1-Laboratório "Prof. Manoel de Castro" - EE/UFRJ and PEMM/COPPE/UFRJ, Caixa Postal 68505, CEP:21945, RJ, Brazil.
2-Depto de Físico-Química - IQ/UFRJ, Rio de Janeiro, Brazil.
3-UPR15 du CNRS, Physique des Liquides et Electrochimie, 4 place Jussieu, 75252 Paris Cedex 05, France.

INTRODUCTION

Recently, Barcia et al [1] have studied iron dissolution in high anodic overpotential, for a rotating disk electrode under mass transport control in 1M of sulfate, pH=0. The authors have studied the system by polarization curves and electrohydrodynamical (EHD) impedance [2] and these results have indicated that on one hand the interface of the iron dissolution under mass transport control is uniformly accessible and on the other hand the presence of an important viscosity gradient localized in the diffusion layer.

In this paper the influence of the viscosity of the medium, changed by glycerol additions, on the polarization curves and EHD impedance diagrams for iron dissolution in sulfate medium at pH=0 is studied. The viscosity effect on the current oscillations observed at the beginning of the plateau is also considered.

EXPERIMENTAL RESULTS AND DISCUSSION

The anodic polarization curves for an iron electrode in sulfate 1M, pH=0, shows for a high overpotential a current plateau for each rotation speed (Ω). At the beginning of the plateau a current oscillation process is noted [3]. This process is a function of Ω and is observed only in a very precise potential range for each polarization curve. The limiting currents decrease when the viscosity increases and it is possible to note the absence of current oscillations for 100 rpm at 2M in glycerol.

The current-time waveform obtained for different potentials, within the range where the oscillations process occurs, shows that this process is a function of potential. From the beginning to the end of the current instabilities, the oscillation spectrum becomes more complex with increasing potential, and the transition from current instabilities to a continuous value is very abrupt without glycerol. 1M of glycerol changes significantly the oscillation diagrams, the oscillation spectrum is less complex than the spectrum without glycerol and the transition from current instabilities to a continuous value is smooth. 2M is able to eliminate the oscillations completely for 100 rpm. The FFT analyses in progress will give a better characterization of these instabilities [4].

INVESTIGATION OF THE ELECTROCHEMICAL OXIDATION OF COPPER IN MOLTEN NH_4HF_2-HF

Denis J.-F. Filliaudeau and Gérard S. Picard

Laboratoire d'Electrochimie Analytique et Appliquée
(Unité associée au C.N.R.S., URA n°216)
Ecole Nationale Supérieure de Chimie de Paris
11, rue Pierre et Marie Curie - 75231 Paris Cedex 05 (France)
Tel : 43 54 53 84 - FAX : 44 27 67 50

Introduction

Fluorine and nitrogen trifluoride can be prepared from electrolysis of molten NH_4HF_2-HF mixtures . Various studies are actually in progress to look for a good anodic material for realizing the electrowinning of F_2 and NF_3 . In order to test electrochemically the anode material, a reference electrode is needed . The electrochemical oxidation of copper, which appeared to be a good candidate, was investigated in molten NH_4HF_2-HF mixtures at room temperature by linear sweep voltammetry (LSV) and electrochemical impedance spectroscopy (EIS) .

Technical

Experiments were carried out in a 1.37HF-NH_4HF_2 mixture at 25°C . The electrolytic cell was made of altuglass . The working electrode was a pure copper wire covered with Teflon (surface area = 0.0078 cm^2) and the counter electrode was a nickel plate with a large surface area . The reference electrode was a copper wire dipped into the melt , into a Teflon cylinder closed by porous Teflon .

Voltammetric experiments were performed with a EG&G PAR Model 273 potentiostat-galvanostat connected to an IBM microcomputer . EIS experiments were performed with this potentiostat coupled to a Schlumberger Model SI 1255 frequency response analyser .

Main experimental results

A preliminary linear sweep voltammetric study has shown the complex character of the oxidation mechanism of copper in molten NH_4HF_2-HF mixture (figure 1) , probably involving ohmic loss , diffusion and adsorption-desorption processes depending on the potential range . This paper deals only with the initial steps of the copper oxidation for low overvoltages .

A semilog analysis applied to i/E curves , resulting from the semi-integration of voltammograms obtained with various scan rates , shows that the first step of the anodic oxidation corresponds to the exchange of one electron . Figure 2 shows the evolution of impedance spectra with the overvoltage . A diffusional step , corresponding to soluble species (Cu(I)) , is evidenced (figure 2a) and , when the overvoltage increases , capacitive and inductive loops , involving adsorption or precipitation processes , appear (figures 2b,c,d) .

Acknowledgement

This work was supported by COMURHEX (Société pour la conversion de l'uranium en métal et hexafluorure) . The authors thank Professor B. Trémillon and Dr. F. Nicolas for their interest in this work, and one of them (D. F.) thank the French Ministry of Research and Technology for providing a doctoral grant .

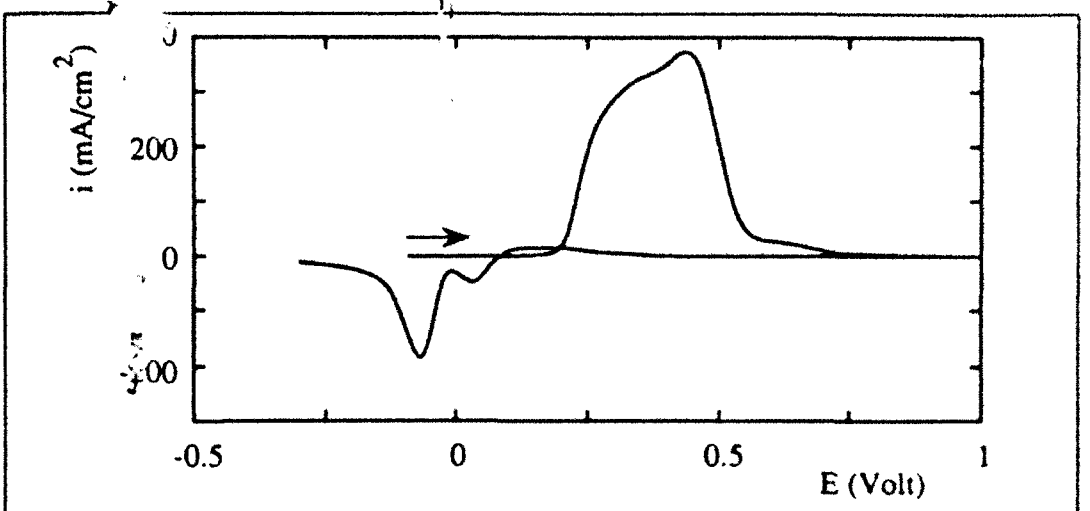

Figure 1 : Linear sweep voltammogram at Cu electrode in a 1.37HF-NH_4HF_2 mixture at 25°C (scan rate : 0.1 V.s^{-1})

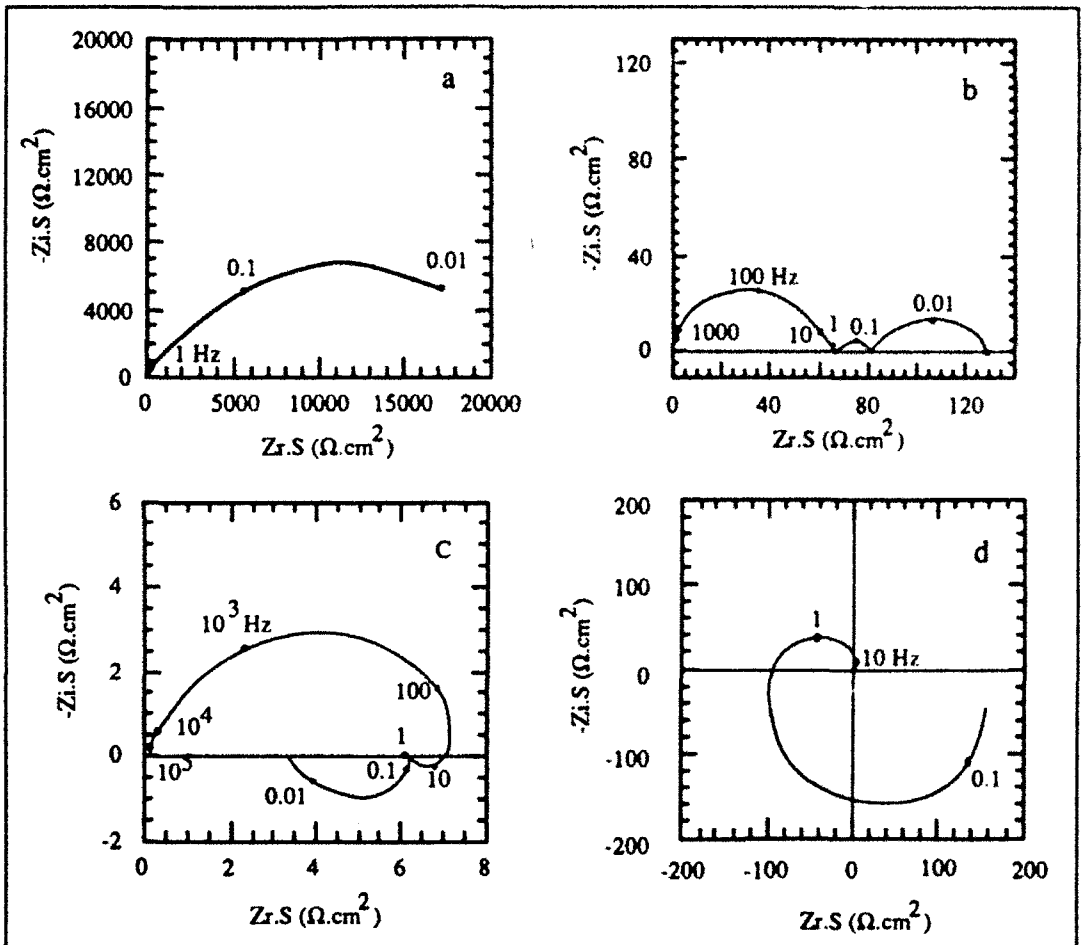

Figure 2 : A.C. Impedance spectroscopy in the 1.37HF-NH_4HF_2 mixture at 25°C ; Nyquist plots obtained with a Cu working electrode at various applied potentials : a) 0 V ; b) 0.08 V ; c) 0.1 V ; d) 0.2 V

AN IMPEDANCE INVESTIGATION OF THIN OXIDE LAYERS ON PURE ALUMINIUM AND OF THEIR WATER CONTENT.

A. FRICHET*, P. GIMENEZ* and M. KEDDAM**

* Centre de Recherche de Voreppe (Groupe Péchiney).
BP 27-38340 VOREPPE France.
** UPR 15 CNRS "Physique des Liquides et Electrochimie"
Université P. & M. Curie - 4 Place Jussieu - 75252 PARIS CEDEX 05 France.

INTRODUCTION.

Several important applications of pure aluminium thin foils (corrosion resistance, adhesion of polymers for bonding and coating technologies...) are recognized as strongly dependent upon the water content of the oxide layer grown spontaneously during processing and storage of the material. a.c. impedances were assessed as a way of evaluating the amount of water in these films with a view to develop a practical test.

EXPERIMENTAL.

Degreasing, etching, chemical brightening produced on pure aluminium a very thin oxide layer (10 to 30 Å thick as measured by ellipsometry).
Impedance measurements (4 kHz - 10 mHz) were performed with a Schlumberger-Solartron equipment (1186 + 1253) . Electrolytes were either aqueous (Na_2SO_4 or NH_4 tartrate) or organic (*Ethanol* + $Zn(NO_3)_2$ *and* THF + Li ClO_4). Samples were potentiostatically maintained at their spontaneous rest potential.

Impedances were basically capacitive. Most relevant informations are drawn from the Cole-Cole plot : $C = C' + jC''$ of C, the capacitance equivalent to the interface impedance $Z = \frac{1}{j\omega C}$.

RESULTS.

Oxide layers with various amounts of water were investigated. The main features of the impedance plots are independent of electrolyte composition. Their Cole-Cole plot displays a high frequency real limit C_{inf} and a broad frequency dispersion. The low frequency tail suggests the existence of a real low frequency limit C_0. The curve can be assimilated to a circle centered well below the real axis (Cole-Cole dispersion law).They were fitted by a least square procedure providing an extrapolated estimate for C_0

De-hydration = in order not to induce structure changes in the layer, water content was decreased simply by vacuum processing (room temperature, 10^{-1} Pa, 64 hours). The thickness is not modified. Impedance measurements were performed in ethanol+0.44M $Zn(NO_3)_2$.

Fig. 1 below shows a comparison of the Cole-Cole plots obtained before and after vacuum processing. Solid line are fits to Cole-Cole circular diagrams. The general shape is not modified by the amount of water in the film whilst C_0 and C_{inf} are clearly increased.

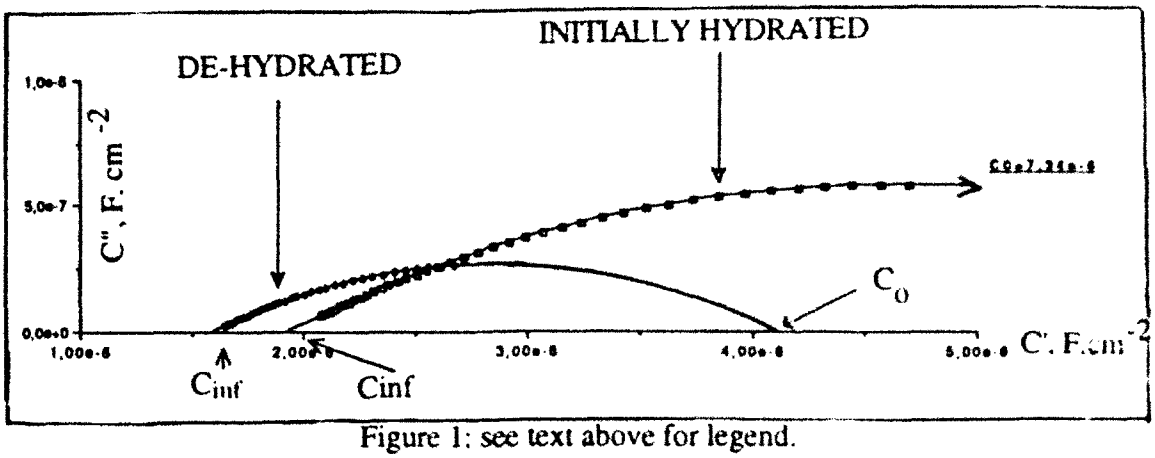

Figure 1: see text above for legend.

Hydration : . Both C_{inf} and C_0 are increased by water immersion of the film (20°C) not producing film growth.

MODELLING OF CAPACITANCE DISPERSION and DISCUSSION.

Interpretation of the Cole-Cole dispersion by a microscopic distribution of time constants in a macroscopically homogeneous material was rejected in the present study since C_{inf} yields a dielectric constant ε_r significantly lower than 9 (value for Al_2O_3). A series connection of two capacitors C_0 and C^{ox} corresponding to a sandwich structure of the layer was explored as an alternative possibility. This decomposition is supported by the values of ε_r close to 9 (ranging from 8.77 to 9.5 within the experimental errors). In this case consistency with the Cole-Cole dispersion behaviour implies that C^{ox} must obey a Jonscher type dispersion law:

$$C^{ox} = C^{ox}_{inf} + \frac{B}{(j\omega)^{1-n}}$$

C_0 must be considered as the capacitance of an outer layer with negligible frequency dispersion. C_{inf} simply arises from the series connection of C_0 and C^{ox}_{inf}.

- The more consistent interpretation of the whole body of experiments, dealing with role of solvent, electrolyte, temperature on the capacitance parameters, is a sandwich structure of the alumina film represented by a series connection of :

. a constant capacitor C_0 standing for the outer layer and depending upon water content and solvent nature but not influenced by the nature of ionic component of the electrolyte.

. a capacitor C^{ox} of the bulk oxide exhibiting a Jonscher type dispersion. The HF limit of C^{ox} can be regarded as resulting from the dielectric behaviour of a rigid Al_2O_3 lattice not altered by water content whilst the dispersion term is increased by the amount of water incorporated to the oxide and is thermally activated.

Common practice of thickness determination based on capacitance measurements is likely to be incorrect but a-c impedance proved to be a suitable technique for investigating the hydration of very thin oxide layers on pure aluminium.

THE INFLUENCE OF EXTENDER PIGMENTS ON THE PERFORMANCE OF ETHYL SILICATE ZINC RICH PAINTS

F.L.Fragata[1], C.R.S.Mussoi[1], C.Moulin[2], I.C.P.Margarit[2], O.R.Mattos[2]

1-CEPEL-Centro de Pesquisas de Energia Elétrica
2-Lab. de Corrosão "Prof. Manoel de Castro", EE/UFRJ and COPPE/UFRJ, Caixa Postal 68505, CEP 21945, RJ, Brasil.

INTRODUCTION

Zinc rich paints are one of the most effective coatings for anticorrosive protection of iron surfaces, especially in strongly agressive environments. Good performences have been observed whether if the zinc rich primes are applied in atmospheric or total immersion conditions.

Although the metallic zinc content is the parameter focused in most technical specifications, it is known that this is not the only factor wich determines the zinc rich paints performance (1-5). Amongst the various binders normally used in zinc rich primers, it seems to be the general consensus that the ethyl silicate based paints is the one that provides best performance.

Concerning the ethyl silicate paints, the minimum metallic zinc content specified is, in general, about 75%w, in the dry film. To apply this condition, the solids balance can be done by two different ways:

- using only the zinc powder and the binder, or
- using the zinc powder, the binder and some other auxiliary pigments, with a view to obtaining films of higer PVC (Pigment Volume Content).

In respect to this latter alternative, different auxiliary pigments may be used. Some producers include chromium oxide or iron oxide to proportion contrast between the paint and the substrate to be painted. Others, for technical reasons, include mineral fillers as for instance barite,mica, talc.

As a consequence of the presence of pigments other than zinc powder, a question has arise concerning interferences of these pigments on the zinc galvanic action over the steel substrate. The aim of this paper is to analyse this question. Using electrochemical techniques, salt-spray and field exposure tests, the paper describes a study on the performance of specially formulated paints where the mettalic zinc content in the dry film is the same, with and without extender pigments.

EXPERIMENTAL

The paints were prepared with 75% and 60%w of zinc powder (95,1% metallic zinc), 7μm average particle size. The first zinc content (75%) is the classical quantity used in the zinc rich paints. The second zinc content (60%) was used for testing the influence of the total PVC on the anticorrosive properties of the paints with lower zinc contents in the dry film.

For each zinc content three kinds of paints were produced: one with only zinc powder and resin, another with zinc powder resin and agamaltolite (aluminium and potassium hidrated silicate; 350 mesh) and the third paint with zinc powder, resin and barite (barium sulfate; 500 mesh).

CONCLUSION

All experiments performed clearly showed that filler additions can, at least in some cases, improve the corrosion protection offered by zinc rich paints, instead of causing harmful effects on it. However, it is important to remember that the final performance of zinc rich primers, in a paint system, do not depend only on electrochemical features of the film but, on the equilibrium of electrochemical and physical properties as for instance flexibility, cohesion and adherence.

REFERENCES

1-Charles G. Munger, "Corrosion Prevention by Protective Coatings", NACE ed., 2nd edition, 1986
2-S. A. Lindquist, L. Mészáros and L. Svenson, JOCCA, 68(1), p.10, 1985.
3-F. L. Fragata, M. Zebrão and C. T. Serra, Corrosão e Proteção de Materiais, 6, p.12, Lisboa, 1987.
4-B. Del Amo and C. A. Giúdice, XI Int. Corros. Congress, 2, p.347, Florence, 1990.
5-D.Pereira, J. D. Scantlebury, M. G. S. Ferreira and M. C. Almeida, Corrosion Science, 30(11), p.1135, 1990.

ACETYLENIC DERIVATIVES AS INHIBITORS OF ARMCO IRON ACID CORROSION

A. Frignani, M. Tassinari, C. Monticelli, G. Trabanelli

Corrosion Study Center "A. Daccò",
Chemistry Department, University of Ferrara
46 L. Borsari, 44100 Ferrara, Italy.

Electrochemical Impedance Spectroscopy (EIS) is applied to study Armco iron corrosion in N_2 purged 1 N H_2SO_4 at 70 °C, in the presence of some acetylenic compounds: 3-methyl-1-butyne (3M1B) derivatives

Y = $-O-CH_2-CH_2-O-H$, X = H (H1); Cl (C1); Br (B1); I (I1)

Y = $-O-H$, X = Cl (C2); Br (B2); I (I2)

or

1-octyn-3-ol (OCT).

The following techniques are used: analysis of dissolved iron as a function of time (SA), recording of the potentiodynamic (0.5 mV s^{-1}) polarization curves (PC), and EIS measurements (+/- 5 mV rms applied sinusoidal perturbation; 10^4-10^{-2} Hz; 5 frequencies per decade; 10% standard deviation).

In the case of 3M1B derivatives, the substitution of the acetylenic H atom with Cl, Br or particularly I improves the inhibitive performances of the base molecule. OCT does not afford a protective action as high as iodo-derivatives, although it is highly efficient and its action persistent.

Small differences are found between the impedance spectra of the blank and H, C or B, whereas much higher in the case of I1, I2 or OCT. The impedance spectra of 3M1B derivatives may be characterized by one capacitive time constant, although, in the case of iodo-compounds, mainly at long test times, very depressed semicircles are recorded. In the presence of OCT two capacitive time constants may be observed, even though poorly resolved at short test times (Fig. 1).

EIS technique allows us to evaluate the inhibitive effects of the acetylenic compounds in relation either to their structure, concentration, or test time. Nevertheless the corresponding corrosion rates, calculated by simply applying the Stern-Geary (S-G) equation, are lower than those from SA, mainly with OCT (Table 1). This fact has been previously observed with other organic inhibitors of iron acid corrosion (1). If R_p instead of R_t had been used, the differences between SA and EIS corrosion rates would have been lower in the case of less efficient inhibitors, but not in the case of I1 and I2, or OCT, owing to the

limited extension of a low frequency inductive loop. In our tests this loop is fairly reproducible, and, as a rule, its extension tends to decrease by using the most efficient inhibitors, or by increasing the additive concentration or the test time.

As regards 3M1B derivatives, a possible explanation for the differences observed may be related to the uncertainity in the B value introduced in the S-G equation, since the evaluation of the anodic Tafel slope can be very approximated owing to the tendency of the anodic reaction to unpolarizability, even for low anodic overpotentials. In the case of OCT the film formed onto the metal surface acts as a physical barrier to H^+ discharge (its cathodic Tafel slope tends to infinitive value). This renders the S-G equation no more applicable when diffusion of reacting species through a more or less thick film controls the corrosion process (2,3).

References

1) A. Frignani, M. Tassinari, C. Monticelli, G. Trabanelli, Werkst. u. Korros., **42**, 208 (1991)

2) A. Bonnel, F. Dabosi, C. Deslouis, M. Duprat, M. Keddam, B. Tribollet, J. Electrochem. Soc., **130**, 753 (1983)

3) G. Mengoli, M.M. Musiani, C. Pagura, F. Paolucci, Proc. 7 SEIC, Ann. Univ. Ferrara, Suppl. n.9, p.61, Ferrara, Italy (1990)

Table 1 - Corrosion rates ($\mu A\ cm^{-2}$) of Armco iron from SA and EIS in 1 N H_2SO_4 at 70 °C, in the presence of the tested acetylenic derivatives at 1 mM concentration.

		A D D I T I V E							
	none	H1	C1	B1	I1	C2	B2	I2	OCT
SA	5500	3880	2600	1040	45	2812	1580	30	256
EIS	2800	1618	1170	500	21	1442	955	7.4	24

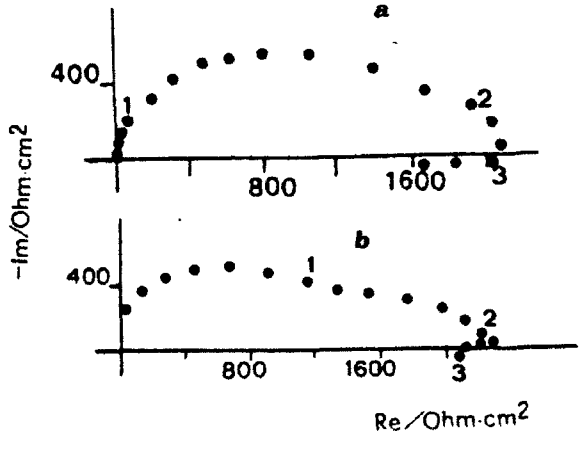

Figure 1 - Examples of impedance diagrams of Armco iron in 1 N H_2SO_4 at 70 °C, in the presence of 1 mM I2 (a), or 1 mM OCT (b), after 24 h test time. Frequencies: 1 = 1 KHz; 2 = 1 Hz; 3 = 10 mHz.

Acknowledgements - Work financially supported by MURST 60% Fund.

ASSESSMENT OF THE EFFICIENCY OF DIFFERENT INHIBITORS ON RUSTED STEEL BY IMPEDANCE SPECTROSCOPY.

J.C. Galván, M. Morcillo, S. Feliu Jr., J.M. Bastidas, J. Simancas, E.M. Almeida (*) and S. Feliu.

Centro Nacional de Investigaciones Metalúrgicas
Avda. Gregorio del Amo 8, 28040 Madrid (Spain).

(*) *SCPM, LNETI, 1069 Lisboa Codex (Portugal).*

The electrochemical impedance spectroscopy was applied to study the inhibitor ability of different chemical compounds over rusted steel samples pretreated with tannic, gallic and phosphoric acids, respectively. These pretreatments are utilized for stabilizing the rust layer before applying paint coatings. However, treating rusted steel with tannic or gallic acid solutions hardly modified the impedance diagrams with reference to those obtained with untreated rusted steel (Fig. 1), which suggested that neither acid has an important effect on the features of the rust layer [1]. In other way, although the treatment of rusted steel with phosphoric acid may result in marked changes in the shape of the impedance diagrams (Fig. 1), the impedance values are still quite low [2].

The scarce influence of treatments based on the use of solutions of the acids assayed in order to reduce the corrosive activity on the rusted steel/electrolyte system makes it advisable to study the effect of more complex treatment specially designed to inhibit or block the anodic and/or cathodic reaction of the corrosion process in this system. Notwithstanding, the surface pretreatments with phosphoric acid may be interesting, in order to get the final objectives of this study for obtaining, not just a paint/rusted steel system with a good anticorrosive performance, but also a good adherence between the paint coating and the phosphate anchorage layer.

In this context, addition of inhibitors (usually sodium chromate, nitrite, molybdate or hydroxide) to the sodium sulphate solution improved the results with the untreated rusted steel (Fig. 2). Nevertheless, when the rust steel has been pretreated with a H_3PO_4 solution, the inhibitors activity decreased, and it is necessary to increase the inhibitor concentrations in order to obtain appreciable changes in the Nyquist plots (Fig. 2). One explanation of the descent of this inhibitor ability may be in the increase of the intrinsic porosity of the rust layer pretreated with phosphoric acid solutions.

Acknowledgement- To the European Communities Commission (agreements 7210/KB931 and 932) for financial support.

References:

1. J.C. Galván, S. Feliu Jr., J. Simancas, M. Morcillo, J.M. Bastidas, E.M. Almeida and S. Feliu. *Electrochimica Acta* (to be published).
2. S. Feliu, J.M. Bastidas, J.C. Galván, S. Feliu Jr., J. Simancas, M. Morcillo and E. M. Almeida. *Journal of Applied Electrochemistry* (to be published).

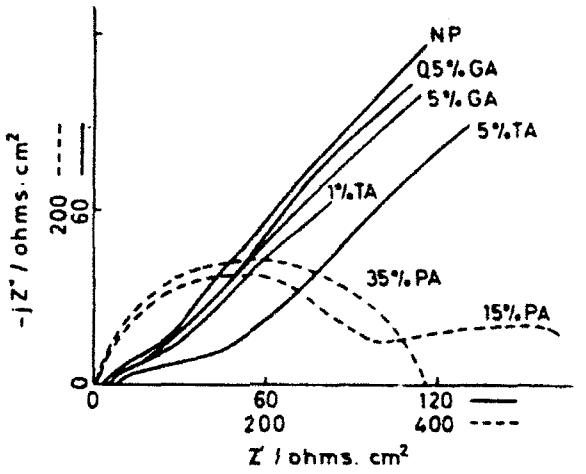

Fig. 1.- Nyquist plots for unpretreated (NP), tannic acid (TA), gallic acid (GA) and phosphoric acid (PA) pretreated rusted steel, respectively. Exposure time: 1h, electrolyte: 0.1M Na_2SO_4, frequency range: 15 kHz- 1 mHz.

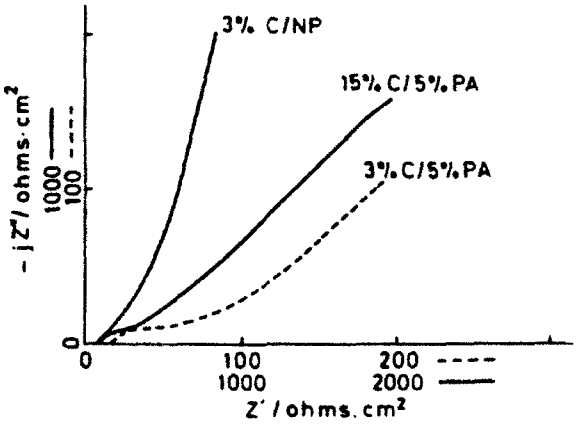

Fig. 2.- Effect of the sodium chromate over the Nyquist plots for unpretreated (NP) and phosphoric acid (PA) pretreated rusted steel, respectively. Exposure time: 1h, electrolyte: 0.1M Na_2SO_4, frequency range: 15 kHz- 1 mHz.

ELECTROCHEMICAL IMPEDANCE SPECTROSCOPY OF ELECTROCHEMICALLY POLYMERISED POLYPHENYLENE FILMS ON PLATINUM ELECTRODE

Zhiqiang Gao, Carita Kvarnström and Ari Ivaska
Laboratory of Analytical Chemistry, Åbo Akademi University
SF-20500 Turku-Åbo, Finland

Electrochemical impedance of polyphenylene films polymerised on Pt substrate is studied in 1 M solutions of different supporting electrolytes in acetonitrile. The change of transfer resistance and the capacitance related to reduction and oxidation of polymer film are studied at different polarisation potentials and also of different thickness of the films. The polymer lost its electrochemical activity when polymerised to 2.0 V where irreversible overoxidation of the film takes place. The change in the electrochemical activity of polyphenylene was clearly observable in the impedance spectrum of the film at lower polarisation potentials where it normally undergoes reversible oxidation.

Polyphenylene films prepared in perchlorate electrolytes showed in SEM pictures a more compact structure than films prepared in tetrafluoroborate and hexafluorophosphate electrolytes. The charge transfer resistances measured in perchlorate electrolytes were found to be much higher than in the other electrolytes used in this study. The more compact structure of the polymer obviously makes the anion intercalation reaction, connected with the charge transfer reaction, more difficult to take place and therefore making the overall process slower in perchlorate electrolytes.

ELECTROCHEMICAL IMPEDANCE SPECTROSCOPY OF GALENA/XANTHATE SYSTEM

J.Genesca, A. Huerta and J.M. Valverde. Facultad Quimica. Universidad Nacional Autonoma de Mexico. 04510 Mexico D.F.

INTRODUCTION

The surface properties of sulfide minerals and the properties of the solid/aqueous solution interface have an important or even decisive part in the processing of these mineral. Impedance spectroscopy is one of the few techniques available for "in situ" characterization of solid/liquid interfaces. The use of this technique thus seems particularly relevant to basic studies connected with mineral processings and specially flotation.

In this work, the first results related with the impedance spectra of galena electrodes in the flotation conditions are presented. The experimental results are analyzed in terms of the equivalent circuit that best reproduces them.

EXPERIMENTAL

Specimens of the galena mineral were obtained from Chilpancingo Mining Company, Guerrero, Mexico. The composition of mineral, 93.04% PbS, 5.66% CuS and 1.29% FeS has been determined by X-Ray Diffraction, SEM-EDAX and Atomic Absorption Spectroscopy. About 5-6 mm thick and 1 cm^2 surface area specimens were cut from massive materials and used as working electrode. Then was mounted in a cold-mount resin, with one surface exposed. The exposed surface was polished wet prior to each measurement on a 600 grit SiC paper using distilled water. The impedance spectra was obtained at the open circuit potential of the electrode. Measurements were carried out between 0.1 Hz and 10 kHz with a FRA CAPCIS VOLTECH CV 2001 and a CAPCIS MARCH Potentiostat/Interface. The amplitude of the AC signal was 10 mV during the impedance measurements. The CORRSOFT SHEILA software (1) was employed to obtain the impedance diagrams. All measurements were made at room temperature. Potassium Borate (0.1 M) was used as buffer. The pH was equal to 9.2 (a pH near to that of the flotation process). Experiments were made with 0.001 M Potassium Ethylxanthate (KEX).

RESULTS AND DISCUSSION

The approach used to analyze the impedance spectra was a qualitative comparison of the shape of the observed spectrum with the spectrum obtained on the basis of various models (2). From such a comparison, the most appropiate model might be selected. Next, parameters could be estimated based either on a few measurement points or the value of impedance at low or high frequency limits. The choice of the circuit was based on the experimental spectra obtained for galena/solution interface. The two-layer model with surface rougness (TLMR) is the equivalent circuit that best describes and reproduces the experimental results. The parameters of the model are given in Table 1. This model takes into account that the

layers produced on the surface of an electrode may be porous and rough. In such a case, a roughness impedance term, B/w may be added in parallel to the coating layer capacitance (2). As can see from Table 1, R_t, R_p and B values are lower without KEX in solution. The R_t values in the solution with KEX are in the order of 1.1 $k\Omega/cm^2$ in the first minutes to 6.5 after 48 hours. The R_t values decrease with time indicating that the anodic dissolution of galena is inhibited. As pointed out by Ahlberg et al (3), for low concentrations of xanthate the dissolution of PbS still prevails at the rest potential. At higher concentrations of xanthate, the surface seems to be saturated and no further inhibition occurs. Instead, the oxidation of xanthate will be observable.

Thus, the results obtained with EIS and other techniques like cyclic voltammetry, seem to probe that the anodic oxidation of galena at the rest potential can be regarded as surface reaction, yielding PbOH surface complexes and an underlying metal deficient sulfide (3). The effect of xanthate ions can thus be regarded as an inhibition of the galena oxidation reaction.

Table 1. The effect of KEX on equivalent circuit parameters for a galena electrode in 0.1 M potassium borate + 0.001 M potassium ethylxanthate

Parameter	System	
	$PbS/KEX/O_2$	PbS/O_2
R_o, Ω/cm^2	35-37	35-38
R_t, $k\Omega/cm^2$	6.5-6.8	1.5
R_p, $k\Omega/cm^2$	1.9-2.0	1.0
B, $k\Omega\ s^{-1}cm^{-2}$	6.5-9.0	3.5

REFERENCES.

1. Capcis March Ltd., Manchester, United Kingdom.
2. J. Pang, A. Briceno and S. Chander, J. Electrochem. Soc. 137 (11) 3447 (1990)
3. E. Ahlberg and A.E. Broo, Int. J. Miner. Process. 33, 135 (1990).

ANALYSIS OF IMPEDANCE SPECTROSCOPY FOR POROUS SILICA GELS

Rosario Gerhardt and Guangqun Zhang
School of Materials Engineering
Georgia Institute of Technology
Atlanta, GA 30332

and

Wanqing Cao
Energy and Environment Division
Lawrence Berkeley Laboratory
University of California, Berkeley, CA 94720

It is customary to study the conductivity of ionic materials by measuring the a.c. electrical behavior and plotting the results in complex impedance terms. However, there are a number of dielectric functions that can be used to analyze experimental data obtained by impedance spectroscopy. These include the electric modulus, the dissipation factor as well as the dielectric permittivity in addition to the complex impedance.

In this paper we will apply some newly derived equations [1] to the interpretation of the complex dielectric behavior of a series of porous silica gels which were measured in an environmental chamber under controlled relative humidity. The measurements were carried out at 10%-98% RH for frequencies ranging from 10Hz-100kHz.

Figure 1 shows the complex impedance spectra at 66% RH for a series of porous silica gels which had been soaked in various KCl solutions. The conductivities vs. % RH shown in Figure 2 were obtained from similar plots at all relative humidities for both samples listed. If we compare the normalized imaginary electric modulus, the dissipation factor and the imaginary impedance plotted versus the logarithm of the frequency (Figures 3 and 4), it is clear that at low relative humidities (<40%_) there is no correspondence between the imaginary impedance and the electric modulus while at higher relative humidities the 2 spectra essentially overlap while the dissipation factor has barely moved to a higher frequency. This difference can be attributed to the fact that at low relative humidities the conductivity is expected to be localized, i.e. at isolated pockets of K-OH on the silica surfaces while at higher relative humidities the conductivity ought to be long range motion of K ions through a continuous water film (hence the higher conductivity).

1. W. Cao and R. Gerhardt, "Calculation of various relaxation times and conductivity for a single relaxation process," Solid State Ionics 42, 213-221(1990).

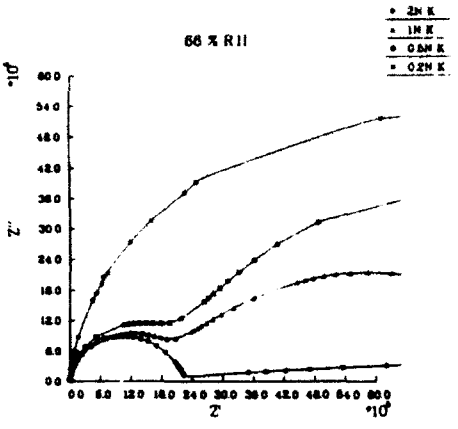

FIGURE 1.

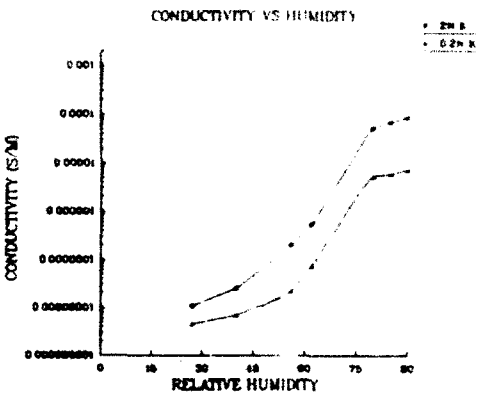

FIGURE 2.

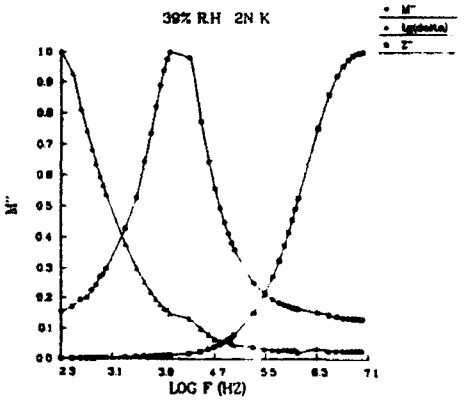

FIGURE 3.

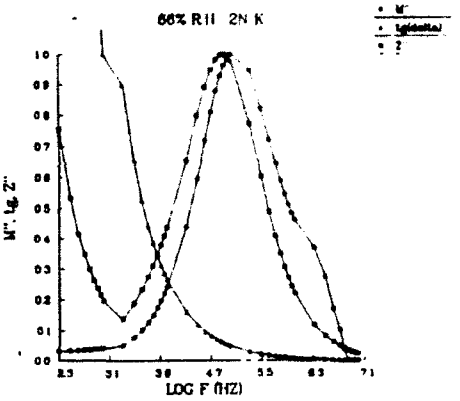

FIGURE 4.

ELECTRODE KINETICS OF OXYGEN REDUCTION ON POROUS NICKEL IN CARBONATE MELT

L. Giorgi, E. Simonetti
ENEA - C.R.E. Casaccia
Division of Electrochemical Technologies and Plants
Via Anguillarese n. 301
00060 S. Maria di Galeria (Rome), Italy

F. Croce, A. Pozio
Department of Chemistry, University of Rome "La Sapienza"
P.le A. Moro n.5, 00185 Rome, Italy

The general equation for the oxygen electroreduction in molten carbonate fuel cell (MCFC) is the following:

$$1/2\ O_2 + CO_2 + 2e^- \longrightarrow CO_3^{2-},$$

but the mechanism is complicated by several steps with the possibility to have intermediate species like superoxides, peroxides and peroxi-monocarbonates [1,2,3].

The aim of the present paper is to investigate the porous NiO(Li) electrode/molten carbonates interface by means of electrochemical impedance spectroscopy (EIS).

A symmetric cell made of recrystallized allumina was used. The electrodes were two identical porous (75±5 %) Ni electrodes, in situ oxidized and lithium doped, with a geometrical surface area of 3 cm^2 and a mean pore size of 9±1 μm. The electrolyte was constituted by 48 $\%_w$ γ-$LiAlO_2$ and 52 $\%_w$ lithium and potassium carbonate mixture (Li/K=62/38 $\%_{mol}$).

The cell was operated at 650±2 °C and fed with a variable composition of CO_2/O_2 mixture.

The cell was controlled by a galvanostatic polarization at i=0, with a superimposed sinusoidal signal of 236 $\mu A/cm^2$, in the frequency range from 0.1 Hz to 65 kHz.

A typical EIS spectrum is shown in fig.1. At a first look the spectrum is evidently depressed (this phenomena is correlated to the porous electrode structure)and it is clear the presence of several processes.

The spectra can be subdivided in two region: low frequencies in which the diffusion is predominant and high frequencies in which the charge transfer aspect is predominant. The equivalent circuit for the interface is a R-C-O network, where the O element is characteristic of a system in which is present a finite diffusion layer [4]. This latter is a confirmation that the pores of the cathode are not completely flooded, but the walls of the pore are coated with a thin film of electrolyte; this film is so thin that the concentration gradient of active species is concentrated in the film itself.

Following Appleby [2] it is possible to derive the relationship between the exchange current density (i_o) and partial pressure:

$$i_o = k\ pO_2^a\ pCO_2^b$$

where a and b are, respectively, the reaction order relative to oxygen and carbon dioxide. In the following, the theoretical reaction orders for the different mechanism are: peroxide path (POP): a=0.375, b=-1.25; superoxide path (SOP): a=0.625, b=-0.75; peroximonocarbonate path (POMCP): a=0.375, b=-0.25.

The value of charge transfer resistance (R_{ct}) in the case of a porous electrode [5], is inversely proportional to the partial pressures of O_2 and CO_2:

$$1/R_{ct}^2 = k\ pO_2^a\ pCO_2^b$$

The problems arising from the depression of the spectra and the closed time constants were overcome by using a non linear last square fit (NLLSF) [6] made on the whole spetrum.

$$\log R_{hf} = -1/2 \log k' - a/2 \log pO_2$$

A similar relationship can be obtained in the case of constant pO_2:

$$\log R_{hf} = -1/2 \log k'' - b/2 \log pCO_2$$

Therefore from the slope of the previous equations it is possible to draw out the reaction orders.

In order to get a very reliable correlation the medium-low frequencies data points were subtracted from the spectra and a high frequencies region fitting was carried out [7,8].

The following procedure was adopted: subtraction of wires' inductance; simulation of RQ circuit at medium-low frequencies; medium-low frequencies fit with the RQ circuit; subtraction of RQ from the spectrum; simulation with a R(RQ) of the remaining data; final fit with R(RQ) circuit on the remaining data.

Adopting such a procedure the fitting errors were very low, and a very good correlation between log R_{ct} values and partial pressures of O_2 and CO_2 was obtained (fig.2).

The data obtained from several series of measurements, made on two different cells, gave the following mean calculated reaction orders: a=0.38±0.09 and b=-1.2±0.2.

These results are in good agreement with the theoretical values for the peroxide mechanism (a=0.375, b=-1.250), expecially in the case of oxygen reaction order. Therefore it was established that the predominant mechanism is the peroxide path.

REFERENCES

1. A.J. Appleby, S.B. Nicholson, J. Electroanal. Chem. 83, 309 (1977)
2. A.J. Appleby, S.B. Nicholson, J. Electroanal. Chem. 112, 71 (1980)
3. I. Uchida, T. Nishina, Y. Mugikura, K. Itaya, J. Electroanal. Chem. 206, 229 (1986)
4. L. Giorgi, E. Simonetti, G. Gavelli, Proceeding of the NATO-ASI "Electrified Interfaces in Physics, Chemistry and Biology", p.16, Varenna (Italy), 23 July÷3 August 1990

5. R. de Levie, in Adv. in Electrochem. and Electrochemical Engineering, ed. P. Delahay, C.W. Tobias, Vol.6, p.329÷397, J. Wiley & Sons, N.Y. (1967)
6. B.A. Boukamp, EQUIVCRT.PAS, Users Manual, 1988
7. A. Pozio, Thesis, University of Rome, 1991
8. L. Giorgi, E. Simonetti, A. Pozio, Proceeding of the International Fuel Cell Conference, Makuhari (Japan), 3÷6 February 1992

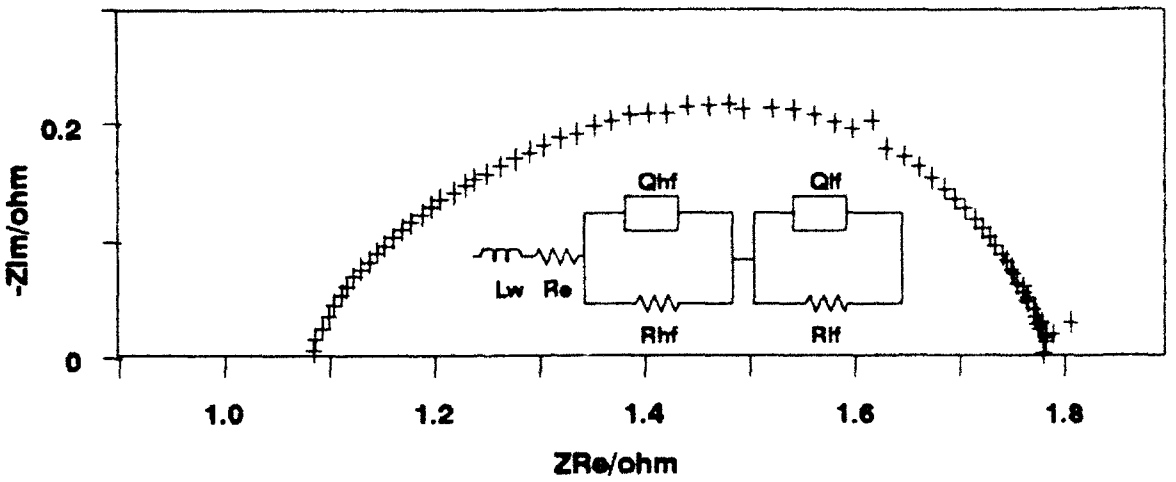

Fig. 1 - Example of experimental and simulated data by means of a total fitting. (pCO_2=0.30 atm, pO_2=0.15 atm, T=650 °C)

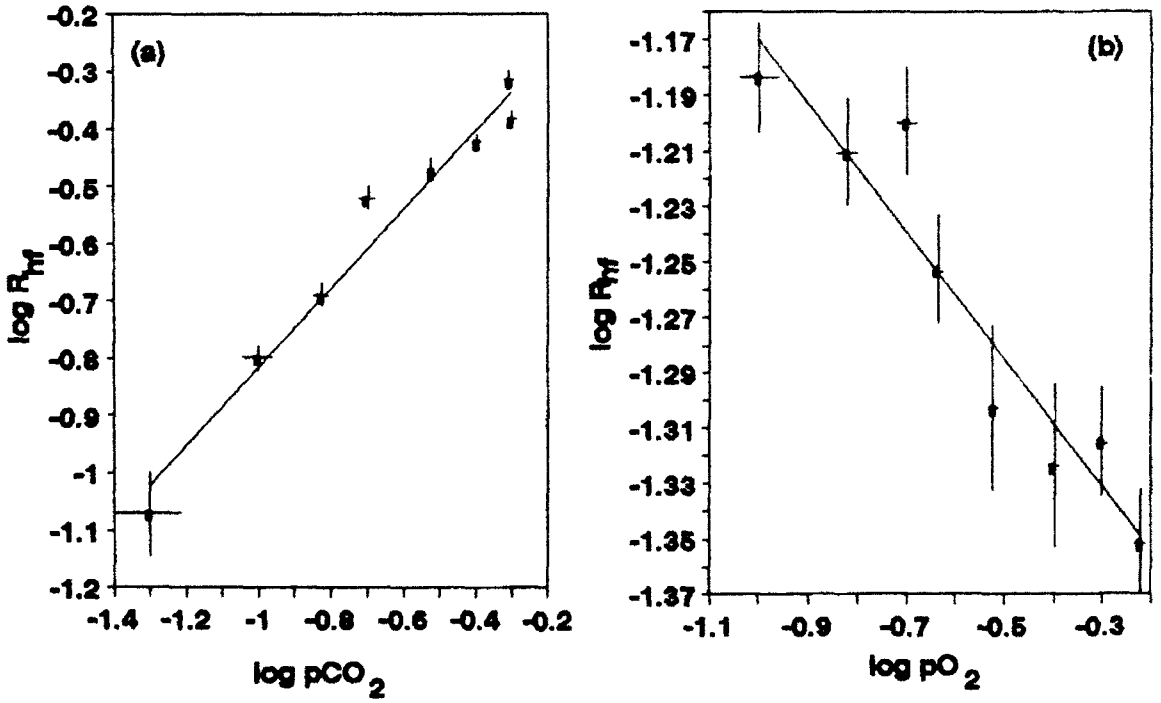

Fig. 2 - Log-log correlation between the high frequencies real impedance and the partial pressure of carbon dioxide (a) and oxygen (b).

IMPEDANCE MEASUREMENT AT ELECTRODES OF CONTINUOUSLY CHANGING STATE

H. GOEHR, *H. BODE*, A. BURGHART, C.-A. SCHILLER
Institut für Physikalische und Theoretische Chemie, Universität Erlangen-Nürnberg, D-8520 Erlangen, F.R.G.

One of the prerequisites of impedance measurement is a quasi-steady state of the system studied. Thus, recording of impedance spectra of an electrode during continuous changes of its state is on principle restricted to sufficiently slow changes of impedance controlling parameters. No perceptible change is admitted during at least one periode $\tau_{lo} = f_{lo}^{-1}$ at the lower limit f_{lo} of the frequency band. Of course the evaluation of spectra causes no additional problems, if no significant drift occurs during the whole recording time τ_s of the spectrum. Within a range of rates between these limits points of measurement at different frequencies may belong to significantly different states. On the premise that the real time t_i of acquisition at each frequency f_i is available, by means of an algorithm of **interpolation** data can be transformed leading to impedance spectra at unique times t_s. Each of these **interpolated spectra** then represents a certain state of the electrode.

We have developed a technique of non-linear interpolation using four consecutive spectra of a series, which are nearest to the selected interpolation time t_s. This technique has been applied to different time dependent systems, e.g. Pd in alkaline solution after intensive cathodic charging with hydrogen. In **Fig. 1** four original empiric spectra of a series of eight – on the left – are compared with four interpolated spectra – on the right –, showing that the decrease of impedance with increasing frequencies at the lower end of the frequency band is totally caused by the influence of time and is therefore a deception. The empiric spectra, contrary to the interpolated ones, are not consistent to KRAMERS-KRONIG transform. The results of fitting the interpolated spectra are much more consistent and therefore the resulting values of parameters are more reliable.

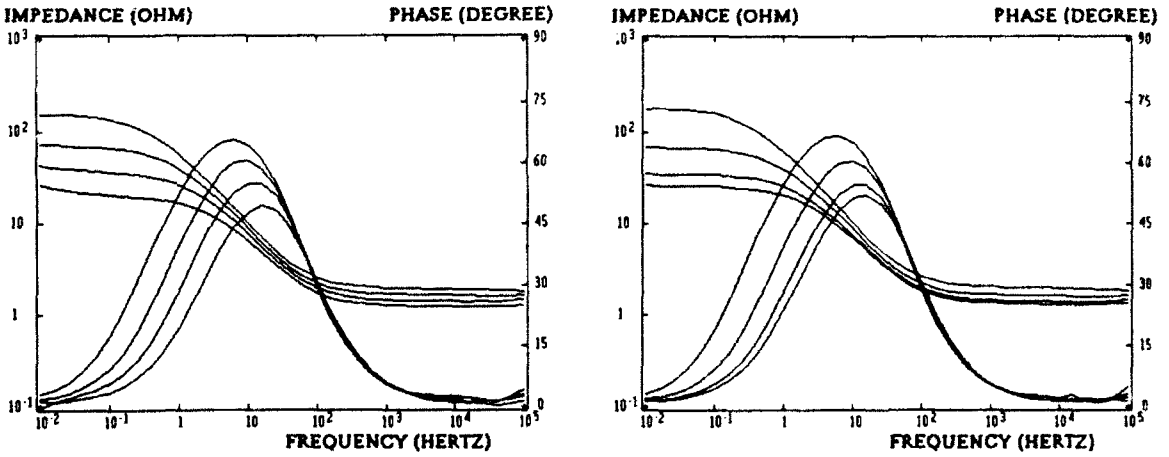

Fig. 1: Pd / 0.1 M LiOH after 5 h hydrogen charging at 100 mA cm^{-2} (end: $t = 0$). 4 spectra selected from a set of 8. Chronological sequence corresponding to increasing impedance and phase resp.
Left plot: empiric spectra.
Right plot: interpolated spectra at t_s = 30min, 44min, 1h40min, 23h34min.

The behaviour has also been tested by a set of simulated spectra **calculated** according to a rather complicated model. This network consists of seven impedance elements with nine **time dependent parameters**. The complex impedance at any frequency point of each of the spectra is calculated as a function of the actual values X_n of the parameters according to individual dependences on time t,

$$X_n(t) = X_n(0) \cdot F_n(t) \,, \tag{1}$$

at realistic times $t = t_i$ of measurement. The starting values $X_n(0)$ are chosen in a way that within the whole frequency range some of the parameters have only a very poor influence on the impedance. Applying the mentioned interpolation program to this set of spectra we get a set of interpolated spectra. Also in this case the results of fitting these spectra are considerably more exact. The reconstruction of the time dependent values of all parameters is achieved within the limits of the estimated accuracy according to their significance.

Generally, the reliability of the results is higher using the set of interpolated spectra instead of the set of empiric (or calculated) spectra. As a typical example this can be seen from **Fig. 2** for one of the parameters. The plotted curves in **Fig. 2** represent the real dependence on time of the parameter which is mostly not available for measured spectra of real systems. An additional advantage of the results from interpolated spectra is due to the fact that the time of acquisition is equal to the known time t_i of interpolation. Parameter values estimated from original spectra, however, are weighted mean values over the duration of recording the whole spectrum.

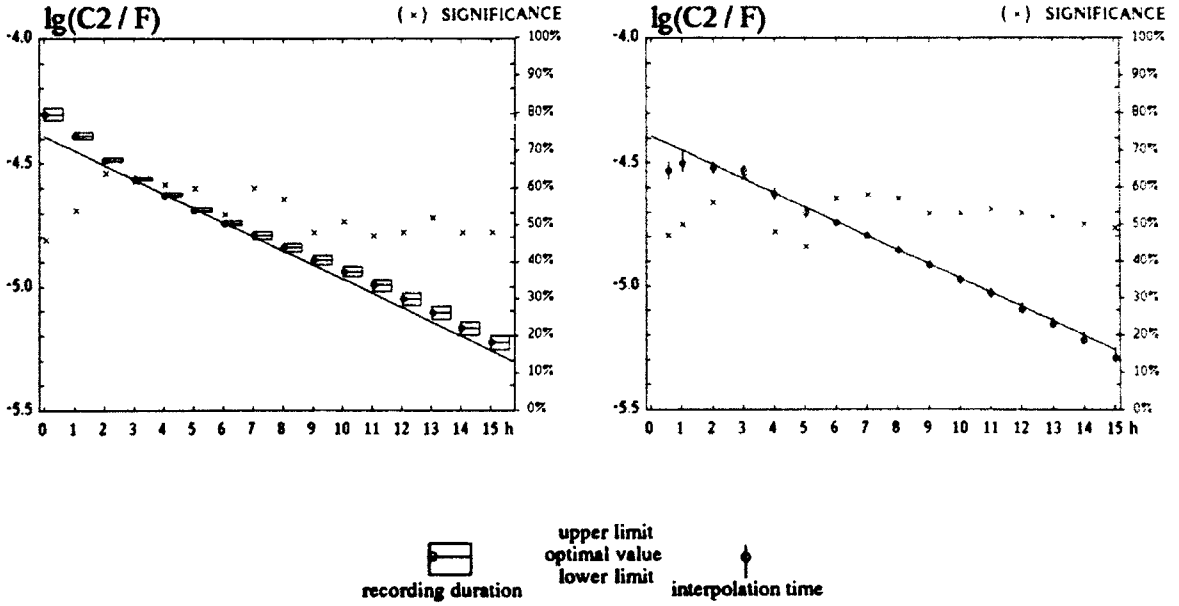

Fig. 2: Dependence on time of capacity C_2 with rather poor significance (×).
Left plot: results from original spectra calculated according to Eq. (1).
Right plot: results from interpolated spectra. Limits of deviation are automatically yielded by our evaluation program ("IMR").

IMPEDANCE STUDIES OF THE OXIDE LAYER ON ZIRCALOY AFTER PREVIOUS OXIDATION IN WATER VAPOUR AT 400°C

H. GOEHR, J. SCHALLER and C.-A. SCHILLER
Institut für Physikalische und Theoretische Chemie, Universität Erlangen-Nürnberg, D-8520 Erlangen, F.R.G.

Zircaloy samples were oxidized in water vapour at 400°C and 105 bar. After different times of oxidation up to 90 days the surface of the samples was studied by recording impedance spectra in 0.5 M K_2SO_4 in the range from room temperature to 200°C (1 to 15 bar) using a three electrode cell inserted in an autoclave. All spectra can well be fitted with the same model, shown in the left part of **Fig. 2**, consisting of five impedance elements with altogether eight parameters. The physical meaning of this model is based on a growing layer with porous sections beside compact areas. The compact layer is properly described by the YOUNG model with a vertical decay of conductivity in an outer zone. Its impedance[1] is given by

$$Z_Y = \frac{p_Y}{j\cdot\omega\cdot C_Y} \ln\left[\frac{1 + j\cdot\omega\cdot\tau\cdot\exp(p_Y^{-1})}{1 + j\cdot\omega\cdot\tau}\right] . \qquad (1)$$

Evaluation of the spectra yields significant data about e. g.

(1) layer thickness,
(2) irreversible penetration of electrolyte into the pores aided by increasing pressure,
(3) activation energies of transport processes from the dependence of kinetic parameters on the temperature.

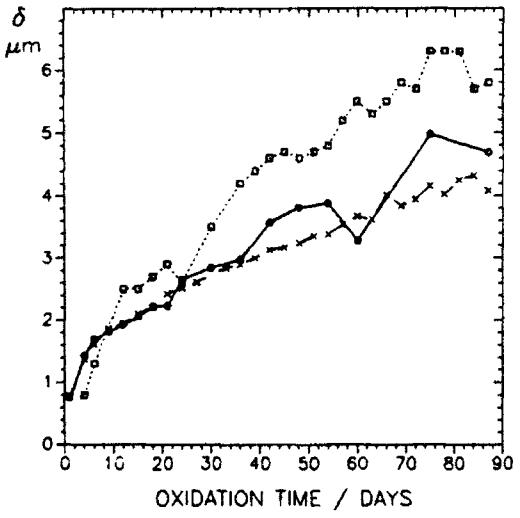

Fig. 1: Thickness of the oxide layer on Zircaloy after oxidation in water at 400°C. Comparison of different methods: EIS ——, FTIR – – –, gravim. · · · ·.

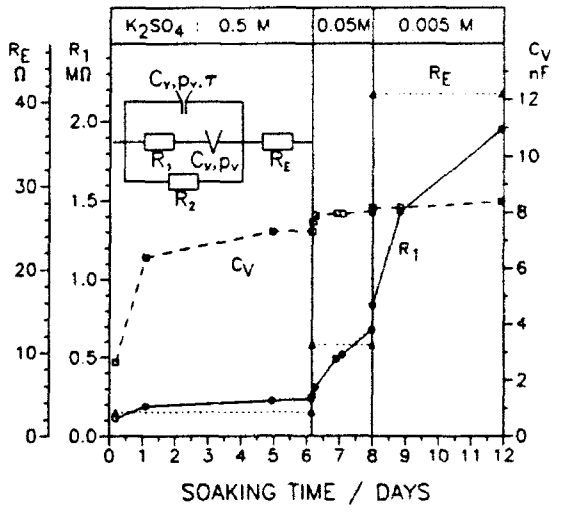

Fig. 2: Sample, 87 days oxidized at 400°C. Dependence on time at 20°C of R_1 (——), C_V (– – –) and R_E (· · · ·) while the concentration of K_2SO_4 after 6 and 8 days is stepwise diminished.

The thickness δ of the oxide layer is obtained from the capacity C_Y of the YOUNG impedance assuming a dielectric constant of 20 and a roughness factor of 1.2. The results in a range of about 0.1 to 10 μm within reasonable limits prove accordance with results on similarly pretreated samples obtained by other authors using gravimetric[2], spectrscopic (FTIR)[3] and wirling current methods[4] (**Fig. 1**).

The immersion of the sample into the solution (0.5 M K_2SO_4) results in an electrolyte penetration into the pores. This is accompanied by an increase of penetration depth and also of wetted pore surface until a steady state is reached. The irreversible penetration is indicated by dependences of resistance R_1 and capacitance C_V on time (**Fig. 2**). These parameters can be correlated with the electrolyte inside the pores and the distributed double layer of the inner pore surfaces. The distribution causes loss angles of about 5°. Therefore, the double layer capacitance is represented by a constant phase element. After stepwise dilution (to 0.05 M and then to 0.005 M) the exchange of the electrolyte inside the pores is extremely delayed, causing a very slow decrease of conductivity and thus an increase of R_1 continuing for several days. The surface of the pores and therefore capacity C_V, however, remain approximately constant. As expected concerning the other parameters of the model, only resistance R_E of the electrolyte depends on the concentration, and no influence of penetration is observed (**Fig. 2**).

According to Eq. (1) the YOUNG impedance* converges with decreasing frequency asymptotically to a resistance[1,5]

$$R_Y = p_Y \cdot \tau \cdot C_Y^{-1} \cdot [\exp(p_Y^{-1}) - 1]. \tag{2}$$

If resistance R_2 is due to the bulk conductivity of the oxide, the transport of ions in the layer is described by R_Y and R_2 in parallel,

$$R_0 = (R_Y^{-1} + R_2^{-1})^{-1}. \tag{3}$$

From the dependence of R_0 on temperature we get **energies of activation**

$$\begin{aligned} E_A &= 55 \pm 5 \text{ kJ mol}^{-1} \quad \text{during heating from 20 to 200°C,} \\ E_A &= 24 \pm 3 \text{ kJ mol}^{-1} \quad \text{during cooling from 200 to 20°C.} \end{aligned} \tag{4}$$

The difference of the values obtained at increasing and at decreasing temperatures show that near 200°C a considerable change of state of the layer occurs. The reversal process at lower temperatures, however, obviously proceeds very slowly.

REFERENCES

1. H. GOEHR, Ber. Bunsenges. Phys. Chem. *85*, 274 (1981)
2. H. RUHMANN, Siemens UB KWU BT 63, Erlangen D-8520
3. K. KASPAR, Siemens UB KWU BT 61, Erlangen D-8520
4. O. GEBHARDT, Paul-Scherer-Institut, Villingen CH-5282
5. N. MUELLER, Thesis, Erlangen 1980

*Eq's. (21) and (22) in [1] are erroneous and should be replaced by Eq's. (1) und (2) resp.

THE DOUBLE LAYER IMPEDANCE AT A ROUGH ELECTRODE: A RANDOM WALK APPROACH

Thomas C. Halsey and Michael Leibig
The James Franck Institute
The University of Chicago
5640 S. Ellis Ave.
Chicago, Illinois 60637

It has long been recognized that surface roughness, even on macroscopic scales, can significantly affect the frequency dispersion of the double layer impedance at a surface.[1] This effect results from the inhomogeneities in the current flowing from the bulk to the surface in question. In principle, this is a very complicated problem, involving both diffusive and migratory transport in the bulk, and the full range of double layer complexity. It will be our purpose in this contribution to show that in one physically relevant limit, this problem can be reduced to a problem of measuring the statistical properties of random walks moving in the vicinity of the electrode surface. Furthermore, this leads to a numerical method that can efficiently compute the frequency dependence of the double layer impedance for an arbitrary surface. For fractal surfaces, this computation leads to a stretched-exponential type relaxation, which at high frequencies resembles the phenomonological "Constant Phase Angle" (CPA) form.

The model that we shall discuss assumes a linear charge-voltage relation in the double layer. This will be true for sufficiently small voltages. We also require that the dominant contribution to the currents outside the double layer is migratory (i.e., induced by the electric field) rather than diffusive. These diffusive currents can be minimized by using electrodes with very high Faradaic resistances (blocking electrodes), by using electrodes with a minimum roughness scale a much greater than the Debye-Hückel length λ_D, and by studying the impedance at relatively high frequencies. The aim is to insure that the diffusion length $\sqrt{D/\omega} \ll a$, where D is an ionic diffusion constant.

If these requirements are met, then the dominant physical effects that determine the double layer impedance are the capacitance of the double layer and the resistance of the surrounding electrolyte.[2] At short times, or high frequencies, only at the geometrical protrusions of the electrode does the double layer charge; at longer times, or lower frequencies, the double layer charges in a much larger surface area of the electrode. The variation of this effective electrode surface area with frequency underlies the frequency dispersion of the impedance. This is the physical insight behind the lumped RC circuit models of Liu et al. and of Sapoval et al.[3,4]

Using the relationship between solutions of the Laplace equation and random walks, the impedance in this RC limit of an arbitrary surface can be expressed as a sum involving the statistics of random walks. Consider an electrolyte bounded by a counter-electrode (CE) and the electrode of interest, the blocking electrode (BE). Suppose that random walkers are emitted from the CE, are reflected at the BE an arbitrary number of times, and are destroyed when the first return to the CE. The probability that a random walker strikes the BE n times before returning to the CE is b_n. It can be shown that the double layer admittance $Z^{-1}(\omega)$ is given by a sum,[5]

$$Z^{-1}(\omega) \propto 1 - \sum_{n=1}^{\infty} b_n (1-\omega)^{-n}. \tag{1}$$

The coefficients $\{b_n\}$ can be computed using techniques for performing random walks in arbitrary geometries that have been developed in the study of diffusion-limited aggregation. Thus Eq. (1) gives a method for computing the double layer impedance for electrodes of arbitrary geometry, and we have in fact used this technique to study a variety of types of surface.

One interesting type of surface is the fractal surface, with a Hausdorff dimension D_0 that is in general non-integral. For these types of surfaces, we have performed a theoretical analysis of the coefficents b_n, based on the properties of random walks near fractal surfaces. The result is that the impedance at fractal surfaces will show a stretched-exponential behavior. In the time domain, this implies that if a voltage step is applied at time $t = 0$, then the current to the surface $I(t)$ will have the form,[6]

$$I(t) \propto \exp(-t^{\beta}), \tag{2}$$

where the exponent $\beta < 1$. β is a function of the Hausdorff dimension D_0 and the "multifractal" properties of the surface.[7] Our numerical results support this conclusion. At high frequencies, the stretched-exponential form Eq. (2) gives a power law in frequency, as in the experimentally observed CPA form.

1. P.H. Bottelberghs, in *Solid Electrolytes*, edited by P. Hagenmüller and W. Van Gool (Academic, New York, 1978) Chap. 10.
2. T.C. Halsey, Phys. Rev. A **35**, 3512 (1987).
3. S.H. Liu, Phys. Rev. Lett. **55**, 529 (1985)
4. B. Sapoval, Solid State Ionics **23**, 253 (1987)
5. T.C. Halsey and M. Leibig, Europhys. Letts. **14**, 815 (1991)
6. T.C. Halsey and M. Leibig, Phys. Rev. A **43**, 7087 (1991).
7. T.C. Halsey, M.H. Jensen, L.P. Kadanoff, I. Procaccia, and E. Shraiman, Phys. Rev. A **33**, 1141 (1986).

ELECTROCHEMICAL IMPEDANCE FOR LARGE STRUCTURE IN SOIL

Shiro Haruyama (Plenary) and Shirohi Sudo*
Tokyo National College of Technology
1220-2, Kunugida, Hachioji, Tokyo 193, Japan
* Tohoku Electric Power Co., Inc.
7-2-1, Nakayama, Sendai, Miyagi 981, Japan

Electrochemical impedance for a two-electrode cell consisted of a metallic large structure and a non-polarizable disk electrode has been discussed considering the distribution of signal current. The current distribution, namely an effective measuring area, extends wider with increasing the electrochemical polarization at interface. Since the interfacial impedance decreases with increasing a-c frequency, the electrochemical impedances at extremely high and low frequencies corresponds to those for the primary and secondary current distribution respectively. Namely, in the measurement of electrochemical impedance of buried large structure, the effective measurring area decreases with increasing a-c frequency.

The current distribution and the partial impedance on the structure has been obtained by conformal mapping. Then, the electrochemical impedance for buried structure has been experessed as the parallel combination of infinite number of the partial impedances, thus

$$RZ(\omega) = \int^{x_s}\int^{x_s} RZ(x,\omega)\cdot ds \qquad (1)$$

$$IZ(\omega) = \int^{x_s}\int^{x_s} IZ(x,\omega)\cdot ds \qquad (2)$$

where ds represents an infinitesimal area on the structure, $RZ(\omega)$ and $IZ(\omega)$ the real and imaginary parts of the total impedance respectively, $RZ(x,\omega)$ and $IZ(x,\omega)$ the real and imaginary parts of the partial impedance respectively and x indicates the coordinate.

The complex plane plot of the electrochemical impedance for buried 1- and 2-dimensional structures exhibit a semi-circle and semi-ellipse respectively, the intercept of which on the real axis is not proportional to the transfer resistance, as distinct from usual electrochemical impedance.

The impedance diagrams for a buried structure in the presence of a local corrosion deviate from those in the absence of the local corrosion below a threshold frequency which is determined by the distance of of the local corrosion site, without depending on the rate and size of the local corrosion. The threshold frequency serves as a tool for detecting the location of local corrosion site of buried large structure.

IMPEDANCE SPECTRA FOR CORRODING ZINC AND ALUMINUM

Joseph Hazan

Materials Engineering Department
Technion, Israel Institute of Technology
Haifa, Israel

A transparent chromic passivation layer on galvanised steel was found to provoke a decrease in the double layer capacitance C_{dl}, an increase in the charge transfer resistance (Rt), and an increase of the value of the impedance at very high frequencies (limiting value of the impedance Z as the frequency goes to infinity). In d.c. measurements the polarization resistance, Rp, increased and the symmetry of the polarisation curve near the corrosion potential was reversed due to the conversion coating. All the changes in the d.c. and a.c. parameters indicate the existence of a protective layer.

The extent of depression was measured by the beta parameter which is the exponent of the complex term in the experimental impedance Z, which consists of the parallel circuit composed of a resistance R and a capacitance C:

$$Z=R/1+(jwRC)^{\beta}.$$

The conversion layer was found to increase the extent of depression. This behaviour is related to an increased inhomogeneity of the surface of the chromated electrode. The almost completely non-depressed semi-circle obtained for an as plated hot deep galvanized sample (with $\beta \approx 1$) indicates that the layer of the zinc oxide on the surface is dry, non-porous and homogeneous. But, the extent of depression of the semi-circle in the high frequency region was found to be high for the electrogalvanized steel samples, even before a conversion treatment.

The limiting value of the impedance at very high frequencies increases by more than 10Ω for chromated samples relatively to the non chromated ones with the same configuration and surface ($1cm^2$). This may be an indication for an existence of a small capacitive loop at very high frequencies, corresponding to the intact conversion layer. The whole loop however is not observed and its full appearance depends first on the high frequencies that can be reached in the experiment. Similarly, in some cases, we have found that the capacitance of the porous layer Cc of an anodic oxide film on aluminum cannot be determined from the experimental a.c. impedance measurement since it is expected at frequencies exceeding the highest values reached by the experimental set-up. But, from the known conditions of formation of the anodic film, the capacitance of the porous layer can be roughly estimated. The expected value of the characteristic frequency of the hypothetic high frequency capacitive loop was found in the simulated impedance diagram greater than 10^7 Hz.

Finally, experimental results for the non protected zinc using a rotating disk electrode in an alkaline and in a low conducting chloride solution are confronted to simulated data obtained with the use of different expressions for the diffusion impedance Z_D.

USE OF ELECTROCHEMICAL NOISE IN THE STUDY OF CORROSION INHIBITION: 2. gem-DIPHOSPHONATES

Stanley T. Hirozawa, David E. Turcotte and Michael C. Welch
BASF Corporation
1419 Biddle Avenue
Wyandotte, Michigan, 48192

Abstract

AC impedance measurements in the $1X10^{-3}$Hz to $1X10^{5}$ Hz frequency range were performed on aluminum at open circuit potential. New corrosion inhibitors were examined in chloride containing water/ethylene glycol solution. The inhibitors are based on gem-diphosphonates and were synthesized[1] from alkyl carboxylic acids (R_c) and PCl_3 by equation 1.

1. $R_cCOOH + 2PCl_3 + 5H_2O \longrightarrow R_cC(PO_3H_2)_2(OH) + 6HCl$

Compounds with varying phosphonate basicity and hydrophobic character (R_c= 1, 7, 11 carbons) were investigated.

Equivalent circuit modelling of Electrochemical Impedance (EI) spectra was used to deconvolute and validate experimental data. This is important in corroding systems because passive circuit elements and data represented by passive circuit elements follow the Kramers-Kronig relations[2,3] . Pitting corrosion was observed visually and electrically for inadequately inhibited aluminum. It influenced the lower frequency EI spectra and required large capacitance values to model[4]. Noise was defined for EI spectra from analysis of fitting residuals.

Qualitative electrochemical noise in open circuit potential versus time measurements and noise defined from EI spectra correlated with corrosion inhibition by the new compounds. Increasing inhibition lead to a decrease in frequency at which qualitative noise is observed in EI spectra[5]. Unstable protective films probably cause electrochemical noise[5,6]. Noise reduction correlates with the elevation of open circuit potential and polarization resistance (R_p) following inhibition of aluminum.

References

1. H.G. Germscheld, US Patent 3,855,284.
2. D.D. Macdonald and M. Urquidi-Macdonald, J. Electrochem. Soc., 137, 515 (1990).
3. J.M. Esteban and M.E. Orazem, J. Electochem. Soc., 138, No. 1, 67 (1991).
4. R. Oltra and M. Keddam, Corr. Science, 28, 1 (1988).
5. S.T. Hirozawa and D.E. Turcotte, Materials Performance Maintenance, Can. Inst. Min. Metal. and Petro., vol. 25, p. 207 (1991).
6. S.T. Hirozawa and D.E. Turcotte, Proc. Symp. Electrochem. Imped. of Practical Corrosion Predictions, ASTM, in press, 1992.

THE COATING/METAL/ELECTROLYTE INTERFACIAL IMPEDANCE AND ITS GLOBAL FRACTAL MODEL.

J. Hubrecht*, M. Embrechts**, W. Bogaerts*

* Katholieke Universiteit Leuven, Dept. MTM, de Croylaan 2, 3001 Heverlee, Belgium

** Rensselaer Polytechnic Institute, Nuclear Engineering Dept., Troy, New York 12181-2000, USA

Comparative tests and quality checks of organic coatings are of vital importance, if corrosion is to be controlled in the most effective way and if the best protecting systems are to be applied.

Electrochemical impedance spectroscopy (EIS) means a well-established value as a technique to characterize electrochemical systems and, consequently, to evaluate corrosion systems. Also metal samples, provided with an organic coating, may be tested by EIS.

The interpretation, however, of such EIS spectra is another matter and only makes sense if one has a plausible, chemically and physically founded model at hand, in function of which system characteristics may then be derived.

Deviations between idealized models (electrical equivalents) and real spectra remain up till now a stumbling block. Empirical models generally fit the measured data, but then lack a physical explanation. The theory of fractals, developed by Mandelbrot [1] and introduced into electrochemistry by Le Méhauté [2-4], appears to be able to elucidate these problems largely.

Figure 1 shows a Nyquist EIS record of an iron/coating/solution system, the full description of which can be found in reference [5]. The coating is a water-base organic paint of an average thickness of 80 µm on a sample surface area of 28.3 cm^2. The immersion test occurs in an aqueous 0.5 M NaCl solution and the record, made between the frequencies 10 kHz and 10 mHz, reflects the system condition after 16 days.

The part of the spectrum at high frequencies (HF) is the response of the coating layer, which is penetrated with electrolyte. Because of the whimsical distribution of coating substance and electrolyte on a microscopic scale, this interface doesn't behave as a perfect parallel connection of a resistance and a capacitance, but leads to a depressed semi-circle in the Nyquist representation. This part of the impedance spectrum corresponds to a model of the Cole-Cole [6] or Davidson-Cole [7] type; in this paper it is attempted to provide that correspondance with a fractal foundation.

Similar comment holds for the impedance part at intermediate frequencies (IF), which stems from the processes at the double layer interface at the basis of the coating pores, where electrolyte contacts the substrate. The Randles equivalent circuit, in a first approximation constituting a satisfactory model for the double layer capacitive behaviour and the charge transfer process, should in a second approximation be corrected for the microscopic interface irregularities. The depressed semi-circle, which indeed appears in this IF area, may again be modelled as indicated above, but fractal theory offers a more elegant interpretation, as also supported by e.g. Nyikos and Pajkossy [8] and de Levie [9].

The mass transfer process, more particularly the diffusion process of the

electroactive substance [10,11] and the coupling with the charge transfer process [12] may as well be dealt with in a fractal way. The impedance response of the diffusion process appears at LF. The metal/coating/solution system, however, may in this frequency domain no longer be described with the aid of the semi-infinite diffusion model or the simple Warburg impedance, but should be seen as two serial diffusion layers of different characteristics.

The impedance expressions, belonging to the different frequency area's, can be integrated into a global impedance model, based on the fractal approach, for the complete metal/coating/solution system. The global model, tested for compatibility with a real spectrum, gives a number of best model parameter values, which characterize the system investigated.

Acknowledgement.

J.H. wants to thank the Dept. of Metallurgy, Electrochemistry and Materials Science of the Vrije Universiteit Brussel which supported the experimental work referred to in this paper.

References.

1. B. B. Mandelbrot, The Fractal Geometry of Nature, Freeman, San Francisco, 1982.
2. A. Le Méhauté and G. Crepy, Compt. Rend. Acad. Sc. Paris, 294, 685 (1982).
3. A. Le Méhauté and G. Crepy, Solid St. Ionics, 9-10, 17 (1983).
4. A. Le Méhauté, J. Stat. Phys., 36, 665 (1984).
5. J. Hubrecht, J. Vereecken and M. Piens, J. Electrochem. Soc., 131, 2010 (1984).
6. K. S. Cole and R. H. Cole, J. chem. Phys. 9, 341 (1941).
7. D. W. Davidson and R. H. Cole, J. chem. Phys. 18, 1417 (1950); 19, 1484 (1951).
8. L. Nyikos and T. Pajkossy, Electrochim. Acta, 30, 1533 (1985).
9. R. de Levie, J. Electroanal. Chem., 261, 1 (1989).
10. L. Nyikos and T. Pajkossy, Electrochim. Acta, 31, 1347 (1986).
11. T. Pajkossy and L. Nyikos, Electrochim. Acta, 34, 171 (1989).
12. R. de Levie, J. Electroanal. Chem., 281, 1 (1990).

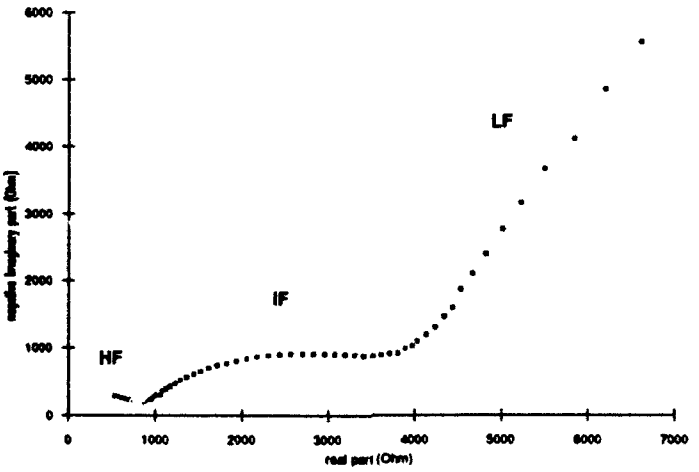

Figure 1 : Complex impedance diagram of an Armco iron/organic coating/NaCl solution system after 16 days; HF,IF,LF: high, intermediate and low frequencies, resp..

Anodic Dissolution and Passivation of Iron Analyzed in Frequency and Time Domains with Channel Flow Double Electrode

Masayuki ITAGAKI and Tooru TSURU

Dept. of Metallurgical Engineering, Tokyo Institute of Technology,
O-okayama, Meguro-ku, Tokyo, Japan

Using a channel flow double electrode (CFDE) system, the species emitted from the upstream electrode are detected on the downstream electrode. Under non steady state, it is impossible to use the steady state collection efficiency Ns because of a travelling time of ions for the gap between the working (upstream) and collector (downstream) electrodes. Therefore, it is necessary to correct with a dynamic collection efficiency $N(\omega)$, which is a function of freaquency.

The aims of this presentation are (1) to establish a dynamic collection efficiency for CFDE, and (2) to separate the partial current of surface accumulation and that of the dissolved ferrous ions during active dissolution and passivation of iron in acidic sulfate solutions, in both time and frequency domains.

Details of CFDE can be found elsewhere. Material of the working electrode was a pure iron ($4x1mm^2$), the collector electrode was a pure gold ($4x1mm^2$), and the gap between them was 0.05mm.

Using Frequency Response Analyzer (FRA), $N(\omega)$ was determined from the current ratio of the working electrode, $I_w(\omega)$, and the collector electrode, $I_c(\omega)$, at a certain frequency, ω;

$$N(\omega) = n_w I_c(\omega)/n_c I_w(\omega)$$

in an alkaline solution containing sulfate, where ferricyanide was reduced to ferrocyanide on the working electrode, then it was oxidized again on the collector electrode.

Measurement of current transient was performed by potential steps in the potential ranges of active dissolution and passivation in sulfate solution of pH1 and 4. Transient datas were recorded in a digital wave memory, which has 2048 sampling points and sampling rate of 2 μ s to 2ms, and processed by a desk top computer. Ferrous ions emitted from the working electrode were continuously monitored by the collector electrode, detecting with an electrochemical oxidation from ferrous to ferric ions at 1.4Vvs.SSE.

The emission efficiency of ferrous ions, $\Phi_{diss}(\omega)$, which corresponds to the ratio of ferrous ions dissolution partial current to the total working electrode current, and the film formation efficiency, $\Phi_f(\omega)$, are assessed as

$$\Phi_{diss}(\omega) = \mathrm{FFT}\{i_c(t)\}/N(\omega)\mathrm{FFT}\{i_w(t)\}, \qquad \Phi_f(\omega) = 1 - \Phi_{diss}(\omega)$$

where, $i_w(t)$ and $i_c(t)$ are working and collector electrode currents measured in this experiment, respectively. The partial currents for dissolution, $i_{diss}(t)$, and film formation, $i_f(t)$, in time domain are derived as follows

$$i_{diss}(t) = \mathrm{IFFT}[\,\mathrm{FFT}\{i_c(t)\}/N(\omega)\,], \qquad i_f(t) = i_w(t) - i_{diss}(t).$$

A NEW APPROACH FOR THE COMPUTATION OF THE FREQUENCY RESPONSE OF SPACE CHARGE-CONTAINING INTERFACES

J. Jamnik[1,2], S. Pejovnik[2], J. Maier[1]

[1]Max-Planck-Institut für Festkörperforschung,
Heisenberg str. 1, D-7000 Stuttgart 80, FRG

[2]Institute of Chemistry,
P.O. Box 30, Ljubljana, Slovenia

A thin single crystal placed between two equal electrodes is considered. It is assumed that there is Schottky disorder in the crystal with intrinsic space charge layers adjacent to the electrodes (Fig.1a) and that there is only one type of charge carriers mobile.

Frequency response of the considered system is calculated on the basis of general transport equations for current involving drift, diffusion and displacement terms. The equations are solved for the electric field perturbation due to the applied potential in a standard numerical way by applying the Galerkin method [1,2]. However, for the basis set of functions, which are used for a series approximation of the solution, harmonics are used. When taking into account the boundary conditions such a basis set leads to an analogy with waves. Namely, in the blocking case there are nodes at the boundaries since the faradaic current is confined within the crystal, while in the opposite case there are antinodes at the boundaries because there is no barrier for the current. Using this method the computational time is greatly reduced in comparison with the use of polynomials as basis functions [1,2].

Numerical results are analysed on the basis of the simple equivalent circuit (Fig.1). A method is proposed for the estimation of the interfacial capacitance C_i which then has a well defined geometrical meaning. The corresponding thickness is just equal to the distance from the electrode to the center of perturbed charge (Fig.1b). The dependence of C_i on the voltage drop across the space charge layer is evaluated and compared for the blocking and nonblocking case.

For the nonblocking case also the degree of influence of the geometrical shape of the space charge region on the interfacial capacitance is inspected. In the approximation, where all the space charge is stretched close to the electrode, e.g. approximated by a δ function, C_i is only twice as large as in the exact case.

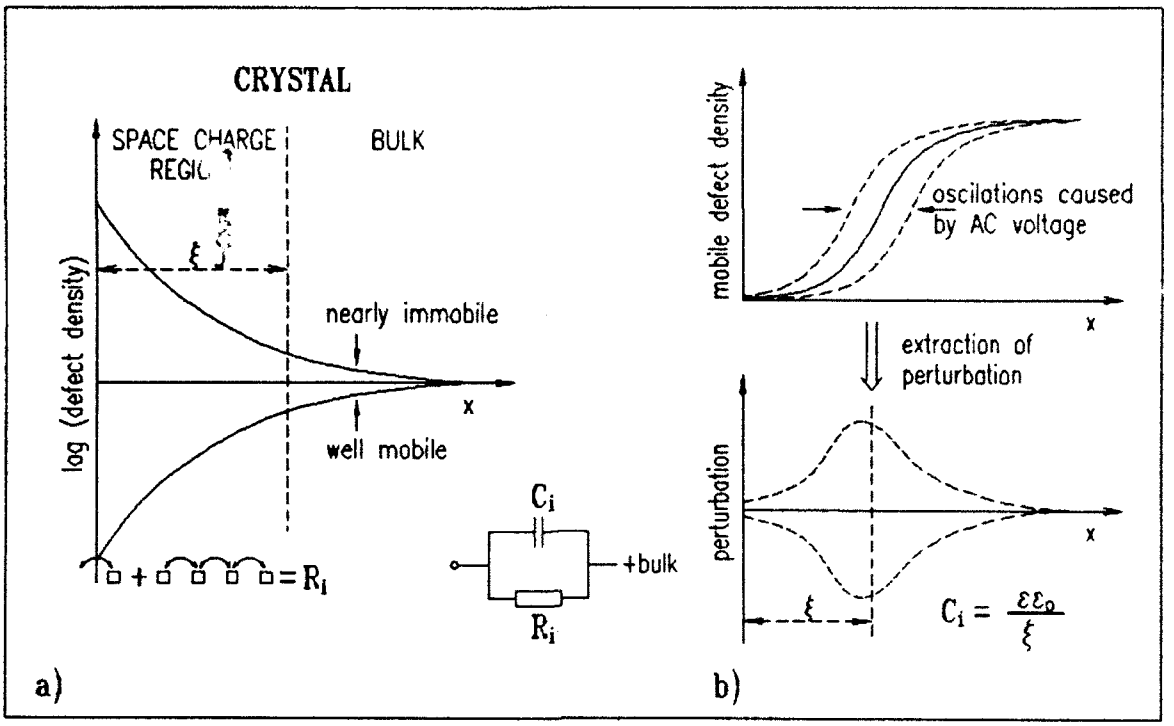

Fig. 1: a)Defect density distribution in thermodynamic equilibrium. b)Perturbation of mobile defect density due to the applied potential. The effect is greatly exaggerated for diagrammatic reasons.

The interfacial resistance R_i is derived analytically as a limiting case when the frequency approaches zero. The result is the same as one would expect from a pure thermodynamic picture [3].

References

1. H.A. Hoyen, J.A. Strozier, Che-Yu-Li, Surf. Sci., **20**, 258 (1970).
2. D.R. Franceschetti, J.R. Macdonald, J. Electroanal. Chem., **100**, 583 (1979).
3. J. Maier, Ber. Bunsenges, Phys. Chem., **90**, 26 (1986).

DIFFUSION IMPEDANCE IN PLANAR, CYLINDRICAL AND SPHERICAL SYMMETRY

T.Jacobsen and K.West

Fysisk-Kemisk Institut, The Technical University of Denmark
DK-2800 Lyngby - DENMARK

For a diffusion controlled electrode reaction

$$0 \rightarrow ne^- + \sum \nu_i S_i \qquad (1)$$

the diffusion impedance, $z_d(s)$ is defined as

$$z_d(s) = \frac{\eta(s)}{i(s)} = \sum \frac{\nu_i}{nF} \cdot \frac{\partial \epsilon}{\partial c_i} \cdot \frac{\Delta c_i(s,x_o)}{J_i(s,x_o)} \qquad (2)$$

where $\eta(s)$, $i(s)$ are Laplace transforms of potential and current perturbations from a steady state and $(\partial\epsilon/\partial c_i)$ is the partial derivative of the electrode equilibrium potential with respect to the concentration of the species i. The dependence on the frequency parameter,s ,is confined to the ratio between the transform of the concentration perturbation, $\Delta c_i(s,x_o)$, and the flux density, $J_i(s,x_o)$, at the electrode surface, x_o.

In the present work the concentration to flux ratio in eq.(2) is determined for electrodes of planar, cylindrical and spherical geometry in a finite diffusion region with both Nernstian and blocking boundary conditions at the diffusion layer boundary.

SOLUTIONS. The Laplace transformed diffusion equation

$$\nabla^2(\Delta c(s,x)) - (s/D)\Delta c(s,x) = 0 \qquad (3)$$

is solved with the flux boundary condition at the electrode surface

$$J(s,x_o) = -D\nabla(\Delta c(s,x))\Big|_{x_o} \qquad (4)$$

and on the other boundary of the diffusion region, x_δ, either a constant concentration, Nernstian diffusion layer

$$\Delta c(s,x_\delta) = 0 \qquad (5)$$

or an impermeable barrier, blocking conditions

$$J(s,x_\delta) = 0 \qquad (6)$$

Introducing the dimensionless functions

$$\psi_o = x_o \sqrt{\frac{s}{D}} \quad , \quad \psi_\delta = x_\delta \sqrt{\frac{s}{D}} \qquad (7)$$

and the notation

$$\Delta c_o = \Delta c(s,x_o) \quad , \quad J_o = J(s,x_o)$$

the solutions are

Planar symmetry, diffusion layer thickness δ

Nernstian
$$\frac{\Delta c_o}{J_o} = \frac{\delta}{D} \frac{\tanh[\psi_\delta]}{\psi_\delta} \qquad (8)$$

Blocking
$$\frac{\Delta c_o}{J_o} = \frac{\delta}{D} \frac{\coth[\psi_\delta]}{\psi_\delta} \qquad (9)$$

Cylindrical symmetry, electrode radius r_o

$$\textit{Nernstian} \quad \frac{\Delta c_o}{J_o} = \frac{r_o}{D} \frac{I_o[\psi_\delta]\cdot K_o[\psi_o] - I_o[\psi_o]\cdot K_o[\psi_\delta]}{\psi_o(I_1[\psi_o]\cdot K_o[\psi_\delta] + I_o[\psi_\delta]\cdot K_1[\psi_o])} \tag{10}$$

$$\textit{Blocking} \quad \frac{\Delta c_o}{J_o} = \frac{r_o}{D} \frac{I_o[\psi_o]\cdot K_1[\psi_\delta] + I_1[\psi_\delta]\cdot K_o[\psi_o]}{\psi_o(I_1[\psi_\delta]\cdot K_1[\psi_o] - I_1[\psi_o]\cdot K_1[\psi_\delta])} \tag{11}$$

where I and K are modified Bessel functions.

Spherical symmetry, electrode radius r_o

$$\textit{Nernstian} \quad \frac{\Delta c_o}{J_o} = \frac{r_o}{D} \frac{1}{1 + \psi_o \coth[\psi_\delta - \psi_o]} \tag{12}$$

$$\textit{Blocking} \quad \frac{\Delta c_o}{J_o} = \frac{r_o}{D} \frac{\psi_\delta - \tanh[\psi_\delta - \psi_o]}{(\psi_\delta - \psi_o) + (\psi_o\psi_\delta - 1)\tanh[\psi_\delta - \psi_o]} \tag{13}$$

DISCUSSION. A few examples of the various diffusion impedances as function of frequency ($s=j\omega$) are given below. The quantity plotted is the reduced impedance $\Delta c_o D/J_o\delta$ eq.(8-9) or $\Delta c_o D/J_o r_o$ eq.(10-13). The parameter values in the graphs are the reduced frequencies $\delta^2\omega/D$ or $r_\delta^2\omega/D$.

Fig.1 shows the behavior for finite boundary conditions. The general observation is a decrease in impedance and phase angle when going from planar to spherical geometry reflecting the increase in transport area and amount of substance with the distance from the electrode surface.

In fig.2 the cylindrical and spherical cases are compared for infinite diffusion regions. Whereas the spherical electrode has a steady state at DC the cylindrical impedance has a low frequency asymptote with constant imaginary part of $-\pi/4$.

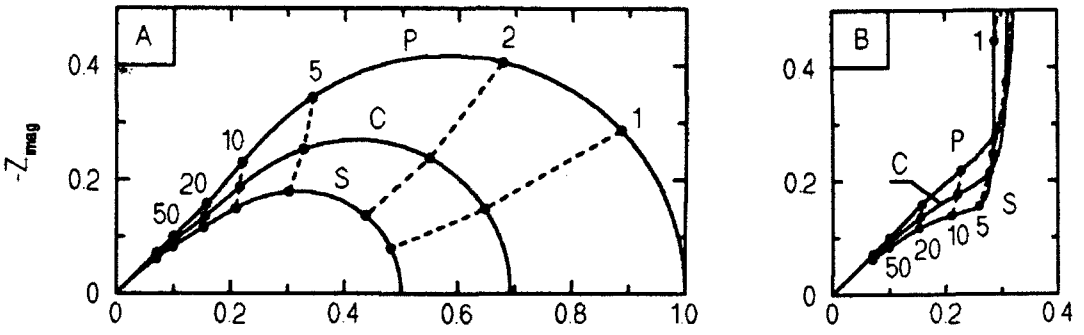

Fig.1 Reduced impedance for finite diffusion with (A) Nernstian and (B) blocking boundaries. (P) planar, (C) cylindrical and (S) spherical symmetry. Geometrical parameters used: $\delta = r_o = r_\delta - r_o$.

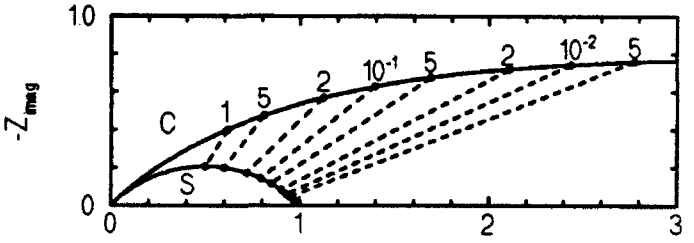

Fig.2 Reduced impedance for infinite diffusion in cylindrical (C) and spherical (S) symmetry.

IMPEDANCE SPECTROSCOPY
A METHOD FOR IN-SITU CHARACTERIZATION OF EXPERIMENTAL FUEL CELLS

W. Jenseit, O. Böhme, F.U. Leidich, H. Wendt
Institut für Chemische Technologie der TH Darmstadt
Petersenstraße 20, 6100 Darmstadt, Germany

1.Introduction Fuel cell development deals mainly with materials development and development of production technologies of fuel cell components - in particular in developing optimal micro-morphologies of porous gas diffusion electrodes. It is obvious, that for the delicate structural features of gas diffusion electrodes for different types of fuel cells common rules for microengineering the respective optimal structure do not exist and a cumbersome experimental approach to find the optimum structural features by trial and error is unavoidable. Adding to the usual measurements of current voltage curves impedance spectroscopy allows to obtain additional useful information of morphological significance.

2. Electrode model for evaluating impedance spectroscopic measurements. The transmission line model was generally used adopted according to Mund and Raistrick respectively. The charge transfer resistance includes an R/C combination describing combined mass transfer and reaction of dissolved gas into the nanoporous particles with only partial utilization of the catalyst under load characterized by the electrochemical Thiele modulus $\phi_{k,el}$. It was also necessary to add the Nernst-impedance Z_{diff} for describing the diffusion across the electrolyte film covering the electrode particles.

3. Results This paper describes five case studies in which impedance spectroscopy is applied to help in understanding structural features of gas diffusion electrodes which are under development, facilitating to find improved fabrication methods and to solve particular problems concerning electrode structure and micromorphology. Concerning alcaline fuel cells,(i) Raney - nickel anodes, (ii) PTFE-bonded Pt-activated soot and (iii) Silflon electrodes (Ag-covered microporous PTFE structures) had been investigated. Further this paper reports on impedance spectroscopy of (iv) conventional and modified nickel sponge anodes and (v) nickel oxide cathodes of molten carbonate fuel cells.

3.1 Raney Nickel anodes. The current voltage curve of the Raney-nickel anode is linear as long as current densities are much lower than the mass transfer limited value.The Nyquist plots of the electrode impedance

which had been measured at the anodic overpotential of +5mV show the small semicircle with 45° slope at high frequencies due to the diaphragm resistance followed by a flattened, distorted semicircle also with a slope of roughly 45°, modelled by the TML. According to impedance data the Raney-nickel grains (d_p = 5μm) are too thick and therefore not fully utilized in particular at higher current density accordingly the granulometry of the Raney nickel could be changed.

3.2 Pt-activated Vulcan XC cathode. The evolution of the current voltage curve of cathodic oxygen reduction with time over a period of 770 hours shows that up to 200 h the electrode improves and begins then to deteriorate steadily b t with ever decreasing rate without reaching a limit g behaviour at 770 hrs.
The history of the electrode can be elucidated by impedance spectroscopy. During the first 10 hours the electrode behaves like a flat electrode - as described by Holtze. During the first 70 hours the initially only superficially wetted electrode becomes wetted and subsequently flooded by the electrolyte and only after that time all catalyst particles are available electrochemically. As seen from the charge transfer resistance (related to the effectively wetted surface from the very beginning the catalyst - as far as due to improved wetting it becomes electrochemically available - begins to deteriorate but deterioration due to grain-ripening decelerates with time ($T^{1/5}$-law).

3.3 The Silflon-electrode. The current voltage behaviour of the oxygen-reducing Silflon-electrode manifests that the Silflon electrode is certainly the most effective oxygen-cathode investigated in this paper. The Nyquist plots reveal that the catalyst utilization decreases with increasing current density . Therefore the electrode may be made essentially thinner

3.4 Molten Carbonate fuel cell electrodes. The current voltage curves of molten carbonate fuel cells are essentially linear. With an effective cell resistance of 2 Ω cm^2 and higher conventional cells cannot bear current densities of more than 0.15 A cm^{-2} as efficiencies would become intolerably low. Improving the cathodes and anodes means pursuing two aims: Increasing the electrochemically accessible inner surface by improved micromorphology and stabilizing these morphological features. Comparison of Nyquist plots of improved and conventional cathodes and anodes shows that (i) ohmic resistance is decreased, (ii) charge transfer is improved due to a higher accessible inner surface of cathode and also (iii) mass transfer of dissolved oxygen proceeds much fast as the electrolyte-film is more equally distributed over the surface of smaller NiO(Li)-clusters.

A STUDY ON TOAD BLADDER MEMBRANES BY ELECTROCHEMICAL IMPEDANCE SPECTROSCOPY

Li Jialing, Cui Yanfang, Xiong Yan,
Liu Jie, and Long Guangdou
Laboratory of Membrane Electrochemistry,
Department of Chemistry, Huazhong Normal University,
Wuhan 430070, P.R. China

The electrochemical impedance spectra for isolated toad bladder were obtained by using a double reference electrode electrochemical system (EG&G PARC Model 378 Impedance System). In most cases where the normal Ringer's solutions were used as bathing solutions or some drugs as additives, a semicircle can be seen on the complex plane. The regularity of the semicircles proves that the GHK relationship is suitable over a wide range to the apical membrane transport. And this is also compatible with a two-barrier-one-side channel structure. When the membrane was incubated in Na-Ringer's solution on the serosal side, there was a small semicircle appearing on the low frequency end of normal semicircles (Fig. 1). It disappeared by the use of the high serosal K activity , the so-called K-depolarization for basolateral membranes. So it is reasonable to regard this small semicircle as the impedance spectrum of basolateral transport.

Quinidine, an agent thought to increase the level of cytosolic free calcium ions is found to induce the semicircle to distort markedly when it acted whth the membrane's serosal side. The spectra were undergoing definite but complex evolution with time, as can be seen from curve a to e in Fig. 2. But the distortion is very similar to that in complex planes where absorpted intermediaters are present during electrochemical processes.

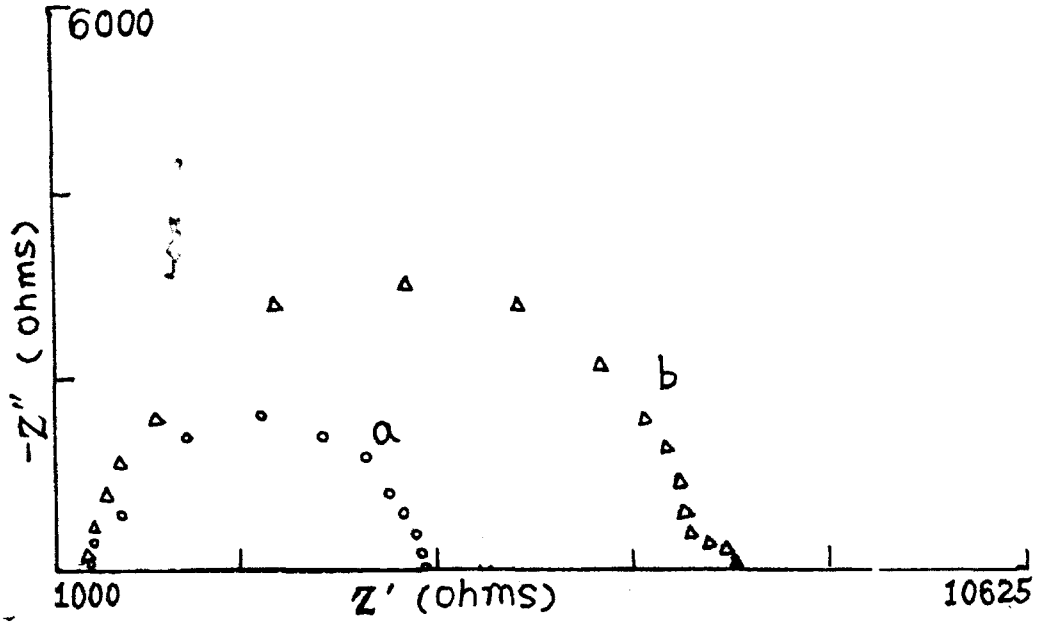

Fig.1. Complex plane plots for toad bladder membranes. serosal solution: a, K-Ringer's solution
b, Na-Ringer's soltion

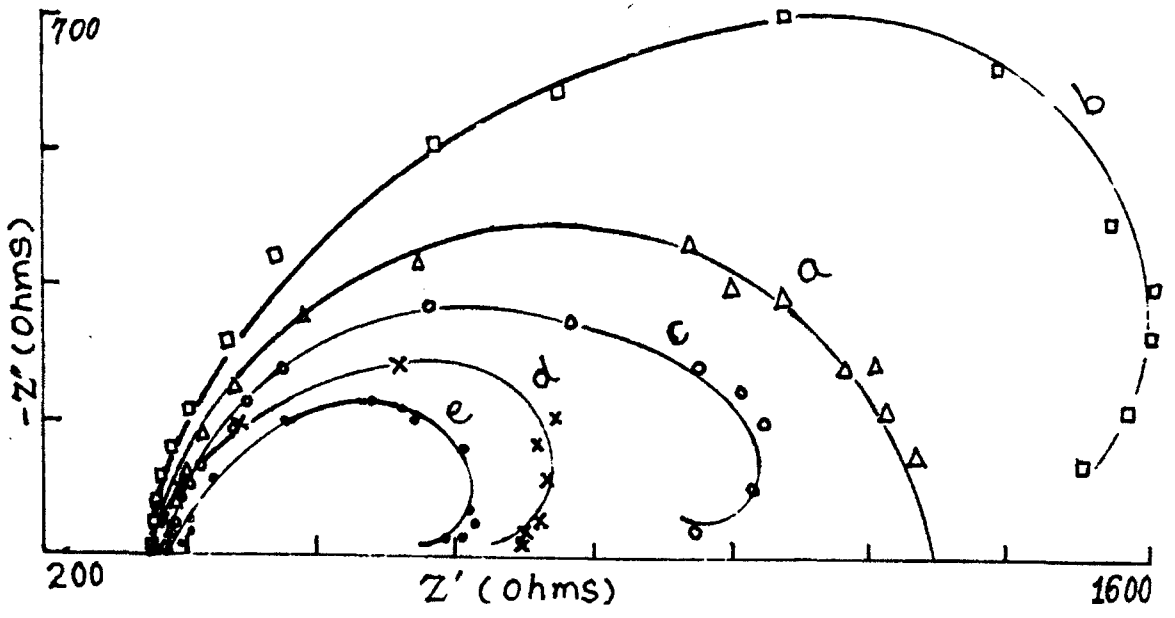

Fig.2. Complex plane plots for toad bladder membranes. incubated with quinidine solution. time sequence: e>d>c>b>a

LOW FREQUENCY MEASUREMENTS IN IMPEDANCE SPECTROSCOPY: CORRECTION OF THE WARBURG IMPEDANCE.

R. Jiménez, M. C. Montemayor and E. Fatás.
Dpt. Química Física. Universidad Autónoma de Madrid.
28049 Madrid. SPAIN.

The classical solution of the faradaic impedance equations, supposes that the transpot processes are in steady state, i. e., the transient behaviour of the a.c. concentration profile is neglected [1]. Therefore, the resulting equations are only applicable when enough cycles of the perturbing signal have elapsed [2].

In order to avoid, partially, this problem, we have deduced more general equations for the faradaic impedance, without the steady state approximation for the mass transfer.

The resulting equations are:

$$Z_{el}'(t) = \frac{\left[R_{ct} + \sigma' A(\omega) \right] D(\omega)}{\left[R_{ct} + \sigma' A(\omega) \right]^2 + \left[\sigma' B(\omega) + \omega C_d D(\omega) \right]^2}$$

$$Z_{el}''(t) = \frac{\left[\sigma' B(\omega) + \omega C_d D(\omega) \right] D(\omega)}{\left[R_{ct} + \sigma' A(\omega) \right]^2 + \left[\sigma' B(\omega) + \omega C_d D(\omega) \right]^2}$$

where $$D(\omega) = \left[R_{ct}' + \sigma' A(\omega) \right]^2 + \left[\sigma' B(\omega) \right]^2$$

being A and B a form of the Fresnel's integrals.

Obviously, replacing $A(\omega)$ and $B(\omega)$ by their limiting values, with $F_c(\infty) = F_c(\omega) = (\pi/2\omega)^{1/2}$, these equations revert to the classical ones of Z'_{el} and Z''_{el} corresponding to the steady state.

The difference between the steady and 'non steady' electrodic impedance, described by this equations, is less in the zone corresponding to pure charge transfer (high frequencies), and becomes considerable in the low frequency region, where mass transfer plays an important role.

The validity of the deduced equations has been confirmed with the system Fe(III)/Fe(II) on a Pt electrode. This couple, with a simple one-electron transfer, has been chosen because of its simplicity.

Figure shows the theoretical lines calculated using the classical stationary equations and the equations deduced in this work, superimposed on the experimental stationary data and measurements carried out during the first cycle of the perturbing signal.

A reasonable concordance, considering the difficulty of the measurement, between non steady points and theoretical line can be observed. On the other hand, the observed deviations, between the steady and non steady measurements, are in agreement with those predicted by the deduced equations. This supports the validity of these equations for the analysis of non steady data.

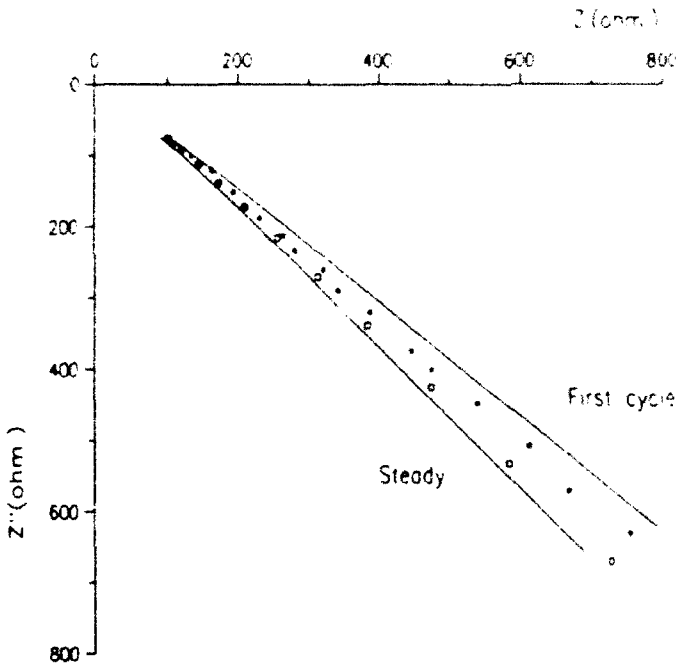

REFERENCES

1. M. Sluyters-Rehbach and J.H. Sluyters in C.H. Bambord and R.D. Compton (Eds), Comprehensive Chemical Kinetics, Vol 26, Elsevier, Amsterdam, 1986.
2. T. Berzins and P. Delahay, Z. Elektrochem. 59, 792 (1955).

MICROSCOPIC AND ELECTROCHEMICAL IMPEDANCE ANALYSIS OF THE DEGRADATION OF POLYIMIDE-COATED AL METALLIZATION

M. Kendig, S. Jeanjaquet, J. Lumsden and R. Addison
Rockwell International Science Center
1049 Camino dos Rios
Thousand Oaks, California 91360

Introduction

The development of non-hermetic packaging for microelectronic devices requires highly resistant passivation layers to eliminate degradation of metallization and microelectronic circuitry under conditions of high water activity, electrical bias and the presence of corrosive ionic species such as chloride. Both anodic and cathodic bias potentials lead to the degradation of the metallization coated with polyimide. Anodic bias on Al metallization has a rather predicted effect of anodically dissolving the metal by the reaction:

$$Al + 3Cl^- \text{ (solution)} \rightarrow AlCl_3 \text{ (solution)} + 3e^-$$

Recently we have documented the accelerated disbonding of 2 μm polyimide coatings on aluminum as a result of cathodic bias.[1] "Cathodic corrosion" of aluminum metallization has been considered to play an even more significant role in the degradation of aluminum conductors in coated microelectronic circuitry.[2] To understand the detailed mechanism of cathodic bias-induced degradation of aluminum metallization under polyimide coatings, a combined *in situ* electrochemical impedance/microscopic analysis experiment has been initiated. Progress on this project will be reported.

Experimental

An array of spade-shaped 0.63 x 0.63 cm^2 electrodes with 0.6 cm x 0.05 cm of aluminum leads were deposited on Si substrates using photolithographic techniques. A polyimide film was applied to the metallized Si wafer. A subsequent photolithographic process left bare a portion on the lead which was subsequently gold plated. Figure 1a shows a schematic of the device.

The wafer was diced and the devices were mounted on a composite circuit board with wire-bonded gold leads connecting the pad on the metallization lead to a solderable connector as shown in Figure 1b. The wire-bond conductor and the edges of the metallized device were masked with an electroplater's mask so that they would not be exposed to the test environment. Alternatively a defect was placed in the center of the device before it was exposed to the environment. The circuit board containing the device could be placed in the cell shown in Figure 2, which allowed simultaneous microscopic (acoustic and light-optical) viewing and electrochemical analysis.

The coated sample was exposed to 0.05 M NaCl under conditions of -5 V vs SCE of cathodic bias. Electrochemical impedance spectra and acoustic and light optical micrographs were periodically taken. A sample with a defect was exposed to the same environment at -2 V vs SCE.

Discussion of Progress

Figures 3a-b show acoustic micrographs taken in a region near the edge of the metallization for the sample soon after initial exposure and after 72 hours of exposure to the 0.05 M

NaCl under -5 V of cathodic bias, respectively. Many of the features on the coating appearing in the acoustic micrograph were not observed by light optical microscopy. Several important observations can be made by comparing Figures 3a and 3b. First, several large heterogeneities appear in the center and near the edge of the metallization. These regions remain with extended exposure. A speckle structure is barely discernible initially, but becomes more pronounced with exposure time. Finally, a large band of high intensity appears diagonally in the acoustic micrograph after several days of exposure to the electrolyte and bias. These latter effects most likely result from the uptake of water by the sample. The quantity of water taken up by the sample is determined to be quite substantial from the following EIS analysis.

Electrochemical impedance spectra obtained in parallel with the microscopy demonstrate that the sample behaves entirely as a capacitor over the frequency range from 1 kHz to 10 mHz, even after 7 days at -5V. Capacitance for the sample as a function of time appears in Figure 4a from which a volume fraction of water may be estimated[3] and follows a $t^{1/2}$ behavior as shown in Figure 4b.

These results will be compared to similar data obtained from a sample which is not biased and one which is biased anodically.

A sample with a macroscopic defect gave impedance spectra which were dominated by the defect. The low frequency impedance spectra correlated with the degradation of the interface as followed by optical microscopy.

These results will be presented and summarized in terms of the possible role played by bias in degrading polyimide, and in water transport and degradation of the polyimide.

Acknowledgment

The authors gratefully acknowledge the help of John Mather of Collins Avionics and Communications Division in providing the test samples used in this work.

References

1. M. Kendig, M. Abdel-Gawad and R. Addison, Corrosion, to be published.

2. R.B. Commozoli, RCA Review, 37, 483 (1976).

3. D.M. Brasher and A.H. Kingsbury, J. Appl. Chem., 4, 62 (1954).

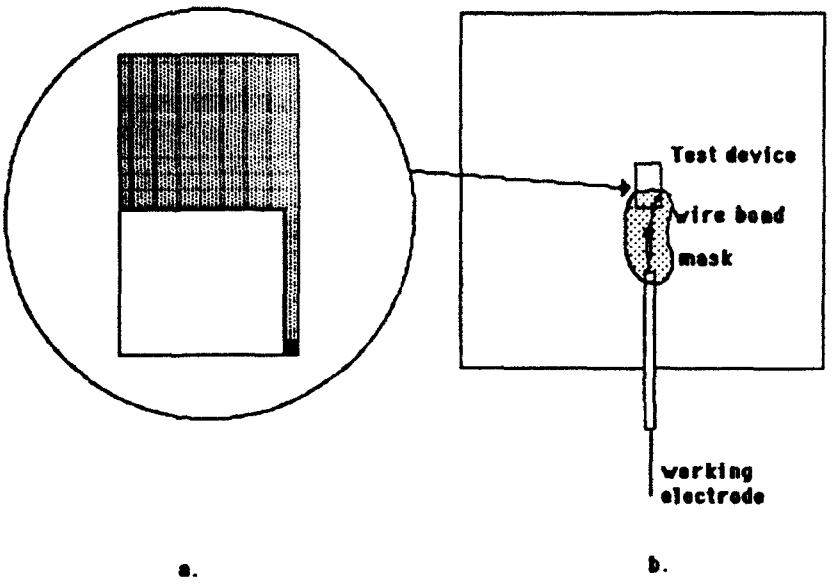

Figure 1 (a) Schematic of the test metallization. (b) Schematic for the mounting and wire-bonding to a solder lead.

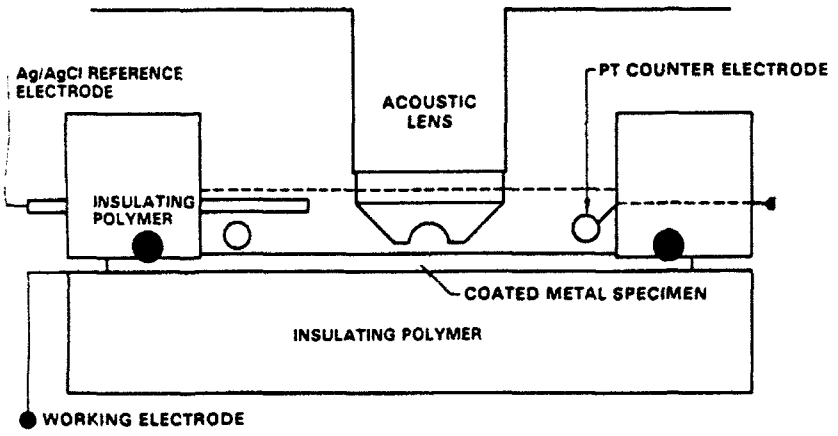

Figure 2 Schematic for the electrochemical cell used for in situ microscopy.

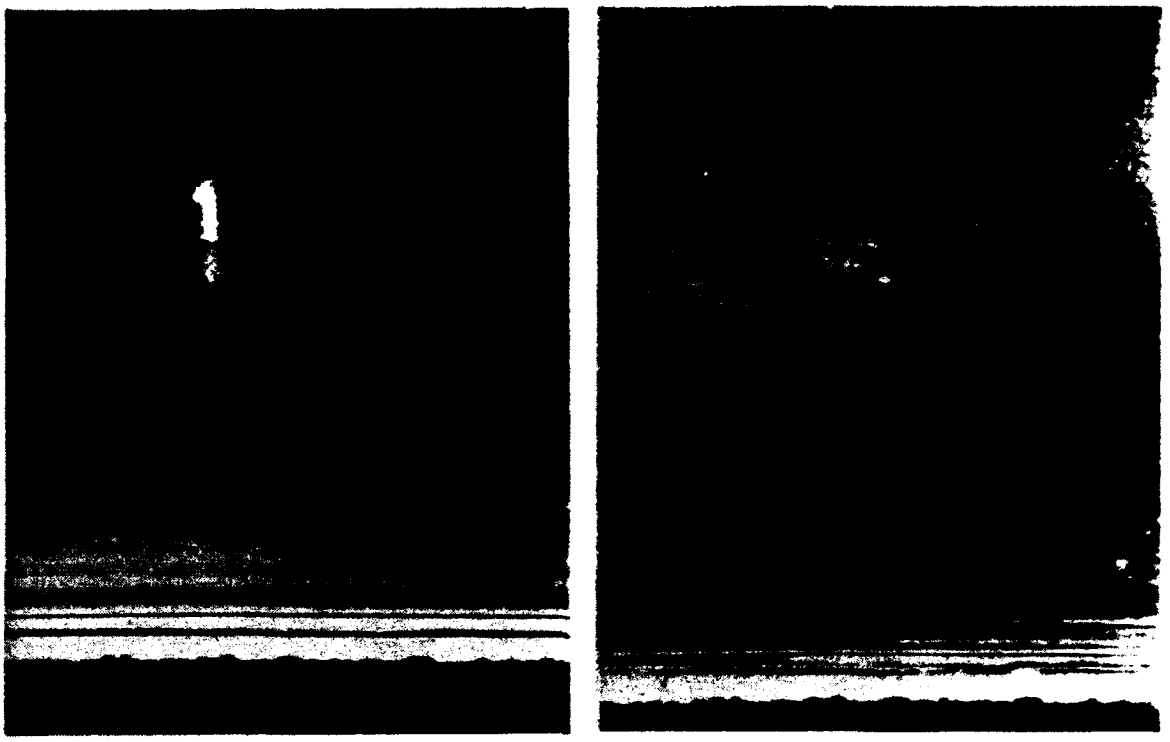

(a) 4 hours (b) 72 hours

Figure 3 Scanning acoustic micrographs of polyimide exposed to 0.05 M NaCl at -5V.

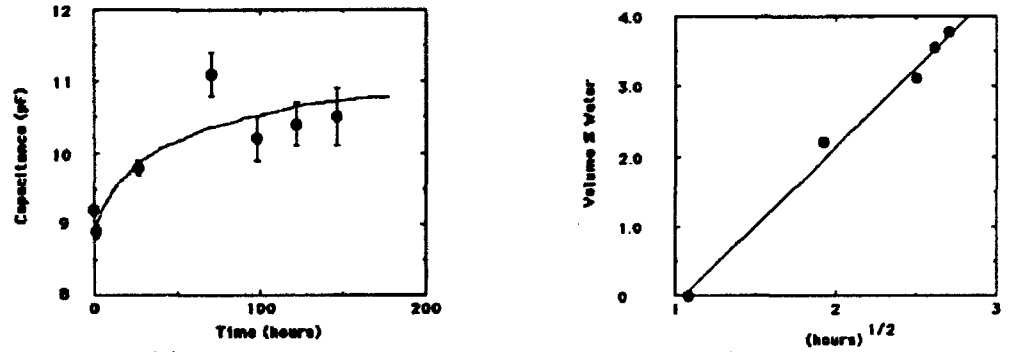

(a) (b)

Figure 4 (a) Capacitance obtained from analysis of the impedance spectrum of the sample of Figure 1 as a function of time of exposure to 0.05 M NaCl at -5 V vs SCE. (b) Calculated volume fraction of water as a function of the square root of time using the capacitance data.

THE PAST AND FUTURE OF ELECTROCHEMICAL IMPEDANCE ANALYSIS OF PROTECTIVE ORGANIC COATINGS ON METAL

Martin Kendig
Rockwell International Science Center
1049 Camino dos Rios
Thousand Oaks, CA

Electrochemical impedance in one form or another has been applied to the evaluation of the kinetics of degradation of organic coatings such as paints and lacquers on metals for over 40 years. The earliest measurements involved the use of impedance bridges to evaluate coating capacitance.[1-2] Certain assumptions regarding the distribution and dielectric nature of the coating allowed the evaluation of the volume fraction of water in the coating dielectric.[2] Menges and Schneider first used frequency dependent impedance for characterizing organic coatings.[3] They noted that a deviation of the impedance from a 1/f dependence at low frequency correlated with coating degradation which was associated with the onset of shorting ionic paths. In the early 1970's several reports[4-5] were made of the frequency dependence of the electrochemical response of organic coatings on steel. Beaunier, Epelboin, Lestrade and Takenouti were the first to use a frequency response analyzer (FRA) to obtain impedance spectra of very thin porous coatings on steel in dilute sulfuric acid. For this work, the impedance of the underlying substrate dominated the spectra.[4]

Since deviations from a purely capacitive frequency dependence marks the degradation of the polymer dielectric, the frequency dependence of EIS is well suited for evaluating the integrity of the organic-coated metal. Furthermore, a decrease in the capacitive impedance (increase in capacitance) can be attributed to the uptake of water. Despite the existence of a few experiments that demonstrate the correlation of parameters extracted from impedance spectra to long term behavior[6-7], there is general agreement that EIS characterizes the state of the coating and, therefore, detects the very earliest stages of degradation. This feature can readily be used to provide an early prediction of longer term behavior.

While there is more or less general agreement on this general equivalent circuit model, the interpretation of the meaning of the specific element has recently become somewhat controversial[8]. Kendig and Leidheiser interpreted the resistance shorting the polymer coating as due to the penetration of electrolyte into the coating in either actual or virtual pores.[5] The motivation for this interpretation has resulted from the observations of Mayne and Scantlebury of the highly heterogeneous nature of organic coatings.[9] Recent interpretations by Haruyama and coworkers suggest that Rpo relates to the disbonding of an organic coating[10], which is hard to justify in light of observations of free films. [11]

The more recent developments in the application of EIS to organic coatings include the trend of transferring the technology from the laboratory to field application. Workers at Nippon Steel have demonstrated an integrated field unit and have presented examples of its application for mapping the degradation on automotive structures.[12]
Kendig, Breitweiser and Hudyma recently applied EIS for monitoring wear of planographic printing plates on customer-owned printing presses. [13]

Another important development of EIS technology has been the demonstration by Chen and Skerry of the relationship between electrochemical noise and EIS.[14]

Basic and applied research using EIS to solve problems of protective organic coatings may well be directed in the future to the following areas:

Application to field studies
Focus on the capacitance (water structure/pigment stucture)
Relationship of adhesion loss to EIS
Application of EIS to coating problems facing microelectronic packaging
Extension of the technique to higher frequencies
Combined techniques (microscopic, spectroscopic, mechanical testing)

These possible future applications of EIS to organic coatings will be discussed in terms of what can be learned with some examples from the author's laboratory.

References

1. F. Wormwell and D. Brasher, J. Iron and Steel Inst., 164 (1950).
2. D. M. Brasher and H. M. Kingsbury, J. Appl. Chem., 4, 62 (1954).
3. G. Menges and W. Schneider as referenced by H. Leidheiser, "Electrical and Electrochemical Measurements as Predictors of Corrosion at the Metal-Organic Coating Interface" in 'Corrosion Control by Coatings', H. Leidheiser ed., Science Press, Princeton (1979).
4.L. Beaunier, I. Epelboin,J.C. Lestrade,H. Takenouti, Surf. Tech.,4,237 (1976)
5.M. Kendig and H. Leidheiser,J. Electrochem. Soc.,123,982 (1976)
6.M. Kendig, S. Tsai and F. Mansfeld,Corr. Sci.,23(4),317(1983).
7. J. Scully,J. Electrochem. Soc.,136,4 (1989) and also J. N. Murray and H. P. Hack, Corrosion,47(6),480 (1991)
8. M. Kendig , F. Mansfeld and C. H. Tsai, Corrosion,47(12), 964 (1992).
9. J. E. O. Mayne and J. D. Scantlebury, Br. Polym. J.,2, 240 (1970)
10. S. Haruyama, M. Asari and T. Tsuru, "Impedance Characteristics During Degradation of Coated Steel", 'Corrosion Protection by Organic Coatings', M. Kendig and H. Leidheiser, eds. Electrochemical Society Proceedings Volume 87-2 (1987).
11. F. Mansfeld and M. Kendig, "Electrochemical Impedance Test for Protective Coatings", 'Laboratory Corrosion Tests and Standards, ASTM STP 866, G. Haynes and R. Baboian eds, ASTM, Philadelphia, 1985, p122.
12.K. Homma, Nippon Steel, paper presented at Corrosion '91.
13. M. Kendig, S. Breitweiser and E. Hudyma, Corrosion,47(1), 62(1991).
14. Chen and Skerry, Corrosion, 47(8),598(1991)

Acknowledgement

Much of this work has been supported by the Office of Naval Research under contract N00014-90-C-0110 for which the author is grateful.

FREQUENCY- AND TIME-DOMAIN INVESTIGATIONS OF MODIFIED ALUMINUM OXIDE LAYERS

K. Kluger, M.M. Lohrengel
Institut für Physikalische Chemie und Elektrochemie
Heinrich-Heine-Universität Düsseldorf
D-4000 Düsseldorf, Germany

The anodic oxide formation on valve metals like Al is described by the high field model where a field-assisted hopping mechanism of the mobile ions is assumed (1). Potentiostatic pulse measurements showed that the high field model has to be extended by a time and field dependent concentration of mobile charge carriers inside the oxide (2-5).

Anodically formed nonporous Al oxide layers (acetate buffer, pH 5.9) were investigated in detail by Electrochemical Impedance Spectroscopy (EIS). The oxide layer can be described by a simple equivalent circuit of a capacity and a resistance in parallel. The oxide behaves like a dielectric material and the capacity is a function of the oxide thickness. The resistance is given by the high field model and is a function of the field strength. Because of the insulating behaviour of the oxide the layer resistance is very high. Therefore, the experiments were carried out using thin oxide films (d_{ox} < 20 nm).

For a constant film thickness the differential layer resistance shows an exponential dependence on the potential (Fig. 1). The differential conductivity decreases with decreasing field strength inside the oxide film. Calculations of the differential conductivity from the high field model lead to a reasonable good fit indicating that the high field model is valid at potentials >0 V. At cathodic potentials (0 to -1 V (HESS)) the differential conductivity increases due to an incorporation of mobile protons into the oxide film. At potentials <-1 V (HESS) a stronger hydrogen evolution takes place and the oxide film is destroyed.

For the investigation of time-dependent effects conventional EIS is not suitable because the time to record a complete impedance spectrum is very long. Realizing the fact that the oxide layer can be described by a simple RC-circuit and that the capacity is constant for a constant oxide layer thickness it is possible to measure phase and impedance at one frequency only. These measurements show a significant time

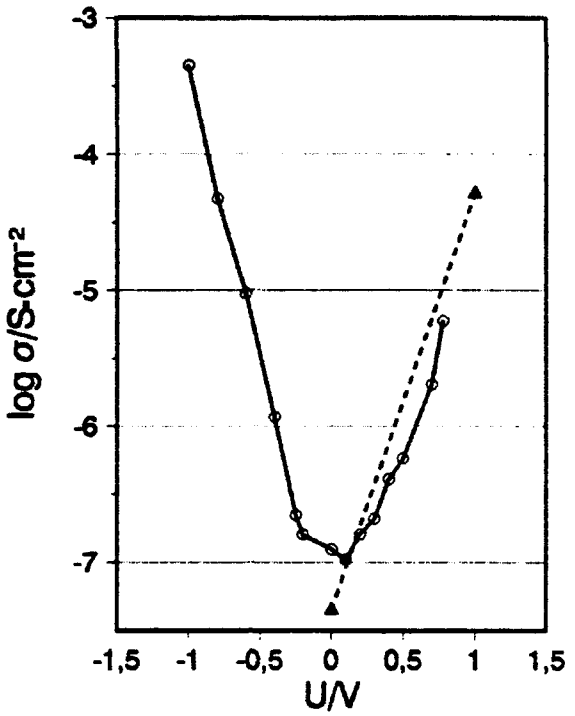

Fig. 1: Logarithm of the differential conductivity σ of an Al oxide layer, formed at 0.8 V, in dependence on the potential (full line). Corresponding values (dashed line) calculated from the high field model.

and potential dependence of the layer resistance. When the field strength is reduced the resistance increases due to an exhaustion of charge carriers by diffusion. For longer periods of time a potential independent corrosion becomes dominant. These results are discussed in terms of the extended high field model.

References:

1. A. Güntherschulze, H. Betz, Z.Phys. 92 (1934) 367.
   E.J.W. Verwey, Physica 2 (1935) 1059.
2. M.M. Lohrengel, D. Ebling, Dechema Monographs 120 (1989) 213.
3. M.M. Lohrengel
   in "Electrochemical and Optical Techniques for the Study and Monitoring of Metallic Corrosion" M.G.S. Ferreira, C.A. Melendres (eds.), Kluwer Academic Publischers, Dordrecht (1991) p. 69-121.
4. K. Kluger, M.M. Lohrengel, Ber. Bunsenges. Physik. Chem., 95 (1991) 1458.
5. M.M. Lohrengel, K. Kluger. Elektrokhimiya, submitted for publication.

CHARACTERIZATION OF SOME III-V SEMICONDUCTOR/ELECTROLYTE INTERFACES UTILIZING ELECTROCHEMICAL IMPEDANCE SPECTROSCOPY

Shyam S. Kocha and Bruce E. Liebert

Materials Research Laboratories, Department of Mechanical Engineering, University of Hawaii at Manoa, Honolulu, HI 96822

The thermodynamic reversible potential required to decompose water into hydrogen and oxygen is about 1.23 eV. An overpotential of 100 - 400 mV may have to be overcome at the semiconductor /electrolyte interface to successfully electrolyze water. Thus, an optimal bandgap of a semiconductor would be in the range 1.6 - 1.8 eV. Single crystal $GaInP_2$, (Eg = 1.83 eV) and $Ga_{1-x}Al_xAs$ (Eg = 1.5 - 1.8 eV) grown epitaxially in a MOCVD reactor (at NREL) were the subject of this study since, by virtue of their bandgaps, they show promise of being capable of splitting water in the absence of an external bias. These materials were studied when immersed in various aqueous electrolyte solutions of different pHs. Electrochemical impedance spectroscopy (EIS) was used to investigate the interface, which was modeled using an equivalent electrical circuit analog that represented the physical phenomena. Based on the space-charge layer capacitance, the flat-band potential and hence, the corresponding position of band edges relative to the hydrogen and oxygen redox levels were determined.

The instrumentation consisted of a Solartron 1255 frequency response analyzer used to generate 20 mV(peak-peak) ac signals with frequencies from 100 μHz to 100 kHz and a PAR 273 potentiostat to subject the sample to various potentials with respect to a reference (SCE) electrode. The electrochemical cell was a standard 3-electrode configuration with platinum gauze as the counter electrode. Nitrogen gas was bubbled through the electrolyte to purge dissolved oxygen. The cell was placed in a Faraday cage and the experiments conducted in the absence of illumination.

On investigating the response of the $GaInP_2$/electrolyte system by means of Nyquist and Bode plots, several features were revealed. The Nyquist plot (-Imag Z vs Real Z) showed two semicircles in the spectrum (Fig. 1), one at low frequencies and the other at high frequencies; i.e., two time constants. The larger, low frequency semicircle varied in diameter with the applied bias, which is attributed to the space charge layer capacitance of the sample. The smaller semicircle, observed at higher frequencies, remained invariant in diameter at all biases, displaying characteristics that would suggest an oxide film of low capacitance and resistance.

In the case of $Ga_{1-x}Al_xAs$ in highly acidic or basic solutions, the samples showed instability in terms of the open circuit potential as well as scatter in the impedance data when a bias is applied. This is attributed to the aluminum constituent which is amphoteric and forms various oxides, some of which are unstable. A Nyquist plot (Fig. 2) at a pH of 4.8 exhibited tilted semicircles which, possibly, indicate the existence of a continuous distribution of overlapping surface states.

A nonlinear least-squares program by B. A. Boukamp [1] was used to fit the model to the data, which resulted in fits with a relative error of < 2-3%. The equivalent circuit describing the phenomena at the $GaInP_2$/electrolyte interface consists of a parallel RC element to represent an oxide film and another RC element to represent the space-charge layer capacitance and polarization resistance, all in series with the electrolyte resistance. Whereas in the case of $Ga_{1-x}Al_xAs$/interface, a constant phase element (CPE) in parallel with a polarization resistance is used to model the interface. Based on the flat-band potential obtained from Mott-Schottky (M-S or C^{-2} vs V) plots, the conduction band edges of both $GaInP_2$ and $Ga_{1-x}Al_xAs$ were found to be negative of the hydrogen redox level. The valence band edge was also negative of the oxygen redox level; i.e., the band edges do not encompass the hydrogen and oxygen redox levels. Hence, they are likely to split water only if suitable surface modifications [2] are carried out or a favorable external bias is imposed. M-S plots obtained for $GaInP_2$ showed a pH dependence of about 60 mV/pH. These results are in agreement with those obtained using traditional capacitance methods, which are performed at a few discrete frequencies [3].

(The work was partially funded through a grant from DOE/SERI (now NREL), which provided all the samples.)

1. B. A. Boukamp, Solid State Ionics, **20**, 31 (1986).
2. A. Heller, Science, **223** 1141 (1984).
3. S. Kocha, J. Turner and A. J. Nozik, submitted for publication.
4. S. R. Morrison, "Electrochemistry at Semiconductor and Oxidized Metal Electrodes," Plenum Press, (1980).
5. V. A. Myamlin and Y. V. Pleskov, "Electrochemistry of Semiconductors," Plenum Press, (1967).

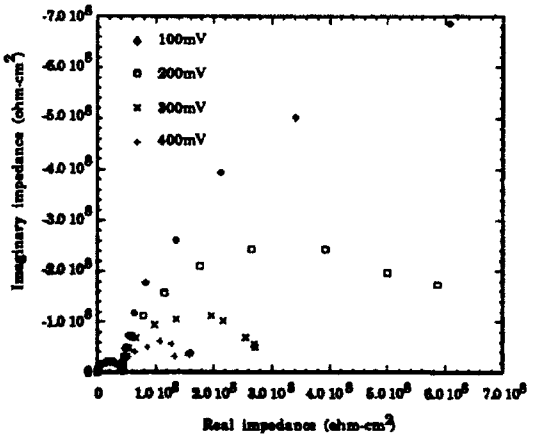

Fig. 1 Nyquist plots of $GaInP_2$ in electrolytes of pH 4.8 at various biases w.r.t SCE reference.

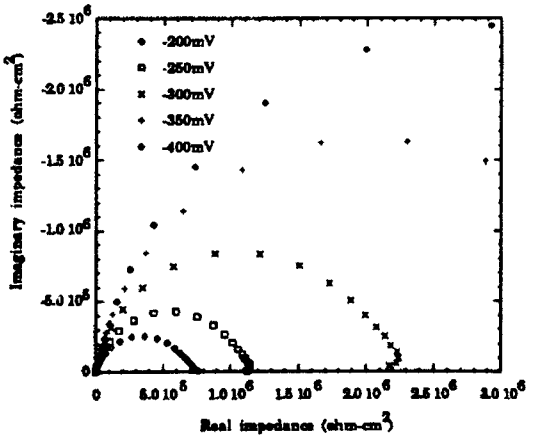

Fig. 2 Nyquist plots of p-$Ga_{1-x}Al_xAs$ in electrolytes of pH 4.8 at various biases w.r.t SCE reference.

POLARIZATION CURRENT DISTRIBUTION AND ELECTROCHEMICAL IMPEDANCE RESPONSE OF REINFORCED CONCRETE WHEN USING GUARD RING ELECTRODES

S. C. Kranc and A. A. Sagüés

Department of Civil Engineering & Mechanics
University of South Florida, Tampa, FL 33620

The electrochemical impedance response of reinforced concrete is complicated by the presence of extended corrosion macrocells and the relatively high resistance of the electrolytic medium. Guard ring electrodes are used in an attempt to confine the excitation current so that the reinforcing steel area sampled by the measurement is well defined. However, the degree of confinement is frequency-dependent because of the presence of high effective interfacial capacitances at the surface of the steel. In this work the distribution of the excitation current and the measured EIS response are examined for a model system using finite difference equations and numerical modeling. The model corresponds to a reinforced concrete plate of finite thickness and large lateral dimensions (as in a simplified bridge deck), with a reinforcing steel mat placed below the deck surface (Figure 1). The excitation electrode, placed on the deck surface, consists of a central disk surrounded by a guard ring, both of variable dimensions. The surface of the steel is considered to be active over a circular region of variable diameter below the excitation electrode. A finite difference spacial grid of rotational symmetry is placed centered on the excitation electrode, covering a circular region of dimensions much larger than those of the electrode. The first problem solved is the polarization current distribution throughout the concrete thickness and laterally from the excitation electrode. This is done starting from the Butler-Volmer equations for iron dissolution and oxygen reduction, and assuming applying to the active and passive steel regions as appropriate. The computations taken into account also the oxygen distribution and transport (assumed to be diffusional) throughout the concrete. The second part of the problem is the solution of the alternating current distribution through the system, by creating a two-dimensional (plus rotational symmetry) equivalent circuit that includes individual impedance elements at each surface node. The impedance elements are keyed to the local polarization currents calculated in the first part, plus an interfacial capacitance term. The output of the problem consists of the complex electrochemical impedance of the entire system as a function of frequency, for a reference electrode placed just below the excitation electrode center. The calculations address the relative distribution of a.c. current over the rebar for various combinations of disk and ring electrode dimensions, active region dimensions, and concrete resistivity. Figure 2 shows results for the case of excitation electrodes consisting of a ring electrode of constant outer radius (15.5 cm) surrounding without gap a disk electrode of variable radius. The rebar is either completely in the active condition, or contains a central 3.5 cm-radius active spot surrounded by passive steel. The solid lines show the average anodic current density present below the disk

electrode, calculated for each case using the DC model. The dashed lines show the average corrosion current density in the same region, estimated from the EIS model calculations (using the appropriate Stearn-Geary relationship) when considering only the portion of the excitation current flowing through the disk electrode. The calculations show that good agreement can be obtained between EIS estimates and actual corrosion rates when corrosion is uniform. However, the calculations show that average corrosion current densities may be severely underestimated in the non-uniform case. This effect has been interpreted as resulting from the difference in current distribution at high and low frequencies [1], further aggravated by limitations in the ability of the ring/disk combination to properly focus the excitation signal when the corroding region is small.

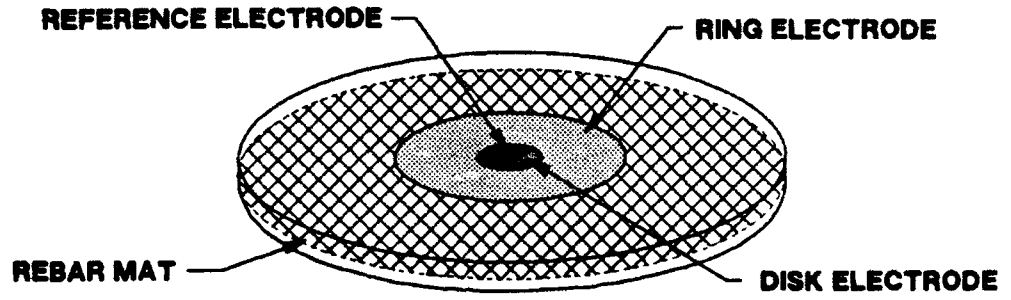

Figure 1. Test system consisting of a circular concrete slab (1m radius, 12 cm thick) containing a reinforcing steel mat halfway through the thickness of the slab. A combination disk/ring electrode is placed centered on top of the slab. The rebar mat is either wholly active or it contains a small (3.5 cm radius) central active spot.

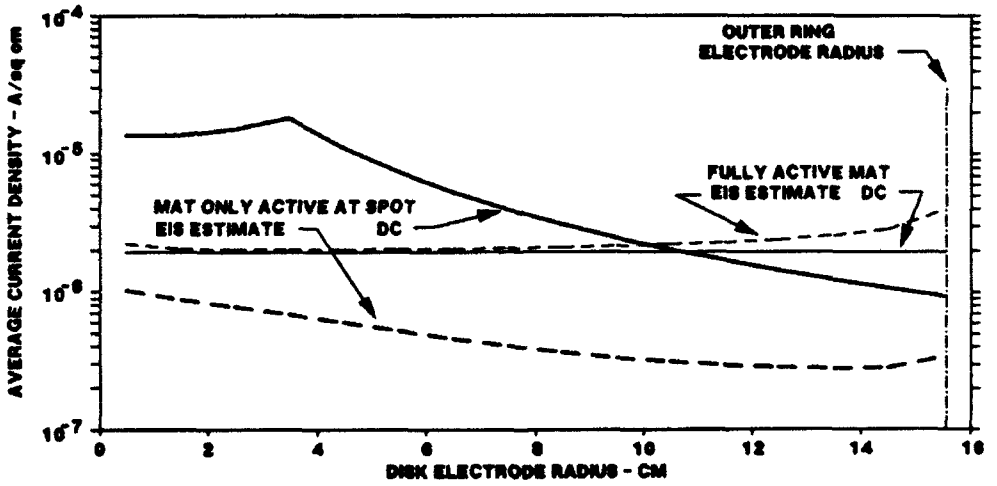

Figure 2. Example showing how the EIS-estimated average corrosion current density immediately below the disk electrode compares with the actual (DC model) average corrosion current density. The disk electrode radius varies from 0.5 cm up to the outer ring electrode radius (constant at 15.5 cm.)

Reference:

[1] Kranc, S.C. and Sagüés. A.A., "Computation of Corrosion Macrocell Current Distribution and Electrochemical Impedance of Reinforcing Steel in Concrete", *Computer Modeling in Corrosion, ASTM STP 1154*, R.S. Munn, Ed., American Society for Testing and Materials, Philadelphia, 1992.

ANODIC BEHAVIOR OF Ni-P ALLOYS STUDIED BY IMPEDANCE SPECTROSCOPY

A. Krolikowski and P. Butkiewicz
Institute of Solid State Technology, Department of Chemistry
Warsaw University of Technology
ul. Noakowskiego 3, PL-00-664 Warsaw

Ni-P alloys as corrosion protective coatings have been the earliest industrial application of amorphous metals [1]. However, there is still no consent as to the essential corrosion characteristics of Ni-P: its ability to passivation [2,3], nature of passive films [2,4] and susceptibility to pitting [2,5]. This work aimed at clarifying the anodic dissolution behavior of Ni-P alloys in relation to their structural state and elemental composition. It was executed by means of comparative studies of Ni-P alloys with varying phosphorus content.

Series of Ni-P alloys with phosphorus content ranging from 6 to 28 at.% were electrodeposited on copper foil to a thickness of 30-40 μm. Results of X-ray diffraction investigations revealed that low P electrodeposits are crystalline whereas samples with high P content exhibit amorphous structure. The transition from crystalline to amorphous state occurs between 10 and 15% of P. Anodic behavior of these samples were studied by impedance spectroscopy, potentiodynamic and potentiostatic polarization methods. The measurements were performed in deaerated sulfate and chloride neutral solutions at 20±2°C.

Polarization studies showed evidently different anodic behaviors of crystalline and amorphous alloys. The former ones dissolve actively with covering of their surface by a greyish black film and their dissolution currents increase with time. The latter ones exhibit current arrest and a continuous suppression of dissolution currents with time. Both these facts suggest passivation. This behavior is fairly insensitive to chloride ions. The surface of amorphous alloys remains lustrous with no visible evidence of pitting.

A deeper insight into the dissolution features of Ni-P was obtained from impedance studies. These measurements were performed at select potentials: at the corrosion potential, and at anodic potentials corresponding to the current arrest. Spectra taken at the corrosion potential are quite similar for all the samples and consist of one capacitive arc, associated with the charge transfer process. When exposed to anodic polarization, crystalline alloys exhibit markedly lower impedance values. The appearance of the greyish black superficial film contributes to impedance data, giving rise to additional response at low frequencies. Spectra obtained for amorphous samples at the same potentials show only one capacitive arc and much higher values of impedance. This differentiation in anodic behavior of crystalline and amorphous alloys is evident upon results of quantitative analysis of impedance data. Fig. 1 shows relation between time constant for the charge transfer process and composition of the Ni-P alloy. At the corrosion potential all samples exhibit quite comparable values of this time constant, irrespective of the alloy structure and composition. How-

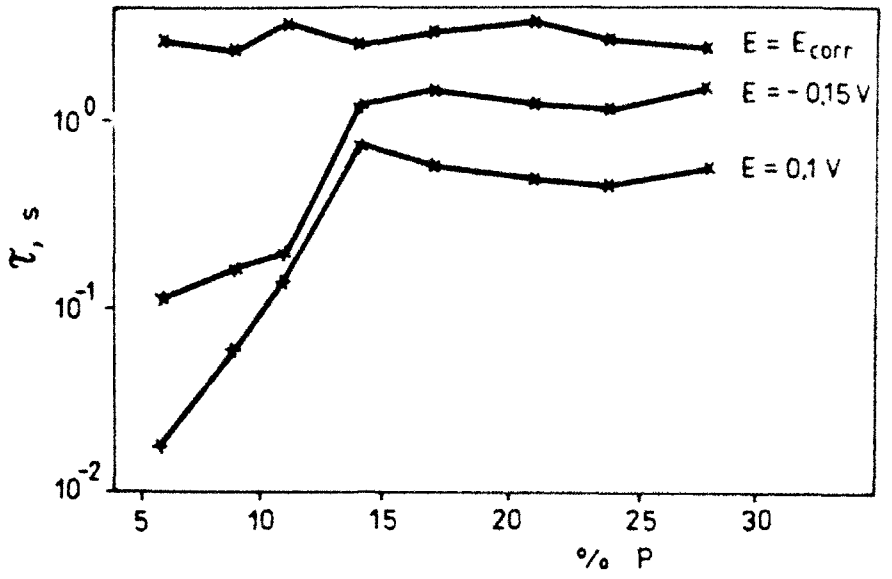

Fig. 1. Time constant for charge transfer process of Ni-P in 0.1 N NaCl as a function of composition of the alloy.

ever, anodic polarization gives rise to the reduction of the time constant. This effect is much more pronounced for crystalline samples.

The results of this work show clearly that, under the open circuit conditions, the nature of the corrosion process is similar for all the Ni-P alloys studied, irrespective of their structure and composition. Anodic polarization, however, gives rise to evident differentiation in the dissolution mechanism. When exposed to anodic polarization, amorphous alloys exhibit suppression of dissolution, like passivation. Features of this process are similar to those observed at the corrosion potential. Under the same conditions, anodic process of crystalline alloys is modified, and active intense dissolution occurs. Thus, anodic behavior of Ni-P is strongly dependent on the structural state of this alloy. Variation in P content has slight effect, although the contribution of alloying phosphorus to the dissolution process is self-evident.

References:

1. C.H. deMinjer and A. Brenner, Plating, 44, 1297, 1957,
2. R.B. Diegle, N.R. Sorensen, C.R. Clayton, M.A. Hefland and Y.C. Yu, J. Electrochem. Soc., 135, 1085, 1988,
3. P.V. Nagarkar, P.C. Searson and R.M. Latanision, Proc. Symp. Corr. Electrochem. Catalysis of Met. Glasses, Proc. Electrochem. Soc., 88-1, 118, 1988,
4. H. Habazaki, S.Q. Ding, A. Kawashima, K. Asami, K. Hashimoto, A. Inoue and T. Masumoto, Corros. Sci., 29, 1319, 1989,
5. H.G. Schenzel and H. Kreye, Plat. Surf. Finish., 77, 50, 1990.

Coating Inspection by a Scanning Electrochemical Impedance Spectroscopy Technique

R.S. Lillard, J. Kruger The Department of Materials Science and Engineering, The Johns Hopkins University, Baltimore, Maryland, 21218. P.J. Moran The Department of Mechanical Engineering, United States Naval Academy, Annapolis, Maryland, 21402. W.S. Tait, S.C. Johnson Wax Company, Racine, Wisconsin, 53403.

Recently, a novel technique for generating quantitative local electrochemical impedance spectroscopy (LEIS) was developed.1 The technique is based on the premise that the ac solution current densities very near the working electrode in a conventional three electrode EIS experiment are proportional to the local impedance properties of the electrode. In this technique, local impedance data are derived by measuring the ratio of the applied ac voltage perturbation to the local ac solution current density normal to the electrode as a function of frequency. The bi-electrode probe used to measure the local ac solution current densities was constructed by drawling gown two parallel and attached glass capillaries to a final diameter of approximately 0.1 mm. The ends of which were displaced horizontally by approximately 0.8 mm. A platinized platinum wire was inserted into each capillary. To obtain the ac solution current density at the tip of this probe, the ac potential difference between the two probe electrodes is measured with a frequency response analyzer or lock-in amplifier. From this ac potential difference the ac solution current density at the tip of the probe is derived with knowledge of the relationship for the solution resistance between the probe electrodes ($R=\ell/\sigma A$), and Ohm's law:

$$i(\omega) = \frac{\Delta V(\omega) \cdot \sigma}{\ell}$$

where: $i(\omega)$ is the local ac solution current density in amps/cm^2, $\Delta V(\omega)_{probe}$ is the ac potential difference between probe electrodes in volts, σ is the solution conductivity in (ohm cm)$^{-1}$, ℓ is the separation distance between openings in the tip of the probe in cm.

In this investigation, Local Electrochemical Impedance Spectroscopy (LEIS) was used to locate defects in a heat cured urea-formaldehyde modified epoxy coating and quantify their impedance. This coating is used to protect the interior of metal aerosol containers which are constructed of mild steel, coated with tin, and sealed by resistance welding. An interior section of this can containing both weld and non-weld areas, was cut from the container and used as a test electrode. This section of can also contained a 0.3 mm diameter artificial defect. LEIS maps of this sample were generated for a select area of this sample which include weld and non-weld areas as well as the artificial defect. These maps were produced at Ecorr for three points per decade frequency over the range of 1 to 10,000 Hz in a 0.1 molar sodium chloride solution buffered with 0.5 molar boric / 0.05 sodium borate, which maintained the pH at 7.2.

Presented in Figure 1 is a typical, LEIS map for the scan area . This map plots the log of the magnitude of the impedance, at 2.4 Hz, as a function of the probe's position above the electrode. It was taken after 2 hours immersion in the test solution. The weld and non-weld coatings as well as the artificial defect are clearly visible in this map. Figure 2 presents a Bode magnitude plot generated from LEIS maps for the artificial defect and weld and non-well coatings after 2 hours of immersion. Each curve in this figure illustrates the behavior of the log of the magnitude of the impedance for one discrete location on the sample, either the defect, weld coating or non-weld coating, as a function of frequency.

In conclusion, LEIS has been successfully used to map the impedance properties of a heat cured urea-formaldehyde modified epoxy coating. Analysis of LEIS impedance maps and Bode magnitude plots generated from these maps reveals that after 216 hours of immersion in 0.1 M sodium chloride the impedance of the weld coating is 63 times lower than that of the non-weld coating. The difference between the impedance properties of these two coatings most likely owes to the corresponding heat treatments used in each area to cure the polymer, since the same polymer is used to coat the steel in both of these areas. The non-weld coating is cured in a convection oven whose temperature is controlled while the weld coating is cured by passing over a flame.

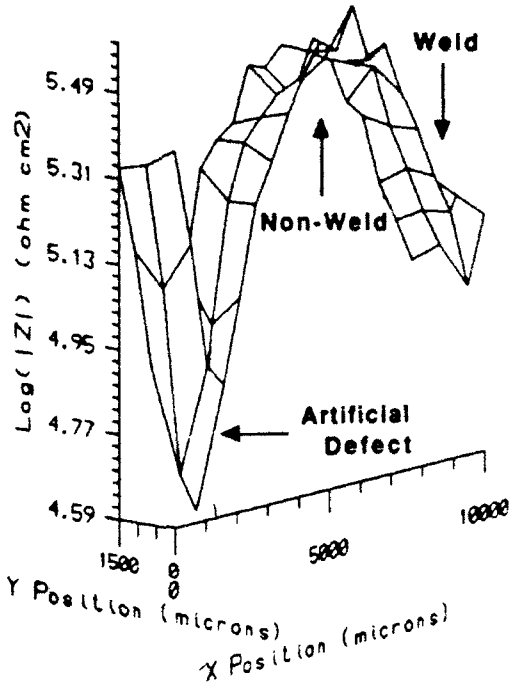

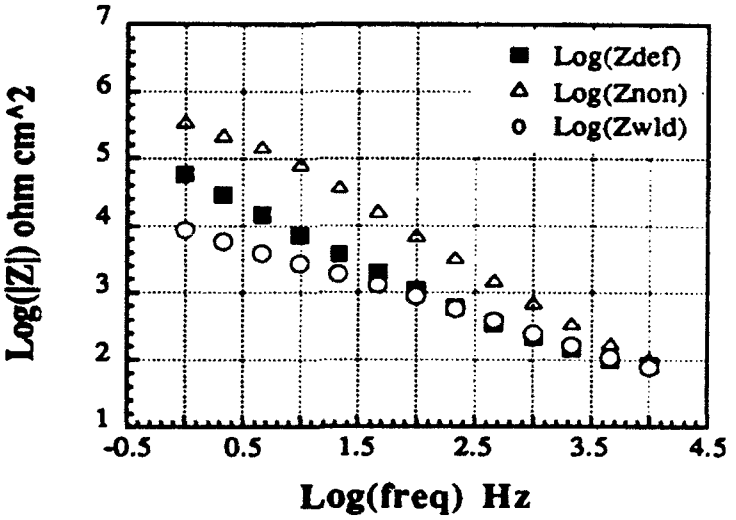

---

1 R.S. Lillard, P.J. Moran, H.S. Isaacs, The Journal of the Elecrochemical Society, vol. 139, no. 4, pp. 1007-12, 1992.

ELECTROCHEMICAL IMPEDANCE SPECTROSCOPY ON METAL HYDRIDE ELECTRODES

Nobuhiro Kuriyama, Tetsuo Sakai, Hiroshi Miyamura,
Itsuki Uehara and Hiroshi Ishikawa
Government Industrial Research Institute, Osaka, AIST, MITI
1-8-31 Midorigaoka, Ikeda, Osaka 563, Japan

Introduction

Nickel / metal hydride batteries have been developed and commercialized because of high energy density, high dischargeability, long charge/discharge cycle life and an advantage to environmental problems, where rare-earth metal based alloys [1] and titanium based alloys [2] have been used for the metal hydride electrode. The reaction on the metal hydride is expressed by Eq.1, where MH_y shows metal hydride,

$$\frac{1}{x}MH_n + OH^- \rightleftarrows \frac{1}{x}MH_{n-x} + H_2O + e^- \qquad \text{(Eq.1)}.$$

Performances of the electrode, such as dischargeability and cycle life, are also affected by many factors, for example, composition of alloy [1d, 1e, 2a], contents of binders and conductive materials in the electrode [1f], and modification of the alloy surface [1b, 1c, 2b]. However, it have not been well realized how those factors contribute to the performances of the electrodes.

Electrochemical impedance spectroscopy [3] enables us to evaluate resistive components of electrodes separately. Hence, the technique is useful to examine electrodes with complex structures and realize effect of the factors on overpotential.

Experimental

A rare-earth based alloy, $MmNi_{3.5}Co_{0.7}Al_{0.8}$ (Mm=mischmetal; La:25.4, Ce:53.6, Pr:5.4, Nd:15.6 in at%), was crushed into fine powder (0.125~0.150 mm). Electrodes examined were prepared from a mixture of the alloy powder coated with copper (20 wt%) and perfluoro-polymer (FEP) as binder (10 wt% of the alloy). The mixture was compacted into a pellet (13 mm in diameter), and the pellet was pressed with a current corrector (nickel mesh) at 300 °C for 5 minutes. 6N KOH solution was used as electrolyte. Charge-discharge cycles were conducted at 20 °C under the following conditions: charge at 40 mA for 2 hours, discharge at 20 mA, -0.6 V (vs. Hg/HgO) cutoff. After 20 cycles, Depth-of-discharge (DOD) dependance of impedance spectra (0.5 mHz~10 kHz) at 20 °C and temperature dependence (-15~30 °C) of them (5 mHz~10 kHz) at a few DODs were recorded under open-circuit condition.

An electrode made from uncoated alloy powder and the binder was also tested in order to examine effect of copper coating to deterioration of the electrodes.

Results and Discussion

Cole-Cole plots of the impedance spectra of the electrode using the copper-coated alloy powder are shown in Fig.1. It is notable in the plots that the low-frequency semicircle and the Warburg slop considerably varied with DOD.

The Cole-Cole plots shown in Fig.1 were well fitted by means of the equivalent circuit shown in Fig.2, where the Warburg impedance was tentatively expressed with a R-Q-C circuit. R_4 and Q_4 related to the semicircle in the low-frequency region varied with DOD, although no appreciable changes in R_2 and Q_2 related to the semicircle in the high-frequency region were observed. And R_4 decreased and Q_4 increased with amount of the alloy, although R_2 and Q_2 were almost constant. Therefore, we assigned R_4 and Q_4 to the reaction resistance on the alloy surface and a double-layer capacitance on the surface, respectively. Since decease in activity of hydrogen atoms in the alloy resulted from increase in DOD suggests increase in the reaction resistance with increase in DOD, the DOD dependence in R_4 is supposed to be resulted from changes in exchange rate of hydrogen atoms between inside and surface of the alloy and/or in charge transfer rate constant on the alloy surface. R_2 and Q_2 were mainly attributed to the contact resistance and capacitance between the current collector and the alloy pellet, respectively. Since R_3 increased with binder content in the electrode, R_3 and C_3 is considered to be related to the contact resistance and capacitance between the alloy particles in the pellet. DOD dependence of R_3 suggests contribution of the reaction

resistance to R_3. R_1 was assigned to the electrolyte resistance between the metal hydride electrode and the reference electrode.

After 440 charge/discharge cycles, R_4 of the electrode using copper-coated alloy powder increased by about 5 times. Very small changes in R_2 and R_3 related to the constant resistances show that the electrical contact in the electrode was preserve after such cycles. Since activation enthalpy of the reaction on the alloy surface evaluated from temperature dependence of R_4 appreciably increased, decrease in reactivity of the alloy surface results in deterioration on the electrode. On the other hand, the electrode using uncoated alloy powder exhibited outstanding increase in R_2 for 130 cycles, which indicates fast deterioration of the electrical contact between the current collector and the alloy pellet. Thus the copper layer coated on the alloy particles is considered to work as a effective "micro-current collector" over many charge/discharge cycles.

References

[1] a) H. F. Bittner and C. C. Badcock, *J. Electrochem. Soc.*, **130**, 193C (1983); b) T. Sakai, H. Ishikawa, K. Oguro, C. Iwakura, and H. Yoneyama, *ibid.*, **134**, 558 (1987); c) H. Ogawa, M. Ikoma, H. Kawano, and I. Matsumoto, *Power Sources*, **12**, 393 (1988); d) T. Sakai, K. Oguro, H. Miyamura, N. Kuriyama, A. Kato, H. Ishikawa, and C. Iwakura, *J. Less-Common Met.*, **161**, 193 (1990); e) T. Sakai, T. Hazama, H. Miyamura, N. Kuriyama, A. Kato, and H. Ishikawa, *J. Less-Common Met.*, **172/174**, 1175 (1991); f) T. Sakai, A. Takagi, K. Kinoshita, N. Kuriyama, H. Miyamura, and H. Ishikawa, *J. Less-Common Met.*, **172/174**, 1185 (1991). [2] a) M. A. Fetcenco; S. Venkatesan, K. C. Hong, and B. Reichman, *Power Sources*, **12**, 411 (1988); b) H. Sawa, M. Ohta, H. Nakano and S. Wakao, *Z. Phys. Chem.* (Munich), **164**, 1527 (1989). [3] J. R. Macdonald, Ed., *Impedance Spectroscopy*, John Wiley & Sons, New York (1987).

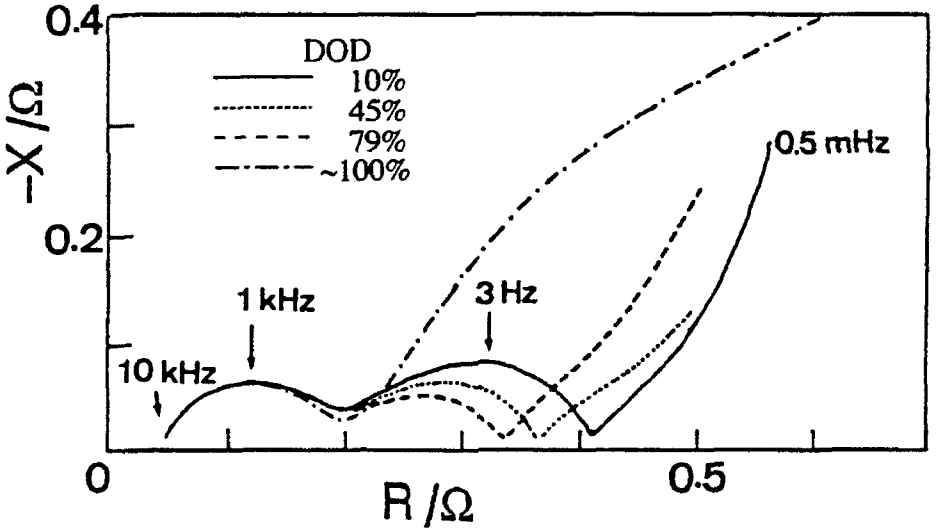

Fig.1 Cole-Cole plots of impedance for the metal hydride electrode.

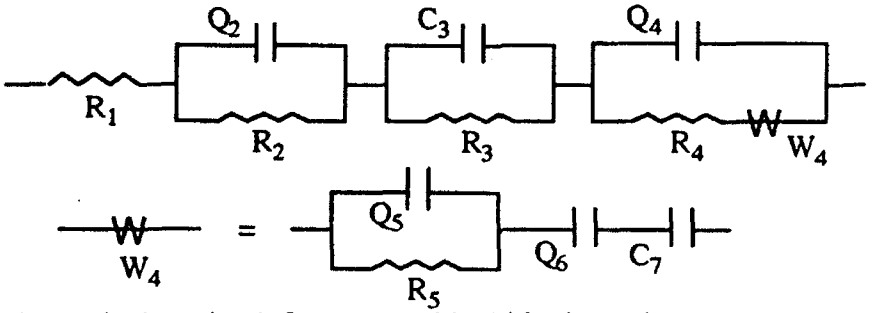

Fig.2 An equivalent circuit for our metal hydride electrodes.
W_4: Warburg Impedance, Q_i: Constant Phase Element; $Q_i(\omega) = \{Y_{i0}(j\omega)^n\}^{-1}$ $(0<n<1)$.

CORROSION INHIBITION STUDY OF PURE IRON IN NEUTRAL SOLUTIONS BY AN ORGANIC COMPOUND USING ELECTROCHEMICAL METHODS

M.C. LAFONT[1], N. PEBERE[1], C. DESLOUIS[2] AND F. DABOSI[1]

1. URA CNRS 445, Equipe de Métallurgie Physique
E.N.S.C.T., 118, Route de Narbonne
31077 Toulouse Cédex - France

2. UPR 15 du CNRS, Physique des Liquides et Electrochimie
Tour 22, Université Pierre et Marie Curie, 4 Place Jussieu
75252 Paris Cédex 05 - France

The present study was designed to acquire a better knowledge of the mechanisms through which an organic surfactant (1-decylimidazole) modifies the corrosion kinetics of pure iron in a 0.5 M NaCl solution. Steady-state and transient (electrohydrodynamical (EHD) impedance) techniques were carried out.

In the cathodic plateau region, the current I_d corresponding to dissolved oxygen reduction is always lower than that predicted by Levich for a uniform active surface [1].

The curves of I_d vs $\Omega^{1/2}$ plotted for different immersion times, under cathodic polarization, show a curvature. When reciprocal coordinates are used (Figure 1), fairly parallel lines are obtained. This means that mass transport in solution is not affected by the inhibitor. Nevertheless, for 30 mn and 180 mn, the system is not stationary, as previously observed [2], whereas for 360 mn there is no more evolution of the current with time.

The non-zero intercepts of the different lines of figure 1 with the ordinate axis are proportional to the quantity $\delta f/Df$, (where δ_f is the diffusion layer thickness and D_f is the diffusivity in the layer). They can therefore be interpreted as indicating a strengthening of the layer which becomes less porous with increasing immersion time.

The curvature observed for 360 mn and for high rotation speeds could be attributed to a partial blocking effect (passage from dependent active sites to independent actives sites).

The EHD impedance diagrams were determined with potentiostatic regulation at - 0.9 V/SCE, recorded at different mean speeds of rotation and reported in Bode coordinates (amplitude and phase shift against the dimensionless frequency, p ($p = \omega/\Omega o$) (Figure 2). These curves correspond to Koutecky-Levich plot of figure 1.

A porous layer effect can be seen in the low frequency domain. The EHD data in the low frequency range were therefore analyzed by use of a simplexe fitting procedure.

Average values of the inhibitor layer thichness ($\delta_f \sim 0.5$ µm) and diffusivity ($D_f \sim 5 \times 10^8$ cm^2 . s^{-1}) were obtained.

However, in the middle frequency range ($0.2 < p < 2$), the curves deviate from those calculated for diffusion through a porous layer [3] and they are simular to those predicted for a partially blocked electrode [4].

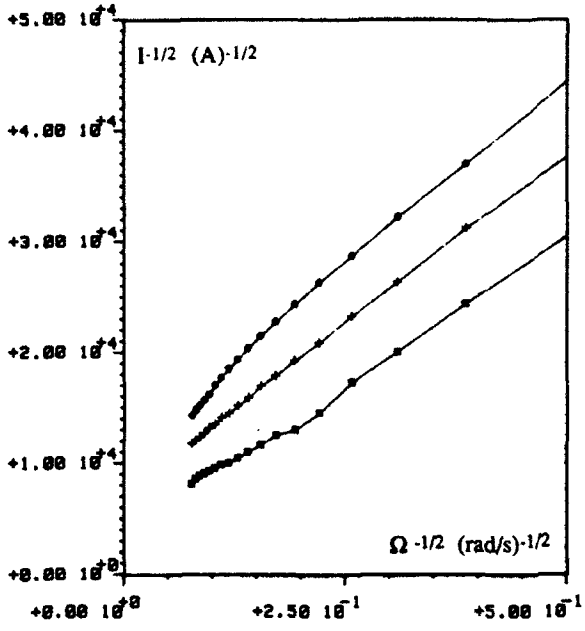

Figure 1 : Koutecky-Levich plots
E = - 0.9V/SCE 10^{-3} M inhibitor
Immersion time : (□) 30 mn, (+) 180 mn and (○) 360 mn.

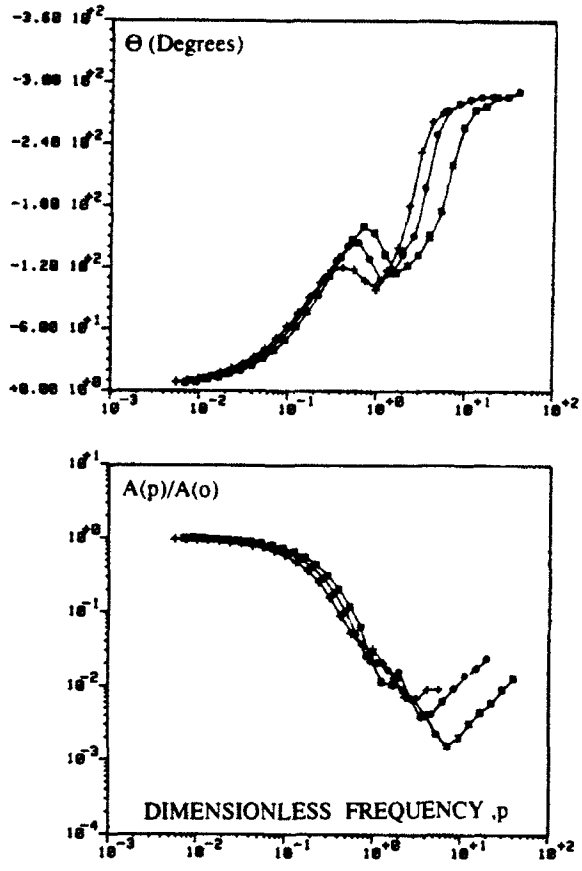

Figure 2 : Potentiostatic EHD impedance diagrams
Preliminary conditions : Ω = 300 rpm ;
5 h at E = - 0.9 V/SCE
(+) 240 rpm ; (○) 120 rpm ; (□) 60 rpm

In the high frequency domain, a significant divergence in the EHD diagram is observed. This new behaviour may be ascribed to mechanical effects on the layer.

In conclusion, it is shown here that the EHD impedance technique is able to provide very useful information on film-forming inhibitors : layer thickness and compactness.

REFERENCES

[1]. V.G. Levich, "Physicochemical Hydrodynamics", Prentice Hall, Englewood Cliffs, New Jersey (1962).

[2] N. Pebere, M.C. Lafont, A. de Savignac and F. Dabosi, Proceedings of the 7th European Symposium on Corrosion Inhibitors Ann. Univ. Ferrara, N.S. Sez V, Suppl. N° 9, 1353 (1990).

[3]. C. Deslouis, B. Tribollet, M. Duprat and F. Moran, J. Electrochem. Soc. 134, 2496 (1987).

[4]. A. Caprani, C. Deslouis, S. Robin and B. Tribollet
J. Electroanal. Chem. 238, 67 (1987).

IMPEDANCE ANALYSIS OF POLYMER FILM ELECTRODES

G. Láng, J. Bácskai and G. Inzelt

Department of Physical Chemistry, Eötvös University,
Budapest 112, P.O. Box 32, H-1518, Hungary

Poly(vinylferrocene) and poly(tetracyanoquinodimethane) electroactive redox polymer films have been studied by electrochemical impedance spectroscopy (EIS). The variation of the impedance spectra as a function of film thickness, thickness distribution, temperature and electrolyte composition has been examined. The reliability of the quantities calculated for the rate of the charge transfer and the charge transport processes, capacitances and resistances on the basis of different models elaborated for the description of the impedance spectra of polymer film electrodes is discussed. Computer simulation and fitting procedures are applied for the evaluation of the impedance data. The possibility of the application of the Kramers-Kronig transformation for the data validation in the case of these systems is also pointed out. By using a constant phase element in the equivalent circuit, which may be justified by assuming e.g. the existence of energetically non-equivalent sites or nonuniform film structure, a better description of the low-frequency part of the spectra can be achieved, and it helps to obtain more reliable data for the low-frequency capacitance. A comparison is made between the data obtained by EIS and other methods.

IMPEDANCE SPECTROSCOPY AT VERY LOW FREQUENCIES

Štefan Lányi
Institute of Physics, Slovak Academy of Sciences,
Bratislava, Czechoslovakia

Impedance spectroscopy is based on a confrontation of a measured frequency dependence of the impedance with that derived using some model. The most elaborate theories assume the action of small harmonic potentials, i. e. having defined frequencies.

As the measuring frequency decreases the impedance measurements become increasingly time consuming. The reduction of the duration of the experiment is desirable for both economical and stability reasons. It is possible using only a few, in the limit only a single period of the measuring signal.

The frequency of a sinusoidal voltage may be considered discrete only if it lasts a sufficient number of periods. The Fourier spectrum of the few periods is no longer discrete or in other words the signal cannot be characterised with an angular frequency equal to the inverse of the period of the voltage. Therefore no strict validity of the data for confrontation with discrete frequency models should be expected. As we found by computer simulation, in practical cases differences in both the amplitude and the phase of the signal arise and it is difficult to predict the magnitude of the arising errors. The situation is further complicated by a dependence on the electrical history of the system, like on time lags between the application of the individual sine wave pulses, on the sequence of the applied "frequencies", etc.

The possible solutions may be i) the confrontation of experimental data with dependences derived from given theoretical expressions for the impedance, respecting the actual sequence of applied pulses, or ii) the solution of differential equations describing the response to the sequence of applied pulses. In the case i) the expression for the impedance is considered correct and instead of the assumption of sinusoidal voltage the correct Laplace transform of the apllied voltage should be used. In the case ii) it is possible to correlate the computed time dependences with an apparatus function correspoding to the used equipment. However, by such correlation much information is sacrificed. It might be then more effective to use the uncorrelated result but this is more a time domain spectroscopy, not ac impedance spectroscopy.

In any case it is necessary to use an experimental equipment transparent enough to know what does it measure. Then a first check, whether a result corresponds to discrete frequency, is the confrontation of a series of readings taken after each period of the signal acting for a longer time.

COPPER DISSOLUTION IN ACIDIC SULFATE MEDIUM STUDIED BY ELECTROGRAVIMETRIC AND ELECTROCOULOMETRIC TRANSMITTANCE TECHNIQUES

A. LE GAL LA SALLE, A. JARDY, R. ROSSET, M. KEDDAM*, H.TAKENOUTI*

Laboratoire de Chimie Analytique de l'Ecole Supérieure de Physique et de Chimie de Paris,10, rue Vauquelin 75231 PARIS Cedex 05, France.
* UPR 15 du CNRS "Physique des Liquides et Electrochimie", Université P&M Curie,Tour 22, 4, place Jussieu 75252 PARIS Cedex 05, France.

INTRODUCTION

Corrosion of copper in Na_2SO_4 aqueous solutions was studied by different methods, including EIS, in order to explain the behavior of Cu in pure water and the cause of releases of solid corrosion products. It was shown that the cyclic phenomena observed came from the poor adherence of the outer layer of cupric oxide to the inner layer of cuprous oxide.

To identify the elementary act by which the copper oxidation starts, the dissolution mechanism in acidic sulfate medium was investigated, using two new transmittance techniques in addition to steady-state current-potential curves and EIS [1]. Electrogravimetric and electrocoulometric transmittances [2] were studied by using respectively a quartz crystal microbalance (QCM) and a rotating ring-disk electrode (*rrde*) under a small *ac* signal. Both techniques give invaluable results when reaction intermediates are involved.

EXPERIMENTAL

All experiments were conducted in Na_2SO_4 10^{-1}mol.l^{-1}, acidified at pH 1.5 by H_2SO_4 addition and deoxygenated with Ar.

Electrogravimetric measurements (QCM)

The oscillation frequency of a quartz crystal (QC) is highly sensitive to its mass variations. The QC used is a disk of 16 mm diameter and its nominal oscillation frequency is 6 MHz. Gold was vacuum deposited at the center of both sides and then copper electrodeposited on one side. The later is the working electrode (area 0.2 cm^2) in a classical set-up for impedance measurements. The difference Δf between the frequency of this QC and that of a reference oscillator is then converted into a voltage difference ΔV, and sent, after substraction of the *dc* component, to a transfer function analyzer (Solartron FRA 1254). By means of this four-input channel analyzer, two transmittances are measured simultaneously :

$Z = \Delta V/\Delta I$ (electrode impedance) ; $M = \Delta m/\Delta V$ (electrogravimetric transmittance)

Experimental calibration gave $\Delta f/\Delta m = 0.052\ 10^9$ Hz cm^2 g^{-1}.

It was shown theoretically that, if there is adsorption of a reaction intermediate, the $\Delta m/\Delta I$ diagram shows a real part.

Electrocoulometric measurements (*rrde*)

The disk of the *rrde* was an electrolytic Cu rod, 5 mm diameter.The thin ring surrounding the disk was in Pt (5.2 mm i.d., 5.54 mm e.d.) and Cu was electrodeposited before each experiment.

With the *rrde*, the species leaving the disk, produced by oxidation, is collected at the ring. The ring and disk currents are measured together with the disk potential, so that the collection efficiency $N(\omega)$ and the electrode impedance are determined simultaneously:

$$N(\omega) = \Delta I_R / \Delta I_D \qquad Z(\omega) = \Delta E_D / \Delta I_D$$

the subscripts R and D stand for ring and disk respectively.

$N(\omega)$ can be split into three terms:

$$N(\omega) = (\Delta I_R / \Delta \Phi_R) \times (\Delta \Phi_R / \Delta \Phi_D) \times (\Delta \Phi_D / \Delta I_D) = (1 / N_R(\omega)) \times (N_t(\omega)) \times (N_D(\omega))$$

where $\Delta \Phi_R$ and $\Delta \Phi_D$ are the flux of species collected at the ring and leaving the disk. $N_R(\omega)$ is known ($=1/n_R F$) and $N_t(\omega)$, characteristic of mass transport, is obtained by calibration; $N_D(\omega)$, which contains the information concerning the disk reaction, can be determined from $N(\omega)$ (n stands for the electron number involved in each electrode reaction).

If now a fraction of the *ac* current leads to the build-up of a surface charge ΔQ involved in a faradic process, such as an adsorbed intermediate or a surface film, then $\Delta Q / \Delta I_D$ is easily deduced from $N_D(\omega)$ according to:

$$n_D F N_D(\omega) + j\omega \Delta Q / \Delta I_D = 1$$

From the corresponding diagram, the adsorbate will be identified as a reaction intermediate or a passivating species.

As $Z(\omega)$ is determined simultaneously, the differential capacitance $\Delta Q / \Delta E_D$ can be calculated.

RESULTS

By means of QCM measurements, it was established that the apparent dissolution valency was dependent on the current density: at low densities, as those encountered in corrosion conditions, Cu dissolves through Cu(I) species, while at high ones, it dissolves through Cu(II) species.

From *rrde* measurements, it was found that $\Delta Q / \Delta E$ had a value of a few mF/cm^2 and that the collection efficiency decreased when the current density or the electrode rotation speed increased. Whereas the Cu(I) disprorpotionation during the transit between ring and disk cannot explain this observation, it was interpreted by a poor reactivity on the ring of the Cu(II) species produced on the disk, which then transforms into a more reactive form by a homogeneous reaction.

All transfer functions studied (EI, electrogravimetric and electrocoulometric transmittances) are in agreement with the formation of an adsorbed reaction intermediate.

MODEL

On the basis of these results, the following reaction model was proposed

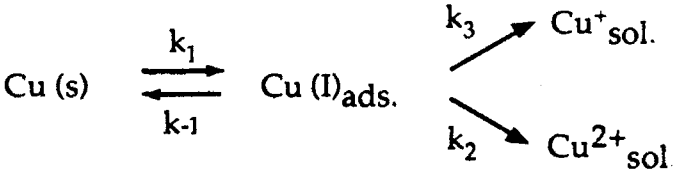

This model and the associated set of parameters were found in good agreement with experimental results by simulation.

REFERENCES

[1] A. JARDY, A. LE GAL LA SALLE-MOLIN, M. KEDDAM,.H. TAKENOUTI, Electrochim. Acta, in press.

[2] C. GABRIELLI, M. KEDDAM, H. TAKENOUTI, Electrochim. Acta, 35, 1990, 1553.

APPLICATIONS OF AC IMPEDANCE SPECTROSCOPY TO THE HYDROGEN EVOLUTION REACTION

Andrzej Lasia, Département de chimie, Université de Sherbrooke
Sherbrooke, Québec, Canada, J1K 2R1

Ac impedance spectroscopy is a very powerful technique for studying interfacial processes. In the present paper ac impedance and steady-state polarization measurements were used to determine the mechanism and kinetics of the hydrogen evolution reaction (HER) in alkaline solutions on various solid electrodes.

The electrical equivalent model, describing the HER on the ideally smooth electrode, consists of the solution resistance, R_s, in series with the parallel connection of the double layer capacitance, C_{dl}, and faradaic impedance, Z_f. The faradaic impedance, in the case when the mass transport can be neglected, is given by [1]:

$$1/Z_f = Y_f = A + \frac{B}{j\omega + C} \tag{1}$$

where ω is the angular frequency and terms A, B and C may be computed from the rate constants of the Volmer, Heyrovsky and Tafel reactions. Very often the condition $A >> B/C$ is fulfilled and then $Z_f = 1/A$.

However, on solid electrodes, this model cannot describe adequately the observed impedance data. The three applicable models have been proposed in the literature:

(i) Constant Phase Element (CPE) model.

In this model C_{dl} is substituted by the CPE and its impedance is:

$$Z_{CPE} = 1/T(j\omega)^{\Phi} \tag{2}$$

where T is the capacity parameter ($T = C_{dl}$ when $\Phi = 1$) and $90°(1-\Phi)$ is the constant phase angle. In this case T is given in units of F cm^{-2} $s^{\Phi-1}$. Brug *et al.* [2] have demonstrated that the average C_{dl} may be represented as:

$$T = C_{dl}^{\Phi}(R_s^{-1} + A)^{1-\Phi} \tag{3}$$

(ii) Fractal model [3].

In this case the electrode impedance is:

$$1/Z_{el} = b(j\omega C_{dl} + A)^{\Phi} \tag{4}$$

where the parameter b depends on the solution conductance and the surface geometry and it is not experimentally accessible.

The fractal model does not allow the determination of C_{dl} and the rate constants. In this case, all the experimentally determined parameters are multiplied by the unknown parameter $b^{1/\Phi}$.

(iii) Porous electrode model.

De Levie [4] has proposed a model of deep cylindrical pores on the electrode surface. Its impedance is described by the equation:

$$Z = R_s + Z_p/n \tag{5}$$

where n is the number of pores and Z_p is given as:

$$Z_p = (1/\pi r)(\rho Z_0/2r)^{1/2}\coth(2\rho l^2/rZ_0)^{1/2} \tag{6}$$

and Z_0 is the specific impedance per unit area of the flat surface of a cylindrical pore, r and l are the radius and length of the pore and ρ is the specific resistivity of the solution. Z_0 consists of the parallel connection of the charge transfer resistance, $R_{ct} = l/A$, and the double layer capacitance, C_{dl}, $Z_0 = R_{ct}/(1 + j\omega R_{ct}C_{dl})$. Gassa *et al.* [5] suggested that Z_0 should be described by the CPE model. In this case, the impedance Z_0 is given as:

$$Z_0 = R_{ct}/[1 + (j\omega)^{\Phi} R_{ct}T] \quad (6)$$

Various electrodes were studied in 1 M NaOH solution using steady-state polarization and ac impedance technique. On the polycristalline Ni [6] and Rh [7] one semi-circle was present. The impedance plots were well approximated using the CPE model with the parameter $\Phi \sim 0.85$-0.99 depending on the overpotential. The average C_{dl}, determined using eqn. (3), was ~40 μF cm^{-2} for Ni and ~50-80 μF cm^{-2} for Rh electrode. The same model could explain the ac impedance spectra for leached Ni-Zn [8], pressed Ni-B powder [9] and $LaPO_4$ bonded electrodes: Ni, Rh on Ni [10] and Ru on Ni [11], and Rh and Pd on graphite [12], with Φ ~0.7-1, despite their rough surface structure.

For the electrode composed of the pressed powders of Raney Ni and Ni (50%) [13], Φ value was very low (~0.52-0.6) and the double layer capacity equaled ~ 0.1 F cm^2, which led to a large surface roughness factor of 10^5. Similar values were obtained for the pressed amorphous Ni-B electrode.

The CPE model could not be applied to the leached Ni-Al alloys [14]. In this case, the fractal model well described the ac impedance data. However, the Φ values were ~0.4-0.45, lower than the theoretically predicted value of 0.5.

The values of the parameters A (B and C) and the steady state current were approximated as functions of the overpotential. It was found that the HER proceeds through the Volmer-Heyrovsky reaction mechanism and the kinetic parameters were estimated.

References

1 D.A. Harrington and B.E. Conway, Electrochim. Acta, 32 (1987) 1703.
2 G.J. Brug, A.L.G. van der Eeden, M. Sluyters-Rehbach and J.H. Sluyters, Electrochim. Acta, 33 (1988) 303.
3 R. de Levie, J. Electroanal. Chem., 261 (1990) 1; 281 (1990) 1.
4 R. de Levie, Adv. Electrochem. Electrochem. Eng., 6 (1967) 329.
5 L.M. Gassa, J.R. Vilche, M. Ebert, K. Jüttner and W.J. Lorenz, J. Appl. Electrochem., 20 (1990) 677.
6 A. Lasia and A. Rami, J. Electroanal. Chem., 294 (1990) 123.
7 P.K. Wrona, A. Lasia, M. Lessard and H. Ménard, Electrochim. Acta, in print.
8 L. Chen and A. Lasia, J. Electrochem. Soc., 138 (1991) 3321.
9 P. Los and A. Lasia, J. Electroanal. Chem., in print.
10 H. Dumont, P. Los, L. Brossard, A. Lasia and H. Ménard, J. Electrochem. Soc., submitted.
11 H. Dumont, P. Los, L. Brossard, A. Lasia and H. Ménard, Electrochim. Acta, submitted.
12 J. Fournier, P.K. Wrona, A. Lasia, R. Lacasse, H. Ménard and L. Brossard, J. Electrochem. Soc., submitted.
13 P. Los, A. Rami and A. Lasia, J. Appl. Electrochem., submitted.
14 A. Rami and A. Lasia, J. Appl. Electrochem., 22 (1992) 376.

AC-SUPERIMPOSED-ON-DC CHARACTERISTICS OF FUEL CELL ELECTRODES

G. L. Lee and J. R. Selman
Illinois Institute of Technology, Chicago, IL 60616, USA

INTRODUCTION

A fuel cell is an electrochemical device that converts chemical energy directly into electrical energy with high energy efficiency. An example is the molten carbonate fuel cell (MCFC). In Yuh and Selman's study[1] AC impedance measurements are recommended as convenient tools for *in situ* determination of relevant process parameters, even for a gas-diffusion porous electrode at an operating temperature of 650°C or above. The overall objectives of this study are: (1) to further develop the theory of AC-superimposed-on-DC (AC/DC) impedance characteristics for both planar and porous electrodes; (2) to analyze the AC/DC impedance characteristics of MCFC electrodes; (3) to illustrate the accuracy and limitation of impedance techniques for MCFC electrodes.

RESULTS AND DISCUSSION

Equivalent Circuit Approach for Planar Electrodes

The equivalent circuit approach is simple and reliable for planar electrode studies. However, in the proposed circuit all significant physical aspects should be represented. A fairly good fit is obtained over a wide range of frequencies by representing the supermeniscus film and also including inductance behavior due to current through the wiring and especially any electric-heating sources(see Fig.1). The simplification gained by pursuing partial fits without considering these two factors will cause 5% to 30% error in the obtained Warburg coefficient for the former factor and approximately 2% for the latter. However, the most important criterion for the validity of an interpretation is to check on the order of magnitude of the corresponding physical parameters, for example, diffusivity. In this study, all the fitted parameters are in a reasonable range when compared to physical properties of all the important aspects, except the values of charge transfer resistance, R_{ct}. It has too large a relative error to be significant, and the validity of this fitted parameter is doubtful. This study concludes that a serious limitation in determining R_{ct} will occur if the mass transfer resistance is large, because the latter will mask the characteristic features of a low R_{ct}.

Distributed Network Approach for Porous Electrodes

For a porous electrode, the distributed network approach is the most reliable method of interpretation but it is too complicated to extract information directly without further simplification. In practice, further simplification can be realized by partial fits of the original distributed circuit under some special conditions, and results for different levels of DC polarizations (see Fig.2) or for different cell temperatures can be obtained[2]. It is clear that kinetic activation and mass transfer resistance vary significantly under different polarization or at different temperatures. These results strongly suggest that the mechanism of oxygen reduction and the associated mass transfer processes are significantly different under current load

than around equilibrium potential (OCV). Therefore, kinetic information obtained under open circuit conditions is not applicable under high current loads.

Validity of Impedance Analysis for Porous Electrodes

The method discussed above is useful since it allows one in a simple way to extract kinetic and mass transfer information separately from a porous electrode EIS signal. However, the uncertainity of the information obtained, e.g., kinetic activation and mass transfer resistance, is about 10%. As observed on an oscilloscope, the noise generated by the environment is of the order of 0.1 mV. The polarization resistance for a fuel cell electrode is low, e.g., of the order of 0.3-0.5 ohm, as expected for an energy generating device. Therefore, in fuel cell studies the EIS signal is more sensitive to noise compared to corrosion studies. Another source of error is the external resistance, which includes the contact resistances between different materials and the ohmic resistances along the current collector, wiring, measuring circuit of the potentiostat and electrolyte matrix. The instability of these resistances may cause poor accuracy in the polarization resistance R_p if the ratio R_{sol}/R_p is not so small as to be negligible.

CONCLUSIONS

AC/DC impedance techniques may not provide information of high accuracy, but it does allow one to visualize kinetic and mass transfer resistances, which other techniques do not. This makes it appear promising to use AC/DC impedance techniques to monitor the cell performance in long term operation.

A limitation common to both planar and porous electrodes is that the order of magnitude of the investigated resistance of the fuel cell electrode may be too small, compared to the Warburg impedance for a planar electrode, and to the external solution resistance for porous electrodes. However, it is to be noted that the same difficulty will also occur in other electrochemical techniques. Therefore, minimizing noise and using more stable measuring equipment are essential condition to increase the accuracy of impedance measurements in fuel cell electrode applications.

REFERENCES

1. C. Y. Yuh and J. R. Selman, *AIChE Journal* **34**, 1949 (1988).
2. G.L. Lee, *Dynamic Analysis of MCFC Porous Electrode*, Ph.D Dissertation, Illinois Institute of Technology, Chicago, IL (1992).

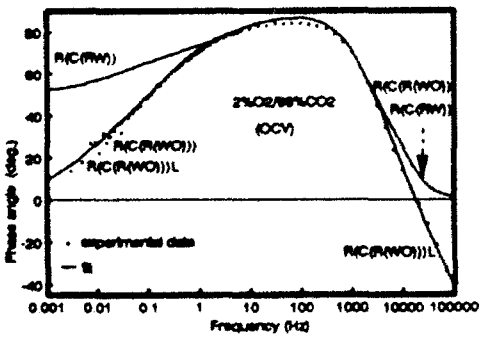

Fig.1 Bode plot for gold flag electrode in MCFC.

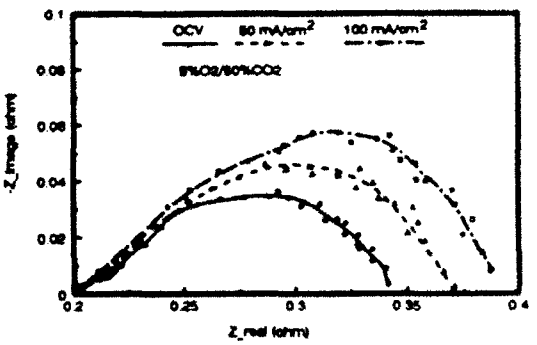

Fig.2 Cole-Cole plot for porous MCFC cathode.

AC IMPEDANCE CHARACTERISTICS OF FUEL CELL POROUS ELECTRODES

Y.P. Lin and J.R. Selman
Illinois Institute of Technology, Department of Chemical Engineering
Chicago, IL 60616

INTRODUCTION A fuel cell is a device which can directly convert fuel and oxidant under production of electrical energy. Depending on the electrolyte used in the fuel cell, one can distinguish five types of fuel cells currently under study. They are (1) polymer electrolyte membrane fuel cell (PEMFC), (2) alkaline fuel cell (AFC), (3) phosphoric acid fuel cell (PAFC), (4) molten carbonate fuel cell (MCFC), (5) solid oxide fuel cell (SOFC). Porous electrodes are used in both cathode and anode of a fuel cell in order to increase the current generated. The principal problems investigated in different types of fuel cell depend on the type of electrolyte used. In the SOFC and PEMFC, the minimization of ionic resistance and maintenance of electrolyte stability are the most critical problems. In the PAFC and MCFC, the ionic conductivity is not a series problem, but the reaction mechanism and kinetics are key points to be investigated.

DYNAMIC AC IMPEDANCE STUDY OF THE MCFC The increased of application of AC Impedance techniques in fuel cell R&D is due to its in-situ characteristics and capability of rapid analysis which is advantageous in a system with relatively fast kinetics.

Based on the agglomerate model of a porous electrode(Fig. 1), Yuh and Selman have developed an analysis of dynamic AC impedance measurement at open circuit[1]. The kinetics of the electrode reaction can be extrapolated according to Fig. 1b[2]. Nishina and Uchida[3] used the equivalent circuit (EC) concept (Fig. 2a) to fit AC impedance measurements of MCFC cathode and anode reactions at a flag electrode. Weewer[4] modified Nishina's EC to study the anode kinetics of the MCFC and used a constant-phase-angle element (CPE) to interpret his results. Lee and Selman[5] studied the cathode reaction of the MCFC at both porous and flag electrodes by AC impedance measurements. They investigated this both at open-circuit and with DC loading. Makkus[6] studied the cathode and anode reactions of the MCFC at flag electrodes, under open circuit conditions(Fig. 2b). A chemical reaction resistance was added to the EC of the cathode reaction. The EIS of other types of fuel cells are described in this presentation.

AC IMPEDANCE STUDY IN FUEL CELL R&D The application of AC Impedance techniques in fuel cell research is still very limited, even though it has been accepted as a useful tool in quite a wide range of electrochemical application. A further investigation of the specific characteristics of different types of fuel cells by means of EIS looks very promise. Some of these characteristics are as follows. In the **MCFC**, the wetting phenomena in conjuction with the mechanism as discussed above; in the **SOFC**, the oxygen diffusion in the air electrode and contact resistance between the electrodes and electrolyte; in the **PAFC**, the kinetics of oxygen reduction in the porous electrode and the influence of oxide film formation on the electrode reaction; in the **PEMFC**, the local heat generation at high power density.

CONCLUSIONS Despite the complexity of the interpretation of FIS data, which

imposes restrictions in modeling as mentioned by Springer [7], the simplified information provided by EIS can still help to understand and, therefore, optimize the processes which control fuel cell performance.

REFERENCES

1. C.Y.Yuh, "Potential Relaxation and AC Impedance of Porous Electrodes", Ph.D. dissertation, Illinois Institute of Technology, (1985).
2. C.Y.Yuh and J.R. Selman, "The Polarization of Molten Carbonate Fuel Cell Electrode, II. Characterization by AC Impedance and Response to Current Interruption", J. Electrochem. Soc., 138, 3649, (1991).
3. T. Nishina and I. Uchida, "Electrochemical Analysis of Oxygen Reduction Path at Au Flag Electrode and Sintered Au Spheres Electrode", Second Symposium Molten Carbonate Fuel Cell Techology, 90-16, The Electrochemical Society Inc., 438, (1990).
4. R. Weewer, "Study of Electrochemical Processes and Wetting Phenomena at the Molten Carbonate Fuel Anode", Ph. D. Thesis, Delft University of Technology, Delft, The Netherlands, (1991).
5. G.L. Lie, Dynamic Analysis of MCFC Porous Electrode, Ph.D. Dissertation, Illinois Institute of Technology, 1992.
6. R. Makkus, Electrochemical Studies on the Oxygen Reduction and NiO(Li) Dissolution in Molten Carbonate Fuel Cells, Ph.D. Dissertation, Delft University of Technology, Delft, The Netherlands, 1991.
7. T.E. Springer and I.D. Raistrick, "Electrical Impedance of a Pore Wall for the Floded-Agglomerate Model of Porous Gas-Diffusion Electrodes", J. Electrochem. Soc., 136, 1594, (1989).

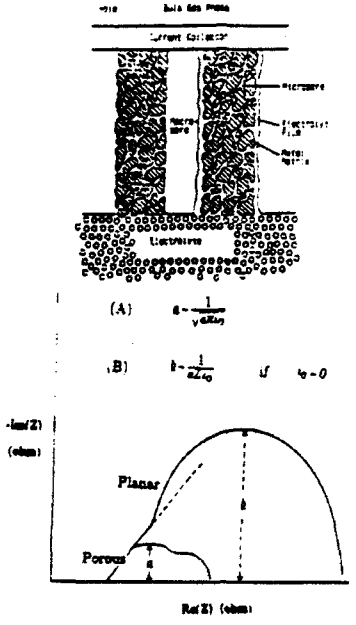

Fig. 1 (a) Schematic of aggolomerate structures in a porous electrode (from Ref. 1); (b) Schematic of expolation for kinetics and other information.

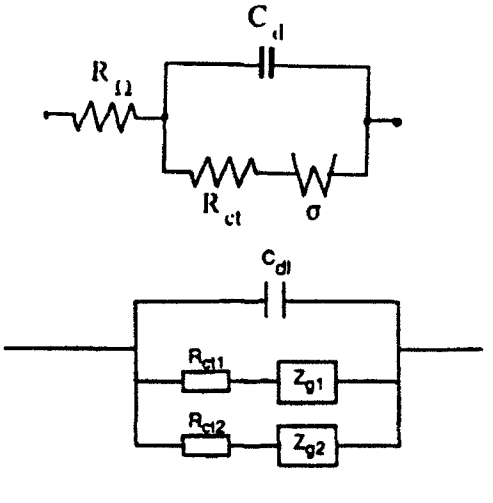

Fig. 2 Equivalent circuit of the cathode reaction in the MCFC (from Ref. 3, 6)

IMPEDANCE SPECTROSCOPY OF ARTIFICIAL MEMBRANES DEPOSITED ON METAL SURFACES WITH LANGMUIR-BLODGETT TECHNIQUE.

Britta Lindholm, Department of Analytical Chemistry, Umeå University, S-901 87 Umeå. Per-Åke Ohlsson, National Defence Research Establishment, Department of NBC Defence, S-901 82 Umeå, Sweden

In recent years the Langmuir-Blodgett technique has been recognized as a powerful tool for surface modification of electrode surfaces on a molecular level. The method takes advantage of that certain molecules, spontaneously form monomolecular films at an air/water-interface. These molecules are in most cases amphiphilic, that is with one or more carbon chains attached to a hydrophilic headgroup. The headgroups are solvated in the aqueous phase whereas the hydrophobic carbon chains point upwards, out of the water phase. The monolayer can be compressed and transferred to a hydrophilic electrode surface by slowly lifting the electrode perpendicular through the air/water-interface. The monolayer adheres to the electrode surface with hydrophilic/hydrophilic interaction. By successively lowering and raising the electrode through the air/water-interface, it is possible to create ordered multilayer structures at the electrode surface. Artificial cell membranes can thus be formed on an electrode surface by transferring two monolayers of phospholipid molecules. [1,2]

In the present work, bilayer and multilayer structures of phosphoplipids on gold electrodes were investigated with impedance spectroscopy. The frequency range was 10kHz - 10mHz and the amplitude 10 mV. The expected equivalent circuits are displayed in figure 1 together with an idealized picture of the molecular structure at th electrode surface. Notice that the membrane constitutes a layered structure of hydrophobic and hydrophilic regimes.

A similar analysis has been performed earlier on black lipid membranes by Coster et al. [3]. We observed low capacitancies (around 0.5 $\mu F/cm^2$) for the hydrophobic part of a phosphatidic acid multilayer film, which is in good agreement with Coster. The resistances of our supported bilayers and multilayers are however substantially lower than what was observed for the black lipid membranes.

The influence of the ionic strength in the supporting electrolyte is discussed as well as the presence of unsaturated groups in the carbon chain.

References:

1.) Puu, Gustafson, Ohlsson, Olofsson and Sellström (1991) In "Progress in Membrane Biotechnology." Ed.: Gomez-Fernandez, Chapman and Parker, Birkhäuser Verlag, Basel, Switzerland.

2) Sellström, Gustafson,Ohlsson, Olofsson ad Puu (1992) Accepted in Colloids and Surfaces.

3) See for instance: 0.Zimmermann, R.G. Ascheroft, H.G.L. Coster and J.R. Smith (1977) Biochim.Biophys.Acta, 469, 23-32.

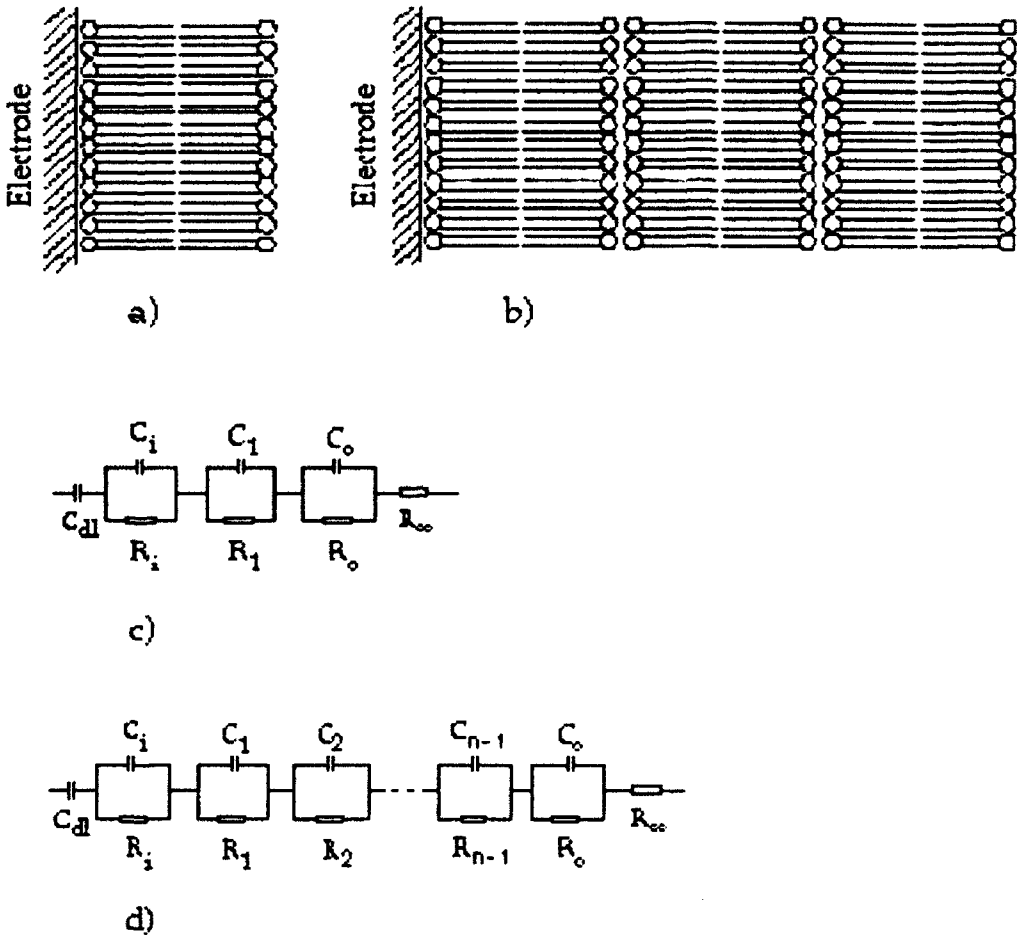

Fig 1. Molecular structures at the electrode surface: a) a bilayer b) a multilayer; Equivalent circuits of c) the bilayer d) the multilayer; n is the number of phospholipid monolayers transferred, which was always an even integer. C_{dl} is the double layer capacitance; R_i and C_i are the resistance and capacitance respectively for the hydrophilic inner part of the membrane, whereas R_o and C_o are those for the hydrophilic outermost part of the membrane; R_k and C_k are the capacitances and resistances for the hydrophobic (k = uneven integer) and hydrophilic (k = even integer) parts in the interior of the film; R_∞ is the uncompensated resistance.

SOME NEW DIRECTIONS IN IMPEDANCE SPECTROSCOPY DATA ANALYSIS

James Ross Macdonald

Department of Physics and Astronomy
University of North Carolina
Chapel Hill, North Carolina 27599-3255

New developments in two main data analysis areas are discussed: (a) complex nonlinear least squares (CNLS) fitting of data, and (b) data-transforming and optimizing integral transforms. In the first category, a Monte Carlo study is used to answer the question of which of several different parameterizations of an ambiguous equivalent circuit model leads to minimum correlation between fitting parameters, a desirable condition. In addition, results are briefly discussed which address the questions of (1) what should be minimized in CNLS fitting? (2) How well can one discriminate between exact small-signal binary electrolyte response and conventional finite-length diffusion response? And (3), what is the ultimate precision of parameter estimates obtained in a CNLS fit?

In the second area, new forms of the Kronig-Kramers relations (KKR) are discussed; the accuracy of several different ways of carrying out the numerical quadratures needed in such transforms is compared; and it is shown how random errors present in complex data are transformed by the KKR. Then, new transforms are described and illustrated that can replace exponential Fourier and KK transforms and, at the same time, can greatly reduce random error and some kinds of systematic errors in real, imaginary, or complex frequency response data, or in transient response data, without the need for making any smoothing or filtering parameter choices.

EVALUATION OF PAINTED STEEL UNDER CATHODIC PROTECTION

I.C.P.MARGARIT[1], O.R.Mattos[1], J.P.Quintela[2]

1-Lab. de Corrosão "Prof. Manoel de Castro", EE/UFRJ and COPPE/UFRJ, Caixa Postal 68505, CEP 21945, RJ, Brasil.
2-PETROBRAS/CENPES/SUPEP/SEMEC, Cid.Univ., Quadra 7, I. Fundão, CEP 21910, RJ, Brasil.

INTRODUCTION

Corrosion prevention of underground or submerged structures is usually a combination of coating and cathodic protection. The two methods are essentially complementary because coating allows the effective use of cathodic protection only for areas with coating damage.

Nevertheless being used for a long time, there are still important problems affecting the use of coatings together with cathodic protection. One problem is concerned with the development of reliable methods for monitoring the cathodic protection efficiency, especially on areas of coating damage. The limitations of potential measurements for this purpose are well known (1). The shielding effect of the coats on delaminated areas is responsible for misleading potential readings (2-4). Although alternative techniques have been proposed in the literature (5-7) more work has to be done before their recognition and widespread application.

Another problem also very important is the unknown factor of the coating aging, i.e., of the *coating efficiency* (%) along the time. This efficiency depends on many factors and it will be greater the better the coating features. It is the knowledge oledge of E that rmines the correct cathodic protection system dimensioning as well as exact adjustments during service.

In general the estimation of % is based on previous field experience or data from the literature . A wrong estimate or super-estimate of the coating efficiency implies serious damage or overprotection, respectively. The overprotection ius damage or overprotection, ree security factor normally applied in cathodic protection designs. Overprotection means not only waste of money but also can cause harmful effects on the coatings (8).

Laboratory methodology to help in more accurate estimations of % has not been developed yet. In this sense preliminary results will be shown in this paper and some aspects concerning the use of electrochemical techniques to monitor coatings efficiency . Particularly we are interested on the study of paints for off-shore structures.

EXPERIMENTAL

Several trials of accelerating the aging process

on paint systems formulated for off-shore structures were performed. They consisted of: 1) Cathodic polarization under -2.0VSCE; 2) Cathodic polarization under -5.0VSCE; 3) alternated immersion in distilled water and 3.5%w NaCl solution with thermal shocks from 5°C to 40°C.

All tests were performed in cycles where the samples remained submited to the "accelerating agent" during 5 days and rested for two days in a 3.5 % NaCl solution, at room temperature and at free potencial. During this period the eletrochemical impedance of the samples was measured. In parallel two control tests were also performed aiming at the evaluation of the proposed tests. The control assays consisted of : total immersion in 3.5% NaCl solution at room temperature without any polarization and total immersion at room temperature with polarization at -1.0 VSCE. This potencial was adopted as one control because it is one of the criteria normally accepted for cathodic protection. Five paint systems were tested.

PRINCIPAL RESULTS AND CONCLUSIONS

The results presented in this paper have shown that the polarization of -5.0V was able to accelerate the deterioration process of the paints submitted to cathodic protection. The polarization at -5.0V followed by impedance monitoring was able to select the more resistive paint system among the five paints proposed. However, it is not obvious if the more resistive paint system will be the best to be used in actual structures where defects are always present in the paint. Indeed, it was shown that in the case of these more resistant paints, when one defect appears, the impedance decreases drastically and consequently the cathodic current increases.

More work using artificial defects in these paint films is in progress in our laboratory.

REFERENCES

1) A. C. Toncre, Materials Performance, p.22, AUG/1984
2) K. Kasahara, T. Sato and H. Adachi, Materials Performance, p.45, SEPT/1980
3) R. R. Fessler, A. J. Markwoth and R. N. Parkins, Corrosion-NACE, 39(1), p.20,1983
4) B. W. Cherry and A. N. Gould, Corrosion'89 Meeting, New Orleans, paper 404,1989
5) J. D. Kellner, Corrosion'86 Meeting, Anaheim, paper 252,1986
6) J. N. Murray, J. K. Scully and P. J. Moran, Corrosion'86 Meeting, Anahein, paper 271, 1986
7) K. Umeyama, S. Takai and T. Tsuru, Corrosion'89 Meeting, paper 423,1989
8) W. R. Mccaffrey, Materials Protection and Performance, FEB/73, part 1,p.10

ANALYSIS OF CHARGE TRANSFER AND MASS TRANSPORT PROCESSES FOR THE REDOX CONTAINING MODIFIED PEO ELECTROLYTE - SNO_2 SYSTEM.

B. MARSAN*, H. CACHET**

(*) Université du Québec à Montréal
Departement of Chimie - CP 8888, Succ. "A"
Montréal, Québec. CANADA H3C 3P8

(**) UPR 15 du CNRS
Physique des Liquides et Electrochimie
Université Pierre et Marie Curie
Tour 22 - 5ème étage - 4, Place Jussieu
75252 Paris cedex 05 - FRANCE

Modified polyethylene oxide (PEO) polymers containing mobile redox species constitute an interesting class of materials for energy applications. A solid state photoelectrochemical (PEC) solar cell has been realized, based on an electrochemically deposited n-CdSe photoelectrode in contact with a polymer electrolyte complexed with an alkali polysulfide[1,2]. A new promising candidate KT/T_2 has been recently proposed for the redox couple: KT, the reduced species, stands for the 5-mercapto-1-methyltetrazole, potassium salt and T_2, the oxidized species, for the dimerized form. The PEC cell is completed by a transparent counter electrode (TCE) constituted by a thin film of a conductive oxide like SnO_2. Under illumination, an oxidation (reduction) reaction occurs at the n-CdSe electrode (at the TCE) respectively. The overall performances of the cell depend for a part on the electrochemical properties of the TCE with respect to the redox couple present in the polymer matrix.

In this work, electrical and electrochemical properties of the MT/T2-modified PEO system (with M=K,Cs) in contact with SnO_2 electrodes are investigated by impedance measurements. A two-terminal potentiostatic arrangement was used in connection with a Transfer Function Analyzer (Voltech TF2000 or Solartron 1174). Polymer electrolyte films are synthetized from acetonitrile solutions of modified PEO, of the metal salt MT and the dimer T_2. The redox and the polymer electrolyte concentrations are taken as MT/T_2=10/1 and O/M=8 respectively. F-doped SnO_2 films are fabricated by spray onto glass substrates, with a square resistance of 10-20 ohms [3]. Sandwich-type structures of a polymer electrolyte layer between two SnO_2 thin film electrodes are assembled at the temperature of 50°C. All this work is performed under argon atmosphere.

Impedance measurements at high frequencies (10kHz-1MHz) without dc polarization give the dielectric constant of the polymer to be 20±4 (with K or Cs salt). The cesium salt is found to be more conductive than the potassium salt.

When a dc polarization is applied to the structure, inverse electrochemical reactions occur at the SnO_2 electrodes. Because of the differenties (size, charge and concentration) between reduced and oxidized species, different impedance response for each electrochemical reaction may be expected. It must be also noted that the externally

applied voltage is distributed through the structure according to the overpotential of each reaction.

Impedance data have been obtained at various dc applied voltage (0-1.5V) and at different temperatures (between 22 and 80°C). They have been analyzed on the basis of the equivalent circuit given in ref.4 (fig.2). From impedance spectra in the range 1-10^5 Hz, a charge transfer resistance R_t is determined and assumed to be related to a Faradaic current $I = I_o.\exp(bv)$, where v is the overpotential for the reaction considered ($v<V$, the applied dc voltage). Our analysis is based on the two following relationships:

(i) $R_t.I = 1/b$

(ii) $\ln R_t = - \ln(I_o b) - b.v.$

v is evaluated to be 20-30% of the applied voltage, indicating that the electrochemical reaction associated to the above R_t is the fastest one, probably the oxidation of MT into T_2. The b factor is found close to 17 V^{-1} indicating a transfer coefficient of 0.5 for a one electron transfer reaction. The pre-exponential factor I_o increases with temperature for a given salt (KT/T_2: 2.10^{-8} to 10^{-7} A/cm^2 from 26 to 60°C) and at the same temperature is four times higher for the cesium salt (4.10^{-7}A/cm2) than for the potassium salt (1.10^{-7} A/cm^2).

REFERENCES:

(1) B. Marsan and A.K. Vijh, First International Symposium on EIS, Bombannes (1989), ext. abstr. C8-16.
(2) B. Marsan and A.K. Vijh, Bull. Electrochem. **5** 456 (1989).
(3) J. Bruneaux, H. Cachet, M. Froment and A. Messad, Thin Solid Films, **197** 129 (1991).
(4) P.R. Sorensen and T. Jacobsen, Electrochim. Acta, **27** 1671 (1982).

THE IMPEDANCE STUDY OF THE OXIDATION OF FORMIC ACID AT A PLATINUM ELECTRODE

H.Matsui, M.Yasuzawa, and A.Kunugi
Department of Chemical Science and Technology, The University of Tokushima, Minamijosanjima-cho, Tokushima 770, Japan

INTRODUCTION

The oxidation of formic acid at a platinum electrode in an acid solution is known[1,2] to be retarded by the formation of adsorbed carbon monoxide. The present paper describes that the oxidation rate of formic acid is approximately independent of the potential at potentials above about 0.35 V vs RHE when the blocking effect of adsorbed carbon monoxide was compensated and the oxidation current was measured at a middle surface coverages. The cause of the potential independency of the oxidation rate has been examined by a faradaic impedance method. A multisine-wave tequnique of an ac-impedance method enabled us to measure some relaxation terms related to reaction kinetics, regardless of the extents of rate retardations.

EXPERIMENTAL

The oxidation current of formic acid was potentiostatically measured at a smooth platinum electrode in 0.1 mol dm^{-3} HCOOH + 0.5 mol dm^{-3} H_2SO_4, and the surface coverage with adsorbed carbon monoxide was obtained by the conventional hydrogen deposition method.

The faradaic impedance was obtained by subtracting the solution resistance and $j\cdot(\omega C_{dl})^{-1}$ from the electrode impedance which was measured by a fast Fourier transformation method. Here, j, ω and C_{dl} are the sign of $(-1)^{1/2}$, the angular frequency and the double-layer capacitance respectively. The obtained faradaic impedance was numerically analyzed according to the equivalent circuit in the inset in Fig. 2. The analysis frequency was limited to values lower than about 100 Hz in order to realize a steady state for any transient term in the equivalent circuit.

All the potentials were referred to a reversible hydrogen electrode in 0.5 mol dm^{-3} H_2SO_4.

RESULTS AND DISCUSSION

Figure 1 shows the i_t - E and $i_t/(1-\theta_{CO})$ - E relationships in the steady-state oxidation of formic acid at a platinum electrode. Here, i_t and θ_{CO} are the overall current density and the surface coverage with adsorbed carbon monoxide respectively. $i_t/(1-\theta_{CO})$ implies the oxidation rate which is compensated for the blocking effect of adsorbed carbon monoxide, and actually this rate was taken at θ_{CO} of 0.5 in order to avoid the rate retardation at high CO coverages (cf. ref. 3). A Tafel-like relationship held between i_t and E in the potential range of about 0.30 - 0.42 V. However, the oxidation rate of formic acid was approximately independent of the potential at potentials above about

0.35 V by expressing it by $i_t/(1-\theta_{CO})$. The cause of the potential independency of $i_t/(1-\theta_{CO})$ was examined by a faradaic impedance method.

Figure 2 shows the complex plane plots of the faradaic impedance for the steady-state oxidation of formic acid at different potentials. The complex impedance plots exhibited a part of a semicircular line in the potential range of about 0.30 - 0.55 V. The complex impedance plots can be explained in terms of the slow adsorption of formic acid molecules coupled with some charge transfer.

At potentials higher than about 0.6 V, θ_{CO} was approximately zero, and the calculated double-layer capacitance agreed with that in the absence of adsorbed carbon monoxide. However, the observed double-layer capacitance was close to that in the presence of a monolayer of adsorbed carbon monoxide, suggesting the presence of some adsorbate other than adsorbed carbon monoxide. This adsorbate corresponded to that detected by the oxygen deposition method, and considered to be formic acid which was adsorbed via its carboxyl group.

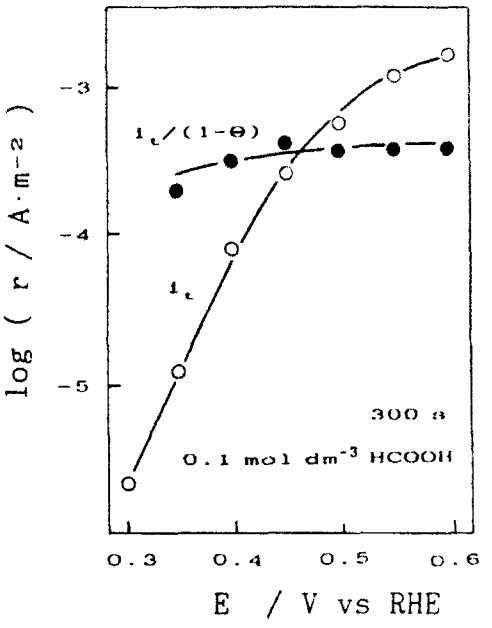

Fig. 1. Potential dependence of i_t and $i_t/(1-\theta_{CO})$.

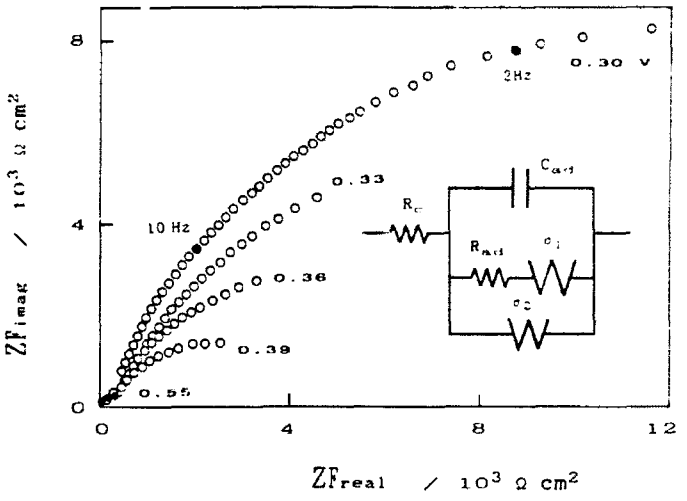

Fig. 2. Complex plane plot of faradaic impedance of HCOOH oxidation.

REFERENCES

1) A.Capon and R.Parsons, *J. electroanal. Chem.*, **44**, 1 (1973).
2) B.Beden, A.Bewick, and C.Lamy, *J. electroanal. Chem.*, **148**, 147 (1983).
3) H.Matsui and A.Kunugi, *Bull. Chem. Soc. Jpn.*, **61**, 3295 (1988); **63**, 507 (1990).

STUDY ON (Y,Ce)-TZP-Al_2O_3 CERAMICS BY AC IMPEDANCE SPECTROSCOPY TECHNIQUE

Guangyao MENG, Zhenghui WEI, Xinqin LIU, Wei WANG & Dingkun PENG and Takao HAKATA*
Department of Materials Science and Engineering, University of Science and Technology of China, Hefei, Anhui 230026, China
* Ibaraki Research Laboratory, Hitachi Chemical CO. Japan

Recently, a number of papers has been devoted to the study of electrical properties of Tetragonal ZrO_2 polycrystalline materials(TZP), because of the practical interest to their applications in solid oxide fuel cell. In this work we studied the electrical and electrochemical parameters of the selected specimens in the (Y,Ce)-TZP-Al_2O_3 composite system by using AC Impedance Spectroscopy technique, in order to give addtional information on its microstructure which should be helpful to the improvement of the TZP's mechanical properties with both Y_2O_3 and CeO_2 stabilizing agents.

The compositions of the specimens are as follows,

No.1: 3Y-97ZrO_2 + 20 wt% Al_2O_3
No.2: 3Y-4Ce-93ZrO_2 + 20 wt% Al_2O_3
No.3: 1.5Y-4Ce-94.5ZrO_2 + 20 wt% Al_2O_3 and
No.4: 1.5Y-4Ce-94.5ZrO_2 + 20 wt% Al_2O_3

All specimens were sintered at 1470 °C for 3 hrs. AC IS measurement was performed in the frequncy range of 12 Hz to 100K Hz and temperature range of 200 °C to 900 °C. XRD was routinely applied to examine the crystallographic structure and SEM was used to observe the surface morphology of the specimens before and after IS measurements.

The impedance spectra of the specimens at temperature lower than 350 °C typically consist of two well separated arcs, indicating the electical behavious associated with grains and grain boundaries, respectively. These two arcs become one stepwisely as temperature rises. With a simplified equivlant circuit shown in FIg. 1, from the IS data analysis we could obtain all electrochemical parameters such as E_{gb}, E_{gr}, C_{gb} and C_g as well as conductivities for both grains and grain boundaries. The results demonstrated that all these values much depended on the composition and treatment procedure of the specimens. The same order of magnitude in conductivity for No.1 and No.2 and also for No.3 and No.4 but noticeablely lower than the former two is related to their Y content hence the oxygen vacancies which are responsible for the oxygen ionic conduction. It appears the different Ce content in the specimens only plays a minor role in the conductivity due to that the Ce atoms are essentially stay in their IV valence[1]. However, the conduction activation energy is distinctly related to the specimen heat treatment process. Specimen No.4 exhibited a remarkably lower E_{gb}(104 kJ/mole) and E_{gr} value(86.6 kJ/mole) due to Y-ZrO_2 powder being pre-heat treated at 1300 °C for 3 hrs. While for other specimens E_{gb} and E_{gr} values were in the range 110 - 112 kJ/mole and 90-96 kJ/mole, respectively. The grain boundary capacitance could give more information about the specimen microstructure. Fig.2 shows that compared with specimens No.1 and No.2, No.3 and No.4 exhibit lower grain boundary capacitance values , indicating better sintering status and thinner interface zone. This should be attributed to their lower Y content and the different heat treatment.

Fig.3 presents the typical XRD patterns of a specimen treasted differently. An unexpected finding is that the AC measurement has caused a change of the relative intencity of T(002) in contrast with Y(200) and of T(113) in contrast with T(131) and peak separation of T(202) from T(220). Wang and Steven[2] discussed the cell distortion on the free crystal surface of TZP in term of geometry of M-T phase transition. It appears the same idea can explain the effect observed here. During CIS measurement Ac electric field would produce electric dipole moment b and induced charge q'. It is easy to find out the free energy of the system increases q'b and the energy barrier for T - M phase transition is lowered

by q'b. This effect of AC electric field on the structure would certainly bring changes in both electric and mechanical properties of the materials, which is worth doing further investigation.

REFERENCES

[1] I. Riess et al., J.Appl. Phys., 61(1987)4921
[2] J. Wang and W. Steven, J. Mater. Sci. Latter, 8(1989) 1195

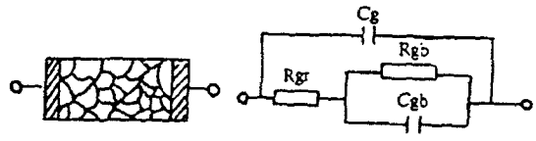

Fig.1 The simplified equivlent circuit for ceramic composite materials

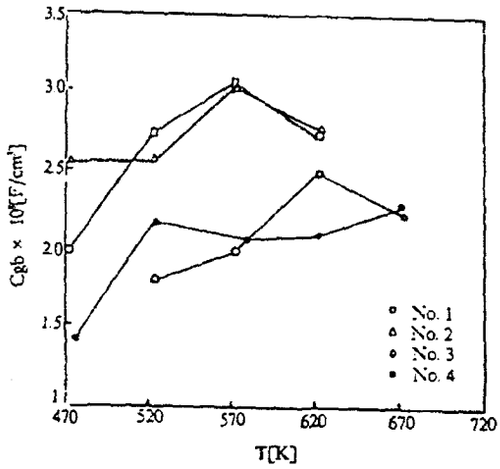

Fig.2 The temperature dependance of grain boundary capacitances for four specimens

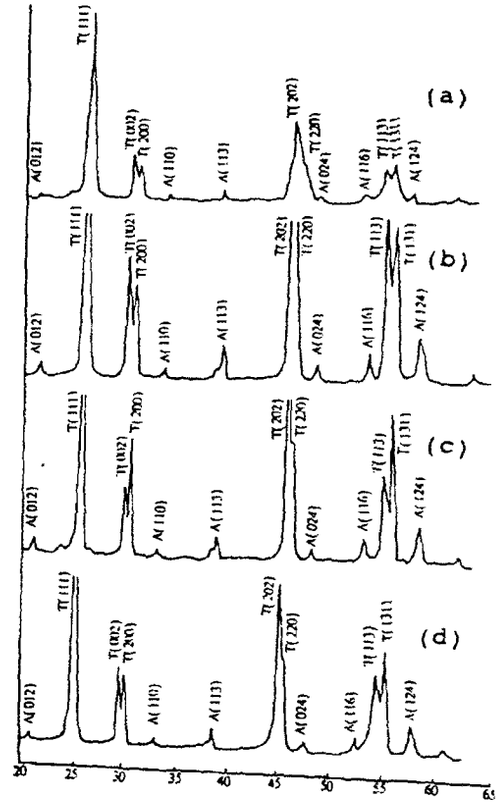

Fig.3 The typical XRD patterns of the specimen(No.2) treated differently
(a) specimen as-sintered
(b) heated to 900 °C and cooled dwon to RT.
(c) underwent IS measurement and strongly polished
(d) strongly polished without IS measurement

ELECTROCHEMICAL IMPEDANCE SPECTROSCOPY OF INTERCALATED ELECTRODES

A. Métrot and A. Harrach
Laboratoire d'Electrochimie et Chimie du Solide
Faculté des Sciences BP 347. 51067 Reims Cedex, France

Electrochemical Intercalation processes in electrodes are of very actual interest as they concern many secondary batteries but practical electrodes are generally porous and difficult to modelize. In contrast HOPG graphite is a well characterized host lattice in which electrochemical intercalation of H_2SO_4 has been demonstrated for decades, leading to the so-called Graphite Salts $C_n^+ X^-, HX$ with $X=HSO_4$. Each pure stage of intercalation does exist in definite Charge Q (or C_n^+) and Potential E "overcharging" ranges [1], while plateaus on the E (Q) curve correspond to two-phases mixtures. The single phase ranges E(Q) relations are quasi linear suggesting a capacitive law related to the internal host-intercalant interfacial capacitance. Indeed this apparent "static" capacitance is roughly proportional to the interfacial area i.e. inversely proportional to the stage number (number of graphene layers separating two intercalant layers): the capacitance is around 170 Farad/g, for the stage 1 (2600 m^2/g), around 80 Farad/g for the stage 2 (1300 m^2/g), etc... in agreement with a realisti- mean surfacic value of 6.5 μFarad/cm^2 [2].

Those results are plainly supported by Impedance measurements performed on pure stage intercalated HOPG in contact with the mother sulphuric electrolyte. On Nyquist plots low frequencies points always appear as a vertical tail leading to Limit Capacitances in good agreement with the static ones. This vertical tail is preceeded by a Warburg-like 45° slope which we consider as a true Transmission Line (T.L.) behaviour of the graphite host seen as a porous blocking electrode. The well defined geometric and cristallographic features of the HOPG sample allow to calculate the Total Resistance R_t and Capacitance C_t of the Line using the intercalated acid resistivity ρ_i and the internal volumic capacitance c_i reported to the intercalant volume, leading to the expression of the Diffusivity D :

$$D = 1/R_t.C_t = 1/3.R_t.C_t = 1/\rho_i.c_i = 1/\rho.c$$

where R_t is the Limit Resistance of the Line, c the volumic capacitance reported to the whole sample volume and ρ the partial ionic resistivity of the electrode. It is noteworthy

that the same expressions of D can be derived from a Nernstian approach [3] as done for the Chemical Diffusion Coefficient $\tilde{D}$ by Weppner et al. [4]. which they carefully distinguish from the Component Diffusion Coefficient D_c according to :

$$\tilde{D} = w.D_c \quad \text{with} \quad w = dLn(a)/dLn(c)$$

where a is the activity and c the concentration of the active specie. Practically, w appears as an ajustement factor that can be very high (75 in the case of H_2SO_4-HOPG) so that we consider the T.L. approach as more natural. To our point of view, D is the actual Diffusivity of Electron-Ion pairs moving along the internal 2D interfaces. Considering now the equilibrium E (Q) curve, static capacitances of two phases mixtures look like infinite as they correspond to Potential plateaus. Nevertheless Impedances Spectra keep their usual capacitive aspect, at least when established using zero centered low sine currents, and the calculated low frequencies capacitances average the pure phase ones. The limit resistances behavior is more complex but can nevertheless be fitted by a T.L. model. If now Impedances are measured with the surimposition of a constant direct current, i.e during stage transformation, the low frequencies tail is no more vertical but more or less incurved, depending on the direct current value. A convenient fitting of the T.L. model is obtained by adding a leak resistance in order to simulate a Charge Transfer Resistance R_{ct}. In the absence of a surimposed direct current, the purely capacitive aspect of the spectra obtained suggests that the overvoltage necessary for the stage transformation is not attained i.e. that R_{ct} is infinite.

Finally, contrary to one-phase "overcharging", diffusion cannot describe, to our point of view, the two-phase processes of stage transformations : a Mobility Coefficient seems more pertinent in this case [5], as moving of the phases boundaries depends directly on the electrical field.

[1].A. Métrot, J. E. Fischer, Synth. Metals 3, 201 (1981).

[2].A. Harrach, A. Métrot, Electrochim. Acta 34, 2, 1877 (1989).

[3].A. Harrach, A. Métrot, Mat. Res. Soc. Symp. Proc., Vol 210, 373, Solid State Ionics II. M.R.S. Edit.(1991).

[4].W. Weppner, R. A. Huggins, J. Electrochem. Soc., 124, 10, 1569 (1977).

[5]. A. Métrot, M. Tihli, Synth. Metals 23, 19 (1988).

IMPEDANCE SPECTROSCOPIC SSTUDIES ON HIGH T_c SUPERCONDUCTORS

M. Mohammad, A.Y. Khan, U. Akhtar, S. Malik, M.S. Subhani and R. Wahab; Electrochemistry Group, Chemistry Department, Quaid-i-Azam University, Islamabad, Pakistan.

Impedance measurements were carried out on superconducting ceramic electrode/electrolyte system. The superconducting ceramic being high Tc, $YBa_2Cu_3O_{7-x}$ and $Y_{1.5}Ba_{2.5}CaCu_5O_{5(3-x)}$, the solution being 2M, 1M and 0.1M tetra n-butylammonium perchlorate in acetonitrile, the temperature being ambient. Impedance were also carried out on an ultramicro ensemble electrode made of superconductor ceramic by making pellet membrane electrode of the ceramic $YBa_2Cu_3O_{7-x}$ Measurements were carried out in oxygen free atmosphere.

The details of the procedure of evaluating Z and Z' from experimentally measured resistances and capacitances are given in refs. [1] and [2]. The calculated Z and Z' were then plotted as impednace plane (Nyquist) plot. From these plots the solution resistance R_Ω, the charge transfer resistance θ and the double layer capacitance C_{dl} etc. were obtained wherever possible. Help was taken from the RC-circuit (equivalent circuit) impedance plots for qualitative interpretation of the electrode/electrolyte impedance data.

Generally for $YBa_2Cu_3O_{7-x}$ (S_1) the Nyquist plots are semi-circle which conforms to the simple Randles circuit. However, sometime a semicircle alongwith low frequency Warburg impedance lines are also obtained which means the equivalent circuit in the latter case is given in fig. given below:

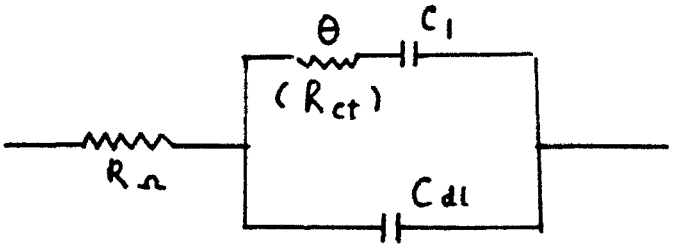

For these cases where low frequency straight lines are obtained, an electrochemical parameter σ, which is a measure of the role of mass transfer resistance, is obtained from the relationship $Z' = Z' - R_\Omega - \theta + 2\sigma^2 C_{dl}$ provided R_Ω, θ and C_{dl} are known from the semicircle. Using the value from the above equation and the lowest frequency used (f = 0.005 KHz, $w = 2\pi f$), the pseudo capacitances were calculated from $C_s = C_1 = 1/\sigma\omega^{1/2}$. A typical value (1M TBAP) being 1.2×10^{-4} (ohm/F)$^{1/2}$ which gives $C_1 = C_s = 750$ uF/cm^2 which is greater than $C_{dl}(C_2) = 650$ uF/cm^2. In all the case θ is small, 120-300 Ω which in principle, means some faradaic process is going on. This indicates that a reaction leading to corrosion of the ceramic electrode, most probably, is taking place but there is no insulating film formation since R_Ω is quite low (80 - 175 Ω). In

the case of S_1 most of time Z - Z' plots were semicircle with Warburg impedance line. In this case θ >> R (θ > 1600 Ω , R 80 - 120 Ω). The equivalent circuit is the same as given in the figure above: C_1 (for 1M TBAP) = 300 uF/cm^2 while C_2 (i.e. C_{dl}) is about 72 uF/cm^2. The ceramic S_2 was found to be rather unstable.

The Z - Z' plots of the $YBa_2Cu_3O_{7-x}$ pellet membrane electrode (ultra-micro ensemble) electrode were similar to the ones obtained for S_2 i.e. a semicircle in the high frequency region and straight line in the low frequency region. For all three concentration R_Ω was very high in the range of 50 - 70 KΩ while C_{dl} was found to be 0.18 to 0.25 uF. θ the charge transfer resistance was found to be about 1000 ohms. Concentration had little effect on these parameters. The equivalent circuits for this electrode is the same as for the two samples S_1 and S_2.

Acknowledgement: The present work was supported by National Scientific Research Development Board Project No. ISB-PH-14(I).

References 1. A.J. Bard and L.R. Faulkner, Electrochemical Methods, Fundamentals and Applications, Chapter 9. John Wiley and Sons, New York (1980). 2. B. Wheeler, AC technique by means of lock in amplifier, University of Texas, Austin, Texas (1985).

STUDY OF THE CONDUCTION MECHANISM OF $MgAl_2O_4$ AT DIFFERENT ENVIRONMENTAL HUMIDITIES

G. Gusmano, G. Montesperelli, P. Nunziante and E. Traversa
Dipartimento di Scienze e Tecnologie Chimiche,
Universita' di Roma "Tor Vergata", 00173 Rome, Italy

In recent years $MgAl_2O_4$ has been proposed as a sensitive material for humidity detection devices [1-3].
In this paper, the electrical properties of $MgAl_2O_4$ in oulk and in thin-film form are discussed in relation to its microstructure.
Three specimens were tested: specimen A was obtained by sintering a commercial powder, specimen B was made up by sintering a powder prepared by the thermal decomposition of a coprecipitated hydroxide mixture to produce a different microstructure. Specimen C was obtained as 80 nm thick thin-film, by radiofrequency sputtering on a Si/SiO_2 substrate using a target prepared from the commercial powder.
Surface area, density and pore size distribution were measured for the pellets. The microstructure of all the specimens was observed by SEM.
The electrical behaviour of the specimens was studied by EIS in the frequency range from 10^{-2} to 10^5 Hz and by measuring I-V curves at relative humidity (rh) values ranging from 5% to 85%. In order to determine the conduction carriers, the samples were polarized at 1 V dc. The study of the charging and discharging currents leads us to conclude that in humid environments the conduction carriers are ions, and that they are both ions and electrons in nearly dry environments.
The typical impedance plot at different rh values shows two semicircles. The one at low frequencies is not complete and its centre is below the real axis. The second at higher frequencies is also inclined, it does not pass through the origin of the complex plane axes and its intercept with the real axis is indepedent of rh. The results show that the same equivalent circuit already proposed by Yeh et al for doped-titania [4] can also be used to describe the electrical behaviour of $MgAl_2O_4$. The circuit is made up of a resistance, characteristic of the crystal grain, and two RC elements, characteristic of the grain surface and the electrode polarization, in series.
Figure 1 shows the resistance of grain surface (Rgs) versus rh for all the specimens.

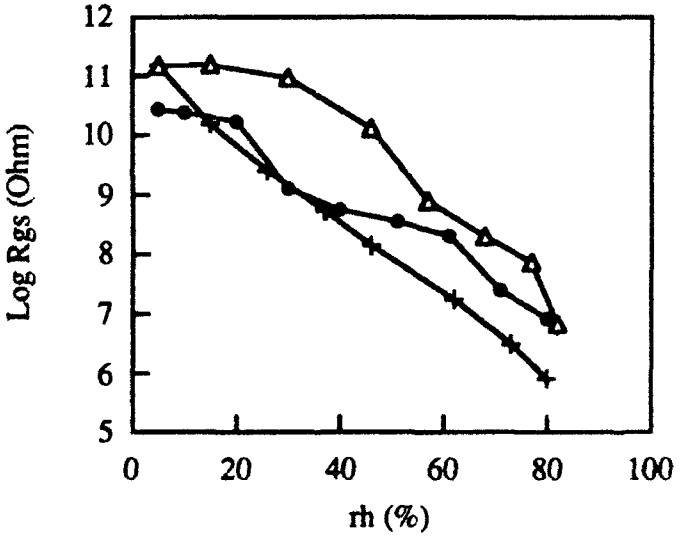

Fig. 1 - The rh-dependence of Rgs for specimens A (+), B(Δ) and C (•), at 40°C.

To study the dielectric characteristics of $MgAl_2O_4$, we calculated the effect of frequency and rh on relative dielectric dispersion k'(ω), on dielectric absorption k"(ω) and on tangent loss (tgδ) for all the specimens. It was found that at low frequencies k' increases more or less regularly with increasing rh. The higher the frequency, the steeper the rise of k' with rh. k' is pratically constant over the entire rh range for frequency values higher than about 1 kHz (fig. 2).

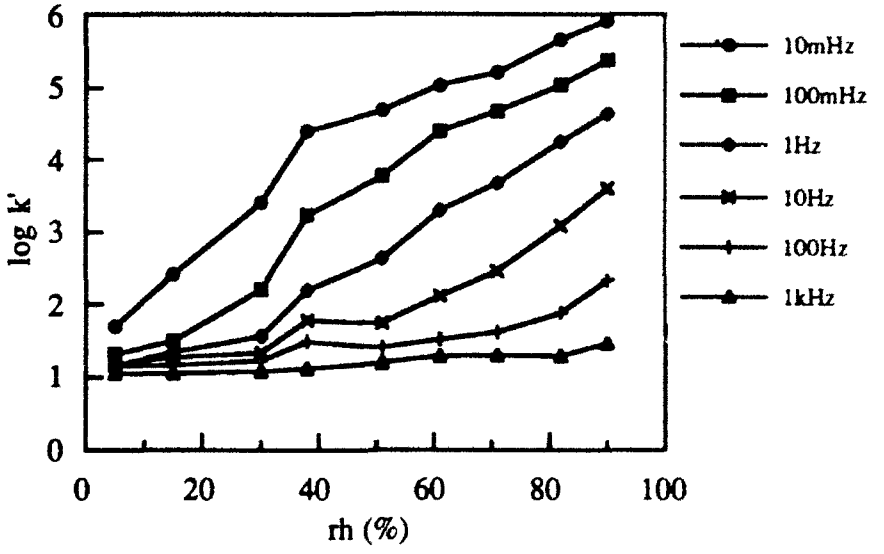

Fig. 2 - Effect of frequency and rh on the relative dielectric dispersion k'(ω) of pellet A.

The electrical behaviour of the specimens was found to be related to their microstructures. Specimen A has a wide pore size distribution and its resistance versus rh sensitivy is about 5 orders of magnitude in the rh range tested. Specimen B, which has a narrow pore size distribution [2], shows a sensitivity 1 order of magnitude lower than that of specimen A. This can be explained in terms of the contribution of water condensed in capillary pores to total conduction, which for specimen A is distributed over a wider rh range. This is confirmed by the analysis of the dielectric behaviour of the specimens: the increase in k' with rh and frequency is much more uniform for specimen A than for specimen B, because of more uniform capillary condensation in its pores. Specimen C does not possess capillary porosity and its sensitivity is only 3 orders of magnitude.

REFERENCES

1. T. Seiyama, N. Yamazoe and H. Arai, *Sens. Actuators* **4**, 85 (1983).
2. G. Gusmano, G. Montesperelli, P. Nunziante and E. Traversa, in *Ceramic Transactions, Vol. 22: Ceramic Powder Science IV*, Ed. by S.i. Hirano, G.L.Messing and H. Hausner, p. 545. The Am. Ceram. Soc., Westerville, Ohio, USA (1991).
3. G. Gusmano, G. Montesperelli, E. Traversa, A. Bearzotti, G. Petrocco, A. D'Amico and C. Di Natale, *Sens. Actuators B* **7**, 460 (1992).
4. Y. C. Yeh, T. Y. Tseng and D. A. Chang, *J. Am. Ceram. Soc.* **73**, 1992 (1990).

Impedance Spectroscopy Under Steady-State Currents of Plasticized PVC Membranes Containing Valinomycin and Mobile Sites

Tal M. Nahir and Richard P. Buck
Department of Chemistry, University of North Carolina
Chapel Hill, NC 27599-3290

Most Carrier-type ion-selective membranes contain additional lipophilic anionic negative sites [1]. A common potassium-selective membrane, for example, has four major active components: valinomycin (val), Kval$^+$ complex, tetraphenylborate (TPB$^-$) or equivalent anion, and KvalTPB ion pair. Typically, these are incorporated in an inert matrix such as plasticized PVC membranes [2].

Upon application of an external voltage across the membrane, a significant concentration polarization of many of the species may take place, depending on the amount of constituents and coupling. In this work, two extreme circumstances are isolated:

a. concentration polarization of valinomycin only;

b. concentration polarization of the ionic species (Kval$^+$, TPB$^-$ and, therefore, KvalTPB) only.

The steady-state current-voltage plots show limiting currents in both instances (Figure 1).

In the first case, the membrane is made with a large amount of TPB$^-$ species. Upon the application of external potential steps, only the valinomycin concentration profiles are significantly perturbed, in a similar way to what was shown for the fixed-site membranes [3]. Examination of impedance spectra reveals a gradual increase in the length of the 45°-angle Warburg lines (in impedance plane plots) at steady-state at higher applied voltages (Figure 2). This result can be related to the decrease of valinomycin at the interface where K^+ enters the membrane.

In the second type of system, the current is limited by the ionic species in a manner described by Sandblom *et al* [4]. As a result of polarization of ionic species, the bulk membrane resistance increases as the applied potentials increase (Figure 3). The concentration of valinomycin is large, and no significant changes in the Warburg impedance can be noticed throughout the experiment.

REFERENCES

1. R. Eugster, P. M. Gehrig, W. E. Morf, U. E. Spichiger and W. Simon, *Anal. Chem.* **63,** 2285 (1991).
2. R. D. Armstrong and G. Horvai, *Electrochim. Acta* **35,** 1 (1990).
3. M. L. Iglehart, R. P. Buck and E. Pungor, *Anal. Chem.* **60,** 290 (1988).
4. J. Sandblom, G. Eisenman and J. L. Walker, Jr., *J. Phys. Chem.* **71,** 3871 (1967).

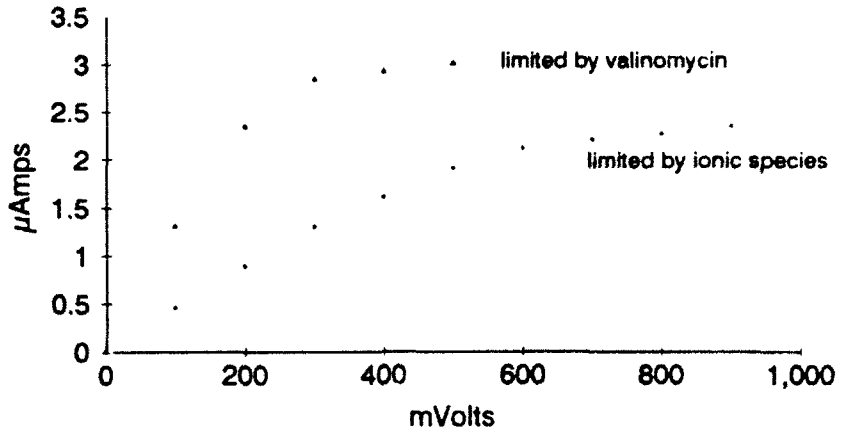

Figure 1. Steady-state current-voltage curves in two membranes, each exhibiting a limiting current.

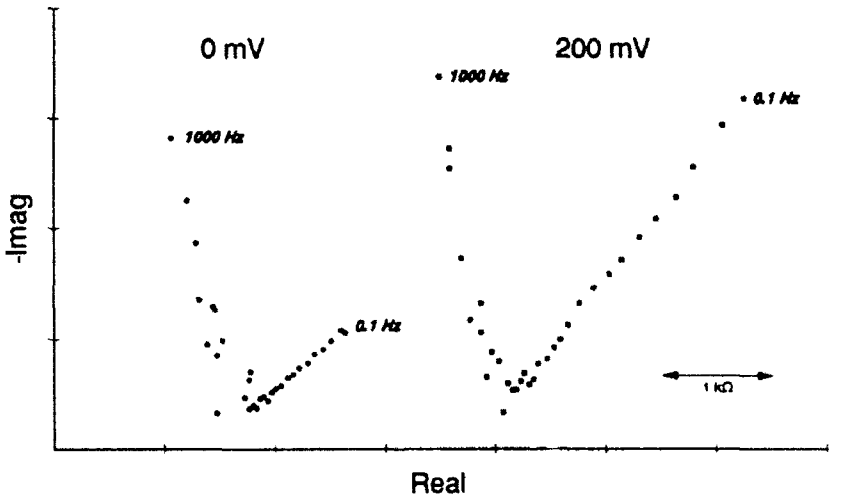

Figure 2. Changes in Warburg impedance in valinomycin-limited steady-state i-V.

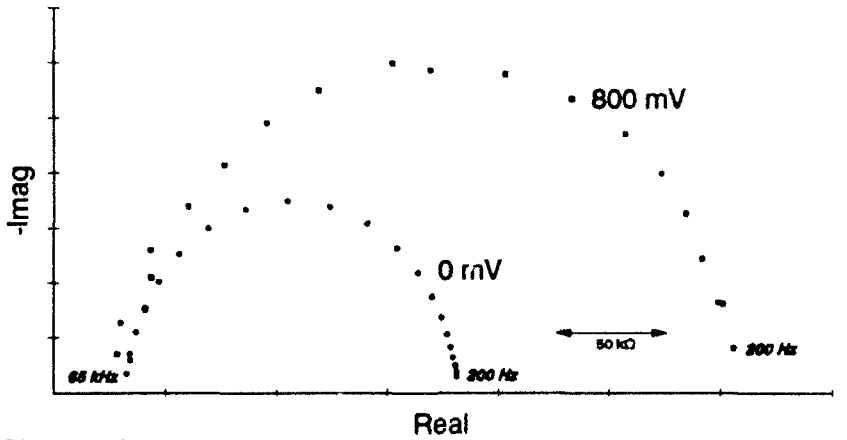

Figure 3. Changes in bulk resistance in ionic-species-limited steady-state i-V.

CALCULATION OF IMPEDANCE SPECTRA BY LAPLACE TRANSFORMATION OF VOLTAGE TRANSIENTS GENERATED BY CURRENT STEP EXCITATION

Michael Neumann-Spallart[$] and Mohamed Etman[@]
C.N.R.S., 1, place Aristide Briand, F-92195 Meudon, France
$ Laboratoire de Physique des Solides
@ Laboratoire d'Electrochimie Interfaciale

Impedence data over a broad frequency range are obtained by converting the transient voltage response of a passive network on current step excitation into the frequency domain using Laplace transformation. The merits and limitations of the method and the quality and type of the required data are discussed and examples of impedance plots obtained with this method are given. Impedance spectra are of great importance for the analysis of electrochemical interfaces and cells. Transient perturbations (single potential or current steps) allow to probe the system during a very short period of time (which is particularly important for rapidly evolving systems). The response contains all the information needed for the calculation of the impedance (Z) of the system over the whole frequency range.

Here, we describe the calculation of impedance spectra from voltage transients generated by current step excitation. The advantage of the current step method is the accessibility of the high frequency range, since fast potential control is not necessary, but on the contrary must be suppressed by deliberately slowing down the response of a potentiostat connected to the circuit [1c]. On the other hand, in the low frequency range (< 1 Hz for a reasonable damping of the potentiostat response) potential control would set in and thus precludes the use of data in the corresponding time domain. This method is therefore complementary to the more frequently used voltage step method.

For most test circuits so far investigated with the present setup, a good quality of the obtained Nyquist and Bode plots was found, agreeing well with the theoretical curves. In general, a higher (> 1 ksamples) memory dephth is desirable. Presently, experiments are carried out in order to evaluate the complex impedance of electrochemical circuits and to compare these results with results obtained by conventional methods of impedance measurement.

AC IMPEDANCE ANALYSIS FOR ATMOSPHERIC CORROSION

Atsushi NISHIKATA and Tooru TSURU
Department of Metallurgical Engineering
Tokyo Institute of Technology
2-12-1, O-okayama, Meguro-ku, Japan

AC impedance technique has been applied to the corrosion monitoring of metals in wet/dry cycle condition. As atmospheric corrosion proceeds under extremely thin, often invisible, electrolyte layers, application of electrochemical techniques to the monitoring of corrosion rates is quite difficult. Because a solution resistance becomes an extremely high value when the electrolyte layer is very thin. In such a condition, the current and potential are not evenly distributed on a working electrode when a small perturbation (voltage or current) is applied.

In outdoor corrosion, electrochemical monitoring has been carried out mainly by a measurement of time-of wetness with a galvanic couple because the galvanic current is easily measured. Such data give an information on changes in environmental condition, but the determination of the correct corrosion rates from them is impossible. The first aim of this study is monitoring of the corrosion rates of copper and carbon steel during alternating wet and dry cycles using as impedance technique. Then, the current distribution on the electrode used in this study is calculated using one dimensional distributed constant equivalent circuit, and the validity of the data obtained by AC impedance technique and a limitation of monitoring is discussed.

Two electrode cell arrangement was used for impedance measurements. Two copper electrodes(10mm long, 0.1mm wide) were embedded 0.1mm apart in parallel in epoxy resign. The carbon steel electrodes also was prepared as specimen. The wet/dry cycles were automatically conducted by exposure to alternate conditions of 1hr.-immersion in a solution and 5hr.-drying at 25C and 60%RH in chamber. The solutions of 1mM Na_2SO_4 and 1mM NaCl were used for copper. Carbon steel was wetted in 0.5M NaCl solution. The instantaneous corrosion rate and solution resistance of thin electrolyte layers were monitored in wet/dry cycle condition by the continuous measurements of the impedance at 10mHz and 100kHz respectively, using a frequency response analyzer and a potentiostat.

Copper in wet/dry cycle condition shows a large increase in corrosion rates, immediately before drying out of the surface. This indicates that oxygen reduction, which is usually controlled by the rate of O_2 transport through thin electrolyte layers, is accelerated because the electrolyte layer becomes very thin. However, further decrease in the thickness of electrolyte film decreases the corrosion rates probably because the anodic dissolution rate is inhibited, where the surface almost dries out and no continuous electrolyte films exist. The corrosion of copper is slightly accelerated by wet/dry cycle. Carbon steel also shows similar corrosion behaviors in each cycle to that of copper, but it is strongly accelerated by wet/dry cycle. The current distribution on the electrode is calculated using a transmission-line model, and a limitation of monitoring is discussed.

"EIS Characterization of Candidate Coating Materials for Aerospace Applications"

H. L. Novak
USBI Company
P.O. Box 21212
Kennedy Space Center, FL 32815

J. F. McIntyre and L. Hang
Florida Atlantic University
Department of Ocean Engineering
Boca Raton, FL 33431

A study was initiated to evaluate environmentally compliant replacement coatings for use in various aerospace programs. Although coatings that employ chromate primers and conversion coatings work effectively, the Clean Air Act Amendments of 1990 and pending changes in the Clean Water Act make it imperative that alternative coating systems be developed and evaluated. An integral part of this investigation involved the use of Electrochemical Impedance Spectroscopy (EIS) to provide screening of candidate coating systems. Mendreck, et al., successfully used EIS to study the corrosion protection of conventional aerospace coating systems applied to AISI 4130-steel substrates.[1] Work reported on herein is a natural extension of this earlier study.

Ion vapor deposited aluminum (IVD/Al) was identified as a probable replacement for chromate primers, a description of the IVD coating process is provided elsewhere.[2] The objective of this work was to establish the effectiveness of IVD/Al as a primer coating. Coated AISI 4340-steel and AA2219 panels (10.16 cm X 15.24 cm X 0.32 cm) were prepared with and without an IVD/Al (MIL-C-83488C, Class I, Type II) basecoat with 76μm polyurethane topcoats. In addition, several steel substrates were coated with a conventional system consisting of a 44 μm organic zinc primer and a 76 μm epoxy-polyamide topcoat. Coated panels were exposed to three environments, including: constant immersion in quiescent seawater; constant immersion in aerated seawater; and, exposure to a marine coastal environment with periodic seawater wetdown. Specimens were exposed in the as received condition or mechanically damaged by scribing an "X" through the coating to expose bare metal. Coated specimens were evaluated using EIS and by employing ASTM D610 and ASTM D714 visual standards. EIS measurements were made using a Solartron 1260 Gain Phase Analyzer interfaced to an EG&G PARC 273A potentiostat; the system was computer interfaced for scanning and data manipulation. A three-electrode cell configuration was employed, where a glass cell was clamped onto the painted panel exposing a surface area of 24.6 cm^2. Impedance scans were conducted between 10 mHz and 65 kHz.

Preliminary results indicated that IVD/Al afforded significant additional protection for the AA2219 substrate in comparison to specimens receiving only a chromate conversion pretreatment prior to application of the polyurethane topcoat. Coating performance has been correlated by others to changes in coating capacitance, C_c, and the ionic pore resistance, R_{po}, of the coating as a function of time.[3,4] As a coating absorbs water the C_c increases because of an increase in the dielectric constant of the coating; therefore, the magnitude of ΔC_c as a function of time is a qualitative measure of water uptake. A large water uptake is often an indication that the coating is porous; hence, the probability for early deterioration is high. However, a better predictor of coating performance is the change in R_{po} with time: a decrease to values below about $10^6\ \Omega \cdot cm^2$ is generally indicative of impending poor performance. Inspection of Figure 1 shows that for IVD/Al coated AA2219 with polyurethane topcoat #1 exposed to aerated seawater, R_{po} remained around $10^6\ \Omega \cdot cm^2$, which indicated that good protection was afforded. ASTM D610 and D714 ratings were 10 and #8 blisters (10 corresponds to the smallest blisters visible with an unaided eye), medium density (located only along edges where the topcoating is thin), respectively. In addition, no undercutting or blistering near the scribe defect was observed. On the other hand, in the absence of an IVD/Al basecoat R_{po} decreased to around $4 \times 10^4\ \Omega \cdot cm^2$, which indicated poor performance. Although

this coating had an ASTM D610 rating of 10, a significant number of large blisters (ASTM D714 #2 blisters, moderate density) were present. Decrease in R_{po} occurred prior to formation of visible blisters. These blisters contained voluminous "reddish" corrosion products surrounded by an area of high pH. Results summarized in Figure 1 also revealed that aerated seawater was more severe than quiescent seawater. EIS data for polyurethane topcoat #6 indicated that performance would be poor in comparison to topcoat #1; this was confirmed by visual observations of specimens exposed to various environments.

Mixed results for coated steel substrates were obtained as indicated by the EIS data given Figure 2. In general, the polyurethane topcoat #6 performed better under all exposure conditions as reflected by ASTM D610 ratings of 10 and the presence of fewer blisters than for topcoat #1. Although an IVD/Al coated steel specimen with polyurethane #6 topcoat exposed to aerated seawater gave low R_{po} values compared to a specimen with topcoat #1, the polyurethane #6 resisted blistering near the scribed defect whereas the polyurethane #1 topcoated specimen showed blistering in this area. However, the IVD/Al basecoat provided adequate sacrificial protection for specimens coated with either the #1 or #6 polyurethane. Conversely, specimens without the IVD/Al basecoat showed early signs of deterioration as noted by rusting in the scribe and the formation and growth of cathodic blisters adjacent to the scribe. In addition, the R_{po} values were lower in aerated than in quiescent environments and ΔC_c were values greatest in the absence of an IVD/Al basecoat. The IVD/Al-Polyurethane system provided better protection than the conventional organic zinc primer/epoxy-polyamide system. For coated specimens with intentional defects exposed to a natural marine coastal environment, the conventional organic zinc primer afforded only minimal protection to the bare steel, while the IVD/Al basecoat provided excellent sacrificial protection with no signs of rusting in the scribe. In general, EIS results for specimens exposed to quiescent seawater showed better performance for the IVD/Al-polyurethane system in comparison to the organic zinc-epoxy-polyamide system.

[1] M. Mendreck, R. Higgins and M. Danford, NASA Tech. Paper 28-20, May 1988.
[2] D. Muehlberger and J. Reilly, Proc. 19th An. Airline Plat & Metal Finishing Forum, p. 127, 1985.
[3] F. Mansfeld, et al., Corr., Vol. 38, No. 9, p. 478, 1982.
[4] M. Kendig and J. Scully, CORROSION/89, Paper #32, NACE:Houston, 1989.

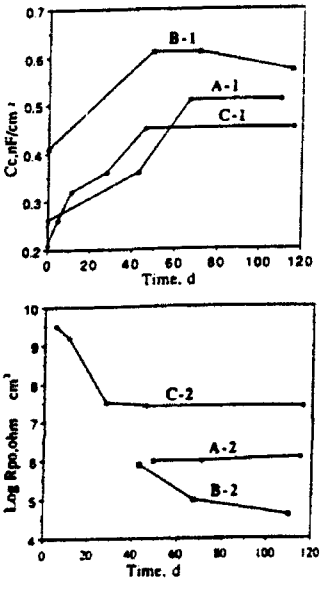

Fig. 1 - R_{po}, C_c Plots for Coated AA2219 Exposed to Seawater. IVD/Al + Polyurethane #1, aerated, A1 & A2; Polyurethane #1, aerated, B1 & B2; IVD/Al + Polyurethane #1, quiescent, C1 & C2.

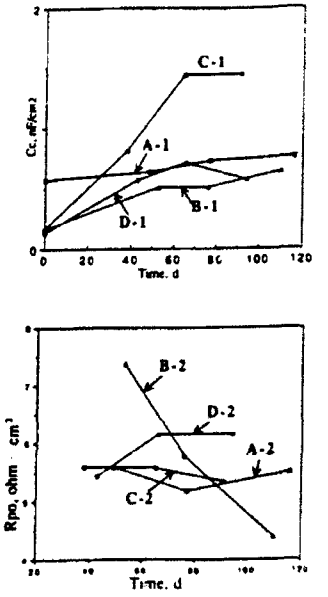

Fig. 2 - R_{po}, C_c Plots for Coated St-4340 Exposed to Aerated Seawater. Polyurethane #6, A1 & A2; IVD/Al+ Polyurethane #6, B1 & B2; Polyurethane #1, C1 & C2; IVD/Al + Polyurethane #1, D1 & D2.

ELECTROCHEMICAL IMPEDANCE IN ELECTROLESS PLATING

Izumi Ohno* and Shiro Haruyama
Tokyo National College of Technology
1220-2, Kunugida, Hachioji, Tokyo 193, Japan
* Tokyo Institute of Technology
2-12-1, O-okayama, Meguro-ku, Tokyo 152, Japan

Electroless plating proceeds spontaneously along the electrochemical mechanism as a simultaneous reaction of two partial reactions: cathodic metal deposition and anodic oxidation of reductant. Therefore, the electrochemical impedance for electroless plating is a parallel combination of the two partial impedances corresponding the respective partial reactions at the mixed potential, as similar to that for metallic corrosion.

The electrochemical impedance for electroless plating has been studied on the basis of computer simulation, using the cupric sulfate-formaldehyde-EDTA·2Na bath as an example.

The cathodic deposition of copper in this bath is very rapid and exhibits a limiting current which is controlled by the diffusion of a copper complex ion. The Warburg impedance during a stationary polarization is written as

$$G_f^W(j\omega) = \frac{1}{(1-\alpha)n^2F^2C\sqrt{j\omega D}} \tanh\left(\delta\sqrt{\frac{j\omega}{D}}\right) \qquad (1)$$

where δ indicates the thickness of the Nernst diffusion layer and D and C are the diffusion coefficient and the surface concentration of the reactant respctively. According to the Nernst layer model,

$$C = \frac{C_o(i_{lim}-1)}{i_{lim}} \qquad (2)$$

where i_{lim} and C^o are the limiting current and bulk concentration of the reactant respectively.

The anodic oxidation of the reductant is controlled by an interfacial activation process. The reaction is very complicated, consisted of several steps which involve some adsorbed intermediates. The impedance for the anodic oxidation of the reductant has been discussed elsewhere[1]. Because the time constant for the adsorption/desorption is usually small, the partial impedance for the anodic oxidation can be assumed to be of transfer reaction at the mixed potential.

The electrochemical impedance for electroless copper plating has been discussed as the parallel combination of the two partial impedances.

[1] S. Haruyama and I. Ohno, Proc. of the Symposium on Electroless Deposition of Metals and Alloys, Proceedings Volume 88-12, The Electrochemical Society, (1988) p.20.

was suggested by the high C_L values.

In such systems described above, we can effectively use an ac impedance analysis to evaluate the basically electrochemical film properties, and the Li/polymer battery performances reflect their basic film properties estimated with an impedance analysis.

PAn/PPy dual-layer

PAn/PPy dual-layer was obtained by electropolymerization of aniline onto the electrode pre-coated with PPy. The dual-layer showed good mechanical strength as a free-standing film peeled off from the substrate. The cathode performances of the film were influenced by the properties of PPy under-layer. The properties of electropolymerized PPy films were significantly affected by the polymerizing conditions(5). Onto two types of PPy films, which were tight film and rough film, PAn was polymerized to investigate the influences of under-layer on the properties of the PAn/PPy dual-layer(6). The impedance responses of dual-layers were measured as a function of upper-layer thickness on the two type under-layers. In the case of thin PAn upper-layer, the activity of doping-undoping reaction and the diffusion of the dopant anion are affected by under-layer PPy activity, while in the case of thicker PAn upper-layer, those of two dual-layers becomes quite the same. So increasing the polymerization charges of upper-layer, the differences between the dual-layers with tight and with rough under-layers disappear. From these results, it is suggested that the cell performances using the dual-layers become almost the same when the PAn upper-layer becomes thicker even using the PPy under-layer of different activity.

However, the results of cell performance assembled with those dual-layers became quite different from this expectation. The charging-discharging efficiency of dual-layer using the tight PPy under-layer was deduced significantly at high current density and/or at large charging depth even using the very thicker PAn upper-layer(6). This disagreements between the cell performance and the impedance results, can be explained as follows; the ac impedance results reflect only the thinner part of the polymer near electrolyte interface, on the contrary the charging-discharging performances of the cell is governed by the all part of the cathode. In such a case of this dual-layer film system, an ac impedance analysis sometimes has a limitation to predict the cell performance as mentioned above.

By using ac impedance method, electrochemical properties of polymer cathodes are able to be evaluated, and the battery performances usually correspond to the electrochemically basic evaluation of cathode film by an ac impedance method, however, sometimes the battery performances can not be judged only by the ac impedance method, when the cathode film electrode becomes thicker and is composed of dual-layer.

References

1) T. Osaka, S. Ogano, K. Naoi and N. Oyama, *J. Electrochem. Soc.*, 136, 306 (1989).
2) T. Osaka, T. Nakajima, K. Naoi and B. B. Owens, *ibid.*, 137, 2139 (1990).
3) T. Osaka, T. Nakajima, K. Shiota and T. Momma, *ibid.*, 138, 2853 (1991).
4) K. Naoi, K. Ueyama, T. Osaka and W. H. Smyrl, *ibid.*, 137, 494(1990).
5) T. Osaka, K. Naoi and S. Ogano, *ibid.*, 135, 1071(1988).
6) T. Osaka, K. Shiota, T. Momma and S. Nakamura, *Abst. of ISE 42nd Meeting*, 3-52(1991).

Impedance Analysis of Electropolymerized Conducting Polymers for Polymer Battery Cathodes

Tetsuya Osaka and Toshiyuki Momma
Department of Applied Chemistry,
School of Science and Engineering, Waseda University,
3-4-1 Okubo, Shinjuku-ku, Tokyo 169, JAPAN

In recent years, the requirement of high power density battery becomes greater with the acceleration of the electronic device performances, and electropolymerized conducting polymers have been regarded to one of the promising candidates as a rechargeable lithium battery cathode. And the electrochemical characteristics of the cathode greatly affect the cell performances. Here, we introduce ac impedance investigations of the electrochemical properties of conducting polymers for the purpose to examine the correlation between the lithium/polymer battery performances and the electrochemical properties by ac analysis.

PAn films polymerized from organic solvents

In our previous work(1,2), the PAn film deposited from a nonaqueous solution with an organic acid, such as propylene carbonate (PC) solution containing CF_3COOH, showed good electrochemical properties. We have already found that the properties of the PAn films deposited from organic solutions are much influenced by the polymerizing conditions(1-3). We also investigated the electrochemical properties of the PAn films electrodeposited from various organic solutions, such as mixed solvents of PC blended with ethylene carbonate (EC), which has a high permittivity, or 1,2-dimethoxyethane (DME), which has a low viscosity(3), and the electrochemical activities were compared in the $LiClO_4$/PC electrolyte solution by ac impedance measurements. The charge transfer resistances of PAn films deposited from the PC-EC solution is smaller than those from the other two cases. The order of the diffusion resistance becomes PC-EC > PC > PC-DME(3). Then, the PAn film formed from PC-EC solution has the highest activity for doping-undoping ion reaction and the fastest rate for ion diffusion process in the film.

We assembled Li/PAn cells using PAn films deposited from various organic solutions and examined the cell performances, and the results exactly corresponded to the impedance results, namely, the battery using PAn deposited from the PC-EC solution gives better power performance.

PPy/PAz copolymer

PAz and PPy can be copolymerized from the solution containing both of pyrrole monomer and azulene monomer(4). In our research about the PPy/PAz copolymer films, it is cleared from the elemental analysis of the composite films that the ratios of the monomeric units in the films are exactly the same as the monomer ratios of the polymerization solutions(4). The values of D and C_L, which is diffusion coefficient and low frequency capacitance respectively, of the films estimated from the impedance results. The D value increases largely in the films of monomeric ratio above 25 Az%, while the C_L value increases in the films of monomeric ratio above 50 Az%. The cell performances of lithium/copolymer batteries exactly corresponded to the electrochemical characteristics of the films obtained from the impedance measurements. The cell using the films of monomeric ratio above 25 Az% showed faster charge or discharge with high current density owing to the fast diffusion of dopant ion in the films, and the cell with the film of monomeric ratio above 50 Az% gave larger battery capacity, as

DEVELOPMENT OF PHYSICO-CHEMICAL MODELS FOR ELECTROCHEMICAL IMPEDANCE SPECTROSCOPY

Mark E. Orazem
Department of Chemical Engineering
University of Florida
Gainesville, Florida 32611-2021

While impedance spectroscopy has become a powerful tool for investigating the properties of electronic materials and electrochemical systems, identification of appropriate models for interpretation of impedance spectra remains a critical issue. The objective of this presentation is to present tools that can be used to guide selection of an appropriate model. The approach is illustrated by development and application of detailed physico-electrochemical model for the impedance response of a number of electrochemical and electronic systems.

In this work, models are classified as being one of two types. **Process models** are used to predict the response of a system from physical phenomena hypothesized to be important. Regression of process models to data allows identification of physical parameters based upon the original hypothesis. In contrast, **measurement models** are built by sequential regression of line shapes to the data. The model can be used to identify characteristics of the data set that could facilitate selection of an appropriate process model. The measurement model can be used, for example, to determine whether a given data set is consistent with the Kramers-Kronig relations. A system with data that are consistent with the Kramers-Kronig relations can be considered to have been stationary during the course of the experiment. If the system were to have changed significantly during the time in which data were collected, non-stationary behavior would need to be incorporated into the process model. Other characteristics of impedance data (such as the number of time constants evident in the spectrum, the frequency-dependent error structure, and sensitivity to system parameters) can be determined through use of measurement models.

Process models for electrochemical systems are obtained by solving the coupled equations describing the physics and chemistry assumed to govern the system. For example, the impedance response associated with deep-level states in semiconductors can be modeled by equations that account for diffusion and migration of electrons and holes, charging of the space charge region, and electronic transitions between energy levels within the semiconductor. A model for the impedance response of electrochemical reactions on metal hydrides incorporates diffusion of hydrogen into the metal. A model for the impedance response of copper in alkaline chloride environments includes convective diffusion of species that engage in homogeneous and heterogeneous reactions. The influence of film growth is also treated. The coupled (often non-linear) equations derived for a given system generally require numerical solution. The equations are first solved under a pseudo-steady-state assumption using iterative techniques to account for non-linear terms.

The equations are then linearized about the steady state solution and the sinusoidal steady state solution is obtained.

The approach taken here involves a considerable degree of interaction between collection of data, application of measurement models as a data screening, and development of physico-chemical process models. Measurement models are used to determine whether data are consistent with the Kramers-Kronig relations. If inconsistency is attributed to non-stationary behavior, the experimental parameters are changed to reduce the experimental time required to collect data. Inconsistency attributed to nonlinear instrumental artifacts or excessive errors may suggest changes in instrumental parameters. The measurement model can be used to check whether data obtained for different operating conditions are replicate. Subtle influences of parameters can be identified in this way, and experiments can be redesigned to enhance sensitivity. The results of the measurement model are then used to guide development of process models.

Physical parameters can be obtained from impedance data through regression of appropriate process models. Process models can be developed by solving the algebraic and differential equations derived from physical and chemical phenomena that govern the system. Development of such process models is fascilitated by use of measurement models as an intermediate step in the development. The measurement model may suggest changes in the experimental design and can guide development of models.

AC-IMPEDANCE STUDY OF THE OXYGEN REDUCTION MECHANISM ON $La_{1-x}Sr_xMnO_3$ IN SOLID OXIDE FUEL CELLS

M.J.L.Østergård & M. Mogensen
Risø National Laboratory
Materials Department, P.O. Box 49
DK-4000 Roskilde, Denmark

Extended Abstract

The performance of the cathode material in a Solid Oxide Fuel Cell (SOFC) is very important since the cell efficiency is to a great extent controlled by the cathodic process. $La_{1-x}Sr_xMnO_3$ (LSM) is considered as one of the most promising cathode materials for SOFC due to its good chemical and thermal compatibility with the electrolyte (Yttria-Stabilized Zirconia, YSZ) and its catalytic activity for the reduction of oxygen.

Although several kinetic studies /1-4/ on the oxygen reduction mechanism on LSM cathodes have been reported, it is still uncertain, how the electrode reaction proceeds.

Electrochemical impedance spectroscopy (EIS) has been used in this work to study the influence of temperature and oxygen partial pressure on the oxygen reduction mechanism on LSM as a cathode material. DC-measurements, cyclic voltammetry and chronoamperometry, have been performed as a supplement to the EIS. The objective of this work is to obtain a better understanding of the mechanism of oxygen reduction on LSM and through this to be able to optimise the LSM cathode performance.

AC- and DC-electrochemical measurements have been performed on a three-electrode cell where the sample under study was the working electrode and two platinum electrodes were used as counter and reference electrodes. The electrolyte was yttria stabilized zirconia (YSZ, 8 mol %). The cell was placed in a furnace where air passed over the manganite electrode.

Temperatures in the range between 900 and 1000 °C, and oxygen partial pressures from 1 to 0.01 atm have been used. Cyclic voltammetry measurements have been performed in the potential range 0 to -300 mV/air. Chronoamperometric and impedance measurements have been performed at different polarisation values within this potential range.

The results obtained show that the polarisation resistance, R_p, increases with decreasing temperature, decreasing pO_2 and increasing (more negative) cathodic polarisations (Fig.1). The current passing through the cell at stady state (I in Fig. 1) increases with increasing temperature, increasing pO_2 and increasing cathodic polarisations.

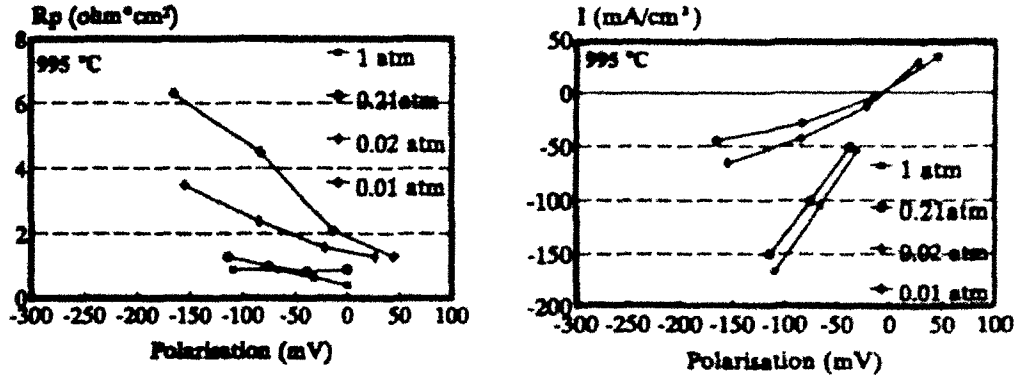

Figure 1: Polarisation resistance and steady state current as a function of pO_2 and polarisation

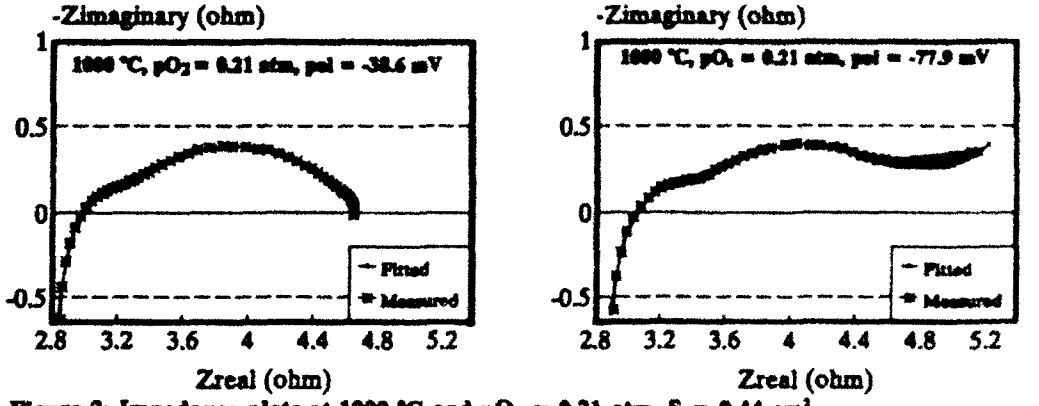

Figure 2: Impedance plots at 1000 °C and pO_2 = 0.21 atm. S = 0.44 cm^2

Curve fitting of the obtained impedance measurements (performed with the computer program "Equivalent Circuit" /5/) has shown that there are three time constants present in the process, each one corresponding to a slow partial reaction step. The two smallest time constants are a function of temperature, partial pressure and polarisation. For all the temperatures and oxygen partial pressures used, diffusion effects have been observed at low frequencies for polarisation values more cathodic than -50 mV/air (Fig.2).

References

/1/ A. Hammouche, E. Siebert, M. Kleitz & A. Hammou. Proc. - Electrochem. Soc., **89-91** (Int. Symp. Solid Oxide Fuel Cells, 1st. 1989), 265-276 (1989)

/2/ J. Mizusaki, H. Tagawa, K. Tsuneyoshi & A. Sawata, J. Electrochem. Soc. **138**, 1867-1873 (1991).

/3/ H.Yanagida, R.J. Brook & F.A. Kröger, J. Electrochem. Soc. **117**, 593-602 (1970)

/4/ E.J.L. Schouler, Solid State Ionics **9 & 10**, 945-952 (1983).

/5/ B.A. Boukamp, Solid State Ionics, **20**, 31-34 (1986).

Acknowledgements

This work has been carried out under the "DK-SOFC" programme sponsored by the Danish Energy Agency (the EFP program, ref. 1443/90-1) and the Danish electric utility groups ELKRAFT & ELSAM.

MICROSCOPIC, SELF-OSCILLATING DOMAINS AT THE SILICON SURFACE DURING ITS ANODIC DISSOLUTION IN A FLUORIDE ELECTROLYTE.

F. Ozanam, N. Blanchard and J.-N. Chazalviel

Laboratoire de Physique de la Matière Condensée,
Ecole Polytechnique, 91128 Palaiseau, France.

The anodic dissolution of silicon in fluoride electrolytes exhibits a *resonant* behavior: for a given potential $V \geq 3V_{SCE}$, a constant current is obtained, but any variation of the electrode potential (even very small) makes the current undergo *damped* oscillations at a frequency T_0^{-1}, with T_0 in the 0.1-1000 s range, depending upon the electrolyte [1]. Correspondingly, the admittance of the interface exhibits resonances at T_0^{-1} *and* its overtones $2T_0^{-1}$, $3T_0^{-1}$... We have elaborated a macroscopic model, based upon the picture of an heterogeneous surface, partitioned into small, independent, self-oscillating domains [2], which is able to account for the experimental impedance diagrams [3]. Noise measurements which give access to the typical size of these domains, are reported here.

Experimental results: In the picture of an interface considered as a collection of self-oscillating domains, but which exhibits a constant steady-state current, the current noise at constant potential is expected to contain the fingerprint of the microscopic oscillation. We have performed noise measurements on a single-crystal p-Si electrode (diameter 0.1 cm, $N_a = 4 \times 10^{15}$ cm^{-3}) sealed in a 2-cm-diameter rotating holder with epoxy resin. The current was amplified and recorded in a 0.5-200 mHz band during a few hours. A special care was taken to reach the steady state before starting the data recording, in order to avoid the presence of any residual damped oscillation resulting from a previous excitation. The noise spectrum, obtained after signal processing, exhibits a maximum at the resonance frequency and at its overtones, just like the impedance spectra (see Fig. 1).

Theory and data analysis: We have modeled the electrical response of an electrochemical interface viewed as a collection of parallel, self-oscillating domains. The current flowing across each domain is supposed to be a periodic succession of non-over-

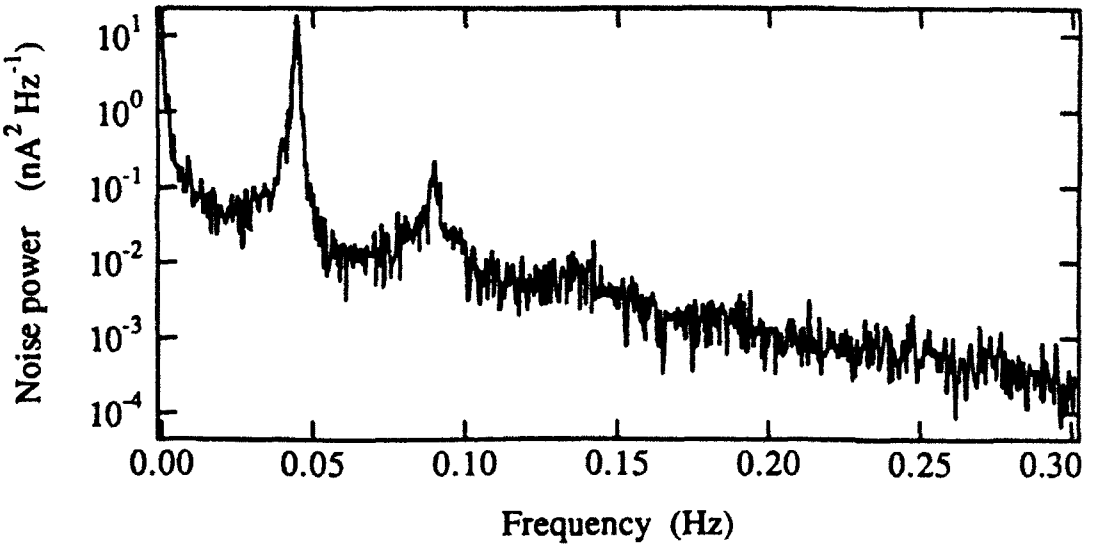

Fig. 1 : Current noise spectrum of a p-Si / 0.025 M HF + 0.025 M NH_4F + 0.95 M NH_4Cl (c_F=0.05 M, pH=3) at V=4 V vs. Ag/AgCl. Notice the presence of peaks at the resonance frequency 0.045 Hz, and at its overtones.

lapping pulses, which is described by its period T_0, by the normalized shape function of the elementary pulse f(t) and by the surface charge density σ corresponding to the current integral over one period. For a constant applied potential V, the domains are uncorrelated, so that, at the macroscopic scale, one observes a stable, average current density $J_0=\sigma/T_0$. Under a small (step or sinewave) potential perturbation, the oscillations of the various domains may be synchronized together, giving rise to a macroscopic current oscillation. A crucial ingredient for allowing both the coming back to the steady state and the existence of a linear response regime is to introduce a source of relaxation in the process. In particular, this may be done by assuming that the pulse succession for each domain is not strictly periodic, but affected by a small "jitter" described by a random function R(t). Then, noting $f(\nu)$ and $R(\nu)$ the Fourier transforms of f(t) and R(t) respectively, the current noise power spectrum is found to be:

$$P_i(\nu) = \frac{S}{N} J_0 S \sigma |f(\nu)|^2 \left[1 - 2\,\mathrm{Re}\left(\frac{1}{1 - e^{j2\pi\nu T_0} R(\nu)^{-1}}\right)\right] \qquad (1)$$

with S the area of the electrode and N the number of microscopic domains. It can be seen that (1) exhibits lorentzian resonances at the fundamental frequency T_0^{-1} and at its overtones. If $f(\nu)$ and $R(\nu)$ are known, one may access the domain area S/N. However, by using impedance data, one can determine S/N independently of $f(\nu)$ and $R(\nu)$, because in our theory, the admittance exhibits lorentzian resonances similar to those of $P_i(\nu)$. Specifically, in the vicinity of a resonance, by noting 1/Z the admittance per unit area and C the specific areal capacitance given by $C=d\sigma/dV$, the domain area comes:

$$\frac{S}{N} \approx -\frac{\pi\nu C}{\mathrm{Im}[1/Z(\nu)]} \frac{P_i(\nu)}{J_0 S \sigma} \qquad (2)$$

Im(1/Z) is a small quantity, except in the near vicinity of resonance. It is more reliably obtained by noting that if $1/Z \approx -A\,(\delta\nu - j/2\pi\tau)^{-1}$, then $\mathrm{Im}(1/Z) \approx -|1/Z|^2\,(2\pi\tau A)^{-1}$. We have then fitted the wings of the fundamental resonance of $P_i(\nu)$ and $|1/Z(\nu)|^2$ with a $1/\delta\nu^2$ lineshape (see Fig. 2); τ is identified to the characteristic damping time of the oscillations triggered by a small potential step (here τ=3000 s). The other parameters are obtained from the impedance data: C=2 mF cm^{-2}, A=3×10^{-6} Ω^{-1} Hz cm^{-2}, T_0=22 s, and J_0=0.5 mA cm^{-2}. One finally obtains for the data presented here S/N=6×10^{-12} cm^2, hence a typical domain size of about 300 Å.

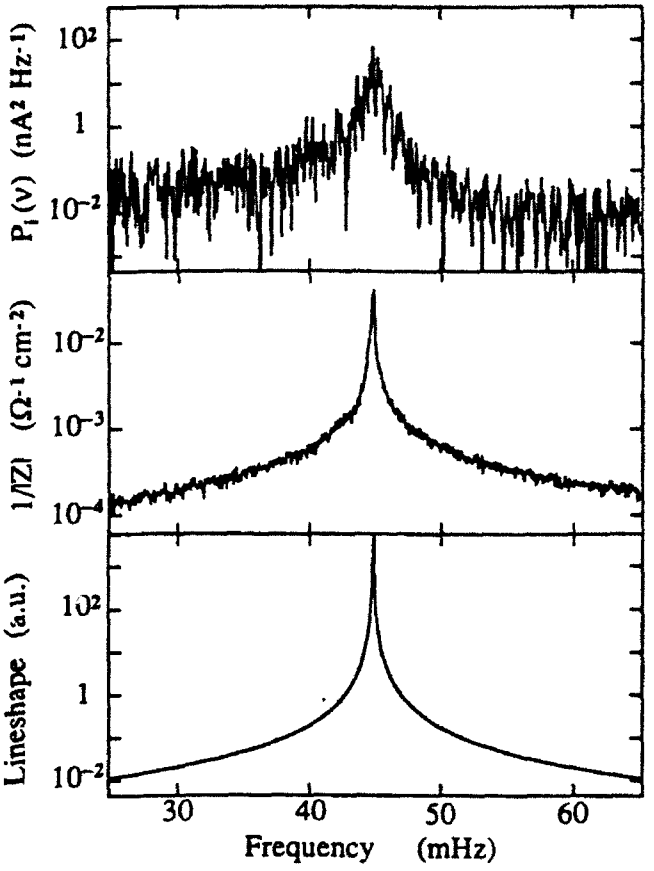

Fig. 2 : Fit of noise and admittance resonances with lorentzian lineshapes (same system as in Fig. 1).

[1] F. Ozanam, J.-N. Chazalviel, A. Radi and M. Etman, *Ber. Bunsenges. Phys. Chem.*, **95**, 98 (1991).

[2] J.-N. Chazalviel and F. Ozanam, *J. Electrochem. Soc.* (in press).

[3] F. Ozanam, J.-N. Chazalviel, A. Radi and M. Etman, *J. Electrochem. Soc.* (in press).

IMPEDANCE STUDY ON TITANIUM NITRIDE COATINGS

J. Piippo, B. Elsener, H. Böhni
Swiss Federal Institute of Technology
Institute of Materials Chemistry and Corrosion
ETH-Hönggerberg, CH-8093 Zürich, Switzerland

Titanium nitride (TiN) coatings produced by chemical (CVD) or physical vapor deposition (PVD) methods are used in order to improve the tribological, optical and chemical properties of substrate material. The corrosion resistance of TiN coated system is determined by the pores that expose the substrate material to the aggressive environment. The corrosion rate in the galvanic couple between the substrate and the noble coating is accelerated by the small anode / cathode area ratio. Various transfer functions based on two parallel connected RC-circuits have been proposed to describe the impedance response of such systems [1-4]. A 3-D physical model taking into account the effects of coating thickness and of specific resistivities of coating and electrolyte is introduced. The model using the transmission line principle simulates the situation of a pore reaching through a coating [5].

The corrosion behavior of 7 μm thick TiN CVD coatings deposited on AISI 316 stainless steel in hydrochloric acid of various concentrations is investigated. The polarization resistance of the coating decreases as the the concentration of hydrochloric acid increases. While TiN remains unattacked in 1M HCl, there is a passive / active transition in 1.5M HCl. When immersed into 2M HCl the system is destroyed because of crevice corrosion. The measured impedance spectra are successfully fitted with the model [5].

In order to study the effect of coating thickness on corrosion resistance the electrochemical behavior of AISI 316 probes deposited with 2.2 μm thick CVD TiN was studied. Both ac and dc methods indicate that thin coatings improve the corrosion resistance of the substrate material, but the better protection is achieved with thicker coating.

The electrochemical behavior of TiN coating on AISI 316 stainless steel can be divided into active and passive behavior according to the state of substrate: when the substrate is passive most of the current flows through the coating and the electrochemical measurements describe mainly the behavior of the coating. When the substrate is active the corrosion potential and the polarization resistance are lower than in the case of passive systems. The impedance measurements are supposed to describe the dissolution of the substrate and the mass transfer through a pore.

The behavior of TiN both on passive stainless steel and on inert Si_3N_4 substrate depends on the pretreatment. After cathodic polarization (15 minutes in -1000 mV) the corrosion potential decreases about 400 mV and the overpotential for hydrogen evolution detected on "as received" samples disappears. XPS measurements indicate that there is an oxide film on TiN that inhibits the hydrogen evolution and that is responsible for the noble electrochemical behavior of TiN.

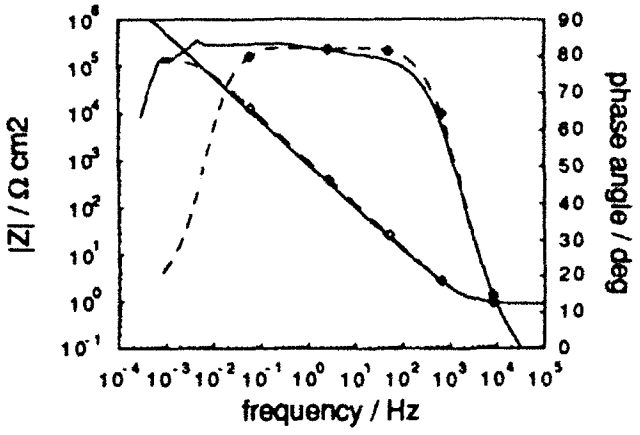

Figure 1. Impedance response of 7 μm thick TiN on AISI 316 in 1.5M HCl. The solid curves describe the passive behavior after the immersion of 4 hours and the broken curves active behavior after 54 hours.

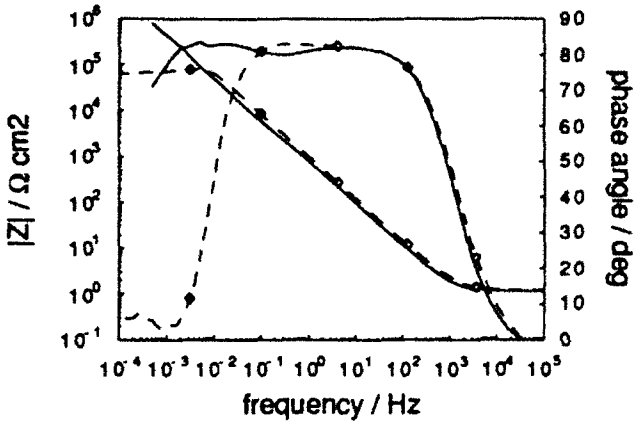

Figure 2. The impedance spectra of 7 μm (solid curves) and of 2.2 μm (broken curves) thick TiN on AISI 316 in 1M HCl.

References

1. B. Elsener, A. Rota and H. Böhni, *Materials Science Forum*, **44&45**, pp. 29-38, (1989)
2. K. Jüttner, *Electrochimica Acta*, **35**, pp. 1501-08, (1990)
3. F. Mansfeld, S. Lin, S. Kim and H. Shih, *Materials Science Forum*, **44&45**, pp. 89-96, (1989)
4. R. Oltra and M. Keddam, *Electrochimica Acta*, **35**, pp. 1619-1629, (1990)
5. J. Piippo, B. Elsener and H. Böhni, Fourth International Symposium on Electrochemical Methods in Corrosion Research, Helsinki, (1991)

CATION MOBILITY IN POLY(ETHYLENE OXIDE) SOLID ELECTROLYTES

M.J.C. Plancha, C.M. Rangel and C.A.C. Sequeira
Laboratório Nacional de Engenharia e Tecnologia Industrial - LNETI
Materials Technology Department
Paço do Lumiar, 22, 1699 Lisboa Codex, Portugal

EXTENDED ABSTRACT

In previous work [1] we reported basic information on the properties of divalent polymer electrolyte films formed by complexes of poly(ethylene oxide), PEO, and nickel chloride, $NiCl_2$ prepared by the casting procedure commonly used for the preparation of PEO-based complexes.

Considering the basic intrinsic interest in these materials and the impact that they may have in the developing electrochemical technology, we have extended their characterization and commenced a parallel study of NiI_2, $ZnCl_2$ and ZnI_2 systems. This paper reports on conductivity and transport number data for $(PEO)_xNiCl_2$, $(PEO)_xNiI_2$, $(PEO)_xZnCl_2$ and $(PEO)_xZnI_2$ films, with x varying between 4 and 24. The measurements were performed using AC impedance spectroscopy.

The electrochemical characteristics were determined by sandwiching the polymer complexes between two cleaned nonblocking Ni or Zn electrodes. The contact area was 6.25 cm^2, except for the $(PEO)_xNiCl_2$ electrolytes which was 1 cm^2. The cell assembly was spring-loaded between acrylic glass plates to maintain good electrical contact. The entire sample holder was kept in a oven, which enabled the control of the temperature in the range 20-200 °C, with a precision of ± 1°C. The AC conductivity was obtained by using a Solartron, model 1250 frequency response analyser, controlled by a model 9000 HP microcomputer. The impedance response was measured in the frequency range 65 KHz-0.01 Hz, and the transport numbers were estimated over the temperature range 20 to 140 °C.

Figure 1 shows typical results of the dependence of the conductivity on temperature for polymer electrolyte with compositions PEO_xNiCl_2 (x=6, 12, 19 and 24), PEO_xNiI_2, PEO_xNiCl_2 electrolytes behaved as almost purely anionic conductors, while PEO_xZnCl_2 and PEO_xZnI_2 have considerable cation mobility, being mixed ionic conductors.

Transport number results for the PEO_xZnI_2 system can be compared with those reported by Yang and Farrington [2] for the same system. Their transport number values, obteined by AC and DC polarization measurements, indicated a negligable cation mobility. However, when they used SEM and EDAX techniques they obtained enhanced transport numbers for Zn^{2+}, at high temperatures.

Findings of Ni^{2+} transport numbers also do not differ too much from those found by Huq and Farrington [3] for the PEO_8NiBr_2 as cast/dried electrolyte.

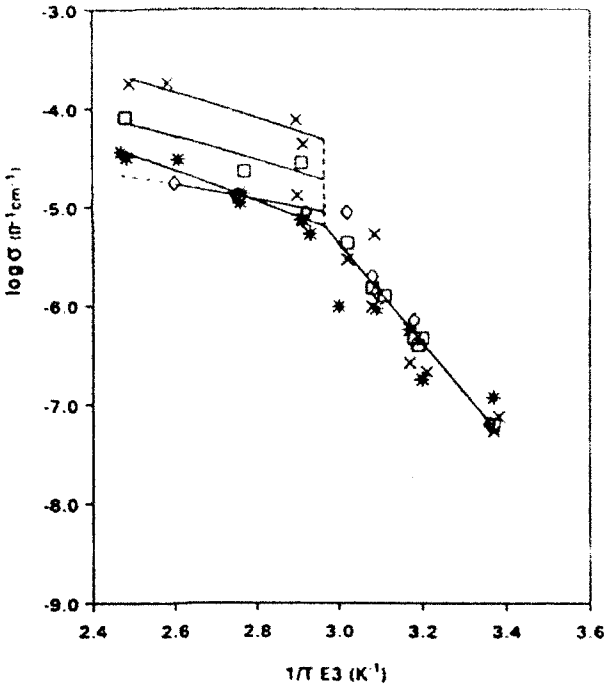

Fig. 1 - Log (conductivity) againts 1/T for films of PEO_xNiCl_2 with x=6 (x), 12 (•), 19 (•) and 24 (*)

ACKNOWLEDGMENTS

M.J.C. Plancha acknowledges a grant within the Ciência Program, Portugal.

REFERENCES

1. M.J.C. Plancha, C.M. Rangel and C.A.C. Sequeira, submitted to Solid State Ionics (1992).

2. H. Yang and G.C. Farrington, Electrochemical Society Meeting, Extended Abstract 728, Chicago (1988).

3. R. Huq and G.C. Farrington, J. Electrochem. Soc., 135, 524 (1988).

A NEW APPROACH TO THE PROBLEM OF "GOOD" AND "BAD" IMPEDANCE DATA IN ELECTROCHEMICAL IMPEDANCE SPECTROSCOPY

G.S.Popkirov and R.N.Schindler

Institut fuer Physikalische Chemie, Universitaet Kiel
Olshausenstr. 40-60, 2300 Kiel, Germany.

Impedance can be defined as transfer function that correlates the response of a system to an input perturbation, if the conditions of linearity, stability, time invariance and causality are obeyed at least during the time of measurement. Unfortunately, it is not always possible to assure the adherence to these conditions. Diagnostic tools for validation of the electrochemical impedance data are needed to make their fitting to a particular mechanistic or equivalent cell model meaningful. It has been shown recently /1/ that the Kramers-Kronig (K-K) integral relationships are applicable to check if experimental impedance spectra are "good" or "bad".

We present an alternative approach to the problem of validation of experimental EIS data. It is based on a comparison of the frequency spectrum of the perturbation voltage and the spectrum of the current response after performing FFT in the time domain technique.

The experimental set-up for EIS measurements consisted of an FFT impedance spectrometer and a fast potentioscat /2/. A sum of 52 sine waves distributed over 4 1/2 decades was used to synthesize the perturbation signal. The impedance of the sample is calculated only for these frequencies that are identified as such from the perturbation signal. If the spectrum of the sample response include not only the frequencies from the perturbation, but also with significant power new frequencies, their origin must be thoroughly analysed. We use just this feature as an indicator for "bad" measurement data.

Polycrystaline Ag- electrodes of 0.38 cm^2 geometrical area were polished to 1 μm and were used as working electrode in 1 M NaOH with a saturated calomel electrode (SCE) as reference. After a two-step oxidation at 0.4 V and 0.6 V for 180 sec each, a cathodic voltage of -1.0 V was applied to reduce the oxide layer back to silver. EIS measurements were carried out at t = 10 s and 300 s after cathodic polarisation. The relative power spectra (RPS) of the perturbation voltage and of the resulting current response are presented in logarithmic scale in Fig.1. The respective impedance spectra are shown on Fig.2 as complex impedance plots.

The existence of new frequencies at t = 10 s with a significant power is obvious, especially in the low-frequency range. This result indicates that the relaxation process of the electrode interphase following the cathodic polarisation was not completed at the time when the first

EIS measurement was started. Thus, the electrode must be classified as being not stationary during the first measurement and impedance spectrum calculated with this input data cannot be valid. The measured response spectrum (Fig.1-b) is a superposition of a response to the perturbation and a response to an additional signal which is attributed to the current decay due to relaxation. This is the reason why the power spectrum of the cell response contains frequencies that are not present in the original perturbation.

New frequencies also appear in the response spectrum of samples if large perturbation signals are used and the condition for linearity is violated. The existence of such new frequencies can be used to indicate, that the cell response was not "pure", and to classify the impedance spectrum as false.

The comparison of the response power spectrum with the perturbation spectrum can be used as a diagnostic tool in the electrochemical impedance spectroscopy if the measurements are made by means of the time domain technique. A number of examples will be presented.

REFERENCES

1. M.Urquidi-Macdonald, S.Real and D.D. Macdonald, Electrochim. Acta 35, 1559-1566, 1990.
2. G.S.Popkirov and R.N.Schindler, in press, Rev.Sci.Instrum. (1992).

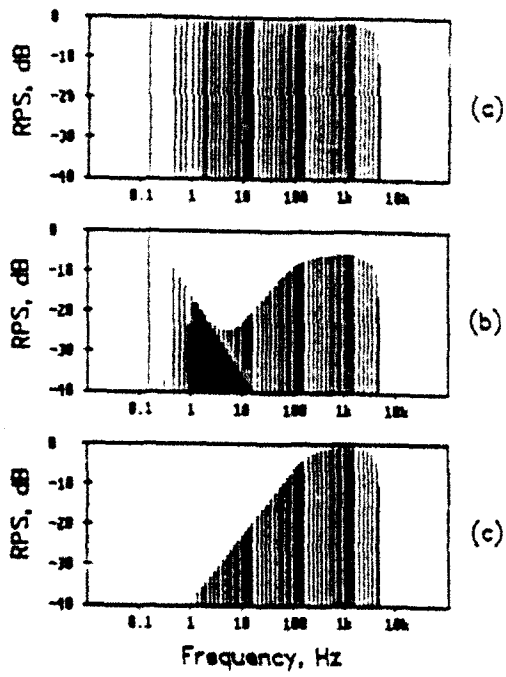

Fig.1 a - perturbation, b,c - response t=10s, t=300s.

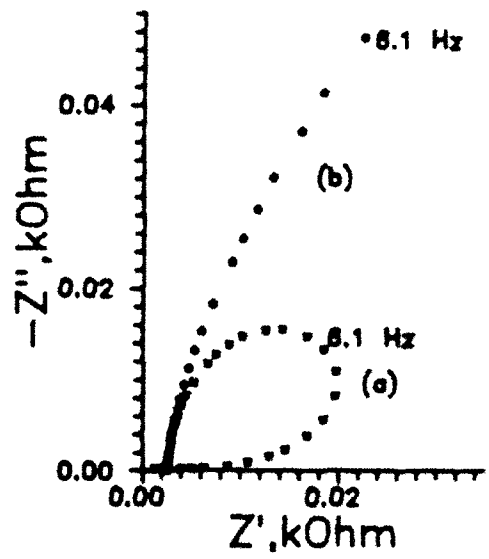

Fig.2 Impedance spectra: a - t=10s, b - t=300s.

THE EFFECT OF SURFACE ROUGHNESS ON THE AC IMPEDANCE OF PALLADIUM IN SULFURIC ACID

B. G. Pound

SRI International
333 Ravenswood Ave
Menlo Park, CA 94025

Introduction

Various preconditioning treatments have been applied to stainless steel pipes to reduce the buildup of activated corrosion products on out-of-core surfaces of nuclear reactors. The present study involved depositing a thin film of palladium onto a stainless steel surface using electroless deposition. In this part of the work, *ac* impedance spectroscopy was used to characterize the electrochemical behavior of palladium foil and palladium-coated AISI 304 stainless steel in deaerated 1 mol l^{-1} H_2SO_4 at the open-circuit potential of each specimen. Impedance spectra for the two materials were compared to determine whether there were any major differences in their frequency response, and more importantly, to demonstrate that the palladium coating can protect the stainless steel substrate in a corrosive environment. It became evident that the interfacial impedance of both specimens was affected by surface roughness, and so the analysis was modified to account for the observed behavior.

Results and Analysis

The surface of the as-received stainless steel specimens was rough, and so the palladium coating exhibited an irregular topography that reflected the contours of the substrate. Nevertheless, Nyquist plots for the palladium foil (mechanically polished with 1000 grit SiC paper) and palladium-plated stainless steel bar were of similar shape, indicating that the plated bar behaves electrochemically as bulk palladium. In both cases, Bode plots of log |Z| as a function of log ω exhibited a single linear region of slope -0.9 over at least four decades of frequency, and the phase angle was typically 77-83° throughout the intermediate frequency range. Further analysis showed that the measured or apparent capacitance (C_a) varied with frequency. Such behavior has been observed in other cases [1, 2] and can be attributed to roughness of the electrode surface [3]. Hence, the frequency response for the two palladium specimens was considered to be indicative of capacitative behavior that is affected by surface roughness.

De Levie [3] has treated the effects of surface roughness on the double layer capacitance (C_d) using a model of grooves. At high frequencies, the apparent admittance can be expressed as

$$Y_a = a\omega^{1/2} + j(\omega C_d + b\omega^{1/2}) \quad (1)$$

whereas at lower frequencies, the apparent parallel capacitance (C_{ap}) due to surface roughness is independent of ω, and Y_a is given by

$$Y_a = a'\omega^n + j\omega C_{ap} \quad (2)$$

where a and b are the high frequency roughness coefficients, and a' is the low frequency roughness coefficient. The value of n determined from the groove model is 2, but previous experimental data indicate that it is more likely to be 1.

For both the palladium foil and plated stainless steel, the real component of the admittance, as predicted, was found to vary linearly with $\omega^{1/2}$ at high frequencies and with ω at low frequencies. The imaginary component also followed a linear dependence on ω at low frequencies but exhibits a more complicated dependence at higher frequencies, as expected from Eq. (1). The agreement between the observed and predicted dependence at both low and high frequencies indicates that the surface roughness model, as represented by Eqs. (1) and (2), is appropriate for the palladium/H_2SO_4 interface under the present test conditions.

The roughness coefficients, a' and a, were determined for both the low and high frequency regions, respectively. The values of the low-frequency coefficient indicated that the effective roughness of the plated stainless steel was higher than that of the foil, as might be expected from the morphology of the palladium deposit. The apparent capacitance also differed considerably for the palladium foil and plated stainless steel, with values of 60 $\mu F\ cm^{-2}$ and 177 $\mu F\ cm^{-2}$, respectively. The higher capacitance for the plated bar is consistent with the higher value of a' for this specimen and reflects its larger real surface area. The differences between the values of C_{ap} and between the low-frequency coefficients supported the incorporation of surface roughness effects to account for the observed deviation from ideal capacitative behavior.

The high-frequency coefficient, unlike its low-frequency counterpart, indicated that the effective surface roughness was similar between the two specimens. This similarity is attributed to a less pronounced difference between surface defects in their contribution to the apparent roughness at high frequencies [3].

Acknowledgements

Financial support of this work by the Electric Power Research Institute under Contract RP2549-10 is gratefully acknowledged.

References

1. B. G. Pound, D. D. Macdonald, and J. W. Tomlinson, *Electrochim. Acta* **27**, 1489 (1982).
2. R. D. Giles, J. A. Harrison, and H. R. Thirsk, *J. Electroanal. Chem.* **22**, 375 (1969).
3. R. de Levie, *Electrochim. Acta* **10**, 113 (1965).

IMPEDANCE ANALYSIS OF LAYERS ON IRON

U.Rammelt, G.Reinhard

Dresden University of Technology, Department of Chemistry, Institute of Physical Chemistry and Electrochemistry,
Mommsenstr. 13, 8027 Dresden, Germany

Surfaces of solid electrodes are usually inhomogeneous in a physical sense because of the presence of geometric effects such as surface roughness. Those geometric effects give a frequency dispersion due to the nonuniform distribution in the current density. Over a fairly wide range of frequencies such effects may be described with the empirical concept of a "Constant Phase Element" (CPE) /1/. This concept has to be extended when adsorption products, oxides or porous conversion layers result in a partially covered electrode surface in a chemical sense.
Transport phenomena of electroactive species to and from a metallic surface may be modified by the presence of an inhomogeneous layer and can be the dominant controlling process.
In this paper two types of diffusion behaviour are distinguished:
- the diffusion toward a surface partially covered with an organic complex compound (phosphonate) and
- the diffusion through insoluble porous phosphate layers, reactively formed on iron.

Phosphonate layers on iron

In aerated neutral solution the corrosion of iron is complicated by the formation of inhomogeneous corrosion product layers at the corroding surface. The corrosion process is strongly effected by additives such as organic phosphorus compounds which form protective layers at the iron surface. The structure and the effect of these nonconducting porous layers on charge transfer and transport phenomena are discussed in terms of transfer function analysis proposed by J.W.Lorenz /2/.
If the electrode area is considered to consist of a set of active sites seperated by passive sites, the mass transport is influenced by convection parallel to the electrode surface /3, 4/. This leads to a hyperbolic expression of the diffusion impedance as can be seen in figure 1.
The impedance of such an electrode may be represented by a parallel combination of the double layer capacity C_{dl}, the polarization resistance R_{pol} and the transport impedance Z_T, which describes the deviation from linear transport conditions. Using a NLLS-Fit procedure of Boukamp /5/ C_{dl}, R_{pol} and the dimension of the active sites of the partially covered surface can be evaluated.

Diffusion transport through a porous layer

The impedance spectra of porous phosphate layer on iron (see figure 2) can be represented by a modified Randles equivalent circuit, where the double layer capacity C_{dl} is replaced by the CPE. The porous layer may slow down the mass

transfer rate of diffusing species. This decrease includes as well the effect of the layer thickness and of the layer porosity. The diffusion coefficient D, which is inveresly related to the Warburg coefficient σ, depends on the average cross-section of the pores in the phosphate layer. Therefore it is reasonable to think that the greater the value of σ, the greater will be the hindrance to the diffusion process.

For cathodic electropainting it is necessary that the pores of the phosphate layer are very small and sufficiently numerous /6/. It has been observed that in this case the polarization resistance R_{pol} and the Warburg coefficient σ are of the same order of magnitude.

References

1. U.Rammelt, G.Reinhard; Electrochim. Acta 35 (1990) 1045.
2. E.Schmidt, J.Hitzig, J.Titz, K.Jüttner, W.J.Lorenz; Electrochim.Acta 31 (1987) 1041.
3. M.Fleischmann, S.K.Rangarajan, H.R.Thirsk; Trans. Far.Soc. 63 (1967) 1240.
4. T.Gueshi, K.Tokuda, H.Matsuda; J. Electroanal. Chem. 89 (1978) 247.
5. B.A.Boukamp; Solid State Ionics 20 (1986) 31.
6. U.Rammelt, G.Reinhard; farbe + lack 98 (1992) 261.

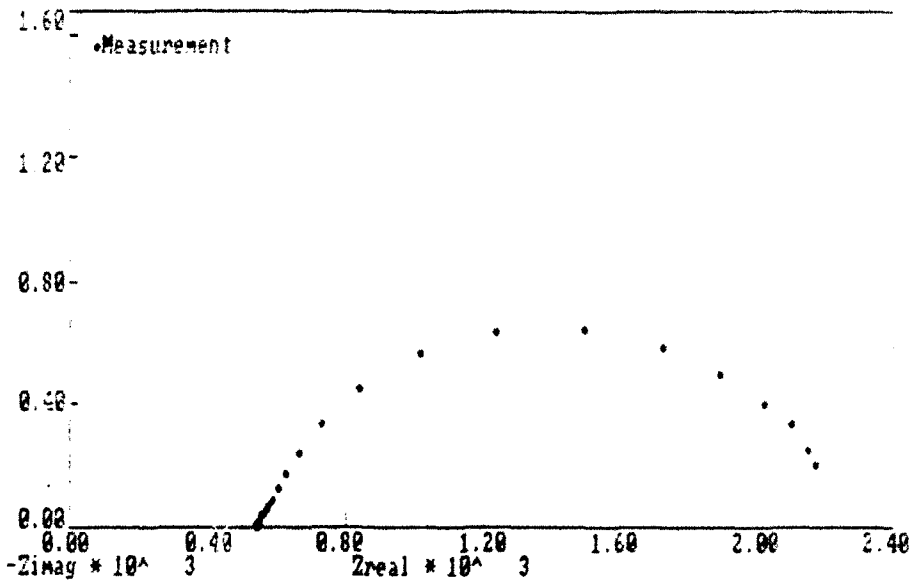

Fig. 1: Nyquist plot representing impedance data for iron in sulfate solution with HEDP

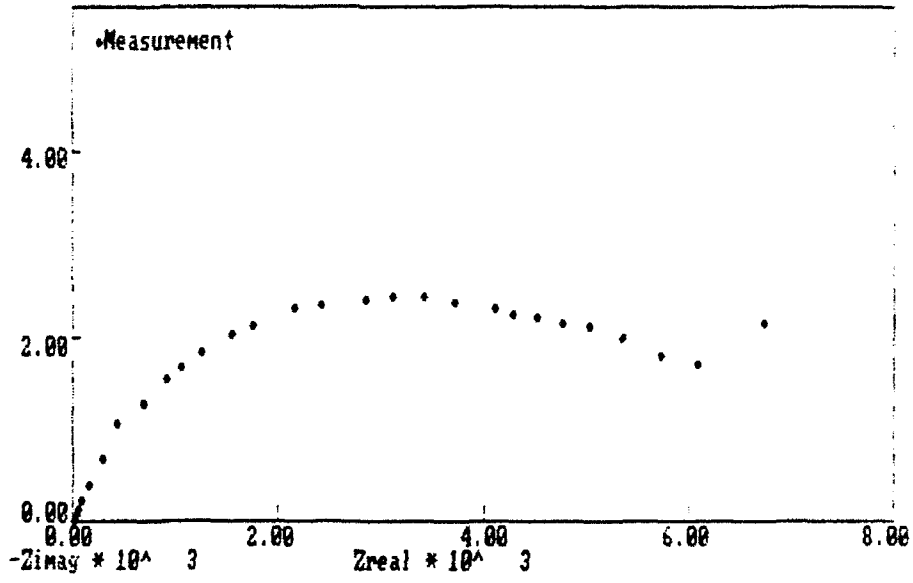

Fig. 2: Nyquist plot representing impedance data for iron with phosphate layer

ELECTROCHEMICAL IMPEDANCE SPECTROSCOPY OF TUNGSTEN IMPLANTED ALUMINIUM SURFACES

C.M.Rangel and M.A.Travassos
Laboratório Nacional de Engenharia e Tecnologia Industrial - LNETI
Materials Technology Department
Paco do Lumiar, 22 1699 LISBOA Codex PORTUGAL

EXTENDED ABSTRACT

Aluminium and its alloys are known to suffer localized attack of the pitting type in aqueous chloride containing environments. It is also known that elements such as Cr, Mo,Ta, Zr and W enhance passivity but exhibit low solubility limits in Al, typically below 1%, exerting at these concentrations very little influence on corrosion behaviour.
However, these limits can be increased using non-equilibrium alloying methods such as ion implantation.

A study has been made of the influence of surface ion implantation of Tungsten upon the electrochemical behaviour of pure Aluminium using Electrochemical Impedance Spectroscopy(EIS).

Tungsten implantation was performed using an analyzed 40 KeV W+ ion beam to a fluence of 4E16 cm^{-2} . Characterization was performed in aqueous solutions at different pH values.
EIS indicated passivation by the formation of a thin film in acid media. Open circuit potentials in a 0.25 M sulphuric acid solution at room temperature indicated an increased of ~400 mV in the noble direction for immersion times up to 70 hours when compared with the behaviour of pure Aluminium in the same experimental conditions. Ennoblement is probably due to the influence of Tungsten in the formation of an oxide around -400 mV(SCE). In acid media the oxide probably contains WO_2.

For alkaline media two regions of stability were found according to applied potential. This is associated to to compositional variation of tungsten concentration and also to the presence of intermetallic compounds as dissolution eats aways the first layers.EIS and joint voltammetric studies suggest dissolution under ohmic control. Results also report the effect of chloride on both stability zones.

ACKNOWLEDGEMENTS. This work is co-financed by JNICT, Portugal, under Research Contract nº 87 177 MATR.

AN ELECTROCHEMICAL IMPEDANCE SPECTROSCOPY STUDY OF ZINC RICH PAINTS ON STEELS IN ARTIFICIAL SEA WATER BY A TRANSMISSION LINE MODEL

S.G. Real, A.C. Elias and J.R. Vilche

Instituto de Investigaciones Fisicoquímicas Teóricas y Aplicadas (INIFTA), Facultad de Ciencias Exactas, Universidad Nacional de La Plata, Sucursal 4, Casilla de Correo 16, (1900) La Plata, Argentina.

C.A. Gervasi and A. Di Sarli

Centro de Investigación y Desarrollo en Tecnología de Pinturas (CIDEPINT), 52/ e 121 y 122, (1900) La Plata, Argentina.

The characteristic feature of a zinc rich paint coating for corrosion prevention is its high content of metallic zinc powder (typically greater than 83% w/w in the dry film) dispersed in a vehicle either organic or inorganic. Due to the presence of voids, the coating is accepted to behave like a porous electrode. EIS has previously been applied to study the protective behaviour of ZRP[1]. However, at present, there has been no attempt to model the impedance response of these systems in that fashion.

The objective of this paper is to establish the feasibility of interpreting the EIS data of a steel/ZRP/sea water system according to a porous-electrode model and to derive the corresponding parameters to assess the coating deterioration with time.

Electrochemical impedance spectroscopy (EIS) was applied to characterize the corrosion protection behaviour of zinc rich ethyl-silicate paints (ZRP) on steel using a Solartron 1250 FRA and 1186 EI controlled by a personal computer. Impedance spectra were collected in the frequency range 1 mHz $\leq f \leq$ 50 kHz at the open-circuit potential as a function of exposure times in artificial sea water.

Typical Nyquist diagrams, after ohmic drop correction, exhibit in the high-frequency domain a constant phase angle of about -45°. This behaviour is typical for porous systems and can be explained using the cylindrical-pore model[2]. At low frequencies the shape of the impedance diagrams involves a slightly distorted capacitive semicircle. With increasing immersion time the impedance spectra exhibit the same general characteristic features whereas the magnitude of the overall impedance gradually increases.

A fairly good description of the experimental admittance diagrams after ohmic drop correction was obtained in terms of a transfer function analysis using nonlinear fit routines based on a transmission line model[3] for n cylindrical pores linked in parallel in the coating structure (Fig. 1).

The parameters derived from EIS results show that the electrochemically active area of the zinc rich ethyl-silicate paints decreases markedly with increasing immersion time. This time dependence corresponds mainly to a decrease of the pore radius. The charge transfer resistance values resulting from the fitting procedure are comparable to that reported in the literature[4] for a plain Zn electrode/sea water system.

ZRP coatings were examined using SEM as a function of exposure time. The micrographs of the coatings exhibit that the amount of corrosion products increases with time generating a strong blocking effect on the porous structure.

The results indicate that ZRP coatings are described as cylindrical pore electrodes whose radii are smaller than that predicted by SEM before immersion.

REFERENCES

[1] D.J. Frydrych, G.C. Farrington and H.E. Townsend, in Corrosion Protection by Organic Coating, Edited by M. Kendig and H. Leidheiser, The Electrochemical Society Inc., Vol. 87-2, Pennigton, NJ (1987).

[2] R. de Levie , in Advances in Electrochemistry and Electrochemical Engineering, Vol. VI, Edited by P. Delahay, p. 329, Interscience, New York (1967).

[3] H. Keiser, K.D. Beccu and M.A. Gutjhar, Eletrochim Acta, 29, 539 (1976).

[4] A. Díaz, S. González and A. Arévalo, Rev. Iberoam. de Corros. y Protección, 19, 15 (1988).

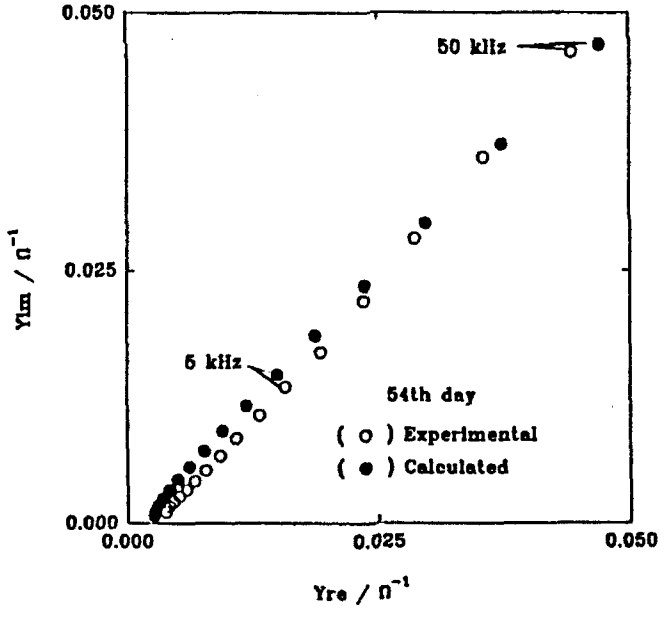

Fig.1 Calculated and experimental admittance plots obtained for ZRP coatings after 54th immersion day.

CHANGES IN IMPEDANCES OF Ni/Cd CELLS WITH VOLTAGE AND CYCLE LIFE

Margaret A. Reid
Electrochemical Technology Branch
NASA Lewis Research Center
Cleveland, OH 44135

As part of a long-term study of the feasibility of using impedance spectroscopy for prediction of cycle life and diagnosis of failures in space flight cells, measurements are being taken on two 19 AH aerospace design Super Ni/Cd cells. The cells are being cycled in a low earth orbit (LEO) regime at 50% depth of discharge (DOD). Impedances are being measured periodically at eight voltages over the entire range of state of charge (SOC). The cells have now been cycled for over 3500 cycles, equivalent to seven months in LEO. The use of sealed cells is essential in studying the effects of long-term cycling in order to avoid changes in electrolyte composition. Unfortunately, the cadmium electrode is connected to the case, so the impedances of the individual electrodes cannot be determined separately by using the case as a reference as was done earlier [1], but parallel studies being carried out in sealed Ni/H_2 cells should help in assigning the observed effects to either the Ni or the Cd electrode.

Measurements are made from 1000 Hz to 0.001 Hz using an AC signal of 1 mv RMS (5 mv RMS at the lowest frequencies and voltages). The cells are held at the desired voltage until the DC current falls to a few mA.

Most of the earlier measurements in this lab were made on Ni/H_2 cells and Ni electrodes at very low states of charge where the greatest differences between cells and electrodes from different manufacturers were observed. The measurements at very low frequencies (0.05 to 0.001 Hz) were the most useful. Measurements at these low frequencies and voltages are time-consuming and are not suitable for routine monitoring of cells on test. One goal of the present study is to develop criteria for monitoring cells at higher states of charge and frequencies so that it can be done routinely.

The two cells currently being cycled are performing satisfactorily (the anticipated life is about 20,000 cycles). Complex plane plots are shown in Figure 1 for one of the cells after 3000 cycles. Preliminary analyses are given in Table I for some of the data using a typical equivalent circuit consisting of an ohmic resistance in series with a circuit consisting of a double-layer capacitance in parallel with a kinetic resistance and Warburg impedance. There has been little change with cycling at the higher states of charge so far. At low states of charge (below 10%), the kinetic resistance and Warburg slope fell initially but have remained reasonably constant since. This can be interpreted as an initial improvement in the electrode, followed by a long period of constant behavior. No signature for prediction of end of life has been seen as yet.

Analysis of the data is also being done using several other equivalent circuit models using a complex nonlinear least squares fitting program [2]. A completely satisfactory

equivalent circuit which will be valid over the whole range of states of charge has not yet been found. We have done preliminary work following an earlier study [3] which used an electrical engineering program, PSpice, incorporating non-linear elements [4].

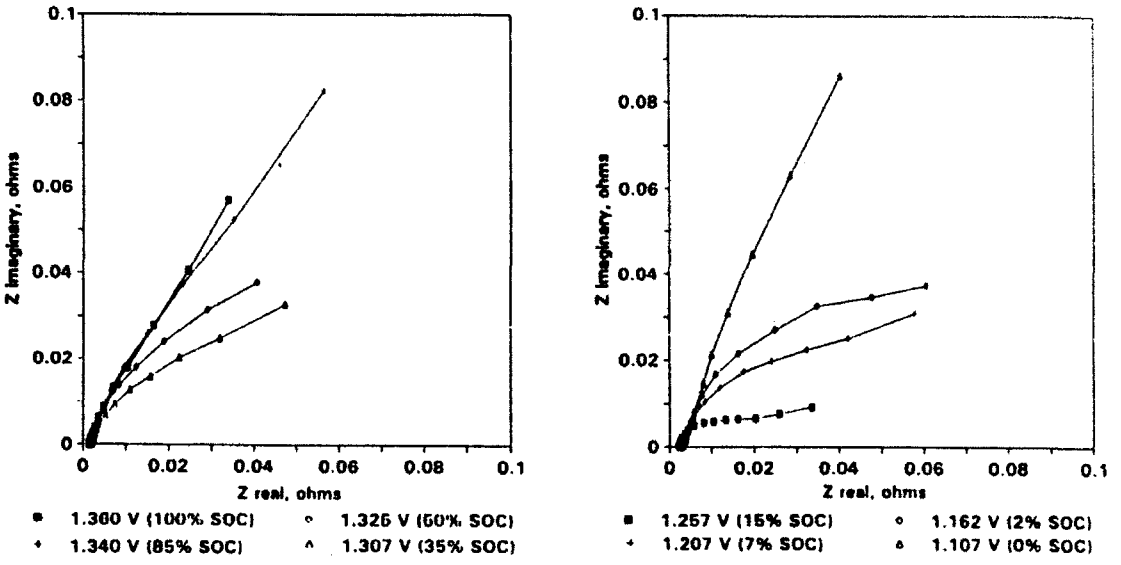

Fig. 1. Complex plane plots for Super Ni/Cd cell after 3000 cycles.

Table I. Parameters for the data of Fig. 1 using simplified circuit.

Voltage	R ohmic, mOhm	R kinetic, mOhm	Warburg Slope, mOhm $sec^{-1/2}$	Capacitance, Farads
1.360	1.38	--	3.51	1100
1.257	1.54	13	2.13	800
1.162	1.65	50	6.51	650

Conclusion

Measurements in Super Ni/Cd cells during long term cycling (over 3000 cycles) have not shown any major changes in impedance parameters, however, cell failure is not expected for some time. The data is being analyzed by several methods.

References

[1] M. A. Reid, *J. Power Sources* **29**, 467 (1990).

[2] J. R. Macdonald, U. of North Carolina at Chapel Hill, CNLS program.

[3] S. Waaben, I. Moskowitz, J. Federico, and C.K. Dyer, *J. Electrochem. Soc.* **136**, 1356 (1985).

[4] J. T. Maloy and M. A. Reid, 1992 Power Sources Symposium, IEEE Inc., New York, N.Y., 1992.

DETERMINATION OF DIELECTRIC CHARACTERISTICS OF ORGANIC COATINGS BY ALTERNATING CURRENT

G. Rocchini* and P. Spinelli†

* ENEL-CRTN, Via Rubattino 54, Milano, Italy
† Politecnico di Torino, Corso Duca degli Abruzzi 24, Torino, Italy

The mathematical validity and physical meaning of the metal/coating/electrolyte schematization by means of equivalent electric circuits is discussed and it is shown that a model based on a quadripole cascade provides satisfactory results.

The analysis of a representation based on two quadripoles, which, in spite of its simplicity, proved to be useful, allowed to verify that the presence of defects changes the value of the leakage resistance but does not significantly affect the value of the capacitance.

This work, which reports the results obtained using aluminium brass samples, coated with a commercial product and immersed in artificial sea water, was aimed at evaluating the effectiveness and the porosity degree of an organic film.

The tests were carried out under dynamic conditions using a laboratory loop. The specimens of aluminium brass were coated with the commercial product Saekaphen HR60 extra G which is an epoxy resin and has been employed using about 10% acetone as a solvent. This product was applied at room temperature and all the samples were aged for 72 hours before the tests. The sample surface was prepared by blasting with synthetic sand Asilikos by Krupp having a granulometry between 0.5 and 1.4 μm. The exposed area of these samples was about 35 cm^2. The choice of aluminium brass is justified by the fact that tubes of this alloy are commonly employed in steam condensers, cooled with sea water, of ENEL thermal power plants.

The behaviour of three different thickness values of the coating (40, 80, 120 μm) was examined. The flow rates of artificial sea water at 40 °C were 1, 1.5, 2 ms^{-1}. Electrochemical measurements were based on alternating current (a.c.) techniques.

From an experimental point of view, the alternating current technique should be preferred to direct current methods, since, by taking advantage of the change of the electrode impedance with the frequency of the sinusoidal signal, measurement of the current is easy and requires a small amplitude signal. The use of direct current demands, on the contrary, the application of high voltages when the film resistance is of the order of 10^9 Ωcm^2. The same remark also applies in the case of a.c. measurements performed at frequencies lower than a few Hz.

Electrochemical impedance measurements during dynamic tests were carried out by means of the EG&G computerized system including mod. 173 potentiostat with mod. 276 interface and mod. 5206 lock-in amplifier. The potentiostat had been modified to perform long distance measurements by the four wires technique according to the manufacturer indications. This was required because the connecting cables were about 5 m long. All the measurements were carried out under potentiostatic configuration as required by mod. 368 AC software of EG&G, written in "Pascal"

for Apple IIe computers. Two version of this software were employed, the first one for operation at the maximum frequency of 100 kHz, the second one at the maximum frequency of 20 kHz. Generally the frequency range [0.25, 100] kHz was used. The signal amplitude ($\approx$25 mV RMS) was fixed before the tests for all the frequencies. This was necessary because for the above described equipment it is not possible to change by software the output level of the oscillator signal. Our experience has shown that, when a coating has a high effectiveness in restraining the corrosion, the increase in the impedance modulus, which is observed at frequencies less than 200 Hz, drastically reduces the current flowing through the system. This gives rise to some difficulties in the measurement of the current itself, which are due to the choice of the current range and to the noise due to the zero-resistance ammeter.

Analysis of the experimental data has been carried out by means of *RIVESA* code developed in *Quick Basic* for IBM PC's and compatibles. The program provides the determination of the leakage resistance R_t and polarization resistance R_p and allows to verify the reliability of the model by using three different evaluations of the capacitance of the metal/coating/solution interphase. Moreover, the program includes the option for a graphic comparison between the computed and experimental data.

The results showed that the polarisation resistance, computed from impedance data using an extrapolation technique, is a good parameter for a correct characterization of the product and for a qualitative evaluation of the protective properties of an organic coating.

Our results indicate that data processing with a given mathematical model requires the knowledge of the surface conditions of the coated samples, because the presence of defects alters the interpretation of the measurements and may lead to contradictory estimate of the protective effectiveness of a given product. In any case the film defects are uninfluential on the coating effectiveness as far as their overall area is negligible with respect to the sample area.

It is worthwhile to observe that, also for an excellent coating, the experimental data on the Nyquist plot Z_i, Z_r cannot be represented by a semi-circle, even if their best fitting with a circle equation is quite accurate. This is due to the fact that in general the circle center is located below the real axis. In spite of this drawback the use of a circle is very instructive for evaluating the value of the polarisation resistance R_p, which can provide information on the response of the system under a direct current polarisation, because one of the important fact is the knowledge of the free-corrosion behaviour of the coated metal.

Finally the commercial product examined in this work, after two year testing, still shows a good protective effectiveness. Only minor corrosion attacks were observed on some samples (40 μm), but they were limited to very small areas.

IMPEDANCE MEASUREMENTS WITH REAL POTENTIOSTATS: CORRECTIONS FOR POTENTIOSTAT RESPONSE

Robert S. Rodgers, EG&G Princeton Applied Research, P.O. Box 2565, Princeton, NJ 08543-2565 USA

Impedance experiments place great demands on the analog circuitry of any potentiostat. If the potentiostat behavior is "civil", mathematical "post run correction" can be used to improve the impedance measurement. Studies of good quality coatings and films can benefit from compensation for potentiostat response. Further enhancements are possible with flexible potentiostat control- and data acquisition-algorithms. Post-run correction is only possible if the current range information is contained in the data file.

The I/E response is the most significant non-ideality of a potentiostat design, although certain aspects of the electrometer response can be important. It can be shown that for the potentiostat architecture shown in Fig. 1 the true cell impedance can be calculated from the observed voltage and current signals by

$$Z_{true} = R_m*(V_{ELECT}/V_{WE}) - R_m/CMRR$$

where V_{ELECT} is the voltage at the electrometer output, V_{WE} is the voltage at the working electrode ($=I*R_m$), R_m is the current measuring resistor, and CMRR is the common mode rejection ratio of the electrometer. The common mode errors occur only in the real part of the measured impedance. Luckily, the CMRR values for differential amplifiers are high (10^4) and problems can be avoided if the common mode signal ($V_{WE}=I * R_m$) is kept to a minimum by choosing an insensitive current scale. A rational selection of the current range must take the CMRR of the differential electrometer into account.

The selection of current scale must avoid current overloads, whether the source of the overload is the AC current, the DC current, or currents induced by noise picked up by the cell. The common mode signal must also be small: CMRR errors can be minimized by

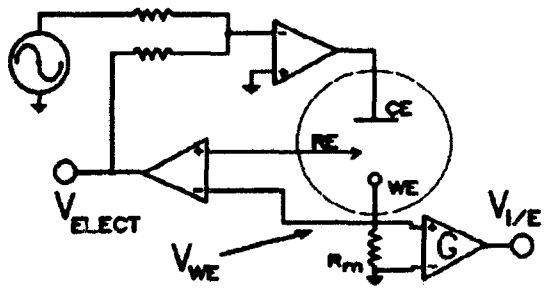

Fig. 1. Block diagram of a potentiostat with a passive current-to-voltage converter[1,2]

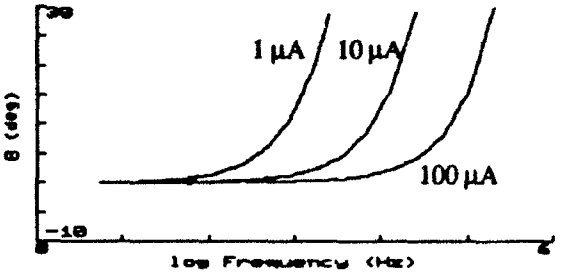

Fig. 2 Phase errors for a 10 Kω resistor measured on the 1 µA, 10 µA, and 100 µA ranges

limiting the common mode signal, V_{WE}. The frequency response of each current range must also be considered since the bandwidth of the I/E converter depends on the current scale. This becomes increasingly important at high frequency and high impedance.

Fig. 2 shows data which was collected for a 10KΩ dummy cell. The phase errors appear to be caused by an inductance, L, in series with the resistor R. Stray capacitance, C, in parallel with the current measuring resistor, R_m, will produce the same effect. The impedance experiment determines the ratio of the voltage drop across the unknown impedance, Z, to that across the current measuring impedance, Z_m. The same ratio will be measured if

$$Z/Z_m = (R+j\omega L)/R_m = R*(1/R_m + j\omega C)$$

A single value of stray capacitance of about 350 pf can be used to correct all current ranges.

Any mismatch between the current and voltage amplifier circuitry will also appear as a gain and phase error in the measured impedance. This mismatch is expected to be independent of the current range selected, and is most apparent for small values of R_m. Although a detailed analysis of the circuitry could be employed to explain this phase shift, an engineering equation is simpler to evaluate and use. The simple engineering model we have selected is a phase shift which is linear with frequency, and a gain error which is quadratic in frequency. This simple model was used to correct the data for all ranges according to

$$\text{Corrected phase} = (\text{raw phase}) * f * p_e$$

where f is the frequency in MHz and p_e is a constant which was found to be 50-60 deg/MHz. The gain or magnitude errors are corrected using

$$|Z|_{true} = |Z|_{raw} * (1-[f/f_o]^2)$$

where f_o is a mythical "break point" frequency, on the order of 2-4 MHz

Stray capacitance corrections are valid for other model potentiostats, however, p_e and f_o corrections are potentiostat model specific. Although they are valid for the M273A design potentiostat, they may not be valid for other poteniostat designs.

1. *M273A Potentiostat/Galvanostat Instruction Manual*, EG&G Princeton Applied Research, Princeton, NJ.

2. *1286 Electrochemical Interface Operating Manual*, Schlumberger Technologies, Farnborough, Hampshire, England.

THE USE OF EIS TO STUDY MEMBRANE TRANSPORT IN NICOTINIC ACETYLCHOLINE RECEPTOR

S. Alonso-Romanowski, A.C. Elias, H.R. Arias*
F.J. Barrantes* and J.R. Vilche.

Instituto de Investigaciones Fisicoquímicas Teóricas y Aplicadas (INIFTA),Facultad de Ciencias Exactas, Universidad Nacional de La Plata, Suc. 4, C.C. 16, (1900) La Plata, Argentina.

(*) Instituto de Investigaciones Bioquímicas (INIBIBB), Universidad Nacional del Sur, (8000) Bahía Blanca, Argentina.

Abstract

The different modes of operation of the nicotinic acetylcholine receptor (AChR) extracted from the electric organ of *Discopige tschudii* were studied by EIS using a thermostatized microcell with either Ag/AgCl or Pt electrodes, in both two-electrodes and three-electrodes techniques. The current signal was amplified in a special electrical circuit made *ad hoc*. For the sake of comparison impedance measurements were carried out also using liposomes made from total lipids of the same origin as the native membranes rich in nicotinic AChR. This is a proper reference system because it allows to investigate the profile of membrane vs. total lipid liposomes. Carbamoylcholine was employed to elicit conductance changes and benzocaine to inhibit them. The agonist-induced response showed a different impedance diagram as those obtained with liposomes or with AChR membranes. Then the system was sweened until complete desensitation could be observed.

To further elucidate the AChR behaviour, the general anesthetic benzocaine was added (it competes for the acetylcholine binding site), followed by carbamoylcholine and waited until complete recovery of the system. This was achieved when obtaining similar impedance spectra as for the AChR membrane.

RESULTS AND DISCUSSION

Prior to each experiment that involves a suspension, the cell used in the EIS experiment was filled with the suspending electrolyte and allowed to stand overnight. The first experiment of each set was done with the pure suspending electrolyte to stablish the blank. Next, the cell was filled with the corresponding suspension.

The experiments sequence precede as follows: a constant volume of the sample was added (500 ul), for e.g., total lipid

(0.3 mg/ml), withdrawing the small volume suspension with a Hamilton syringe and replacing it with the same volume of the pure electrolyte. The measurements were done with total lipids, then change the suspension with AChR rich membrane ; afterwards CCh was added, followed by at least three frequency cycles. The first frequency cycle (0.1 Hz - 10,000 Hz) was done immediately after the CCh was added. We continued cycling until there was no difference with the AChR spectra obtained before the CCh was added. Then we added benzocaine to check if we could detect any surface difference of the lipid-protein interface . The procedure followed with benzocaine was the same as the one when adding CCh.

For the membrane /receptor system (Fig.2), the total impedance Z(t) of the network is given by:

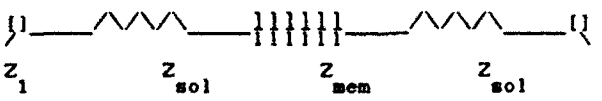

$$Z(t) = 2\,(Z_1) + 2\,(Z_{sol}) + Z_{mem}$$

where Z_1 is the impedance interface-electrode solution, Z_{sol} is the solution impedance and Z_{mem} stands for the membrane impedance that depends on the suspension used. Z_{mem} can be : total lipids liposomes, lipids with AChR embedded liposomes, lipids/AChR and CCh, lipids/AChR and benzocaine, lipids/AChr, benzocaine and CCh.

The experimental results were analyzed and reported as "difference spectra", e.g., the impedance difference between the value obtained for the suspension of total lipids liposomes and the impedance spectra of the buffer (Tris 10 mM, 100 mM NaCL). Note that this procedure eliminates effects due to electrode/electrolyte and solution impedance.

The most striking feature is the increase in the magnitude of the impedance difference when changing the lipid for the protein, by a factor of two. These data show that the impedance (Real and Imaginary part) are strong functions of the element (AChR or CCh or Benzocaine) present near by the membrane interface. The spectra for the total lipids liposomes show only one time constant. When the protein is present we get two time constants.

REFERENCES

1. G. Cotaand E. Stefani, J. Physiol. **351**, 135 (1984).
2. S. G. A. McLaughlin, G. Szabo and G. Eisenman, J. G. Physiol. **54**, 667 (1971).
3. E.B. Castro, S.G. Real, S.B. Saidman, J.R. Vilche, and R.H.Milocco, Materials Science **44 & 45**, 417-432 (1989).

THEORETICAL INVESTIGATION OF THE ELECTROCHEMICAL DEPOSITION OF METAL INVOLVING ADSORPTION ANS DESORPTION STEPS

Sylvie Rouquette-Sanchez, Pierre Cowache
Pascale Boncorps and Jacques Vedel

Laboratoire d'Electrochimie (Unité Associée 216 au CNRS)
ENSCP, 11 rue Pierre et Marie Curie
75005 Paris - France-

The objective of this work is to study the reactional pathway proposed by Sella [1] occuring during the electrochemical reduction of Te(IV) ions into Te(0) deposed at the working electrode.
The proposal mechanism is described as :

a- *Diffusion.*

$$\underset{C_s}{A^{n+}} \xrightarrow{D} \underset{C_{el}}{A^{n+}}$$

b- *Adsorption.*

$$\underset{C_{el}\ \Gamma\theta_0}{A^{n+} + s} \xrightarrow{K_1} \underset{\Gamma\theta_1}{A^{n+},s}$$

c- *Charge transfer.*

$$\underset{\Gamma\theta_1}{A^{n+},s} + ne^- \xrightarrow{k_b} \underset{\Gamma\theta_2}{A,s}$$

d- *Desorption.*

$$\underset{\Gamma\theta_2}{A,s} \xrightarrow{K_2} A + \underset{\Gamma\theta_0}{s}$$

e- *Competitive reaction.*

$$\underset{C_m\ \Gamma\theta_0}{M^{n+} + s} \xrightarrow[K'_3]{K_3} \underset{\Gamma\theta_3}{M^{n+},s}$$

The electrochemical impedance of this mechanism was calculated. We have deduced an electrical equivalent circuit from the analytical expression of the impedance. In fact, two equivalent electrical circuits were obtained which only depends on the relative values of the kinetic parameters K_2 and K'_3 (Figure 1).
The electrical study shows that the capacitive and selfic effects can be observed together when the electrical parameters are are selected independently of the mechanism. However, the influence of the selfs are not seen when their values are correlated by the relations imposed by the mechanism.
Moreover, the diffusion impedance is complex (Figure 1) and we have shown that, in the case for which the diffusion is a limiting step, the impedance shape of this diffusion is different in function of the kinetic parameters.
If $K_2 > K'_3 - K_3C_m$ and $K_2 > \frac{2K_3K'_3C_m}{K_3C_m - K'_3}$ we observe at low frequencies a selfic effect and a loop which is characteristic of the diffusion (Figure 2).
If one of these two conditions is not verified, the Nyquist diagrams show a classical diffusion with a slope equal to one.
That shows a competition beetween the two desorption steps : the diffusion process is modified when the competitive reaction occurs.
The study of the other kinetic parameters shows their influence on the current-potential curves and on the impedance diagrams in all the possible limitations.

[1] C. Sella, P. Boncorps, J. Vedel, J. Electrochem. Soc., 133(1986)2043

Figure 1 :

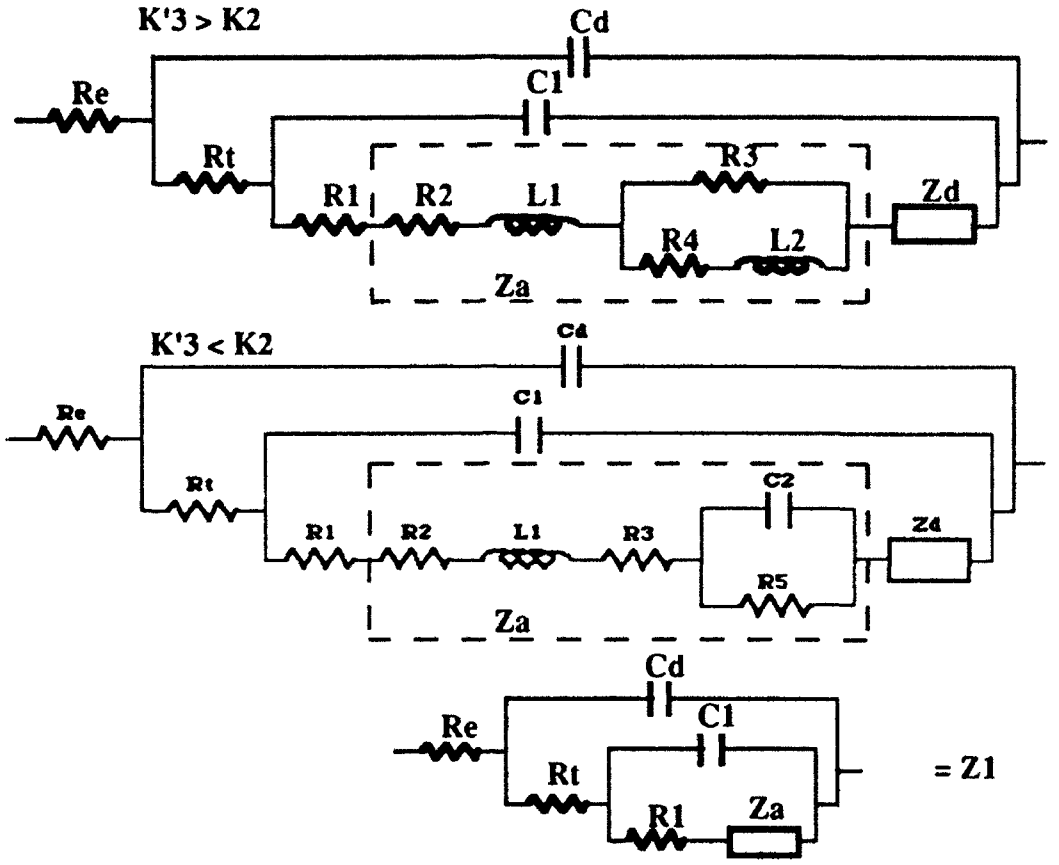

$$Z_d = T(Z_a) \text{ with } T = \frac{th(\delta\sqrt{\frac{j\omega}{D}})}{\sqrt{j\omega D}}$$

Figure 2 :

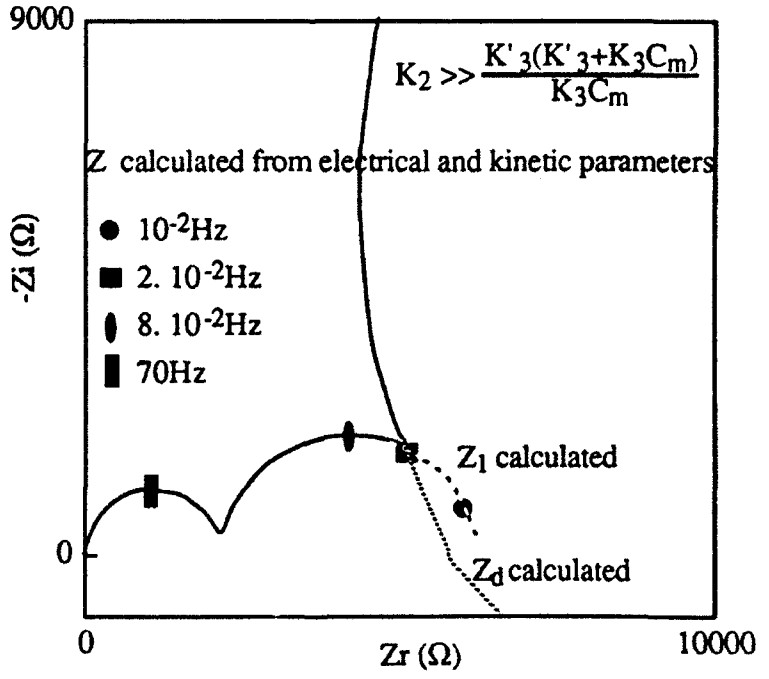

THE STUDY OF MEDIUM EFFECTS ON THE ELECTROCHEMICAL REDUCTION OF NITROMETHANE BY IMPEDANCE ANALYSIS

M. Rueda, F. Prieto and I. Navarro

Department of Physical Chemistry, Faculty of Pharmacy, University of Seville. Spain

Salt effects in electrode kinetics is a classic subject with numerous examples in the field of metal cation discharges. However, little attention has been paid to the influence of the supporting electrolyte in the field of organic electrode reactions. This is probably due to the multistep character of these reactions. The impedance technique is suitable to provide information about every step of the mechanisms [1], therefore, the salt effects can be studied on elementary electrode processes instead of on global reactions.

Nitromethane reduction is the most frequently selected system to show the influence of salts in organic electrode reactions [2–4]. Guidelli et al. [4] proposed an ECe mechanism for nitromethane reduction on mercury. The use of the impedance method proved that in fact the first electron transfer is composite, including another chemical step, so that an ECCe mechanism was proposed, [5].Because no effect was found by changing the pH of the solution in the range pH 7– pH 9, it was accepted that the solvent may be the protonation agent.

In this paper the concentration of the supporting electrolyte is modified in order to detect the influence of the water activity on the chemical steps. The nature of the salt is also varied to investigate the existence of specific double layer effects on the mechanism, as suggested in [4].

The supporting electrolytes have been 1M, 3M and 6M $NaClO_4$ and 1M and 2M NaI aqueous solutions. The pH of the solutions was kept at 8.25 by using 0.2M borate buffer.

Impedance measurements were performed with a computerized system based on the HP192A network analyzer and a home-made potenciostat. The same potenciostat provides also the polarographic data by 14 bits DA/AD converters. The amplitude and phase angle of the admittance were measured and transformed into the impedance and admittance components.

Two kinds of analyses as a function of the frequency have been performed at every potential: a) based on a pseudo-Randles circuit as in ref. [5], so that the charge transfer resistant, R_{ct}, and the warburg coefficient, σ can be obtained and b) based on the complete equations for the admittance deduced for the ECCe mechanism in which the second intermediate can diffuse from the interphase, [6]. This analysis provides R_{ct} and a parameter called C in [6] which depends on the global rate constant for the

first EC steps, k_I. The agreement obtained with both analyses is good in all cases thus confirming that conditions for the pseudo-Randles circuit are fulfilled.

A shift in the half wave potentials towards less negative values is observed when the $NaClO_4$ concentration is increased. The shift is in the opposite direction when changing from $NaClO_4$ to NaI solutions of the same concentration.

The values of the diffusion coefficient and the rate constant for the second chemical step, k_c, are inferred by comparing the dc limiting currents with those obtained in acid solutions of the same concentration (the chemical step is assumed to be very fast in these conditions). The formal standard potentials for the EC steps, E_I°, are estimated from the half-wave potentials. The analysis of R_{ct} and C as a function of potential provides the $k_{a,I}$ and $k_{c,I}$ values for the EC steps.

k_c and $k_{c,I}$ do not change appreciably when increased the $NaClO_4$ concentration but increase somewhat when changing to NaI solutions. These findings contradicts the previous assumptions about the nature of the chemical steps, because they are not compatible with protonation reactions. Reorientation or isomerization is the most plausible nature for the first chemical step and a bond-breaking N-OH reaction for the second. The salt effect on the E_I° can also be understood in the frame of this mechanism because a charged intermediate should be more stabilized by the ionic strength. Differences between the data in $NaClO_4$ and NaI solutions can be explained by the influence of specifically adsorbed anions. It is inferred that the first electron transfer takes place within the inner layer.

REFERENCES

1. C.P.M. Bongenaar, A.G. Remijnse, M. Sluyters-Rehbach and J.H. Sluyters, J. Electroanal. Chem. 111 (1980) 139
2. M. Breiter, M. Kleinerman and P. Delahay, J. Am. Chem. Soc. 80 (1958) 5111
3. M. Suzuki and P.J. Elving, Collect. Czech. Chem. Commun. 25 (1960) 3202
4. R. Guidelli and M.L. Foresti, J. Electroanal. Chem. 18 (1973) 301
5. M. Rueda, M. Sluyters-Rehbach and J.H. Sluyters, J. Electroanal. Chem., 261 (1988) 23
6. F. Prieto, M. Rueda, I. Navarro, M. Sluyters-Rehbach and J.H. Sluyters, J. Electroanal. Chem. , in press

AMTEC ELECTRODE STUDIES USING ELECTROCHEMICAL IMPEDANCE SPECTROSCOPY

M.A. Ryan, M.L. Underwood, R.M. Williams,
D. O'Connor and B. Jeffries-Nakamura

Jet Propulsion Laboratory
California Institute of Technology
Pasadena, CA 91109

The Alkali Metal Thermal to Electric Converter (AMTEC) is a direct energy conversion device capable of near-Carnot efficiencies; it has been demonstrated to perform at high power densities, with open circuit voltages up to 1.6 V and current densities up to 2.0 A/cm^2 [1-3]. The device is a sodium concentration cell which, as it is operated at JPL, uses a β"-alumina solid electrolyte (BASE) ceramic tube as a separator between a high pressure region containing liquid sodium at 900 - 1300 K and a low pressure region containing a condenser at 400 - 700 K. BASE is a sodium ion conductor; sodium metal is oxidized at the liquid sodium/BASE interface and sodium ions are transported to the low pressure side of the BASE. Electrons travel through an external circuit to recombine with sodium ions at a porous, thin film metal electrode which has been sputtered onto the outside wall of the BASE tube; sodium vapor is transported through the porous metal electrode, vaporizes on the low pressure side, and is collected on the condenser. The principles of AMTEC have been described in detail by Weber [1].

A quantitative model of the performance of a porous metal electrode in an AMTEC cell has been developed using electrochemical impedance spectroscopy. This model has been discussed in detail by Williams *et al.* [4,5]. A similar model has also been developed for a simpler, non-power producing cell, the Sodium Exposure TEst Cell (SETC). Parameters which describe the system and which can be derived from the impedance value of R_{ACT} (Apparent charge transfer resistance) include both kinetic and sodium transport parameters. Verification of the model has made it possible to extract transport and kinetic information from current-voltage data. The model has been applied to electrodes of several materials and compositions, including rhodium-tungsten and platinum-tungsten. EIS data have been used to compare the performance of materials as well as the performance of different compositions of the same material. While RhW performance has not been shown to be composition dependent, PtW performance has. Figure 1 shows the impedance spectra for four compositions of PtW alloys electrodes after 1125 hours of operation.

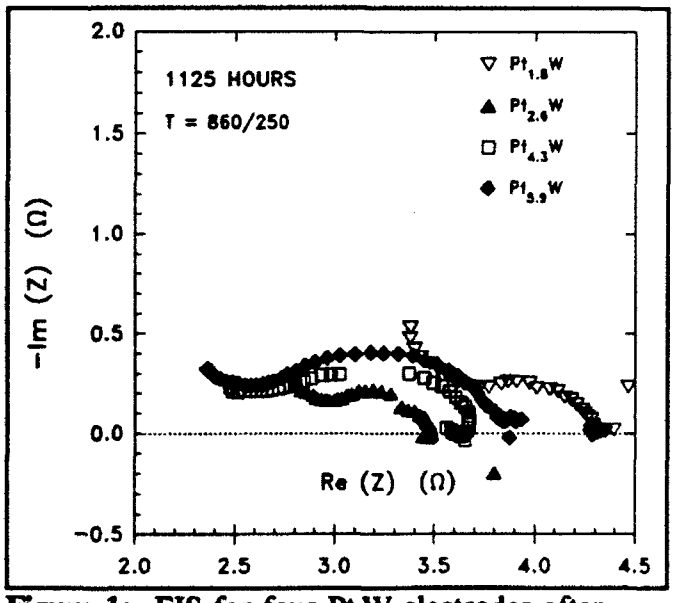

Figure 1: EIS for four Pt$_x$W electrodes after 1125 hours of operation. Frequency was from 1 to 64,000 Hz.

Power density is generally used as an indicator of device performance, but it is not a good indicator of electrode morphology, as it does not differentiate among the various processes contributing to performance. These processes include kinetic and transport processes. The morphological change in a porous metal electrode which will have the greatest long-term effect on performance is sintering of the electrode material. There is a direct relationship between the contact area or perimeter of the metal grains of the electrode on the BASE and the exchange current magnitude. Exchange current, J_0^0, is, then, a sensitive indicator of the progress of sintering. Another process which is significant in changing electrode morphology is migration of electrode material. It has been found that various metals which have been used as current collecting materials, such as nickel and molybdenum, contribute to migration of electrode materials when the electrode is held at high temperature in the presence of sodium vapor. Exchange current will also be an indicator of rearrangement of electrode material.

Because J_0^0 is a function of temperature, and because impedance measurements have been made at a variety of temperatures in the course of an AMTEC experiment, a quantity which can be described as a temperature independent exchange current, or J_0 normalized for collision rate, is used to compare behavior at different temperatures [5]. This quantity, B, can be expressed as: $B = J_0^0 T^{1/2}/P_2$. B has the units A $K^{1/2}$ /m^2 Pa.

Monitoring B as it is calculated from measured impedance or current-voltage data throughout an experiment gives a measure of the morphological condition of the electrode. As sintering goes with the fourth root of time [6] ($t^{1/4}$), then plotting B vs. $t^{1/4}$ if the exchange current is proportional to contact perimeter, $t^{1/2}$ if it is proportional to contact area, makes it possible to predict the functional lifetime of an electrode material. Figure 1 compares the predicted lifetime of a Pt_3W electrode (solid lines shows grain growth) with the decline of B with $t^{1/4}$ and $t^{1/2}$. A Rh_2W electrode declined in performance much more rapidly than predicted because of rearrangement of electrode material caused by interactions with an overlying nickel mesh. Non-contaminated RhW is predicted to have a lifetime of up to 25 years. PtW should operate for up to 15 years.

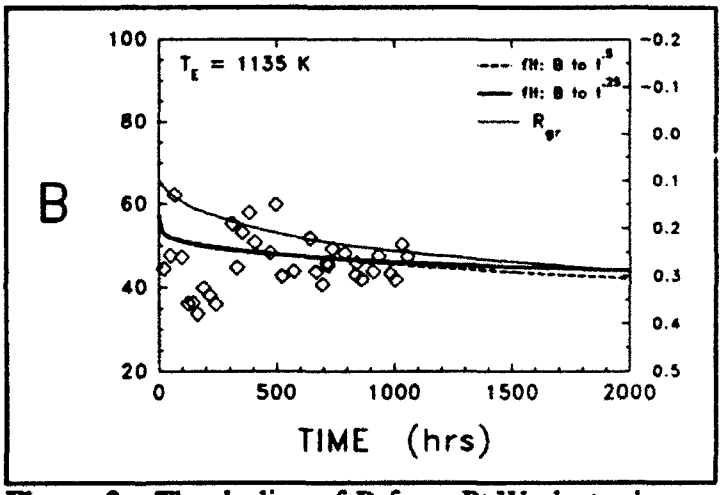

Figure 2: The decline of B for a Pt_3W electrode plotted vs. $t^{1/4}$ and vs. $t^{1/2}$. Grain growth is also plotted against $t^{1/4}$.

REFERENCES

1. N. Weber, *Energy Conv.*, 14, 1 (1974).
2. T. Cole, *Science*, 221, 915 (1983).
3. C.P. Bankston, T. Cole, R. Jones and R. Ewell, *J. Energy* 7, 442 (1983).
4. R.M. Williams, M.E. Loveland, B. Jeffries-Nakamura, M.L. Underwood, C.P. Bankston, H. Leduc and J.T. Kummer, *J. Electrochem. Soc.*, 137, 1709 (1990).
5. R.M. Williams, B. Jeffries-Nakamura, M.L. Underwood, C.P. Bankston and J.T. Kummer, *J. Electrochem. Soc.*, 137, 1716 (1990).
6. F.A. Nichols, *J. Appl. Phys.*, 37, 2805 (1966).

ELECTROCHEMICAL IMPEDANCE FOR PASSIVE IRON IN ORGANIC SOLVENTS CONTAINING SULFURIC ACID AND WATER

V.A. Safonov* and Shiro Haruyama
Tokyo National College of Technology
1220-2 Kunugida, Hachioji, Tokyo 193, Japan
* Moscow State University, Faculty of Science
Leninskie Gorg, Moscow 117234, Russia

The role of water on passivity of iron has been studied by impedance technique in acidic dimethylsulfoxide (DMSO) and dimethylformamide (DMF) solutions containing different amount of water. The passivation potnetial shifted more noble potentials with decreasing the water content of the solvents and no passivation occured in the absence of water. The peak current in the active reigion and the current in the passive region decreased with the decrease in the water content in both the solvents. Both the currents are less in the DMSO than in the DMF.

The Flade potential, namely the potential for passivity breakdown in open-circuit, was not affected by either the nature of organic solvent or the water content, while the time for activation, which is much shorter in DMF than in DMSO, increases with decreasing the water content.

Electrochemical impedance for the passive iron in the acidic organic solvents exhibits partially overlapping two semicircles on the complex plane graph, as similar to that for the passive iron in aqueous solutions. The impedance characteristics of this type are often simulated by a cascade connection of two parallel RC circuits, although the physicochemical meaning of the equivalent circuit is sometimes not clear. It is probable that the R_hC_h couple which appeared at high frequencies is attributable to the passive film formed on surface. The C_h value is of the order of 10^{-6} F/cm^2 without depending on the potential and decreases with decreasing the water content of the solvents. The large value and potential-independency of R_h indicate that the high frequency capacitance is of dielectric nature. The R_h value is of the order of 10 ohm·cm^2 and increases with decreasing the water content. The low frequency R_lC_l couple is attributable to faradaic impedance and double layer capacitance. The C_l value increases with increasing the water content, exhibiting a saturation to $2 \cdot 10^{-5}$ F/cm^2. The R_l value decreases with increasing the water content.

It is likely that the passive film on iron in the acidic organic solvents containing water is created via a hydroxyl-containing intermediate during anodic dissolution process, as similar to that in aqueous solutions. Because of large C_h and small R_h value, it is probable that the R_hC_h couple corresponds to that of the outermost dielectric layer. The decrease in the C_h value with the decrease in the water content of the solvents is attributable to the decrease in water molecule involved in the outer most layer.

NONSTATIONARY MODELLING OF THE BASIC ELECTROCHEMICAL IMPEDANCE

B.Savova-Stoynov and Z.B.Stoynov

Central Laboratory of Electrochemical Power Sources
Bulgarian Academy of Sciences, Sofia 1113, Bulgaria

INTRODUCTION

One of the basic problems of the Electrochemical Impedance Spectroscopy (EIS) is connected with the necessity of studying time-varying phenomena. The new mathematical transforms called Rotating Transforms allow direct treatment of the nonstationary system.To analyze the experimental data measured by Rotating Transform (RT) it is also necessary to develop a theory of the Nonstationary Impedance Models (NIM). This paper is devoted to the derivation of the most simple basic nonstationary models and to the manifestation of the qualitative difference between the results obtained by the classical Fourier Transform (FT) and the Rotating Transform. The basic nonstationary impedance models are derived on the basis of Rotating Transforms.

NONSTATIONARY IDEALLY NONPOLARIZABLE ELECTRODE

After the application of the Rotating Transforms the classical aperiodic noises are totally filtrated.

The resulting impedance becomes:

$$Z^{RT}(j\omega) = R_o \tag{1}$$

in contrast to the classical FT result:

$$Z^{FT}(j\omega) = R_o + \frac{\alpha}{\omega}\left[\frac{\pi}{2} - j\left(\frac{I_{DC}}{I_o} + \frac{1}{4}\right)\right] \tag{2}$$

and as can be seen the errors are completely omited.

NONSTATIONARY IDEALLY POLARIZABLE ELECTRODE

This model contains the electrolyte resistance and the double layer capacity. If one assumes a linear time variation of the capacitance

$$C = C_o + \alpha t \tag{3}$$

under potentiostatic control with an ideal iR correction, the

state equations are:

$$U_c(t) = U_{DC} + U_o \cos\omega t \tag{4}$$

$$i(t) = \alpha U_{DC} + \alpha U_o \cos\omega t + C_o \omega U_o \sin\omega t + \alpha C_o \omega U_o t \sin\omega t \tag{5}$$

After FT the admittance becomes

$$Y^{FT}(j\omega) = \frac{3}{4}\alpha + j(\omega C_o + \frac{\pi}{2}\alpha) \tag{6}$$

including additional error terms in comparison with the stationary case.

When the projection into the frequency domain is performed by RT, the nonstationary admittance is:

$$Y^{RT}(j\omega) = \alpha + j\omega C_o \tag{7}$$

Here, RT filtrates the errors but an additional element appears, directly related with the time evolution of the capacity. In this case the element α brings useful information and can be called a "ghost" element.

NONSTATIONARY POLARIZABLE ELECTRODE

The structural model of the nonstationary polarizable electrode contains the electrolyte resistance, R, the double layer capacity, C and a conductance, g, representing the Faradaic current. For the purpose of simplifying let us assume a linear time evolution of this conductance

$$g = g_o + \alpha t \tag{8}$$

under potentiostac control and an ideal iR correction.

After FT, the nonstationary admittance has the form

$$Y^{FT}(j\omega) = g_o + \frac{\pi}{2}\cdot\frac{\alpha}{\omega} + j\omega(C - \frac{5}{4}) \tag{9}$$

and after RT, the impedance becomes the following:

$$Z^{RT}(j\omega) = g_o + j\omega C \tag{10}$$

The last equation contains again the pure structure of the model with exact identifiable parameters.

It can be concluded from these simple cases that the application of the Rotating Transform enables the filtration of the nonstationary errors. The structure of the nonstationary impedance models contains the stationary model combined with additional elements related directly with the time evolving parameter.

COMBINATION OF IMPEDANCE AND INTENSITY MODULATED PHOTOCURRRENT SPECTROSCOPY FOR THE CHARACTERIZATION OF SEMICONDUCTOR PHOTOELECTRODES

J. Schefold, F. Philipps
Institut für Physikalische Elektronik, Universität Stuttgart,
D-7000 Stuttgart 80

Impedance- and Intensity Modulated Photocurrent Spectroscopy (IMPS) have been used independently for the characterization of semiconductor photoelectrodes. As proposed by Chazalviel [1] both methods can be combined as differential methods based on identical basic principles. This approach reduces or even eliminates the well known transformability problem of impedance data.

Existing models for the current voltage behaviour of semiconductor/electrolyte contacts tend to emphasize either surface recombination or electrochemical charge transfer as the reason for reduced energy conversion efficiencies [2], although, in the general case, both effects will influence the electrode response. Provided that the photocurrent generation process is close to ideal, the equivalent scheme of such a contact which holds for both processes may be written as (Fig. 1) [3]

$$Z = Z_{sc} + Z_{ct} \,, \qquad (1)$$

with Z_{sc} as the impedance related to the semiconductor/surface barrier (including the recombination process) and Z_{ct} related to the electrochemical charge transfer. Both Z_{sc} and Z_{ct} represent a general impedance, i.e. they may - depending on the nature of the recombination and charge transfer processes - actually contain a network of several passive elements (R, C, CPE). The IMPS-transfer function H thereby gets

$$H = \frac{i^-}{i_{ph}^-} = \frac{Z_{sc}}{Z_{sc} + Z_{ct}} \,, \qquad (2)$$

and the general impedance/IMPS correlation from eq. (1) and (2) is [4]

$$Z = Z_{sc} \cdot H^{-1} \qquad (3)$$

with the reciprocal IMPS function H^{-1}. Transformable circuit structures, such as recombination related elements within Z_{sc} and charge transfer related elements within

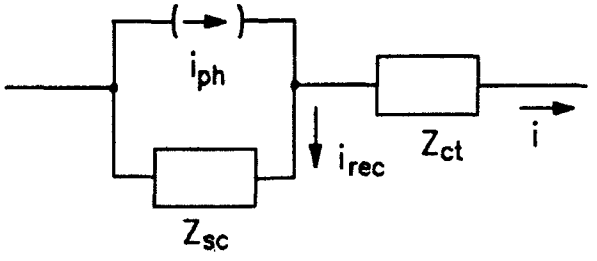

Fig. 1. Differential equivalent circuit for an illuminated semiconductor/electrolyte contact (i_{ph} = ideal photocurrent source, i_{rec} = recombination current density).

Z_{ct} can thereby be identified, since the erroneous interpretation of an impedance element as Z_{sc} will not follow eq. (3).

In the most simple case, each impedance element can be modelled by a parallel (RC)-combination with the two ohmic elements representing the recombination process (R_{sc}) and the electrochemical charge transfer process (R_{ct}), respectively. Measurements at the H_2-evolving p-InP/electrolyte interface verify this approach quantitatively [3,4]. An example for the corresponding impedance and IMPS data is given in Fig. 2. Here, the low frequency impedance semicircle is due to the electrochemical charge transfer reaction ($R_{ct}C_{HH}$) and the high frequency semicircle is defined by the semiconductor depletion layer capacity C_{sc} and the recombination resistance R_{sc}. For $C_{HH} >> C_{sc}$ eqs. (1) and (2) yield a low frequency IMPS value (see Fig. 2)

$$H(\omega \rightarrow 0) = R_{sc}/(R_{sc}+R_{ct}) \qquad (4)$$

The application of both methods was found to be essential for the evaluation of impedance data which perform considerable frequency dispersion or show small values of the Helmholtz capacity as in the case of semiconductors coated with small islands of metal catalysts [4].

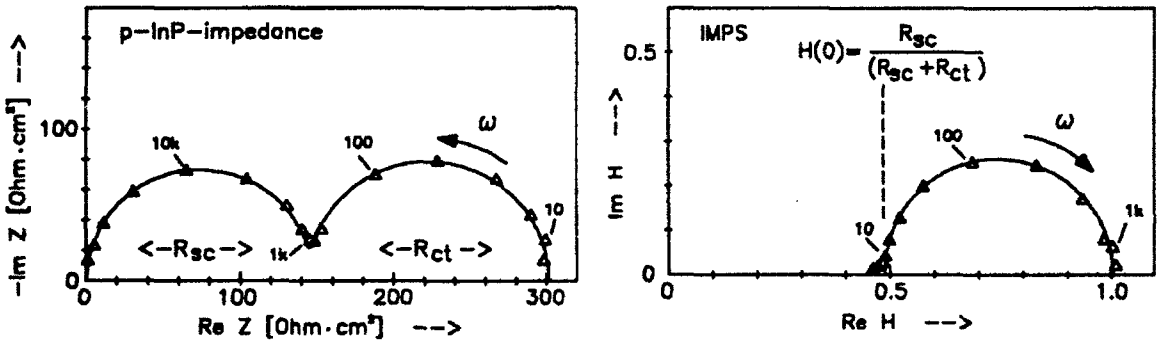

Fig. 2. Impedance and IMPS data for p-InP in 1 M H_2SO_4 for $i_{ph} \approx -450\ \mu A/cm^2$ and $i \approx -220\ \mu A/cm^2$. Measurement points (△) and fitted curves.

Formally, impedance data of Fig. 2 can also be modelled by another, transformable circuit which emphasizes ac-surface state charging effects [2]. This structure could be excluded using the IMPS/impedance correlation given in eq. (3). Since results at p-InP must not necessarily hold for other semiconductors and other redox reactions, it seems an interesting task to extend both methods to other systems.

References

[1] J.-N. Chazalviel, Electrochim. Acta 35, 1545 (1990)

[2] J. Schefold, H.-M. Kühne, J. Electroanal. Chem., **300**, 211 (1991)

[3] J. Schefold, F. Philipps, M. Specht, proc. 42nd ISE Meeting, 7-112, Montreux (1991)

[4] J. Schefold, J. Electroanal. Chem., submitted

THE EFFECT OF SURFACE INHOMOGENEITIES ON THE ELECTROCHEMICAL IMPEDANCE RESPONSE OF ALUMINUM

Gayle R. T. Schueller and S. Ray Taylor

Center for Electrochemical Science and Engineering
Department of Materials Science and Engineering
University of Virginia
Charlottesville, VA 22903

Analysis of the interfacial impedance response of solid electrodes is typically complicated by surface inhomogeneities such as variation in topography and composition[1,2,3]. These effects are virtually unavoidable in macroscopic samples. The present investigation employs high purity aluminum (99.999%) and copper (99.99%) to systematically investigate the effect of (1) surface topography, (2) surface area fraction of chemical heterogeneity, and (3) surface distribution of chemical heterogeneity, on the impedance response of aluminum-copper electrodes. Specifically, this study will evaluate the relative contributions of surface roughness, copper fraction, and copper distribution to the frequency dispersion of the impedance spectra. The intent of this investigation is to provide a controlled study of these features which can subsequently be extrapolated to more applied evaluations of aluminum alloys with different surface roughnesses. Additionally, this study may provide insight into the origins of constant phase element behavior.

Aluminum-copper composite electrodes were formed by arranging parallel copper wires into an array and casting them into high purity aluminum, as depicted in Figure 1. The copper wires and rods chosen for this investigation ranged in diameter from 0.1mm to 5mm. A systematic evaluation of the effects of area fraction and distribution of copper in these electrodes was conducted by arranging the copper wires and rods to form surface area fractions of 0% (100% aluminum), 0.2%, 20%, and 100% copper within a $1cm^2$ exposed surface. Topographic effects were investigated by polishing these electrodes to surface finishes ranging from Mastermet (0.06μm chemical-mechanical silica suspension available from Buehler) to 180 grit. The impedance spectra of all samples were evaluated in aerated 0.1M sodium borate buffered to pH 7 with boric acid.

It will be shown that increased electrode roughness and chemical heterogeneity both result in impedance spectra with increased frequency dispersion. This increased frequency dispersion is evidenced by (1) a reduction in the peak height in the phase angle impedance spectra, and (2) a broadening of the phase angle peak. Additional complications in the impedance spectra arise from the appearance of a second time constant which becomes more pronounced with increased electrode roughness and chemical heterogeneity.

ACKNOWLEDGEMENTS

The financial support of the Virginia Center for Innovative Technology is gratefully acknowledged.

REFERENCES

1. J. R. Macdonald, *Impedance Spectroscopy: Emphasizing Solid Materials and Systems*, John Wiley and Sons, New York, (1987).

2. I. D. Raistrick, *Annual Review of Materials Science*, **16**, pp. 343-370, (1986).

3. R. deLevie, *Advances in Electrochemistry and Electrochemical Engineering*, **6**, edited by P. Delahay, John Wiley and Sons, New York, pp. 329-397, (1967).

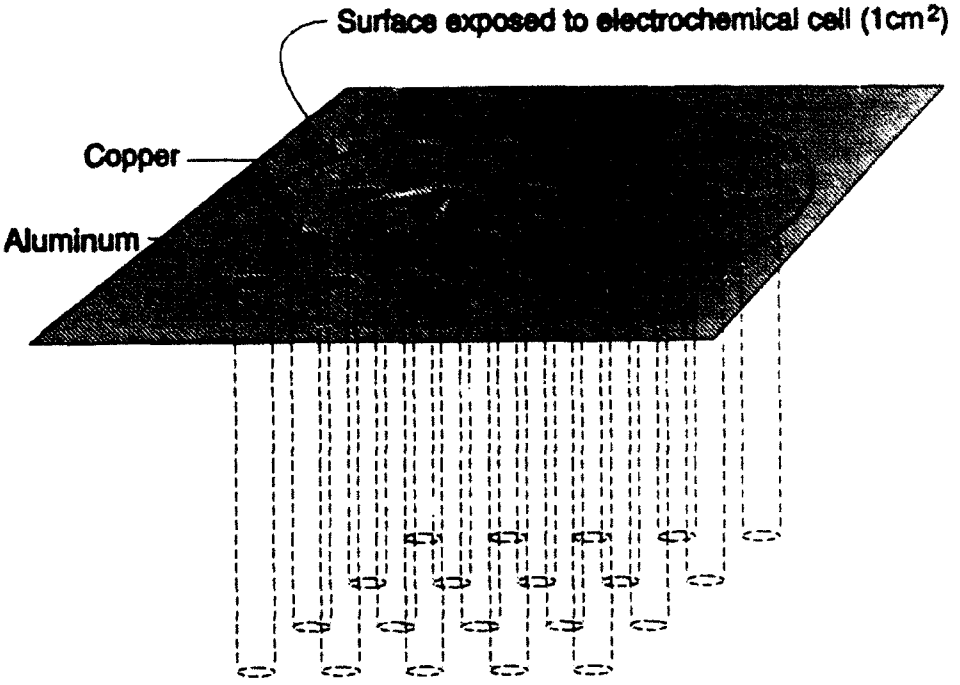

Figure 1 Schematic diagram of aluminum-copper electrodes.

A GENERALIZABLE APPROACH FOR THE ELECTRIC BEHAVIOR IN THE PRESENCE OF CONDUCTING FILMS WITH AN EXAMPLE OF GROWING FILM WITH NERSTIAN REACTIONS

D.SCHUHMANN
Laboratoire de Physico-Chimie des Systèmes Polyphasés, URA 330 CNRS, 1919, Route de Mende, BP 5051, 34033 MONTPELLIER CEDEX 01 (France).

Introduction

The "doctrine" for treating electrochemical systems which can be defined by only one interface, taking into account more or less complex kinetic steps, seems to be definitely established. The situation is not so firm for systems with several interfaces such as conducting solid films, ceramics, membranes etc... Our group was concerned with this problem when discussing impedance data obtained with a galena electrode suggesting a film growth, process met in passivation. In order to interpret the results it was first necessary to look for a rigorous general approach valid for describing systems with several interfaces, and thus not only those related to passivation. The second step was the illustration with a specific kinetic model chosen for its possible application to our data. In order to avoid confusion between the meanings of approach and model in the present context, the approach for defining a system with two interfaces (three media) will be detailed before presenting its application.

The approach

It may be summarized with five items : definition of the charge carriers in each medium ; choice of the transport equations (the simplest ones with solid films are Nernst-Planck or NP equations) and use of Coulomb's law ; definition of the chemical scheme at both interfaces ; definition of boundary conditions : the most important one, stressed by D.Macdonald and col. [1], is related to the distribution of the applied potential into three components : in the film and at both interfaces.

A model consistent with film growth

MA is a film growing at a metal electrode M with an electrolyte containing the anion A^{2-} (2 OH^- H_2O + O^{2-}). Charge carriers are vacancies V^{2+} and V^{2-} [1]. NP equations are used. Concentrations are assumed to be equal (to C) before polarization. If they are weak, Laplace's equation may be substituted to Coulomb's one. It turns out that this approximation leads in fact to a rigourous solution when the interfacial reactions are nernstian. The latter are in this model :

$$M_m <=> M_f + 2e^-_m + V_f^{2+} \qquad (I)$$

$$M_m + V_f^{2-} <=> M_f + 2e^-_m \qquad (II)$$

$$V_f^{2+} + A^{2-}_s <=> A_f \qquad (III)$$

$$A^{2-}_s <=> A_f + V^{2-}_f \qquad (IV)$$

The subscripts indicate the media (m = metal, f = film, s = solution). Couples (I) + (III) and (II) + (IV) lead to film growth and couples (II) - (I) and (III) - (IV) are equivalent to Mott-Schottky pair reaction :

$V_f^{2+} + V_f^{2-} <=> Null$ (V)

It introduces a thermodynamical constraint between the equilibrium constants of reactions (I) to (IV). Boundary conditions for the pseudo-steady state are obtained expressing balances of matter and, in the case investigated, the Nernstian character of reactions. With the latter assumption, the concentrations of vacancies remain constant and equal in the film and the interfacial potentials do not depend on the applied potential V. One finds for the current density :

$$I = 4F^2C(D_+ + D_-)(V - V_0)/(RTL) \quad (1)$$

where L is the film thickness, D_+ and D_- diffusion coefficients V_0 a constant depending on the equilibrium constants. Noting that dL/dt is in proportion with I and taking into account that reaction V occurs in new monolayers, the thickness evolution is given by :

$$L^2 = L_0^2 + h(V - V_0)t \quad (2)$$

where L_0 is the value of L at t = 0 and h a constant. The impedance at t = 0 is thus potential independent but varies with t like L. Such a result was found polarizing galena in alkaline solutions.

In general (nonnersnstian reactions), the boundary conditions to be used in the calculation of impedance are obtained equating flows at interfaces and taking into account film and double-layer capacitances. As in the case of systems with one interface, the impedance is split up into a faradaic component and a capacitive one but here the latter corresponds to the three capacitances in series.

Adding to the chemical scheme described by reactions (I) to (IV) a chemical dissolution and thus introducing the additional term -S/2 in the expression of dL/dt, a steady state is obtained and one has :

$$a : L = (h/S)(V - V_0) ; b : I = 4F^2C(D_+ + D_-)Sh/RT \quad (3)$$

S is influenced by diffusion and a limiting current I_{lim} may be obtained. In agreement with this modified model, impedances proportionnal to $(V - ct)/I_{lim}$ were found in electropolishing experiments.

Conclusion

The approach proposed seems to be quite rigourous and its application to specific models allows to interpret some experimental results without any ad hoc assumption. Attempts for applicating this approach to other kinds of systems, not only those classicaly studied in electrochemistry, are in progress.

Reference

1. C.Y.Chao, L.F.Lin and D.D.Macdonald, *J.Electrochem.Soc.*, 128, 1187 (1981).

FREQUENCY DOMAIN ANALYSIS OF PHOTOPROCESSES AT ILLUMINATED SEMICONDUCTOR ELECTRODES BY TRANSIENT TRANSFORMATION

Peter C. Searson[1] and Digby D. Macdonald[2]

[1] Department of Materials Science & Engineering, The Johns Hopkins University, Baltimore, MD 21218

[2] Center for Advanced Materials, Penn State University, University Park, PA 16802

Relaxations in photoprocesses at illuminated semiconductor electrodes are usually observed as a decay in the photocurrent, or photovoltage, as a function of time. Any attenuation in the response of a photoelectrode represents a decrease in efficiency and a limitation to performance. In order to design more efficient photoelectrodes for applications in energy conversion and photocatalysis it is essential to be able to identify the limiting processes and to determine the kinetics of the controlling reactions. Historically, techniques based on analysis of the transient response to a light pulse, or step, have been used for mechanistic evaluation. The origins of many transient effects have been identified and there are models [1,2] to describe processes such as electron hole pair generation, minority carrier diffusion, bulk recombination (e.g. radiative and Auger), recombination via surface states, and faradaic processes. Analysis of photoprocesses in the time domain is inherently limited, however, since the time constants associated with photorelaxation process span many orders of magnitude.

The photocurrent response to a perturbation in photon flux can be represented in the frequency domain by a frequency dependent quantum efficiency, $\Phi(\omega)$:

$$\Phi(\omega) = \frac{i_{photo}(\omega)}{\varphi(\omega)} \qquad \{1\}$$

where $i_{photo}(\omega)$ is the photocurrent and $\varphi(\omega)$ is the photon flux. Equation {1} can be determined from the photocurrent response to either periodic or transient excitation. Intensity modulated photocurrent spectroscopy, developed by Peter et al. [3], is an example of periodic excitation. In this case, an opto-acoustic coupler is used to generate a sinusoidally modulated light intensity and the corresponding transfer function calculated from the amplitude and phase shift of the a.c. photocurrent response as a function of the amplitude and frequency of the photon flux.

In contrast to periodic perturbation methods, transformation using transient perturbation

techniques has received very little attention in electrochemistry, although Pilla [4] has shown that transformation of the current response to a transient voltage perturbation in an electrochemical system can be performed in Laplace space:

$$F(s) = \int_0^{\infty} f(t)\, e^{-st} dt \qquad \{2\}$$

where s is the Laplace frequency ($s=\sigma+j\omega$) and f(t) is a time dependent function. In this paper, we demonstrate that a similar approach can be used to calculate, $\Phi(\omega)$, where f(t) corresponds to the time dependent photocurrent response, $i_{photo}(t)$, to a transient photon flux, $\varphi(t)$.

The imaginary axis transform is obtained by substituting $s=j\omega$ into equation {2} and rewriting in terms of real and imaginary components:

$$F(j\omega) = \int_0^{\infty} f(t) \cos(\omega t)\, dt - j \int_0^{\infty} f(t) \sin(\omega t)\, dt \qquad \{3\}$$

The frequency dependent quantum efficiency, $\Phi(\omega)$, can be determined by calculating $i_{photo}(\omega)$ and $\varphi(\omega)$ from equation {3} and substituting into equation {1}.

Real and imaginary axis transforms can be used to determine a number of diagnostic parameters related to the photoinduced reactions. Since, both response and perturbation functions are transformed and the transfer function is normalized to the frequency dependent quantum efficiency, this technique can be applied to a wide range of systems for quantitative analysis of relaxation processes, ranging from ultrafast laser pulse experiments to the analysis of interfacial processes with longer time constants. In addition, this approach can be applied to both solid state and semiconductor/electrolyte interfaces in two-electrode and three-electrode configurations.

References

1. Yu.V. Pleskov and Yu.Ya. Gurevich, *Semiconductor Photoelectrochemistry*, Consultants Bureau, New York (1986).
2. L.M. Peter, in Specialist Periodical Reports, Vol.9: Electrochemistry, The Royal Society, London (1984) p.66.
3. L.M. Peter, J. Li, R. Peat, H.J. Lewerenz, and J. Stumper, Electrochim. Acta, **35**, 1657 (1990).
4. A.A. Pilla, J. Electrochem. Soc., **118**, 1295 (1971).

A COMPARATIVE STUDY OF THE IMPEDANCE CHARACTERISTICS OF THIN REDOX-POLYMER FILMS ON ELECTRODES

Michael Sharp and Åsa Genborg

Department of Chemistry,
University of Umeå,
901 87 Umeå, Sweden

Impedance spectra were recorded over the frequency range 65kHz - 5mHz for a series of glassy-carbon electrodes coated with thin layers of Nafion and poly(styrenesulphonate), PSS, containing tris(2,2-dipyridyl)osmium(II/III) electroactive counterions in order to examine the dynamics of charge-transport within the polymer phases as a function of redox-site concentration, C_T, and the ratio of oxidised:reduced sites present, θ.
Analysis of the experimental data in terms of complex capacitance, $C^* = Y^*/j\omega$, revealed significant differences in the properties of the two systems, as illustrated by figure 1 which shows plots obtained at $C_T = 0.36M$ and at the formal potential of the incorporated redox species. Single semicircular arcs were observed for PSS films at all values of C_T, with low frequency limiting capacitances that were in accord with the total quantity of redox sites in the coating as determined from integrated cyclic voltammograms. Such results were adequately explained by a Randles equivalent circuit which included a finite transmission line terminated by an open-circuit. Although similar behaviour was found for Nafion films at low values of C_T, two (or more) arcs appeared in capacitance diagrams at high C_T indicating the presence of multiple charging processes with characteristic time constants on the order of 10^{-2} and 10 seconds. To our knowledge such phenomena have not been reported earlier.

Fig. 1

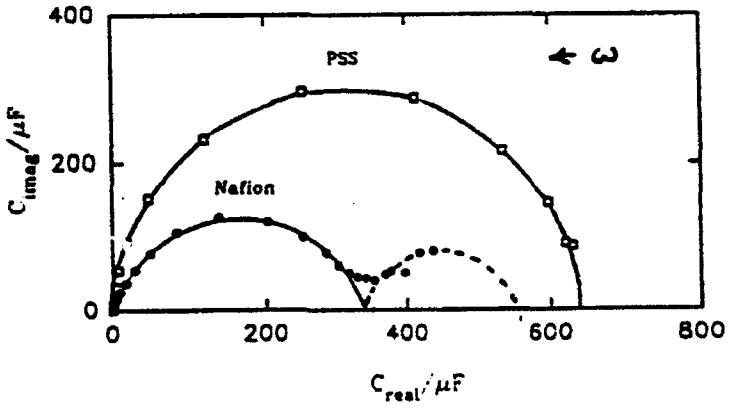

Apparent diffusion coefficients, D_E(app), which provide a measure of charge-propagation rates, were derived from impedance spectra for both systems and are plotted as a function of redox site concentration in figure 2.

Fig. 2

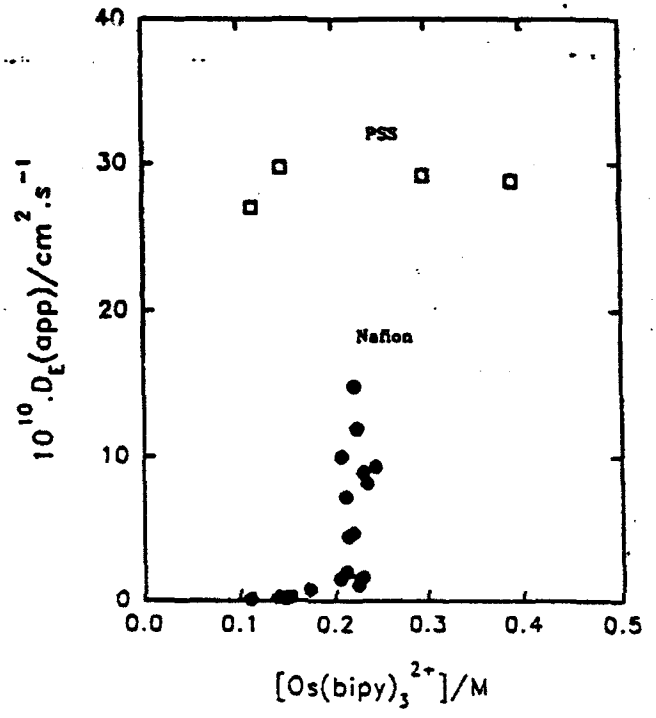

The constancy of the values found for PSS coatings suggests that physical displacements of the redox cations themselves are responsible for charge-transport. The sudden rapid increase in D_E(app) observed for the Nafion system at C_T ~ 0.2M, however, may indicate that conduction proceeds by intersite electron exchange controlled by percolation.
The significance of these results with respect to recent theoretical models of polymer-coated electrodes will be discussed.

APPLICATION OF THE AC IMPEDANCE MAPPING TECHNIQUE TO THE CORROSION DETECTION OF STEEL PIPES IN CONCRETE

M.Shibata, H.Adachi, A.Sakakura, and K.Kasahara

Fundamental Technology Research Laboratory, Tokyo Gas Company,Ltd

Corrosion of steel pipes and rebars in concrete has become a matter of worldwide real concern. Nondestructive detection methods tried so far include the application of AC impedance technique. Irrespective of its possible effectiveness, difficulty in evaluating the actual extent of corrosion damage has been preventing a practical application. Complexity in the current distribution changing for each structure of interest is thought mostly responsible. To overcome such difficulty, 3-dimensional FEM analysis may be incorporated with the conventional. In this paper, comparison is made between the observed and FEM simulated AC impedance data for an idealized piping model.

EXPERIMENTAL PROCEDURES

21 lengths of pipes (28mm diameter, 90mm length, and 79cm^2 surface area) were embedded in concrete in a straight line at regular intervals of 10mm. Lead wires fitted to each end of the unit pipe were connected to each other to obtain a total length of 210cm pipe or disconnected to simulate any particular portion in a 210cm long pipe.

Distribution of applied current was calculated from the current between each adjustment couple of pipes. AC impedance measurements were made by placing four rectangular spaced auxiliary electrodes(Pt) with one Ag/AgCl reference electrode at the center of the rectangle.

3-dimensional FEM ANALYSIS

3-dimensional FEM analyses were made by using a model composed of totalled 2932 nodes. Equivalent circuits were approximated as follows:

(1) pipe/concrete interface : a resistance in parallel with a capacitance
(2) concrete : resistance.
(3) auxiliary electrode/concrete interface : a resistance in parallel with a capacitance

RESULTS

Figure 1 shows the current distribution wherein a set of electrodes was placed immediately above the middle of the 210cm pipe. As evident in the figure, the higher the frequency, the more concentrated was outflow of the current in the vicinity of the auxiliary electrodes. The results of FEM analysis showed an excellent agreement with the observed.

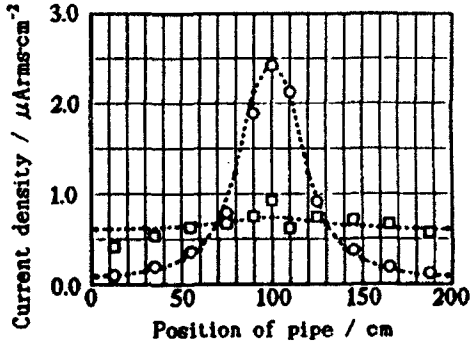

Fig. 1 Current distribution from pipe
Applied current : 1mA rms
○ : 1kHz, □ : 1mHz
Dot line : obtained from 3D-FEM analysis

CONCLUSION

A good agreement between the observed and calculated indicates the validity of the numerical model and the present developed 3-dimensional FEM program.

PARTIALLY BLOCKED SURFACE STUDIED BY THE ELECTROHYDRODYNAMIC IMPEDANCE

C.R.S. SILVA[1], O.E.BARCIA[1,2], O.R. MATTOS[1] and C.DESLOUIS[3]

1-Lab. de Corrosao "Prof. Manuel de Castro" - PEMM/COPPE/UFRJ, Cx Postal 68505, CEP 21945, Rio de Janeiro, Brazil.

2- Departamento de Fisico-Chimica-IQ/UFRJ, Rio de Janeiro, Brazil.

3-UPR 15 du CNRS "Physique des Liquides et Electrochimie", Univ. P. et M. Curie 4 Place Jussieu, 75252 Paris Cedex 05, France.

INTRODUCTION

In electrochemical systems, the interface can be non-uniformly reactive in a macroscopic sense. In this situation, there are different kinetic conditions that lead to the concept of partially blocked electrodes (1). Assessing the non-uniform reactivity is only possible when total or partial mass transfer control is effective on specific areas of the electrode. Electrochemical methods of mass transport study (Levich plots, impedance measurements) are able to reveal and, in some instances, to characterize the blocking geometry.

By using the ac impedance technique, it has been shown that diffusion control over a partially blocked electrode leads to the existence of two time constants (2), the smaller one giving a capacitive loop which could be analyzed as a kinetic one instead of a diffusion one. Also, by use of the electrohydrodynamic (EHD) method (3), a more quantitative analysis of the phenomenon can be done allowing in particular, the possibility of measuring the average dimension of the active sites from the consideration of the two diffusion time constants (4). Until now, the analyses remain qualitative in that they extrapolate results established for one site to the case of a distribution of sites.

In this work, we use an array of microelectrodes with well-defined positions to simulate real blocked electrodes. By doing so, we were able to predict quantitatively their response in a modulated flow for some regimes.

EXPERIMENTAL RESULTS AND DISCUSSION

The experimental model was obtained by covering a platinum disk electrode (area 0.38 cm^2) with a thin photosensitive resin. A photographic mask with a regular array of identical circular sites was placed against the resin and UV illumination was performed. The same pattern was used with different diameters (141, 243,419, 538 and 649 μm), defining respectively a value of the active fraction of the electrode area (2.5, 7, 21, 35, and 52%).

A fast redox reaction:

$$Fe(CN)_6^{3-} + e^- \Leftrightarrow Fe(CN)_6^{4-} \qquad \text{in KCl (M)}$$

was performed on the active sites.

In the quantative model used for the steady-state and non-steady-state conditions, it was considered that the concentration distribution over any site is not influenced by the presence of the other surrounding sites.

The plotting of the limiting diffusion current of the reduction plateau against $\Omega^{1/2}$ for the experimental results and the theoretical currents calculated with the hypothesis of

independent sites, showed that this approach is valid for the smaller sites (d=141 μm). When the diameter is higher, the interaction between the active sites becomes significant.

The EHD data obtained for each diameter at different mean angular velocities show at all frequencies a good reducibility vs the dimensionless frequency (frequency divided by the mean angular velocity). It was observed with the hypothesis of independent sites that for low frequencies the experimental curves present larger deviations with respect to the theoretical response as the diameter increases. For the diameters equal to 419 μm and 538 μm, the lower part of the diagram does not reproduce the response of the totally active disk but when the value of the active fraction is around 50% (d=649 μm), the low frequency behaviour follows that of a fully active disk and this is consistent with the fact that the steady-state current is in practice given by the Levich value over a fully active disk. In addition, the diagrams obtained with the circular disks active or with the complementary pattern are identical when the active fraction of the electrode is 50%.

Also, from the comparison between the experimental and the theoretical phase shifts it is possible to obtain an estimate of the average value of the sites dimensions (4).

CONCLUSION

In this work, we have demonstrated the possibility of using the EHD impedance technique for experimentally characterizing a partially blocked electrode by two parameters, the average dimension of active sites and the active fraction of the interface. Further approach in this direction will require both improved experimental design of the active sites for obtaining smaller and more accurately defined dimensions and more refined theory for considering in the mass transport equation the influence of the diffusion-convection terms normal to the surface.

REFERENCES

1. R.Landsberg and R.Thiele, Electrochimica Acta, 11, 1243 (1966)
2. E.Schmidt, J.Hitzig, K.Juttner and W.J.Lorenz, Electrochimica Acta, 31, 1041 (1986)
3. C. Deslouis, and B. Tribollet, "Flow modulation techniques in Electrochemistry", VCH Series, Advances in Electrochemical Science and Engineering, Eds Gerisher /Tobias Vol 2, pp 205-264 (1991).
4. A.Caprani, C.Deslouis, S.Robin and B.Tribollet, J.Electroanal chem., 238,.67-91 (1987)

RAPID CORROSION ESTIMATION IN POORLY CHARACTERIZED FLUIDS BY ELECTROCHEMICAL IMPEDANCE SPECTROSCOPY (EIS)

David C. Silverman
Monsanto Company
St. Louis, MO 63167

Rapid corrosion determination using with limited testing is often required in process evaluations. EIS can meet this need since the technique can be used to make rapid estimates of corrosion rates from 2.5×10^{-4} to 250 mm/y[1-3] while providing mechanistic information. However, characterization of the chemistry of such streams is often impossible. Thus, when EIS is used for such evaluations, linear circuit analogues often provide the only way to bridge gaps in knowledge so as to successfully predict corrosion rates from the spectra. This paper provides a practitioner's view of some strengths and limitations of using EIS for rapidly estimating corrosion in process waste streams.

Corroboration that corrosion phenomena and rates are being measured by EIS is essential because of the lack of chemical characterization of these systems. This short-coming could increase experimental complexity. However, this complexity was overcome by using independent corrosion measurements made on the same electrode. A DC generated voltage-current curve was curve-fit using Wagner-Traud theory assuming one anodic and one cathodic reaction. The resistance was compared to that determined by EIS. Corrosion rates estimated from mass loss of the electrode were also compared to those obtained by time-averaging the EIS results.

The impedance spectra were generated periodically during the 24 to 72 hour exposures. When the rotating cylinder electrode[4] was used, spectra were generated at 200 rpm, 1000 rpm, and 2000 rpm. The data were analyzed by using the four circuit analogues discussed previously[2] and by the software developed by Boukamp[5].

A failed heat exchanger had to be replaced quickly because of its critical relationship in a process. A HASTELLOY®B-2 heat exchanger was located and installed, the choice based mainly on the waste stream having 3 to 10 wt% hydrochloric acid and the extra exchanger being available. The stream also could contain small amounts of phosphorous and acetic acids. The goal was to quickly determine if the choice was appropriate using limited testing. A mechanistic study could not be undertaken.

Figure 1 shows a typical spectrum generated after 24 hours of exposure for one of the solutions. All of the spectra showed pseudo-inductive behavior. The spectra were analyzed by the method outlined by Epelboin and Keddam[6] and used previously to analyze spectra for steel in a waste stream[7]. The pseudo-inductance was not caused by non-linearity between excitation and response because the amplitude of the excitation was 5 mV. Such a small amplitude is not expected to cause such non-linearities to develop[7]. That the corrosion potential was constant suggests that the spectra were generated under steady state conditions.

The charge transfer resistance was calculated from the curve-fit. These resistances were compared to those obtained from the curve-fit of

the DC polarization results. Figure 2 shows a typical curve. Typical agreement for the three solutions tested was 4400, 1300, and 1600 ohm-cm^2 by EIS and 3800, 1500, and 1100 ohm-cm^2 by the DC technique. In addition, mass losses of the electrode were within a factor of two of those from EIS. This agreement means that corrosion rates were successfully obtained within 24 hours by EIS. Corroboration by an independent measurement was needed because of the complexity of the spectra. Note that the DC-based resistance agreed with the EIS value that was not at the limit of zero frequency. Another electro-active process with slow relaxation was probably occurring.

The ability of steel to withstand a number of environments at a waste site had to be quickly screened. The environment was an aqueous emulsion containing mud and a number of constituents which were to be biologically degraded. Corrosion in a number of these environments was estimated after various periods of biological activity. The effect of fluid motion had to be evaluated because of agitation in the "bioreactors".

The impedance spectra were generated periodically over 72 hours to insure that a steady state corrosion potential was achieved. Similar to other waste studies[2], a number of different types of impedance spectra had to be analyzed. However, most of the spectra could be fit reasonably well by the four circuit analogues previously discussed[2]. Corrosion among the environments varied over several orders of magnitude. The time averaged corrosion rates estimated from resistances extracted from EIS agreed within a factor of two with the corrosion rates estimated from mass loss of the same electrode. The important point is that once again, EIS could be used for rapid corrosion estimation in a complex environment. Corroboration from an independent measurement on the same electrode was needed to provide confidence in the result. Though this need for corroboration in these complex environments is a shortcoming of EIS, the fact that such corroboration can be provided without increasing needed test resources means that EIS can be used for practical, rapid screening of corrosion in complex systems.

1. Silverman, D. C. and Carrico, J. E., Corrosion, 44(5), 280 (1988).
2. Silverman, D. C., Corrosion, 46(7), 589 (1990).
3. Williams, D. E. and Asher, J., Corros. Sci., 24(1), 185 (1984).
4. Silverman, D. C., Corrosion, 40(5), 220 (1984).
5. Boukamp, B., "Equivalent Circuit" (EQUIVCRT.PAS), Vers. 3.97 (1989).
6. Silverman, D. C., Corrosion, 45(10), 824 (1989).
7. Epelboin, I. and Keddam. M., J. Electrochem. Soc., 117, 1052 (1970).

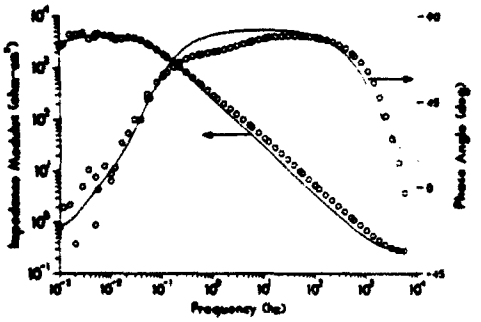

Figure 1 (Points=Measured, Lines=Calculated)

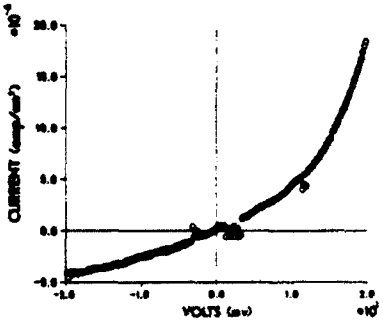

Figure 2

AN INEXPENSIVE LOW FREQUENCY IMPEDANCE ANALYZER BASED ON DIRECT SAMPLING

E. Skou

Department of Chemistry, Odense University, DK-5230 Odense M

Direct digital sampling by the use of A/D converters has not been widely used in impedance analyzers mainly due to limitations in the high frequency regime. At least two sampled points is needed during one period of the frequency to be measured (Nyquist sampling theorem). As an increase in sampling rate of A/D converters is attained at the expense of the number of effective bits, there is a trade off between speed and accuracy, which limits the frequency range which can be covered by this sort of analyzers.

If the frequency of the stimulating sine wave is known this problem can be partly overcome by the use of subsampling. By this method points are not sampled in every period of the sine, but at exactly known time intervals which do not have a simple relation to the period of the sine. In this way the original stimulus and response signals can be reconstructed mathematically and the impedance calculated from the amplitude ratio and the time difference between the two signals. The frequency range will then be limited by the accuracy of the system timer and the gate time of the A/D converter, both of which usually are orders of magnitude lower than the period of the Nyquist frequency.

In the system described, the sampling is performed with a HP6940 Multiprogrammer system equipped with a 20 kHz multiplexed A/D converter. The multiplexing makes the effective sampling rate 10 kHz. The source of the stimulating sine wave is a HP3325A frequency synthesizer and the sampled curves are fitted with a least squares sine fitting routine [1].

An algorithm is presented which, on the basis of the following conditions, calculates a combination of sampling rate and an adjusted frequency close to the set frequency:

1. At least 10 periods are sampled. If the total sampling time exceeds 10 seconds the number of sampled periods is decreased, but will always be at least one.
2. The total sampling time is always an integer multiply of 20 milliseconds. This minimizes the interference from 50 Hz noise.
3. An integer number of periods is sampled. This facilitates the determination of the signal offset and improves the accuracy of the fitting algorithm.
4. The time interval between two sampled points has no simple relation to the period of the sine. This gives a good amplitude coverage.

The systems accuracy has been tested by applying the same signal to both channels of the analyzer and compute the phase difference and amplitude ratio. The amplitude was chosen so that 75% of the input range of the A/D converters was covered. In the frequency range 100 kHz to 0.01Hz the phase difference was not greater than 0.3 deg and the amplitude difference was not greater than 0.3%. None of the figures were correlated to the frequency.

References::

[1]: P.Bloomfield: Fourier Analysis of Time Series: An Introduction p 33
John Wiley 1976

RELATION BETWEEN ADHERENCE OF A PAINT FILM AND CORROSION PROTECTION

E.Spengler, I.C.P.Margarit, O.R.Mattos

Lab. de Corrosão "Prof. Manoel de Castro", EE/UFRJ and COPPE/UFRJ, Caixa Postal 68505, CEP 21945, RJ, Brasil

INTRODUCTION

The relationship between adhesion of a paint film to a substrate and the corrosion protection of this paint film is a controversial subject in the literature (1-3).

In this paper the paint adhesion is previously defined by three surface profiles (roughness) over a carbon steel. Results for an epoxy and an alkyd paint are presented. The adhesion in this work is not used to compare the relative performance of the two paints but only to analyse if a better adhesion always implies a better corrosion protection, whatever the paint.

EXPERIMENTAL

Carbon steel (1020) samples were prepared in order to obtain different roughnesses as shown in Table I.

Table I: Measured roughness

SURFACE	ROUGHNESS
Blasting	14 ± 3 μm
60 Emery Paper Polishing	3 ± 0.3 μm
400 Emery Paper Polishing	0.2 ± 0.06 μm

Samples of each roughness were painted with epoxy and alkyd based paints. The dry thickness were those indicated by the manufacturers, respectively: 80 μm and 60 μm, obtained with at least two layers of paint. The corrosion performance of the samples was tested in salt-spray, continuous immersion monitored by impedance, 100% relative humidity chamber and natural field exposure tests. Three samples were tested for each condition and the results presented in this paper were reproduced at least twice.

The working electrolyte was 10^{-3}M of NaCl and the natural field exposure was performed in a typical marine atmosphere.

RESULTS AND CONCLUSIONS

For scratched samples all tests have shown a direct relationship between the adhesion and the corrosion attack beyond the scratch. Indeed, the blasted samples have shown less attack beyond the scratch. No difference was detected between 60 EP and 400 EP samples, in spite of the difference in roughness of the profiles.

For non-scratched samples all tests have shown an inverse relationship between the adhesion and the corrosion attack. Indeed, the blasted samples were the most corroded. The particular results concerning 60 EP and 400 EP samples is maintained: in spite of the difference in roughness of these two surface treatments polishing. the same attack was detected. By impedance it was possible to predict very soon that the blasted samples would present the worst corrosion protection.

For scratched samples the adhesion of the paint defines the corrosion progress beyond the scratch. Although, similar behaviour detected for 60 EP and 400 EP samples shows the necessity of a minimum difference in the adhesion to impose a distinct corrosion behaviour.

For non-scratched samples, the adhesion is not the most important parameter defining the paint performance. The polymer itself controls the corrosion process whatever the adhesion.

REFERENCES

1- H.Jullien, W. Funke and U.Zorll, 15th FATIPEC Congress Book, (3) III-255/III-272, 1980.
2- K.R.Gowers and J.D.Scantlebury, JOCCA, 70(3), 64/68, 1987.
3- W.Schwenk, Corrosion Control by Organic Coatings (Pap.Conf.) Houston, Texas, 103/110, 1980 (Publ. 1981).

IMPEDANCE OF POLYMER ELECTROLYTE FUEL CELL ELECTRODES

T. E. Springer*, I. D. Raistrick, S. Gottesfeld, M. Wilson and T. Zawodzinski
M.S. D429, Los Alamos National Laboratory, Los Alamos, New Mexico 87545, USA

Polymer electrolyte fuel cells (PEFCs) have a well-hydrated ionomeric membrane separating the air or oxygen cathode and the hydrogen anode structures. Carbon-supported platinum and a soluble ionomeric precursor are cast into a thin (< 5μm) hydrophilic catalyst layer that is bonded to the membrane and backed by teflonized hydrophobic carbon cloth that provides a distribution network for the reactant gases. Because of its rapid kinetics and low overpotential, the anode is ignored in this analysis. We have developed electrode models for the PEFC cathode to explain steady-state voltage-current density (V-I) measurements.[1] We have recently extended the same models to include time-dependence, and we are therefore able to calculate the ac impedance of the fuel cell cathode as a function of dc potential and frequency. An important criterion for a model is its ability to predict correctly both the dc and the ac behavior. The various models are distinguished by the oxygen path from gas inlet to the catalyst and by the ionic conduction path from membrane to catalyst.

Several different models for the cathode catalyst layer have been used previously. In our pore model[2] the gas moves at bulk concentration through macropores whose walls are coated with a thin electrolyte film through which the O_2 diffuses to the catalyst. The electrolyte film provides a distributed ionic resistance path that causes the overpotential to change along the pore depth. In a second model, based on an agglomerate structure[3] for the pore wall[4], O_2 diffuses across a thin electrolyte film and then into the wall to access catalyst distributed uniformly on carbon. In the latter case the O_2 concentration drops as it penetrates the wall, but the overpotential in the radial direction remains constant.

The present model[1] combines both concentration loss and ohmic loss within the catalyst layer using a simpler geometry. We assume a uniformly distributed and superimposed contribution from ionic and electronic conduction, O_2 diffusion, and double-layer capacitance throughout a catalyst layer with a uniform distribution of catalyst sites. The model uses "effective" diffusion coefficients and ionic conductivities that account for the mixed carbon and ionomer medium. The electrode backing layer is also included in both the steady-state and dynamic models.

In the laboratory, impedance and polarization data were obtained on 5 cm^2 cells for currents up to 10 A using a Hewlett Packard HP6060A electronic load in potentiostatic or galvanostatic mode, Stanford Research Systems SR 560 differential preamplifiers (which matched), and either a Solartron 1250 or a Voltech TF 2000 frequency response analyzer. Instrumentation and data collection were managed by National Instruments LabVIEW 2 software on a Macintosh IIx computer. Figure 1 shows typical impedance data for a PEFC (80°C) with 3 atm of H_2 (anode) and 5 atm air (cathode) for various iR-corrected cell voltages along the V-I curve of Fig. 2. We will show model predictions of this and other data.

ACKNOWLEDGMENT: This work was supported by the U.S. Department of Energy, Office of Transportation Technology.

REFERENCES:

1. T. E. Springer and S. Gottesfeld, in "Proceedings of the Symposium on Modeling of Batteries and Fuel Cells" , R. E. White, M. W. Verbrugge and J. F. Stokel, Editor, PV 91-10, p. 197, The Electrochemical Society , Pennington, NJ (1991).

2. T. E. Springer and I. D. Raistrick, *Proc. Electrochem. Soc. Symp. on Electrode Materials & Processes for Energy Conversion,* (Philadelphia, May 11-14, 1987). The Electrochemical Society, 1987.

3. J. Giner and C. Hunter, *J. Electrochem. Soc.* **116**,1124 (1969).

4. T. E. Springer and I. D. Raistrick, *J. Electrochem. Soc.* **136**,1594 (1989).

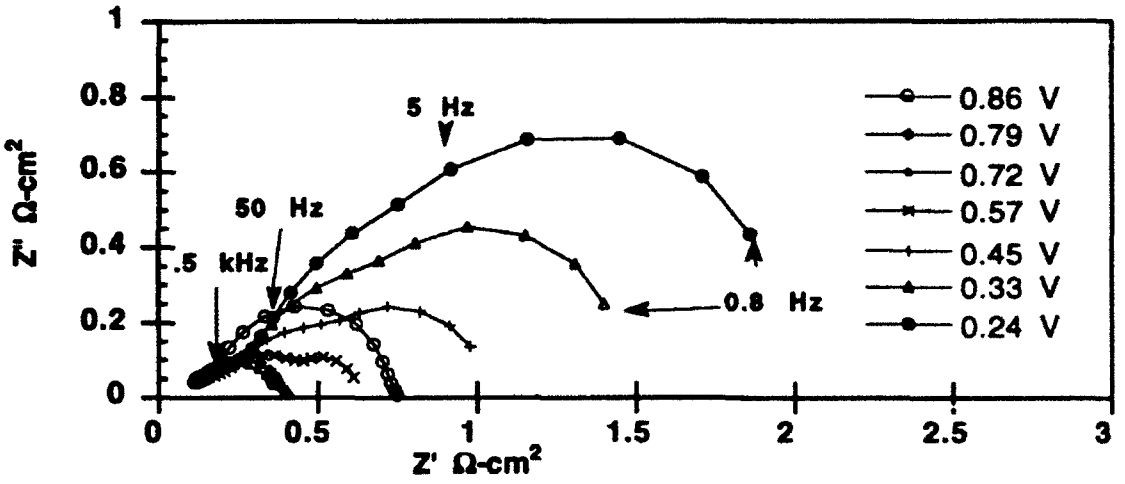

Figure 1. Measured impedance of a 5-cm^2 PEFC with a 5 atm air cathode for various iR-corrected cell voltages.

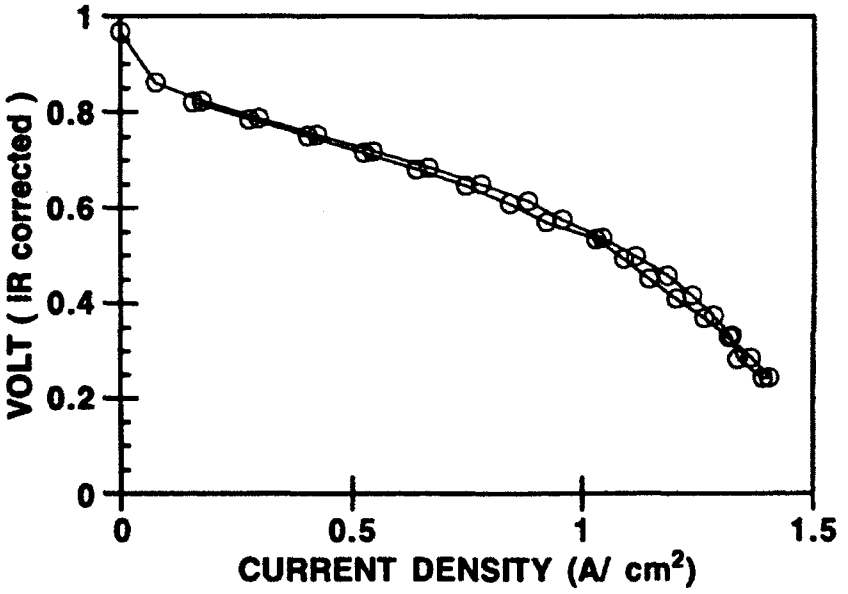

Figure 2. Polarization curve, iR corrected, corresponding to the impedance measurements in Figure 1.

THE EFFECT OF PARASITIC CONDUCTION PATHWAYS ON EIS MEASUREMENTS IN LOW CONDUCTIVITY MEDIA

Kevin C. Stewart, David G. Kolman, and S. Ray Taylor
Center for Electrochemical Science and Engineering
University of Virginia
Charlottesville, Virginia 22903

Artifacts are ubiquitous to electrochemical impedance measurements at sufficiently high frequency. These artifacts can arise from the measurement electronics, the reference electrode, the electrical leads, and/or the electrochemical cell. In high conductivity electrolytes under optimum measurement conditions, artifacts occur at frequencies well above the point where the solution resistance can be resolved, and the artifact is simply ignored. However, in low conductivity electrolytes (e.g. lake water, glacial acetic acid) impedance spectra can be corrupted with artifacts down to 100 Hz or less, which can mask or distort the interfacial response. One explanation for this behavior is that the low conductivity media unmask parasitic pathways within the measuring equipment and electrochemical cell. Previous models by others that have attempted to incorporate parasitic pathways in the cell have not been universally applicable to all systems. This may possibly be due to the exclusion of contributions from within the measuring equipment. The goal of the present research is to develop a universal and portable model which can be used to extract artifactual data from impedance spectra collected in any low conductivity electrolyte.

This study has systematically examined the factors which may contribute to the occurrence of artifacts in low conductivity media. The frequency regime over which artifacts exist was identified for steel in lake water. The value and occurrence of the solution resistance was identified by adjusting the conductivity using either KCl, sodium molybdate or deionized water and comparing the results with calculated values. Possible contributions from the frequency response analyzer, potentiostat, reference electrode, and cell geometry were studied using a series of test resistors. The major contributors to artifacts appear to arise from the potentiostat and associated leads. In addition, the magnitude of the test resistor, the selected current measuring resistor, and the ratio of the resistances between the working and reference and the reference and counter electrodes have been found to contribute to the artifacts. The problem of fitting complex spectra was approached by combining nodal analysis with simplex fitting. A model for a particular make of potentiostat was determined which accurately reproduces the spectra for a set of current measuring resistors used in the voltage drop configuration for two electrode measurements.

Present work seeks to model the virtual earth voltage measuring

configuration as well as three electrode systems. Tests will seek to prove that corrupted data may be deconvoluted from impedance spectra with the use of the circuit models. Initially, experiments incorporating a model electrochemical interface including test resistors and capacitors will be employed. Additionally, an actual electrochemical interface comprising a redox reaction will be studied.

Modeling of the measuring electronics is required as an initial step in analyzing the source of artifacts in an EIS system. Once the electronics are accounted for, contributions from the electrochemical cell may be then quantified so that accurate data may be acquired from corrupted spectra.

NONSTATIONARY IMPEDANCE SPECTROSCOPY :

THEORY AND APPLICATION

Z. Stoynov

Central Laboratory of Electrochemical Power Sources
Bulgarian Academy of Sciences,1113 Sofia,Bulgaria

Developed on the base of the Transfer Function Theory the classical Electrochemical Impedance Spectroscopy (EIS) treats stationary and linearized systems. Many electrochemical systems however contain interesting time-varying phenomena which cannot be simplified as quasi-stationary. To enable the study of such objects the development of tools for nonstationary impedance spectroscopy is quite desirable.

Two main problems arise in this context. The first one is connected with the mode of the consecutive frequency sweep typical of EIS. As a result the data measured are corrupted by typical errors caused by the system evolution during the experiment. An efficient method for solving this problem, called Four - Dimensional Analysis was developed and successfully applied.

The second problem of treating nonstationary systems is related with the mathematical basis - Fourier Transform(FT) of the EIS. The detailed analysis shows that under nonstationary conditions FT becomes an erroneous,biased and inefficient estimator.As a result the theoretical framework of the classical EIS is restricted to stationary objects.

To overcome this limitation a new mathematical transform was created. Named Rotating Transform, this new mathematical basis allows the measurement of intrinsically nonstationary signals and the development of a theory of Nonstationary Impedance Spectroscopy.The key notion of this new method is the INSTANTANEOUS IMPEDANCE - a momentum projection on the frequency domain of the system nonstationary state.

Measured by the Rotating Transform, these instantaneous data should be compared to instantaneous impedance models also derived on the basis of the Rotating Transform.The development of these impedance models must take into account the nonstationary conditions and the new transform properties.

The first steps in this direction have been made successfully. The general conclusion is that under nonstationary conditions the structures of the models are more complicated. The stationary structure of the model is complicated by second "ghost" substructure resulting from the derivatives of the nonstationary phenomenon. Typically this "ghost" structure is in quadrature of the basic stationary one.

A DISCUSSION ON THE MOLECULAR BASIS FOR USING ELECTROCHEMICAL IMPEDANCE SPECTROSCOPY TO ESTIMATE COATING AND CORROSION PARAMETERS

W. Stephen Tait, Ph.D.
S. C. Johnson & Son, Inc.
1525 Howe St.
Racine, WI 53403

Extended Abstract

Electrochemical impedance spectroscopy (EIS) spectra often contain responses for more than one chemical or electrochemical process. In this paper EIS spectra from four systems are discussed in terms of electrical double layer theory[1] and the capacitive nature of organic coatings: a) a coated metal exhibiting single time constant capacitive dielectric behavior, b) a coated metal exhibiting triple time constant capacitive dielectric behavior, c) a coated metal in which undercoating metallic corrosion occurs, and d) polycrystalline steel exposed to etching solution.

It has been demonstrated that when organic coated, tinplated steel exhibits capacitive dielectric behavior after 100 days exposure that no undercoating steel corrosion is observed.[2] Electrolyte is present in the coating in this situation, but it is dispersed through-out the coating.[3] When more than one time constant is observed in the EIS spectrum (for capacitive dielectric behavior) it has been proposed that the different time constants arise from variations in coating thickness. Measurements of coating thickness using an Elcometer 300 coating thickness gauge demonstrated that different coating thicknesses were indeed present.[4]

When sufficient water collects at the coating/metal interface, metallic corrosion occurs.[5] Because electrical double layer capacitances for metallic corrosion are on the order of microfarads/cm^2, and capacitances for coatings are on the order of nanofarads/cm^2, [6] the difference between their corresponding time constants is large enough that separate responses are observed in the EIS spectrum, corresponding to the coating and metallic corrosion.

Nital etchant is used to enhance the grain structure of polycrystalline metals such as mild steel.[7] SEM photomicrographs of a Nital etched mild steel surface revealed that grain details were the result of various grains, presumably different crystal orientations, corroding at different rates. Thus it was hypothesized that several time constants should be observed in EIS data gathered from mild steel exposed to Nital. This was indeed the case. Consequently it is proposed that in this situation the different time constants corresponded to different electrical double layer structures (resistances and capacitances) associated with each crystal orientation.

References

1) J. O'M. Bockris and A. K. N. Reddy, *Modern Electrochemistry*, **Vol. 2**, pp. 623 - 844, Plenum Press, NY (1970)

2) W. S. Tait and J. A. Maier, *J. Coatings Technol.*, **62**(781), pp. 41 - 44 (1990)

3) H. Leidheiser, Jr., *Corrosion*, **39**(5), p. 189 (1983)

4) W. S. Tait, K. A. Handrich and J. A. Maier, *Advances in Accelerated Testing and Coating Characterization, Proceedings of the SSPC Evaluation and Durability Conference*, **SSPC 91-15**, April 29 - May 3, 1991, Pittsburgh PA., Steel Structures Painting Council, Pittsburgh, PA (1991)

5) H. Leidheiser Jr., private communication, September 1986.

6) W. S. Tait, K. A. Handrich, S. W. Tait and J. W. Martin, (to be published in an ASTM special technical publication)

7) G. Petzow, *Metallographic Etching*, p. 27, American Society for Metals, Metals Park OH (1976)

STUDY OF THE ELECTROCHEMICAL GRAFTING AND THE GROWTH OF POLYMERS ON METALLIC SURFACE BY IMPEDANCE SPECTROSCOPY

J. Tanguy, A. Servais, G. Lécayon

DSM/DRECAM/SRSIM, C.E. Saclay
F.91191 Gif sur Yvette, France

Under cathodic polarization some monomers dissolved in an appropriate electrolytic solution can be grafted and polymerized on a metallic electrode. That is the case of the acrylonitrile monomer whose large dipolar moment can be oriented in the high electrical field in the double layer formed at the metal solution interface. In the same time the molecule can be electrochemically reduced at the electrode in order to form an anionic specie chemically bounded to the metal. This anionic specie serves as the first step for a classical anionic electropolymerization which leads to a polyacrylonitrile polymer strongly bounded to the metallic subtrate (nickel for instance) [1]. The chemical bonding on the metal gives to this polymer interesting properties by comparison with other deposition techniques. Electrochemical impedance spectroscopy was used in order to understand the electrochemical polymerization mechanism as well as to study the electrical properties of the polymer layers.

Firstly the impedance diagram obtained on an electrode coated with polyacrylonitrile when using acetonitrile as the solvent in the electrolyte (the same solvent is used for the electropolymerization) is very similar to the diagram obtained on the bare metal before the deposition of the polymer. In other words, the swelling property of acetonitrile makes the polymer "transparent" to the electrolyte and the capacitance of the double layer on the metal can be measured by impedance through the polymer. As a result the difference observed between the capacitance measured on the bare metal before deposition of the polymer and the capacitance measured on the metal coated with the polymer leads to estimate the part of the metallic surface which has been grafted during the electropolymerization.

In fact information on the grafting ratio on a metallic surface is very important in order to understand the polymerization mechanism as well as the structural properties and the electrical properties of the polymer layers. For example it appeared that the grafting ratio was dependent on the monomer concentration in the electrolytic solution used for polymerization and this result allows to make clear the differences in the morphology of the polymers obtained with various monomer concentrations. On the other hand the impedance results allowed us to give a correct interpretation of the different electrochemical characteristics (current-potential curves and current-time curves) recorded during the electropolymerization in various conditions [2].

---

[1] G. Lécayon, P. Viel, C. Le Gressus, C. Boiziau, S. Leroy, C. Reynaud
Journal de Chimie Physique, 1984, 84, n° 2, 260, 267.

[2] P. Viel, Thèse Paris VI, 1990.

THE DETECTION AND ANALYSIS OF CHEMICAL AND ELECTROCHEMICAL DAMAGE IN BMI/GRAPHITE FIBER COMPOSITES USING EIS

S.R. Taylor, D.F. Wall, and G.L. Cahen, Jr.
Center for Electrochemical Science and Engineering
University of Virginia
Charlottesville, VA 22903

The selection of polyimides as a matrix material in graphite fiber composites has been based on the mechanical stability of this polymer system at elevated temperature. The high cross-linking density and high glass transition temperatures (typical T_g between 200° and 400° C) allow retention of mechanical properties at temperatures approaching T_g, and have made polyimide based composites attractive for use as air frictional surfaces and engine components in the aerospace industry. While the analysis of structural stability of these materials has focused on the effects of temperature, loading, and fatigue, it is becoming evident that the impact of moisture, pH and electrochemical polarization must also be considered when projecting long term mechanical integrity.

The degradation of bismaleimide (BMI)/graphite fiber composites when galvanically coupled to an active metal has been a focal issue in the use of high temperature PMC's in the aerospace industry. Recent observation of electrochemically derived damage in these materials has prompted the need for methodologies to sensitively detect and quantify material changes under a variety of environmental conditions, as well as provide insight into the damage mechanism.

Electrochemical impedance spectroscopy (EIS) was used in this study to monitor changes in a BMI/graphite fiber composite resulting from cathodic (-0.050 to -1.7 V_{SCE}) and anodic (1.5 V_{SCE}) polarization, exposure to caustic solutions (0.01M to 4M), and galvanic coupling to various metals (aluminum, steel, copper, and titanium). All test samples were unidirectional, 0°, 8-ply composites made from Im7 fibers and 52504 bismaleimide resin. All EIS tests were performed in a three electrode configuration under potentiostatic control at open circuit (0 V_{SCE}) in 3.5 weight percent NaCl (25° C).

EIS was found to both sensitively detect interfacial changes in the material and possibly differentiate modes of material damage. For a given test condition (e.g. cathodic polarization), EIS spectra were found to change in a manner consistent with the severity of the environmental stress. Impedance spectra indicate interfacial alterations at extremely low overpotentials (20 mV), low caustic concentration (10 mM), and attachment to titanium, a material previously believed to provide a benign couple. More importantly, each test condition (e.g. cathodic polarization, anodic

polarization, caustic, and galvanic coupling) produced distinctive changes in the spectra characteristic to the test condition. It is believed that these characteristics changes are indicative of the damage mode (e.g. fiber/matrix attack) and indirectly indicative of the responsible electrochemical mechanism.

Spectra of composite samples which had been cathodically polarized demonstrated changes suggestive of porous electrode behavior (1-3). It is proposed that this behavior results from attack of the BMI at the fiber/ matrix interface by cathodically generated species. Although OH^- is typically enlisted as the aggressive species, exposure to caustic solution reveals a very different damage "signature" which suggests uniform ablation. It is quite possible that cathodic polarization produces peroxide and superoxide radical intermediates (4) that act as the degrading species which may account for the difference between impedance spectra of cathodic and caustic exposure. Spectra following anodic polarization indicate that uniform ablation of both phases may be occurring, and spectra of galvanically coupled samples demonstrated behavior of both anodic and cathodic polarization.

Additional evidence to support the idea that cathodic polarization causes porous electrode behavior comes from calculations of electrolyte penetration based on changes in the phase angle response and the theoretical impedance response for rough surfaces (3). This method has the inherent advantage in that the phase angle is an intrinsic parameter which does not depend on sample size or fiber numbers. Extrapolation of penetration rates determined from 24 hours of cathodic polarization correspond to penetration rates collected for 12 month exposures of galvanically coupled composites. Present research is focused on performing supportive experiments to verify the interpretation of impedance spectra.

References

1. R. de Levie, *Electrochimica Acta*, **8**:751-780 (1963).

2. R. de Levie, *Electrochimica Acta*, **9**:1231-1245 (1964).

3. R. de Levie, *Electrochimica Acta*, **10**:113-130 (1965).

4. E. Yeager, J.A. Molla and S. Gupta, "The Electrochemical Properties of Graphite and Carbon", in *Proceedings of the Electrochemical Society*, Vol 84-5, p.123 (1984).

EIS STUDY ON THE SOLUBILITY AND DIFFUSIVITY OF O_2^- AND CO_2 IN MOLTEN CARBONATES

Isamu Uchida, Kohta Yamada and Tatsuo Nishina
Department of Molecular Chemistry and Engineering,
Faculty of Engineering, Tohoku University,
Aramaki-Aoba, Aoba-Ku, Sendai 980, JAPAN

The kinetics of gas electrode reactions in molten carbonate, particularly of oxygen reduction (reaction (1)) are very important for understanding the electrode processes in the MCFC. In our earlier paper, we reported the the kinetic parameters of the oxygen reduction at Au[1, 2] and conductive oxides electrodes[3] at an atmospheric pressure, and proved conclusively that the exchange current density i_o was found to be of the order of 10 mA/cm^2, which was much larger than the previously reported values by Appleby and Nicholson[4]. Recently, we also applied the electrochemical impedance spectroscopy (EIS) for the precise measurement of Warburg coefficients and analyzed apparent Warburg coefficients (σ_{app}) in terms of $C\sqrt{D}$ values of the electroactive species in alkali carbonate melt[5]. We concluded that the oxygen reduction reaction proceeds with the superoxide path (SOP), involving the mixed diffusion of O_2^- and CO_2 for alkali carbonate melts of several compositions under moderate partial pressures (0.1-0.9 atm) at temperatures of 600-800°C.

$$\frac{1}{2}O_2 + CO_2 + 2e \rightarrow CO_3^{2-} \quad (1), \qquad 3O_2 + 2CO_3^{2-} \overset{K_1}{\rightleftarrows} 4O_2^- + 2CO_2 \quad (2),$$

$$\left[O_2^-\right] = K_1 P_{O_2}^{0.75} P_{CO_2}^{-0.5} \quad (3), \qquad O_2^- + 2CO_2 + 3e \rightarrow 2CO_3^{2-} \quad (4).$$

The above analysis of Warburg coefficients enables us to go further in to the $C\sqrt{D}$ value analysis. Based on the reaction(4), the apparent Warburg coefficient may be expressed as follows.

$$\sigma_{app} = \frac{RT}{3^2F^2\sqrt{2}K_1P_{O_2}^{0.75}P_{CO_2}^{-0.75}\sqrt{D_{O_2^-}}} + \frac{RT}{1.5^2F^2\sqrt{2}K_hP_{CO_2}\sqrt{DCO_2}} \quad (5)$$

$$\sigma_{app}P_{CO_2} = \frac{RT}{3^2F^2\sqrt{2}K_1\sqrt{D_{O_2^-}}}P_{O_2}^{-0.75}P_{CO_2}^{1.5} + \frac{RT}{1.5^2F^2\sqrt{2}K_h\sqrt{DCO_2}} \quad (6)$$

Thus, the $K_1\sqrt{D_{O_2^-}}$ and $K_h\sqrt{DCO_2}$ values can be determined from the slope and the intercept of the plot using equation(6), and the results are shown in Fig.1 and Fig.2 which are Arrhenius type plots for $K_1\sqrt{D_{O_2^-}}$ and $K_h\sqrt{DCO_2}$, where K_h is the Henry coefficient for CO_2.

As shown in Fig.1, $K_1\sqrt{D_{O_2^-}}$ shows good linearity over the entire temperature range used in this study. According to the heat of activation ($\Delta H^{\neq}$) of $K_1\sqrt{D_{O_2^-}}$, the melts used in this study may be categorized in two groups. One is that of the $(Li+K)CO_3$ binary systems, with $\Delta H^{\neq} \cong$ 100 kJ/mole; the other is that of the $(Li+Na)CO_3$ and $(Li+Na+K)CO_3$ with $\Delta H^{\neq} \cong$65 kJ/mole. The temperature dependence of $K_h\sqrt{DCO_2}$ is more complicated than that of $K_1\sqrt{D_{O_2^-}}$, as shown in Fig.2. The data for (62+38)mol% $(Li+K)CO_3$ show a split around 700°C: at higher temperatures the activation energy $\Delta H^{\neq}$ is 180 kJ/mole, while at lower temperatures it is 34 kJ/mole. We already reported a similar behavior of T/σ_{app} values for the oxygen electrode in (42.7+57.3)mol% $(Li+K)CO_3$ [2], and both findings agree quite well. In our previous paper[2], the gas composition of O_2 and CO_2 was fixed at P_{O_2}=0.9 atm and P_{CO_2}=0.1 atm, so that it was impossible to determine which species dominates the overall process of oxygen reduction. From the present work, it is clear that CO_2 limits the overall process of oxygen reduction.

Similar analysis of Warburg coefficients also applied to the oxygen electrode under pressurized conditions up to 5 atm in (62+38)mole% $(Li+K)CO_3$ at 923K to elucidate the pressurizing effect on molten carbonate fuel cell (MCFC) performance. Again, only the SOP involving the mixed diffusion of O_2^- and CO_2 can explain the reaction order of σ_{app}. The $K_1 \cdot \overline{D_{O_2^-}}$ and $K_h \cdot \overline{D_{CO_2}}$ values thus obtained agreed well with those from the atmospheric pressure as $K_1 \cdot \overline{D_{O_2^-}} = 2.135\times10^{-10}$ mole/$cm^2atm^{0.25}s^{0.5}$ and $K_h \cdot \overline{D_{CO_2}} = 7.315\times10^{-9}$ mole/$cm^2atm^1s^{0.5}$. Using $K_1 \cdot D_{O_2^-}$ and $K_h \cdot D_{CO_2}$ values thus determined, we calculated the diffusion impedance of O_2^- and CO_2 individually, and found that the 15% CO_2+Air is more suitable to reduce the cathode overvoltage in MCFC operation than 30% CO_2+Air which is used in the today's MCFC development. It was concluded that the diffusion of O_2^- is a controlling factor of the overall reaction process, and performance gain of MCFC by pressurized operation is ascribed to the increase of O_2^- concentration.

Thus, the $K_1 \cdot \overline{D_{O_2^-}}$ and $K_h \cdot \overline{D_{CO_2}}$ values determined in this work give the quite important information about the optimum operating conditions of MCFC system.

REFERENCES

1. I. Uchida, T. Nishina, Y. Mugikura and K. Itaya, *J. Electroanal. Chem.*, **206**, 229(1986).
2. I. Uchida, T. Nishina, Y. Mugikura and K. Itaya, *J. Electroanal. Chem.*, **209**, 125(1986).
3. I. Uchida, Y. Mugikura, T. Nishina and K. Itaya, *J. Electroanal. Chem.*, **206**, 241(1986).
4. A.J. Appleby and S.B. Nicholson, *J. Electroanal. Chem.*, **53**, 10(1970), **83**, 309(1977), **112**, 71(1980).
5. T. Nishina and I. Uchida, Proceedings of the Second Symposium on Molten Carbonate Fuel Cell Technology, Proc. Vol.90-16, The Electrochemical Society, Pennington, NJ., p.438-453(1990).

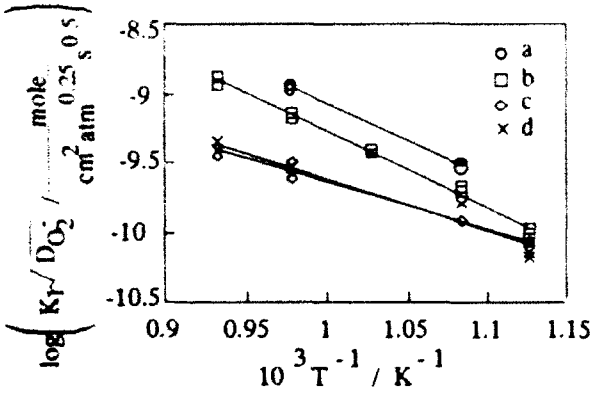

Fig.1 $K_1\sqrt{D_{O_2^-}}$ values for several carbonate melts as a function of temperature.
a-d; (35+65)mol% $(Li+K)CO_3$,
(62+38)mol% $(Li+K)CO_3$,
(52+48)mol% $(Li+Na)CO_3$,
(43.5+31.5+25.0)mol%$(Li+Na+K)CO_3$.

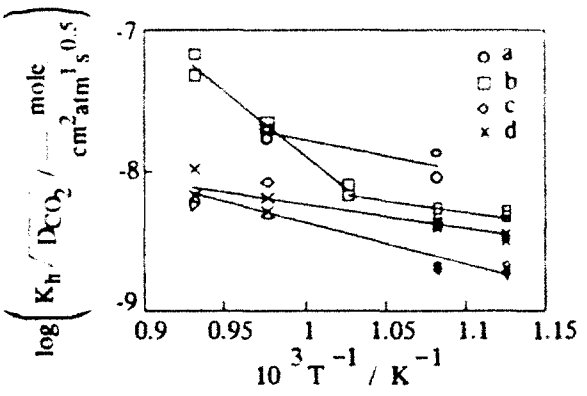

Fig.2 $K_h\sqrt{D_{CO_2}}$ values for several carbonate melts as a function of temperature.
a-d; (35+65)mol% $(Li+K)CO_3$,
(62+38)mol% $(Li+K)CO_3$,
(52+48)mol% $(Li+Na)CO_3$,
(43.5+31.5+25.0)mol%$(Li+Na+K)CO_3$.

KINETIC STUDY OF POROUS ELECTRODES IN MOLTEN CARBONATE FUEL CELL SYSTEM BY POLARIZATION MEASUREMENTS AND AC IMPEDANCE SPECTROSCOPY

Isamu Uchida, Göran Lindbergh and Tatsuo Nishina
Department of Molecular Chemistry and Engineering,
Faculty of Engineering, Tohoku University,
Aramaki-Aoba, Aoba-Ku, Sendai 980, JAPAN

The analyses of steady-state polarization data and electrochemical impedance spectroscopy data for porous gas diffusion electrodes used in molten carbonate fuel cells generally becomes not only rather complicated but also difficult, since many of the kinetic parameters are unknown. An additional difficulty arises from the fact that the actual geometry of these electrodes are not sufficiently well examined. Many of the kinetic parameters can be obtained from analyses of data from nonporous electrodes. However, the difficulties related to experimental work in the molten carbonate system have so far mainly restricted the evaluation of kinetic data to flat electrodes in an excess of electrolyte. The conditions in a porous gas diffusion electrode are quite different and it is important to verify the validity of the kinetic parameters also at these conditions.

In order to overcome some of the difficulties related to analyses of data from real MCFC cathodes, while at the same time preserve some of the important features of a porous electrode, a simpler geometry has been used and only the cathode reaction,

$$\frac{1}{2}O_2 + CO_2 + 2e \rightarrow CO_3^{2-} \qquad (1),$$

has been analyzed in this investigation. The electrode consisted of a sintered structure of equally sized gold spheres, plated with a thin layer of nickel.

In the literature, analyses of the current-potential behavior of MCFC electrodes by means of the thin film model[1,2] and the agglomerate model[3,4] can be found. The later model is considered to better represent the actual geometry of the electrode, but the thin film model has the advantage of greater simplicity. For the evaluation of data in this work, the thin film model was used. In an electrode consisting of gold spheres, the electrochemical reactions can only proceed on the surface of the large solid particles. By assuming that these are covered with a electrolyte film of uniform thickness, the thin film model can be considered to well represent the actual geometry of the electrode. For steady-state conditions the use of this model is well known[1,2], and need not to be further described here.

There are few results for the use of impedance spectroscopy for the analyses of porous MCFC electrodes reported in the literature. Selman et. al.[5] have shown the general usefulness of the method. However, the analyses was mainly restricted to evaluation of the relative importance of of kinetic and mass transfer to the total reaction rate. In this work the impedance data have been analyzed by means of a thin film model, as outlined by Raistrick[6]. Following Raistrick's approach, the total impedance of a porous electrode can be calculated by solving the differential equations

$$\frac{d\bar{i}}{dx} = -\frac{s}{Z_t}\bar{\eta} \qquad \frac{d\bar{\eta}}{dx} = -\frac{1}{\kappa_{eff}}\bar{i} \qquad (2)$$

where k_{eff} is the effective conductivity of the electrolyte thin film inside the electrode, s the specific surface area, L the electrode thickness, x the distance in axial direction of the pores and x=L at the electrolyte tile, $\bar{i}$ the Laplace transformed current density perturbation, $\bar{\eta}$ the Laplace transformed overvoltage perturbation, and Z_t the total local impedance, including the local Faradaic impedance and the double layer capacitance. At the open circuit potential, these equations can be solved analytically for the total impedance as follows.

$$Z_{tot} = \sqrt{\frac{Z_t}{s\,\kappa_{eff}}}\coth\left(L\sqrt{\frac{s}{Z_t\,\kappa_{eff}}}\right) \qquad (3)$$

The analyses can be extended for an electrode at polarized conditions. The local Faradaic impedance is then no longer constant but changes with position in the electrode, since it is a

function of the overvoltage and the concentration of reacting species at the electrode surface. Thus, in order to calculate the impedance the steady-state potential distribution must first be known. Once this has been obtained, the total impedance can be calculated by a complex numerical integration of eq.(2) over the thickness of the electrode.

The steady-state polarization behavior, as well as the impedance at open circuit potential and for polarized conditions have been examined. The experiments have been performed in (62+38)mole% $(Li+K)CO_3$ for different gas compositions and in the temperature range of 550-650°C. The experimental impedance data were fitted to the theoretical model by means of a non-linear least square method. It was found that the model quite well could be used to simulate the behavior of the porous cathode. Fig.1 shows three sets of experimental data for different gas composition fitted with the same set of kinetic parameters, assuming the superoxide path,

$$3O_2 + 2CO_3^{2-} \overset{K_1}{\rightleftarrows} 4O_2^- + 2CO_2 \qquad (4),$$

$$\left[O_2^-\right] = K_1 P_{O_2}^{0.75} P_{CO_2}^{-0.5} \qquad (5).$$

$$O_2^- + 3e \rightarrow 2O^{2-} \qquad (6),$$

$$O^{2-} + CO_2 \rightleftarrows CO_3^{2-} \qquad (7).$$

The kinetic parameters thus obtained were compared with the data of Au flag electrode, and they showed reasonable agreement. This indicates that the same mechanism dominates the reaction for both conditions and that kinetic parameters obtained on Au flag electrode also can be used in order to describe the porous electrode system.

The validity of experimental impedance data has been examined by means of Kramers-Kronig transforms, and found that the validity of data is good except for the low frequency region. This disagreement indicates that these data could be less accurate. This could also explain the deviation between experimental and fitted data in this frequency region as shown in Fig.1.

REFERENCES

1. G. Wilemski, *J. Electrochem. Soc.*, **130**, 117 (1983).
2. J. Jewulski and L. Suski, *J. Appl. Electrochem.*, **14**, 135 (1984).
3. C. Y. Yuh and J.R. Selman, *J. Electrochem. Soc.*, **131**, 2062 (1984).
4. H. R. Kunz and L. J. Bregoli, *J. Electrochem. Soc.*, **131**, 2815 (1984).
5. C. Y. Yuh and J.R. Selman, *AIChE Journal*, **34**, 1949 (1988).
6. I. D. Raistick, *Electrochim. Acta*, **35**, 1579 (1990)

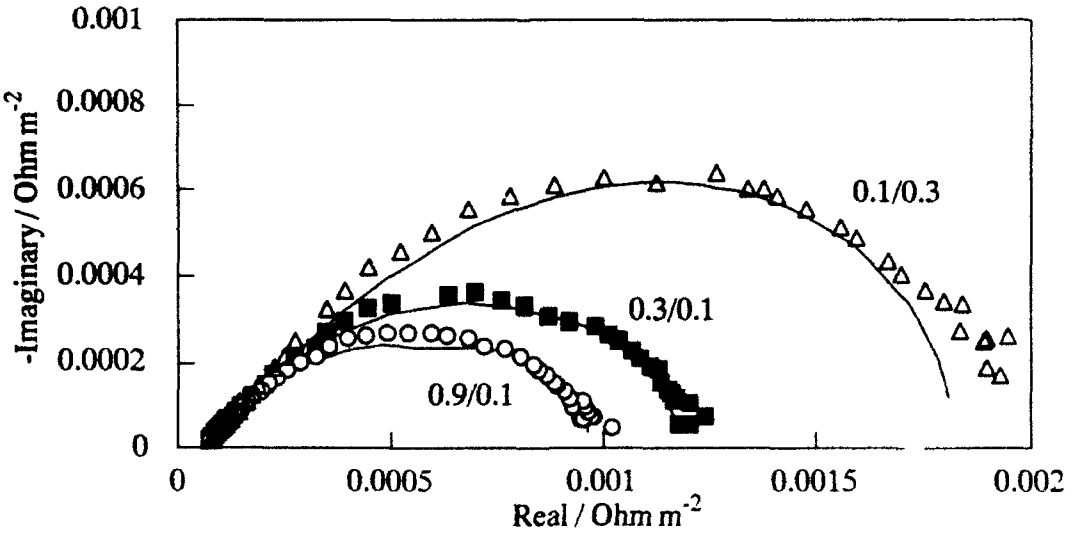

Fig.1 AC-impedance spectra for a porous electrode at open circuit potential at different gas compositions (O_2/CO_2) as indicated in the figure at 650°C. Dots are experimental data and solid lines are fitted data.

ELECTROCHEMICAL IMPEDANCE SPECTROSCOPY OF A YTTRIA-STABILIZED ZIRCONIA CELL AT HIGH OXYGEN PRESSURES

M. L. Underwood, R. M. Williams, D. J. Clark, R. W. Losey, and J. W. Suitor

Jet Propulsion Laboratory
California Institute of Technology
4800 Oak Grove Drive
Pasadena, CA 91109

Spacecraft sensor cooling using Joule-Thomson expansion gas coolers is considered the cooling choice for long life performance. A zirconia based solid electrolyte could be used in the compressor stage of the cooler. A study was conducted to examine the feasibility of such a compressor. In the experimental test, the oxygen inlet pressure was maintained at 7.8 atm, and the discharge pressure was increased to 32 atm by the solid electrolyte compressor. However, the power consumed by the compressor was 4 to 10 times the predicted requirement based on the resistance of zirconia alone. We used *dc* current-voltage curves and Electrochemical Impedance Spectroscopy (EIS) to elucidate the areas of high cell resistance and to give direction to future work.

The zirconia oxygen pump pressure system consisted of a closed end yittria-stabilized zirconia tube with interior and exterior electrodes deposited from platinum ink. The 12 cm^2 external electrode was contacted with a Pt wire mesh as a current collector. Pt ink on the tube surface was used to sense voltage, and a thermocouple wire was used to carry the cell current. The contact to the interior electrode was made by packing the tube interior with ~1 mm diameter, platinum coated, clay balls. Pt wires were used to sense the interior electrode potential and to carry the cell current. The potentials reported are between the two active and nominally identical electrodes.

EIS and *dc* current-voltage characteristics were measured with the same O_2 pressure (P_{O2}) on both sides of the electrolyte. The P_{O2} and cell temperature (T) were varied from 1.1 to 13.9 atm and 745 to 959°C respectively. The cell potential was scanned from as high as 0.8 V to as low as -0.8 V, and currents up to 2 A were measured. A positive potential and a positive current are taken when O_2 is pumped from the interior of the tube to the exterior. For EIS, the cell voltage was set; then the cell current was allowed to stabilize for two minutes before frequency dependent data were collected. At each potential, the EIS frequency was scanned from 1 Hz to 64 kHz in five steps per decade. The EIS data were analyzed using Equivalent Circuit analysis program.[1]

The cell resistance determined from the slope at zero current for the *dc* current-voltage curves generally agreed with the cell resistance determined from the low frequency impedance at zero *dc* current. This resistance was about 65, 40, and 9.7 Ω-cm^2 at 745, 840, and 959°C respectively. These values are 4 to 10 times the expected zirconia resistance. The resistance generally decreased with increasing P_{O2}. This indicates that reaction overpotentials, mass transport limitations, and other cell resistances contributed to the power drain in the cell.

EIS results helped to determine the cause of the excess power drain. Figure 1 shows the basic equivalent circuit used to analyze the EIS data. The CPE_i represents a constant phase element with an admittance of $Y(\omega) = Y_o(j\omega)^n$ with $j = (-1)^{1/2}$ and $0<n\leq1$. The R_1 and CPE_1 elements compose a circuit with a time constant in the mid to high frequency range while the R_2 and CPE_2 elements have a time constant in the low to mid frequency range. Some of the dispersions showed additional, lower frequency behavior that was modeled as necessary with additional R-CPE parallel elements.

The series resistance, R_S, varied only with T. The value of R_S is about twice the expected value due to zirconia resistance alone.[2] Thus, some of the power drain for the oxygen pump was due to excess losses in the contacts and leads. In addition to R_S, an inductance of 2 to 6 μH-cm^2 appeared at high T, probably due to geometrical effects. The inductance was masked in the lower temperature data due to the magnitude of the other elements.

R_1 and R_2 accounted for the remainder of the excess power loss in the cell. These were determined for the 840°C and 959°C data. R_1 did not vary significantly with potential and was in the range of 1.5 to 3.0 Ω-cm^2 at 840°C and 1.0 to 2.0 Ω-cm^2 at 959°C. R_2 accounted for most of the *dc* impedance of the cell. Figure 2 is a plot of R_2 as a function of the magnitude

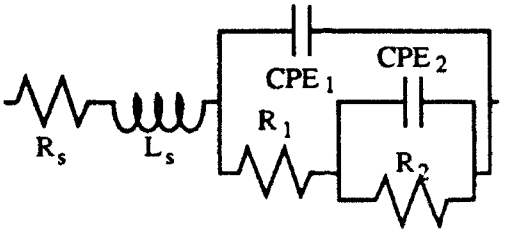

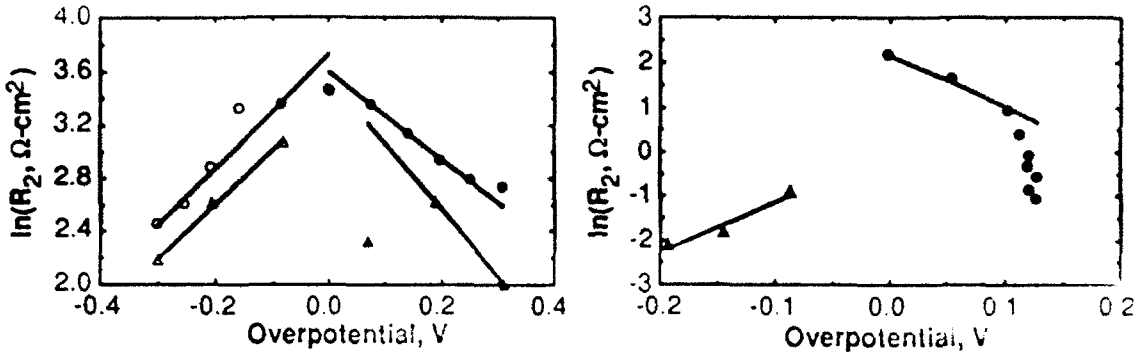

(a) $T = 840°C$ ● $R_2 = 36.6e^{-3.27|\eta|}$ ▲ $R_2 = 35.4e^{-5.02|\eta|}$ ○ $R_2 = 41.4e^{-4.24|\eta|}$ △ $R_2 = 30.4e^{-4.05|\eta|}$ $P_{O2} = 1.1$ atm $P_{O2} = 7.7$ atm

(b) $T = 959°C$ ● $R_2 = 9.05e^{-12.1|\eta|}$ ▲ $R_2 = 0.99e^{-11.4|\eta|}$ $P_{O2} = 13.9$ atm

Figure 2: Variation of R_2 with cell overpotential, (a) 840°C, and (b) 959°C. The symbols represent the data, and the lines are the best fit to the data using to the equations shown.

of the overpotential (η) for two data sets at each temperature. Included on the plots are best fit curves for the exponential decrease of R_2 with η according to the equation: $R_2 = R_0 \exp(-B|\eta|)$. The values of R_0 and B varied with P_{O2}, T, and direction of current. Since R_0 and B depended on the direction of the current, the cell must not have been symmetric. That is, the total η was not evenly distributed between the two electrodes.

A definitive interpretation of these results alone cannot be made. However, R_1 is probably a charge transfer resistance, and R_2 is probably a mass transfer and adsorption-desorption resistance.[3] A simple, mass transport limited model for R_2 as a function of η can be derived assuming the overpotentials are equal at each interface and the mass transport losses are equivalent at the anode and cathode. In such a model B would be equal to nF/RT where n, F, and R have their usual meanings. Similarly, R_0 would equal $K_f RT/nFP_{O2}$ where K_f represents a mass transport loss in Pa m^2/A.

The magnitudes of B for these data are much too small to fit this simple model. The value of F/RT is 10.4 V^{-1} at 840°C and 9.42 V^{-1} at 959°C. Since n must be an integer, B cannot match the slope of the model particularly at 840°C. Similarly, according to the model, R_0 should decrease by a factor of 7 as the P_{O2} increases from 1.1 to 7.7 atm. Instead, the decrease is only a few percent. Of course, K_f could have a strong P_{O2} dependence, but the data are inconclusive. Thus, these data cannot be explained by a simple mass transport limited model. More likely, the single R_2 determined here is composed of several smaller mass transport and adsorption-desorption impedances, some of which are inversely proportional to P_{O2}.

A high mass transfer impedance for Pt electrodes on ZrO_2 is consistent with literature results at lower O_2 pressures. Verkerk et. al. found the electrode resistance to be proportional to $(P_{O2})^{1/2}$ for P_{O2} from 4.5×10^{-2} to 1 atm, and that the reaction rate is limited by the rate of O_2 mass transfer to the anode.[4] Similarly, Robertson reported that the O_2 exchange rate at a Pt / zirconia interface is limited by oxygen diffusion on the Pt surface.[5]

Acknowledgments: The research described in this abstract was performed by the Jet Propulsion Laboratory, California Institute of Technology, and was supported by the Director's Discretionary Fund of the Jet Propulsion Laboratory. The development of the experimental techniques, instrumentation, and software was supported by the National Aeronautics and Space Administration.

References:

1) B. A. Boukamp, *Equivalent Circuit*, University of Twente, the Netherlands.
2) T. H. Estell and S. N. Flengas, *Chemical Reviews*, Vol. 70, No. 3, 1970, p. 348.
3) B. A. van Hassel, B. A. Boukamp, and A. J. Burggraaf, "Oxygen Transfer Properties of Ion Implanted Yttria-Stabilized Zirconia," presented at SSI 8, Lake Louise, Canada, Oct 23, 1991. Also to be published in *Solid State Ionics*.
4) M. J. Verkerk, M. W. J. Hammink, and A. J. Burggraaf, *Journal of the Electrochemical Society*, Vol. 130, No. 1, January 1983, pp. 70-78.
5) N. L. Robertson and J. N. Michaels, *Journal of the Electrochemical Society*, Vol. 137, No. 1, January 1990, pp. 129-135.

EIS AS A MEANS OF EVALUATING ELECTROLESS NICKEL DEPOSITS

E. T. van der Kouwe

Atomic Energy Corporation, P.O. Box 582, Pretoria, 0001 South Africa

Electroless nickel coatings on mild steel have been exposed to quiescent acidic NaCl (pH 3.6) solutions. The open-circuit potential (OCP) of uniform and thick (>20 μm) coatings tends to move towards positive potentials, implying an ennoblement process. During ennoblement a frequency dispersion is observed which has been attributed to a self-protective reaction of the coating involving an enriched phosphorus layer and the electrolyte. The OCP starts moving towards negative potentials as soon as penetration of the coating has taken place, thereby triggering corrosion of the substrate. Non-uniform or porous EN coatings drift towards negative potentials with little or no ennoblement. Degradation of the coating and corrosion of the substrate have been monitored by electrochemical impedance spectroscopy (EIS).

The following conclusions may be drawn from EN coating tests. Good corrosion protection may only be expected of coatings having polarisation resistances (PR) > 45 k .cm^2, a one-time constant equivalent circuit, Y_o values less than 45 μF/cm^2, CPE n values >0.93 and OCP values more positive than -300 mV (SCE). EN coatings are less prone to corrosion attack at more neutral pHs. Coatings under tensile stress offer less corrosion protection than coatings under compressive stress. A minimum thickness of 24 μm is recommended to compensate for the the non-uniformity of a coating. EN coatings do not provide long-term protection to mild steel in acidic (pH 3.6) 3% NaCl solutions.

It is postulated that a thick (>20 μm) EN coating in an HCl-NaCl solution can protect itself spontaneously (in 3% NaCl solutions at pH 3.6 only temporarily) by forming a protective film. This protection will only be effective if the coating is uniform and thick enough for the nickel to dissolve to such an extent that sufficient enrichment of phosphorus takes place to form a protective film before exposure of the substrate to the electrolyte. Diegle *et al.*[1] suggested a chemical passivation process, controlled by the formation and surface retention of hypophosphite anions, protecting the EN coating. Thick and uniform coatings are likely to show a frequency dispersion before coating breakdown, while non-uniform or thin coatings show little or no dispersion before breakdown. Our experiments differed from those of Diegle's in that the samples were not subjected to anodic polarisation, the samples contained only 8 weight per cent phosphorus and the acidic electrolyte contained NaCl.

Two experimental results appear to support Diegle's chemical-passivation model. Elemental depth analysis obtained with glow discharge optical spectroscopy shows that EN coatings are already enriched in phosphorus by the plating process.

Secondly, adding 1% NaH_2PO_2 to the acidic NaCl solution inhibits EN corrosion. Sato[2] suggested that oxyanions added to the electrolyte are capable of converting a less protective anion-selective hydrated metal oxide precipitate into a more protective cation-selective precipitate by adsorption or incorporation. It is relatively easy to visualise the inhibitive role of adsorbed hypophosphite anions precipitating from the electrolyte, but more difficult to give a mechanism of hypophosphite ions being generated by the EN coating itself. Nevertheless, the protective layer is likely to be a

cation-selective precipitate in which the movement of chloride ions is restricted. It is clear from the literature[3] that the presence of phosphorus destabilises the formation of a $Ni(OH)_2$ layer, resulting in increased phosphorus hydrolysis. It is probably the ability of the phosphorus in the EN layer to form a hypophosphite layer (repair hanism) that enhances its protective power against chloride attack. This repair mechanism is particularly evident in less aggressive neutral NaCl media, where the attack is superficial and the exposed surface quickly recovers by generating protective film. These effects are reflected in OCP oscillations.

REFERENCES

1. R. B. Diegle, N. R. Sorensen, C. R. Clayton, M. A. Helfand and Y. C. Yu, *J. Electrochem. Soc.* **135**, 1085 (1988).
2. N. Sato, *Corrosion* **45**, 354 (1989).
3. R. L. Zeller, *Corrosion* **47**, 692 (1991).

FREQUENCY DEPENDENCE OF THE MODULATED SURFACE TENSION OF SOLID METALS

Gintaras VALINCIUS
Department of General & Inorganic Chemistry
Vilnius University, Vilnius 2734, LITHUANIA

Surface tension of metals may be measured by using estance method [1]. Quantity which is measured in this experiment is derivative of the surface tension γ with respect to the surface charge density q or potential E. The first derivative (γ_q) was named q-estance and the second (γ_E) E-estance [1]. Usually, to obtain γ_q or γ_E sinusoidial AC modulation is used. Various frequences are employed. And if there occur slowly relaxing processes on the surface modulated surface tension becomes a complex quantity. That is why a problem of the frequency dependence analysis arises. On the other hand, surface tension is a function both of potential and surface concentration(s) of adsorbed substances. If estance is measured only on a single frequency one cannot conclude what part of a signal is due to potential change and what part due to change of the surface concentrations of adsorbats. This is the second and the main reason why analysis of frequency dependencesis necessary for the interpretation of the data of modulated surface tension measurments.

We analysed frequency dispersions of q- and E-estance for two kineticly controlled adsorbtion processes: one substance's adsorbtion and two substances adsorbtion or adsorbtion of one substance to two different places on the surface. General equations which describe q- and E-estance for both processes are:

$$\gamma_q = \left[\frac{\partial\gamma}{\partial\bar{\alpha}_1}\right]_{\alpha_1,E}\frac{d\alpha_1}{dq} + \left[\frac{\partial\gamma}{\partial\bar{\alpha}_2}\right]_{\alpha_1,E}\frac{d\alpha_2}{dq} + \left[\frac{\partial\gamma}{\partial E}\right]_{\alpha_1,\alpha_2}\frac{dE}{dq} \qquad (1)$$

$$\gamma_E = \left[\frac{\partial\gamma}{\partial\bar{\alpha}_1}\right]_{\alpha_1,E}\frac{d\alpha_1}{dE} + \left[\frac{\partial\gamma}{\partial\bar{\alpha}_2}\right]_{\alpha_1,E}\frac{d\alpha_2}{dE} + \left[\frac{\partial\gamma}{\partial E}\right]_{\alpha_1,\alpha_2} \qquad (2)$$

where α_i-surface concentrations of adsorbed species expressed in the charge density units. First two terms in eqs.1,2 are extensive components and third terms are intensive components of estance. Partial derivatives in eqs.1,2 do not depend upon modulation frequency. They are related to electronic state of the metalic surface. Introducing frequency independent parameters into eqs.1,2 one can obtain final expressions for q- and E-estance as a functions of modulation frequency:

$$Re\,\gamma_q = \frac{\gamma_{q0}}{M^2+(1-\kappa)^2L^2}\left\{\frac{y_1[M+(1-\kappa)\lambda_1 L]}{1+\lambda_1^2}+\frac{y_2[M+(1-\kappa)\lambda_2 L]}{1+\lambda_2^2}+(1-y_1-y_2)M\right\} \qquad (3)$$

$$Im\,\gamma_q = \frac{\gamma_{q0}}{M^2+(1-\kappa)^2L^2}\left\{\frac{y_1[(1-\kappa)L-\lambda_1 M]}{1+\lambda_1^2}+\frac{y_2[(1-\kappa)L-\lambda_2 M]}{1+\lambda_2^2}+(1-y_1-y_2)(1-\kappa)L\right\} \qquad (4)$$

$$Re\,\gamma_E = \gamma_{E_0}\,[1-y_1\lambda_1^2/(1+\lambda_2^2)-y_2\lambda_2^2/(1+\lambda_2^2)] \qquad (5)$$

$$Im\,\gamma_E = -\gamma_{E_0}\,[y_1\lambda_1/(1+\lambda_1^2)+y_2\lambda_2/(1+\lambda_2^2)] \qquad (6)$$

where: $\gamma_{q_0}, \gamma_{E_0}$- equilibrium values, y_1, y_2 - fractions of extensive components in equilibrium estance, κ is a ratio of capacities $\kappa = \lim_{\omega\to\infty}(dq/dE)/\lim_{\omega\to 0}(dq/dE)$, frequency $\omega=2\pi f$, dimensionless frequencies $\lambda_i = \omega/k_i$, where k_i - relaxation rate constants of the corresponding

adsorbtion process [s^{-1}]. Quantities M and L are:
$M = \sum K_i(1+\kappa\lambda_i)^2/(1+\lambda_i)^2$, $L = \sum K_i\lambda_i/(1+\lambda_i)^2$, where $K_i=(1+\tau_i)C\alpha_i/[C_0(1-\kappa)]$ $C\alpha_i=d\alpha_i/dE$, $C_0=dq/dE$. Both last derivatives corresponds to zero frequency. Partial derivatives $\tau_i=(\partial\rho/\partial\alpha_i)_{\alpha_{i\neq j},E}$, where ρ - density of the electrostatic double layer charge.

Electric parameters κ, k_i, K_i and C_0 may be determined by using AC impedance technique. Nevertheless, the question whether there is any possibility to determine non-electric parameters γ_{q0}, γ_{E0} and y_i without additional measurments is important for estance technique. Analysis of eqs.3-6 shows that only E-estance may be described with a unique set of parameters γ_{E0}, k_i and y_i. Frequency dependences of q-estance may not be described in such way. We shall show this considering the adsorbtion of one substance takes place on the electrode. Then eqs.3,4 reduces to

$$Re\gamma_q=\gamma_{q0}\frac{1+\kappa(1-y_1)\lambda_1^2}{1+\kappa^2\lambda_1^2}, \qquad Im\gamma_q=\gamma_{q0}\frac{(1-y_1-\kappa)\lambda_1}{1+\kappa^2\lambda_1^2} \qquad (7,8)$$

It is obvious from eqs.7 and 8 that one may calculate only three independent parameters κ/k_1, $(1-y_1)/k_1$ and γ_q. Parameter y_1 may not be calculated separately and one cannot conclude what is the contribution of potential and adsorbed substances to the surface tension. Thus, additional electric measurments are necessary. Despite this and the fact that eqs.3, 4 are less elegant it is easier in experiments to maintain constant charge density than constant potential drop accross interface.

Eqs.3,4,7,8 were used to simulate hodographs of q-estance for the adsorbtion of one and two substances. Results are presented in figure.

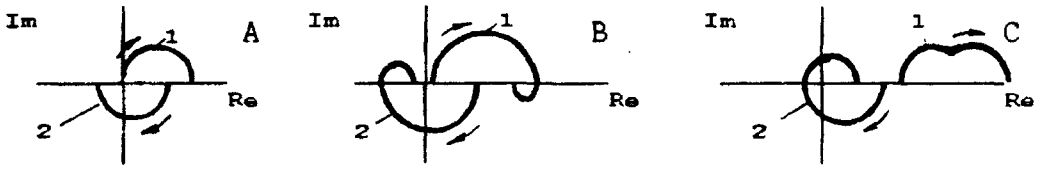

One may hightlight some features of q-estance: i) if there occur adsorbtion of only one substance$q$-estance crosses maximum two quadrants of complex plane (1A,2A) and amplitude of q-estance varies monotonicly, ii)if there occur adsorbtion of two substances q-estance may cross one (1C), two (1B), three (2B) and four (2C) quadrants and the frequency dependence of its amplitude may contain extremums (1B,2C) and steps (2B,1C). It may be noted that change of the sign of the imaginary part of estance is a sufficient criterion for the conclusion that more than one substance is adsorbing on the surface.

We found such frequency dependences in a system Pt/Cd^{2+} in the underpotential region (E = +0.3-+0.7 V vs.s.h.e.). Imaginary part of q-estance in this region changes its sign when frequency is increasing. This definetively proves that in this potential region more than one process is observed in a frequency range from 0.1 to 30 kHz. Contrary to this in the hydrogen region (E = 0.0-0.2 V) in the presence of Cd adatoms 1A type hodographs of q-estance were found. Earlier in the absence of cadmium two stages of hydrogen adsorbtion were detected by using estance technique [1].

REFERENCES

1. A.Gochshtein. Surface tension of solids and adsorbtion. Moscow, Nauka 1976, 400 p. (in russian).

IMPEDANCE SPECTROSCOPY STUDY OF SUPERPLASTIC 0.3 MOLE CuO MODIDIFIED 3YTZP OXYGEN SENSOR MATERIAL

J. Vangrunderbeek, J. Luyten, S. Kuypers, W. Hendrix and F. De Schutter

VITO, Boeretang 200, B-2400 Mol, Belgium

Stabilized $ZrO_2(Y_2O_3)$ compositions (3YTZP) are commonly used as oxygen sensor materials, f.e. the well known Lambda sensor in automotive application. Moreover, very recently these compositions became also of increasing importance because of their superplastic characteristics [1-5]. In sensor fabrication, electroceramics are required in various shapes. Subject of this study is the superplastic deformation and shaping of 3YTZP sensor material.

Superplasticity in ceramics is governed by diffusion controlled grain boundary sliding. The correlation between the grain boundary resistivity, the presence of a glassy phase between the grains and the superplastic deformation has been investigated by complex impedance spectroscopy and scanning and transmission electron microscopy for three categories of samples 3YTZP, 3YTZP + 0.3 mole CuO and 3YTZP + 0.3 mole CuO which had undergone creep deformation. Accurate grain boundary resistivity values have been obtained from non linear least squares fitting of the measured impedance data using the Equivalent Circuit fitting programme of Boukamp [6]. The activation energy associated with the grain boundary resistivity has been investigated as well.

References

[1] S.P.S. Badwal, F.T. Ciacchi, M. V. Swain and V. Z. Zelizko, J. Am. Ceram. Soc. 73 (1990) 2505-2507.
[2] F. Wakai and T. Nagono, J. of Mater. Sci. Lett. 7 (1988) 607-609.
[3] I. Wei Chen and Liang An Xue, J. Am. Ceram. Soc. 73 (1990) 2585-2609.
[4] R. Duclos and J. Crampon, J. Mat. Sci. Lett. 6 (1987) 905-908.
[5] J. Luyten, W. Hendrix, J. Sleurs and W. Vander Meulen, Proc. Mechanics of creep brittle materials 2, Leicester, September 2-4, 1991.
[6] B.A. Boukamp, University of Twente, The Netherlands.

ABSTRACT submitted to the Second International Symposium on Electrochemical Impedance Spectroscopy, University of California, Santa Barbara, California, USA, July 12-17, 1992.

RECOMBINATION IN SEMICONDUCTOR ELECTRODES: INVESTIGATION BY THE ELECTRICAL AND OPTO-ELECTRICAL IMPEDANCE METHOD.

D. Vanmaekelbergh and A.R. de Wit

Debye Research Institute, University of Utrecht
P. O. Box 80.000, 3508 TA Utrecht,
The Netherlands

F. Cardon
Laboratorium voor Kristallografie en Studie van de Vaste Stof
Rijksuniversiteit Gent
Krijgslaan 281
B-9000 Gent
Belgium

The efficiency of photovoltaic solar cells based on semiconductor/electrolyte interfaces is limited by recombination of the photogenerated carriers. In fig.1, an illuminated n-type semiconductor/electrolyte interface is depicted. Electron-hole pairs are separated be migration and/or diffusion leading to an electrical hole flux i_h towards the surface.This hole flux does not depend on the band-bending and is proportional to the incident light intensity if light absorption occurs predominantly in the diffusion layer or in the depletion layer. The photocurrent density i measured in the external circuit corresponds to the transfer of holes through the semiconductor/electrolyte contact. In a large potential range, i is smaller than i_h due to recombination. In fig.1, recombination via one type of centre is shown.

Impedance techniques proved to be successful for the study of recombination in semiconductor electrodes (1). In the electrical impedance method, a small alternating potential $\tilde{V}$ is superimposed on the electrode potential and the incident light intensity (and hence i_h)is kept constant.The ac-recombination current density $\tilde{i}_R$ is measured in the external circuit. The electrical impedance due to recombination is defined as $\tilde{V}/\tilde{i}_R$. In the opto-electrical impedance method, the potential is kept constant and the incident light intensity is modulated. As a consequence, an ac-component $\tilde{i}_h$ in the electrical hole flux arises, which can be measured in the external circuit in the absence of recombination (sufficiently high band-bending). In the potential region where recombination occurs, an ac-photocurrent density $\tilde{i}$ (= $\tilde{i}_h$-$\tilde{i}_R$) is measured. The opto-electrical impedance is defined as $\tilde{i}/\tilde{i}_h$, or hence as $1-(\tilde{i}_R/\tilde{i}_h)$.

Both the electrical- and opto-electrical impedance can be calculated by relating $\tilde{i}_R$ to the recombination processes in the depletion layer or at the surface. The depletion layer is therefore considered as a capacitor, with a free electron and a free hole reservoir at x=d and x=0, respectively (see fig.1). Capture of an electron at a position x' is followed by an instantaneous equilibration in the conduction band and corresponds to a charge flow e(d-x')/d in the external circuit. Capture of a hole corresponds to a charge flow ex'/d.

The ac-recombination current density in the external circuit is hence given by:

$$\tilde{i}_R = e \int_0^d ((1-x/d)\tilde{j}_{R,n} + (x/d)\tilde{j}_{R,p}) \; dx$$

Both types of impedance follow from the above equation if the ac-components of the electron and hole recombination velocities ($\tilde{j}_{R,n}$ and $\tilde{j}_{R,p}$) are calculated as a function of the perturbing signal $\tilde{V}$ or $\tilde{i}_h$. The above equation shows that in the case of surface recombination, i_R corresponds to the flow of free electrons only.

The theoretical results show that the same information can be obtained with both types of impedance method. Recombination in the depletion layer can be distinguished from surface recombination. When recombination occurs predominantly at the surface, the rate constant β_n for electron capture can be obtained.

The theoretical results have been compared with results measured at CdS, InP, GaAs and GaP photoanodes . The results at CdS are presented in poster 28 (2). The electrical and opto-electrical impedance results measured at GaAs photoanodes show that recombination occurs predominantly at the surface via donor-type recombination centers (rate constant for electron capture = 10^{-6} $cm^3 s^{-1}$)(3-4). The electrical impedance results measured at GaP electrodes indicate that both recombination in the depletion layer and at the surface must be taken into account(5).

References

(1) D. Vanmaekelbergh and F. Cardon, Electrochim.Acta,37,837 (1992)
(2) A. R. de Wit, D. Vanmaekelbergh and J. J. Kelly, to be published in J. Electrochemical Soc.
(3) D. Vanmaekelbergh, W. P. Gomes, and F. Cardon, Ber. Bunsenges. Phys. Chem. 89,994(1985)
(4) J. Li and L.M. Peter, J.Electroanal.Chem.,199,1(1986)
(5) D.Vanmaekelbergh, R. P. ter Heide and W. Kruyt, Ber. Bunsenges. Phys. Chem.93, 1103 (1989).

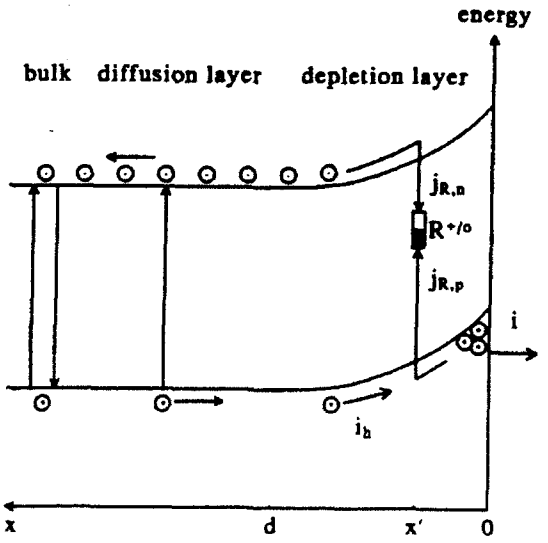

THE DETERMINATION OF COATING PERFORMANCE USING ELECTROCHEMICAL IMPEDANCE SPECTROSCOPY

E.P.M. van Westing, G.M. Ferrari and J.H.W. de Wit*

TNO Centre for Coatings Research, Department for Corrosion Prevention
P.O. Box 6034, 2600 AB Delft, The Netherlands.
*Delft University of Technology, Laboratory for Materials Science
Division for Corrosion Technology and Electrochemistry
P.O. Box 5025, 2600 GA Delft, The Netherlands.

Anti corrosion performance studies of organic coatings have normally been carried out by accelerated weathering or by outdoor exposure of coated panels. Both methods do not provide information about the failure mechanism of the coatings and the former methods can give unpredictable results which cannot very well be compared with the actual outdoor performance of the coatings. Electrochemical Impedance Spectroscopy (EIS) has been used for some years now in the study of the performance of organic coatings. It was observed that the technique has promising possibilities in this field, however the interpretation of the results was mostly carried out in terms of changes in the curves of the Nyquist plot of the impedance (visual or graphical judgement) [eg. 1,2], or by the DC-resistance of the coatings [3]. It was commonly considered that when a coating showed capacitive behaviour or when the DC-resistance exceeded e.g. 100 MOhm.cm^{-2} [3] the coating was performing well and was protecting the substrate against corrosion. This point of view is an oversimplification of the real situation, as barrier type coatings, like epoxies, can remain very high impedant for prolonged time while poorly protective. In earlier investigations it was already shown that epoxy coatings can remain very high DC-resistant while taking up water and corrosive species from the electrolyte [4] during the first stage of the exposure. Consequently it is not unlikely that some electrochemical processes occur locally under a coating along the coating/substrate interface, and hardly affect the impedance of the coating. Oxygen is mostly considered to be rate determining for the corrosion reactions, as the diffusion of water exceeds the suppletion due to the corrosion reactions [5]. However Stratmann and Hoffmann [6] observed that corrosion reactions and transitions of oxides can take place at the coating/substrate interface even without the availability of oxygen. The uptake of water is therefore an important parameter for the evaluation of the anti corrosion properties of a coating.

Epoxy model coatings were investigated while immersed in a 3% NaCl solution using Electrochemical Impedance Spectroscopy (EIS) during the first stage of the exposure where water uptake is the main process and during long term exposure where the corrosion starts. The analysis of the impedance measurements showed the necessity of the use of the Constant Phase Element (CPE) in the equivalent circuit of the impedance. A short review of literature on CPE-interpretations is given. From literature it is derived that deviation from ideal dielectrical properties, that is represented by a CPE originates from interaction (shielding) of polarizable groups.

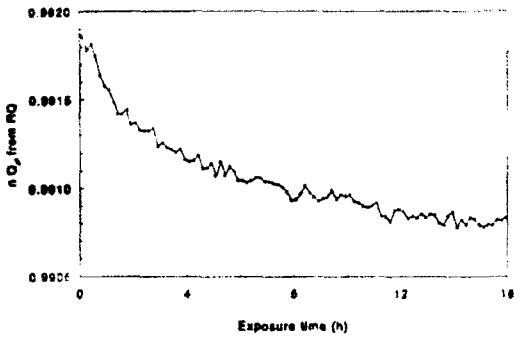

Figure 1: Change of dielectrical properties during wateruptake: n Q_{pf} of a coating as function of time during wateruptake.

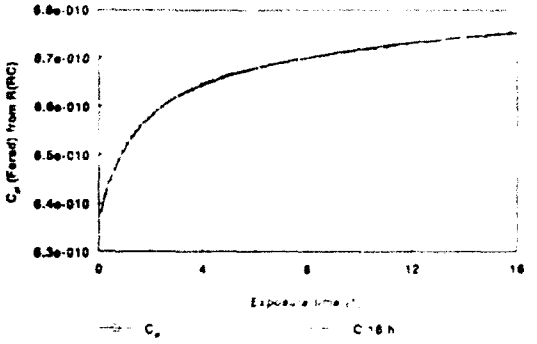

Figure 2: Result of fit on curve of C_{c} of a model epoxy coating as function of time during wateruptake. (capacitance increase curve)

The results of impedance measurements on the water uptake of the coatings, show that the entering water not only affects the dielectrical properties (see figure 1), but also yields swelling of the coating polymer. The water uptake and the swelling of the coating polymer were analyzed and quantified from the results of the impedance measurements using a novel method (see figure 2). Impedance measurements during the long term immersion of the coating show that the start of the corrosion process under high impedant barrier type coating can be detected by changes of the dielectrical properties of the coating, resulting in changes of the parameters of the CPE (see figures 3a and b: 1: no corrosion; 2: one (very smal) corrosion spot; 3: three corrosion spots). The difference in results interpreting the impedance measurements using a condenser or a CPE in the equivalent circuit is also discussed.

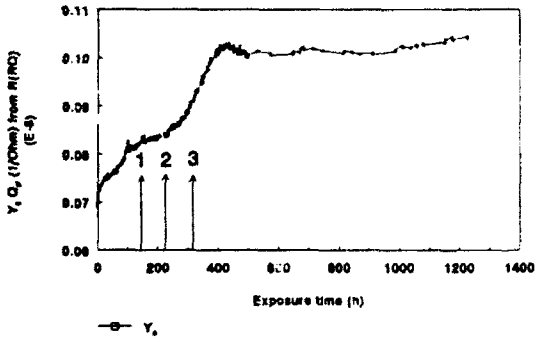

Figure 3a: CPE-parameter Y_0 as function of time during long term immersion in a 3% NaCl-solution.

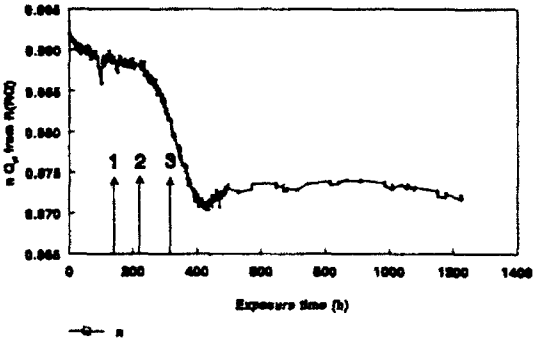

Figure 3b: CPE-parameter n as function of time during long term exposure in a 3% NaCl-solution.

[1] M. Morcillo et. al., *Polymeric Materials for Corrosion Control*, ACS Symposium Series 322, (Ed. R.A. Dickie and F.L Floyd), p. 86. American Chemical Society, Washington (1986).

[2] G.W. Walter, *Corrosion Science*. 26. p. 681 (1986).

[3] G.T. Burstein, G. Gao and J.E.O. Mayne, *J. Oil Col. Chem. Ass.* (10), p. 407 (1989).

[4] E.P.M. van Westing, F.M. Geenen, G.M. Ferrari & J.H.W. de Wit, *Proc. 16th Int. Conf. Org. Coat. Sci. Tech.* Athens, Greece, 1990, p. 541.

[5] J.E.O. Mayne, In 'Corrosion' 2nd edn., L.L. Sheir (ed), Newness-Butterworths, London, 1976, Vol. 2 p. 15:24.

[6] M. Stratmann and K. Hoffmann, Proc. 9th European Congr. on Corrosion, Utrecht, 2-6 October 1989, Paper CO-070 Volume II 1989.

EXTENDED ABSTRACT
Second International Symposium on
Electrochemical Impedance Spectroscopy

University of California
Santa Barbara, California, USA

July 12-17, 1992

MODEL FOR IMPEDANCE OF AN IONIC CONDUCTOR SANDWICHED BETWEEN BLOCKING ELECTRODES*

J. C. Wang

Energy Division
Oak Ridge National Laboratory
Oak Ridge, Tennessee 37831-6185
U. S. A.

April 28, 1992

MODEL FOR IMPEDANCE OF AN IONIC CONDUCTOR SANDWICHED BETWEEN BLOCKING ELECTRODES*

J. C. Wang

Energy Division
Oak Ridge National Laboratory
Oak Ridge, Tennessee 37831-6185
U. S. A.

The conductivity of an ionic material is typically determined from the small-signal ac impedance of a thin specimen sandwiched between two blocking electrodes. This impedance contains contributions from dc ionic conduction, local hopping of bound ions, high-frequency dielectric response, and processes across the electrode-electrolyte interface. While continuum microscopic theories of conductance that account for ion diffusion, migration, and recombination have been developed [1], they are not yet adequate for analyzing experimental data. In practice, equivalent electrical circuits which lump the main physical processes into macroscopic circuit elements are commonly used to extract physical quantities such as the conductivity and high-frequency dielectric constant of a material [2]. This latter, empirical approach is adopted in this work.

An idealized equivalent circuit for the system described above is a resistor in series with a capacitor (rc pair) representing the bulk material and the conductor-electrode interfaces, respectively, and a second capacitor in parallel with the rc pair representing the high-frequency dielectric response of the system [3]. In practice, however, in order to describe the experimental data satisfactorily, it is often found necessary to replace the interface capacitor and the bulk resistor with constant-phase-angle (CPA) elements and/or non-Debye dielectric elements [4-6]. The equivalent circuit proposed and discussed in this work is of this nature. The interface capacitor in the ideal model mentioned above is replaced with a CPA element, and a non-Debye dielectric element is added in parallel with the bulk resistor to represent the local ionic movement.

The capacitor in the circuit represents the dielectric response of the free space and of all other polarizing processes at frequencies which are well above the loss-peak frequency associated with the local ionic hopping around the charge-compensating centers, but are below resonance frequencies of induced polarization processes. The resultant dielectric response can be lumped together as a high-frequency dielectric constant which can be extracted from measured capacitance and the sample dimensions.

A conducting ion in an ionic conductor may contribute to both the ac and dc conduction. In this study, it is assumed that at any given time some of the conducting ions make a dc contribution while the remainder contribute to an ac contribution. This situation is represented by the parallel combination of the resistor and the non-Debye dielectric element. The dc conductivity of the specimen can be extracted from the measured bulk resistance and the sample dimensions.

The complex ac conduction or, equivalently, complex dielectric function of the material is associated with the hopping of conducting ions back and forth among available potential minimas resulting from charge-compensating centers. In the dielectric form, it often exhibits a non-Debye form characterized by a broad loss peak and a CPA behavior at frequencies above the loss peak. In this work, an ion-hopping model which accounts for the fluctuating barrier heights induced by thermal agitations is emphasized [7]. The model yields a dielectric function very close to the empirical Havriliak-Negami function and predicts the invariance of loss-peak shape with temperature, an experimental result observed in many materials [8].

It is assumed in this study that the dominant process at the conductor-blocking electrode interface can be represented by the double layer capacitance between the conducting ions and the blocking electrode. Under the applied field, the conducting ions may have to overcome different magnitudes of resistance to reach the various parts of the rough electrode surface to form the double layer. At lower frequencies, more ions can find time to form a double layer and, therefore, the capacitance is greater. However, at the same time, the total resistance experienced by these ions is also increased. The conditions for the capacitance and resistance to have a CPA behavior will be discussed by comparing the fractal and pore models for the blocking electrode [9-12].

*Research sponsored by the U.S. Department of Energy under contract DE-AC05-84OR-21400 with Martin Marietta Energy Systems, Inc.

REFERENCES

1. J. R. Macdonald, J. Electrochem. Soc. 135, 2274 (1988).
2. J. R. Macdonald, J. Electroanal. Chem. 223, 25 (1987).
3. I. D. Raistrick, Solid State Ionics 18 & 19, 40 (1986).
4. I. D. Raistrick, C. Ho, and R. A. Huggins, J. Electrochem. Soc. 123, 1469 (1976).
5. J. R. Macdonald and G. R. Cook, J. Electroanal. Chem. 168, 335 (1984).
6. J. B. Bates and J. C. Wang, Solid State Ionics 28-30, 115 (1988).
7. J. C. Wang and J. B. Bates, Solid State Ionics 50, 75 (1992).
8. A. K. Jonscher, 'Dielectric Relaxation in Solids,' (Chelsea Dielectrics Press, London 1983).
9. J. C. Wang, Solid State Ionics 28-30, 1436 (1988).
10. J. C. Wang and J. B. Bates, Solid State Ionics 18 & 19, 224 (1986).
11. H. S. Liu, Phys. Rev. Lett. 55, 529 (1985).
12. L. Nyikos and T. Pajkossy, Electrochim. Acta 30 (1985).

CHARACTERIZATION OF PASSIVE LAYERS FORMED ON LEAD BY EIS

F.E. Varela, L.M. Gassa and J.R. Vilche

Instituto de Investigaciones Fisicoquímicas Teóricas y Aplicadas (INIFTA)
Facultad de Ciencias Exactas, Universidad Nacional de La Plata,
Sucursal 4, Casilla de Correo 16, (1900) La Plata, Argentina

Many attemps have made to study the anodic corrosion of lead in aqueous sulphuric acid to establish the properties of the passive layers formed between the equilibrium potentials of $Pb/PbSO_4$ and $PbO_2/PbSO_4$ systems[1], particularly in order to determine the sequence of chemical and electrochemical events which lead to the generation of insulating/semiconducting passive layers. During passivation of the $Pb/PbSO_4$ electrode, the alkalinization of the electrolyte in the pores of the $PbSO_4$ layer promotes the formation of the $Pb/PbO/PbSO_4/H_2SO_4$ system at potentials more positive than -0.40 V. As potential is set more positively than 1.0 V PbO_2 becames the stable oxide phase.

The purpose of this study is to investigate the corrosion process and characteristic of the surface layer formed on lead in concentrated sulphuric acid solutions at 25°C, using electrochemical impedance spectroscopy (EIS) and rotating disc electrodes. Data obtained under a wide variety of experimental conditions show that the passive film formation is a highly irreversible process and the surface films consist of various Pb(II)-containing species, depending upon the formation potential. At formation potentials more cathodic than -0.4 V, the impedance measurements are associated with the thickness and the dielectric properties of a single $PbSO_4$ layer. The impedance diagrams obtained in the potential range where a composite Pb(II) sulphate-oxide passive layer is anodically produced are interpreted trough the influence of its formation potential on the thickness, semiconducting properties and diffusion processes present in the film. The discussion is found in the results of the application of transfer function analysis using non linear fit routines.

REFERENCES

[1] K.R. Bullock and D. Pavlov (Editors), Advances in Lead-Acid Batteries, The Electrochemical Society Inc., Pennington, NJ (1984).

THE CORROSION OF ALUMINIUM ALLOYS BY CHLORINATED HYDROCARBONS

Schalk W. Vorster
and
Ockert J. Van Der Schijff

Department of Metallurgical Engineering
Potchefstroom University for CHE
Private Bag X6001
Potchefstroom 2520
REPUBLIC OF SOUTH AFRICA

ABSTRACT

Chlorinated organic compounds are used extensively in industry as solvents and degreasing agents. In contact with aluminium it can lead to serious corrosion of the metal by virtue of the decomposition of the organic phase. This corrosion process is characterised by an induction period during which very little corrosion is evident. Subsequently, very high corrosion rates ensue. Finely divided aluminium in contact with certain halocarbons can lead to explosive reactions.

Although these reactions have been extensively studied (1,2,3,4,5,6,7,8,9) little information is available about the onset of the corrosion prosess. This investigation concerns the reaction of aluminium with carbon tetrachloride. The objective was to elucidate the role of the existing oxide layer in the initial stages of corrosive attack, by utilising surface impedance measurements. The early stages of the corrosion process were investigated by means of controlled exposure of aluminium coupons to boiling carbon tertrachloride (CCl_4), followed by electrochemical impedance spectroscopy in a 1% sodium nitrate ($NaNO_3$) solution. Computer-analysis of the impedance data provided data to model the system under study in terms of an equivalent circuit model consisting of electronic circuit elements. Aluminium plate (alloy grade H4; see Table 1), with a nominal thickness of 1,2 mm was used in the investigation.

Al (mass %)	Mn (mass %)	Ti (mass %)	Cu (mass %)	Fe (mass %)	Ni (mass %)	Si (mass %)
99.362	0.055	0.034	0.002	0.330	0.026	0.180

Table 1. Chemical composition of aluminium alloy.

Three surface conditions were investigated: (i) "As received", (ii) "as received", followed by oxidation for 1 h at 300°C in air, and (iii) "as received", followed by removal of all existing surface oxides (etched in a 10% caustic soda solution, water rinsed and then dipped in very dilute nitric acid). The carbon tetrachloride used in the study was of unstabilized AR purity. The ratio of the exposed metal surface area to the volume of carbon tetrachloride employed, was found to be significant, and is referred to as the S/V ratio. In a typical experiment a 25 mm x 55 mm aluminium coupon was contacted with 60 cm^3 of boiling carbon tetrachloride under reflux, and removed after a predetermined time for weight loss measurements and/or impedance spectroscopy, using a 1% $NaNO_3$ solution as electrolyte. (Temperatures lower than boiling point were also used). Before weight loss

determination, corrosion products were removed from the surface in an ultrasonic bath. Impedance spectra were generated utilizing an automatic system which included a Solartron Model 1255 Frequency Response Analyser (FRA), and a EG&G PARC Model 273 Potentiostat/Galvanostat, controlled by an IBM personal computer. A three-electrode assembly consisting of an aluminium working electrode, a platinum counter electrode, and a standard calomel reference electrode was used for all experiments.

It was found that the induction period can be resolved into two distinct phases. The first phase of the induction period comprises a series of events that lead to the destruction of the original oxide layer on the aluminium surface, and the stepwise formation of an aluminium chloride-rich surface film. During the second phase of the induction period hexachloroethane is deposited on the metal surface. The concomittant build-up of the Lewis acid, $AlCl_3$, in the organic liquid eventually leads to the destruction of the surface film and the onset of a rapid autocatalytic reaction. The following mechanism for the initial stages in the attack of aluminium by carbon tetrachloride therefore seems plausible: Carbon tetrachloride molecules approach the oxide surface and adsorb, thereby leading to a rise in the surface resistance. A loose complex is formed as discussed above. The aluminium oxide lattice is thereby slowly transformed to firstly, an aluminium oxide/aluminium chloride mixed lattice and finally to a layer of $AlCl_3$ on the metal surface. This would lead to a surface film with lower electronic as well as ionic resistance, facilitating easy metal transport from the film/metal interface to the metal carbon tetrachloride interface. Trichloromethyl free radical species as well as aluminium chloride will be formed readily, the former reacting, and thereby depositing hexachloroethane on the metal surface, and the latter dissolving in the bulk of the organic phase. The surface resistance of the aluminium will increase dramatically as the coverage by the non-conducting organic coating spreads and grows thicker. The $AlCl_3$ dissolved in the CCl_4 constitutes a Lewis acid. As soon as a critical concentration is reached in the carbon tetrachloride, rapid direct attack of the aluminium through the partially protective surface layer becomes possible. Naturally the S/V ratio will be important in defining the onset of this phase. (Small surfaces exposed to large volumes of CCl_4 will require longer times before the onset of rapid reaction). The direct attack on the substrate will have the effect of undermining the black surface film, which will be dispersed in the liquid phase, thereby allowing direct attack by the CCl_4. A rapid fall in surface resistance will signal the onset of this phase. As the reaction will be promoted by the production of $AlCl_3$, an autocatalytic reaction ensues.

---

1. STERN, M. & UHLIG, H.H. (1952a). Corrosion of Aluminum by Carbon Tetrachloride. J Electrochem Soc. 99, 381.
2. STERN, M. & UHLIG, H.H. (1952b). Effect of Oxide Films on the Reaction of Aluminum with Carbon Tetrachloride. J Electrochem Soc. 99, 389.
3. STERN, M. & UHLIG, H.H. (1953).J Electrochem Soc. 100, 543
4. ARCHER, W.L. & SIMPSON, E.L. (1977). Chemical Profile of Polychloroethanes and Polychloroalkenes. Ind. Eng. Chem. Prod. Res. Dev., 16, 158.
5. ARCHER,W.L. & HARTER, H.K. (1978). Reactivity of Carbon Tetrachloride with a Series of Metals. Corrosion-NACE, 34, No 5 pp. 59.
6. ARCHER,W.L. (1982). Aluminum-1,1,1-Trichlorethane. Reactions and Inhibition. Ind. Eng Chem. Prod. Res. Dev., 21, 670.
7. ARCHER,W.L. COOK-KING, M. & ZEMPEL, R.W. (1983) Chlorinated solvents and aluminum: User awareness. Aerosol Age, 6.
8. ARCHER,W.L. (1984).A Laboratory evaluation of 1,1,1-Trichlorethane-Metal-Inhibitor systems. Werkstoffe und Korrosion, 35, 60.
9. ARCHER,W.L. & STEVENS, V.L. Reactivity of Aluminum With Solvents and Additives in Coatings. J Coatings Technol.

APPLICATION OF IMPEDANCE ANALYSIS METHOD, Z_CALC, TO PAINTED AND UNPAINTED METALS

G.W. Walter, D.N. Nguyen and M.A.D. Madurasinghe
BHP Steel - Sheet & Coil Products Division
Research & Technology Centre
Box 77 Port Kembla NSW 2505 Australia

The aim of this paper is to describe and show applications of a new program called Z_CALC, written in Fortran running under HP-UX, for analysis of impedance data for unpainted and painted metals. It consists of two main subprograms - AUTOGUESS and CURVEFIT. AUTOGUESS is a fast, semi-automatic, linear, one stage routine for obtaining initial guesses of equivalent circuit parameter values. CURVEFIT uses these initial guesses in an interactive, complex, non-linear least squares routine to provide refined parameter estimates.

AUTOGUESS only requires the operator to select a region of experimental data points belonging to the arc of the first Nyquist semicircle (that due to the paint film), which has minimum overlap with the second semicircle (that due to the substrate metal). AUTOGUESS can then automatically calculate initial parameter guesses for this first semicircle. The same process is repeated for the second semicircle. This interactive approach is much easier to apply than either graphical methods or two stage semi-automatic linear/non-linear methods. The required parameters of a Nyquist depressed semicircle are centre, radius, and depression angle, α. In order to determine these parameters, the required portion of the impedance data must be fitted to a semicircle. If appropriate transformation of variables is undertaken, this can be a linear least squares problem using the approach taken by Schwiderke and Di Sarli [1]. AUTOGUESS can be applied to cases where the two Nyquist semicircles are not clearly separated, in which case solution resistance, R_S, and paint film capacitance, C_{pf}, can be estimated. After obtaining initial estimates of parameter values for the first Nyquist semicircle, their contributions are subtracted from the impedance data. The same linear least squares method can then be applied to the second Nyquist semicircle to obtain initial guess values for its parameters. The Warburg diffusion tail, if it exists, can then be calculated, after subtraction of the second semicircle's contribution to the remaining impedance. Thus, the whole approach in AUTOGUESS is simple even for a relatively non-expert operator because the method operates semi-automatically on the input data file which is obtained from a data base built into Z_CALC. AUTOGUESS differs from Schwiderke and Di Sarli's method [1] in that it takes into account special cases where initial guesses are difficult to obtain (semicircles not clearly separated, and determination of estimates for Warburg diffusion impedance). After AUTOGUESS has returned parameter initial guess values, the operator can obtain a visual estimate of the goodness of fit by requesting a Nyquist plot which compares the discrepancy between experimental data points and the fitted curve using AUTOGUESS's initial guess parameter values. A curve fitting error is also displayed.

Subprogram CURVEFIT uses the parameter initial guess values and improves their accuracy. In order to do this, the operator first chooses either non-weighted or weighted curve fitting. Weighted, using the inverse of the modulus, is recommended so as to avoid a bias towards low frequency data. The operator then chooses one of three curve fitting algorithms (Gauss-Newton, Levenberg-Marquardt, Modified Gauss-Newton). A description of the benefits and recommended procedure for each of these has been given elsewhere [2]. If CURVEFIT converges successfully, the operator has to judge whether the parameter estimates obtained are reasonable by examining all of the following criteria. A Bode or Nyquist plot on the VDU screen will show discrepancies between experimental and curve fitted data. The curve fitting error is also shown on this plot along with a readout of each parameter and its standard deviation.

Examples of the application of the impedance analysis program, Z_CALC, to unpainted and painted metals is given in Figures 1 and 2. Equivalent circuit models used for the analysis are described in the full paper and elsewhere [2].

References:

[1] E.E. Schwiderke, A.R. Di Sarli, Bull Electrochem 3, 107 (1987).
[2] G.W. Walter, D.N. Nguyen, M.A.D. Madurasinghe, Electrochim Acta 37, 245 (1992).

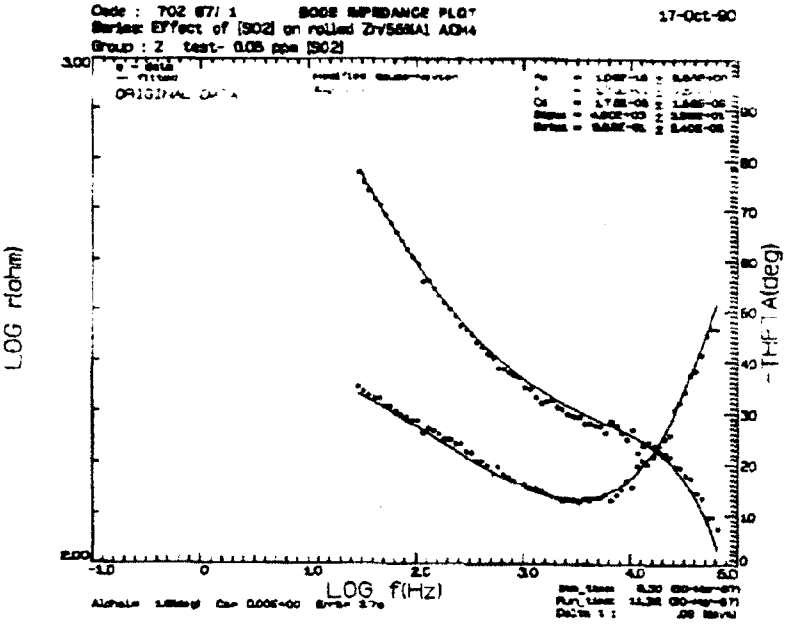

Figure 1. Bode plot, showing experimental data and curve-fitted line, of modulus, r, and phase angle, θ, components of impedance as a function of frequency for a three-electrode Atmospheric Corrosion Monitor, ACM, (55%Al-Zn alloy) during evaporation of 0.5 mm distilled water film applied to the surface in the presence of laboratory air containing 0.05 ppm [SO_2].

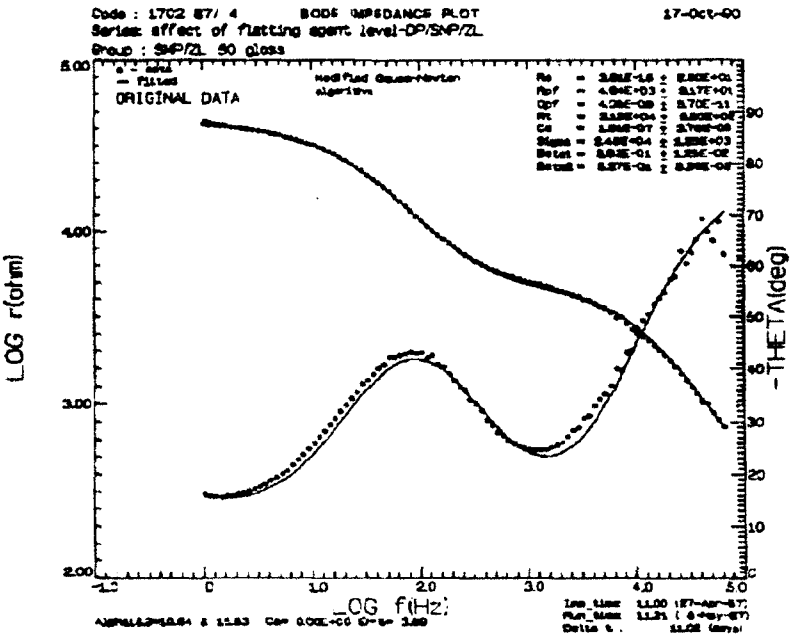

Figure 2. Bode plot, showing experimental data and curve-fitted line, of modulus, r, and phase angle, θ, components of impedance as a function of frequency for painted ZINCALUME (55%Al-Zn alloy coating on a steel substrate) with epoxy primer and silicone modified polyester, SMP, top coat, immersed for 11 days in 5% NaCl solution at 50°C.

TIME RESOLVED IMPEDANCE SPECTROSCOPY OF ELECTROCATALYTIC SURFACES

Markus Weidenauer, Michael Wanner, and Konrad G. Weil

Institut für Physikalische Chemie, Technische Hochschule Darmstadt
Petersenstrasse 20, D-6100 Darmstadt, GERMANY

We developed a Fourier transform impedance spectrometer, which is based on sampling in logarithmically equally spaced time intervals [1]. Basically the instrument consists of a PC with a fast A/D converter and a low noise potentio/galvanostate. The set-up enables us to obtain impedance spectra from 1 to 10^4 Hz with a time resolution of about one second. When the system can be described as a simple RCR circuit, differential double layer capacities C_d and charge transfer resistances R_{ct} can also be obtained with this time resolution. Thus, C_d and R_{ct} can be monitored quasi-continuosly as a function of time or of potential.

As an example for the applicability of this technique we studied the impedance of copper surfaces during autocatalytic copper deposition with formaldehyde as reducing agent. It turns out that the impedance characteristics of this surface are entirely different during and after the process, even when the surface remains in contact with a solution. During the autocatalytic copper reduction C_d is of the order of 500 $\mu F/cm^2$, while when the process is interrupted, C_d drops to values below 100 $\mu F/cm^2$.

The autocatalytic copper deposition consists of two partial processes: copper ion reduction and formaldehyde oxidation. Both processes are far from equilibrium. However, for the formaldehyde oxidation to be sufficiently fast, a very specific surface microstructure is required. This microstructure is formed by a selforganization mechanism during the deposition of copper. The surface roughness, monitored through the double layer capacity, provides the feedback between the two processes, which is necessary for the system to show the properties of a selforganizing synergistic process.

This interpretation is corroborated by results, which demonstrate that the copper surface during the autocatalytic copper deposition enhances the raman scattering of adsorbed scatterers.

[1] H. Wiese and K. G. Weil, IEEE Transactions on Acoustics, Speech, and Signal Processing, 36, 1096 (1988).

IMPEDANCE STUDIES OF THE INTERFACE ELECTRODE/Zn-MONTORILLONITE

Wang Wenlou, Liu Wanyu*, Lin Fengliang, Yu Wenhai*
Department of Modern Chemistry,
*Department of Materials Science and Engineering,
University of Science and Technology of China
Hefei, Anhui 230027
P.R. China

EXTEND ABSTRACT

The interfaces of both Ni/Zn-montmorillonite (mont.) and Zn/Zn-mont. have been studied by means of A.C. Technology. The impedance responses on the interface are dependent on water content in Zn-mont. and electrodic materials. For Ni/Zn-mont. system, the complex impedance plane shows gradually departure from the more ideal vertical spike as the water content decrease. Figure 1 is the complex impedance planes which were measured by a ZL5-LCR intellectual instrument, frequency scanning range 12-10^5 Hz, controlled by an computer with a working voltage of 50 mV. A, B and C in Fig.1 are correlated to the samples which are in a moist chamber of water , a moist chamber of $Mg(NO_3)_2$ saturated solution and atmosphere respectively. The influence of the water content on the departure of vertical spike results from changing roughness from the sample surface, which has been identified by SEM. The more rough the surface is, the larger the departure from the vertical spike is[1].

The reason why water content could change the roughness of the surface is that mont. possesses a high expansibility. The d_{001} value of mont. is the criterion of its expansibility. The d_{001} value of Zn-mont. for A,B and C samples are 1.9267nm, 1.5494nm and 1.5104nm respectively. While it absorbs water, each particulate of mont. starts expanding which makes contact between particulate get much better and makes the surface more smooth owing to improving the plasticity of mont. so that the surface behavior closes up that of the ideal blocking electrode.

To a certain extent, the change of the impedance response on the interface takes place during the certain period. The changing tendency is that the resistance at low frequency decreases and the turning point between the interface and the body resistance increases towards the higher resistance, which may be due to forming water films on the interfaces. The water film formed needs some water that comes from the sample. The decrease of water content in the sample raises the body resistance [2]. The water film may also modify the interface and improve the contact between the electrode and the sample.

The samples of two sizes sieved by 80 mesh and 220 mesh standard sieve were examined. The particulate size of mont. seems no influence on the complex impedance plot. The results of XRD and SEM also show that the difference of both is little.

For Zn/Zn-mont. system, the water content in the sample has an effect on the interface behavior. Figure 2 shows the results of sample A, B and C in the cell of Zn/Zn-mont./Zn. The change of the interface behavior of sample A takes place from the non-blocking electrode to the

blocking electrode after assembling 24 hours. This shows that Zinc electrode has been heavily corroded and an inactive film has been formed on its surface. Within the same time, The change of chemical reaction to chemical reaction and diffusion, is clearly observed in sample B, this change in sample C is little. Comparing sample A with B and C, it can be found that Zinc electrode in B and C still maintains higher active. It is also found that the resistance of the reaction on the interface increases from A to B to C. Those may be interpreted on the basis of "free water" content in the sample. Mont. which contains three layers water (d_{001}-- 1.9 nm) is possessed of higher corrosive that which does two layers water (d_{001}--1.5 nm). This is because the "free water" content in sample A is much more, and the "free water" is of higher active in reacting with Zinc electrode. The resistance of reaction depends on that whether the water film is formed on the interface. While the interface is full of the water, the reaction resistance is small, vice versa, the resistance is larger.

Reference:
[1] W.B.Reid and A.R.West. Solid State Ionics, 451(1991)239
[2] Wang Wenlou and Lin Fengliang, Solid State Ionics 40/41 (1990)125

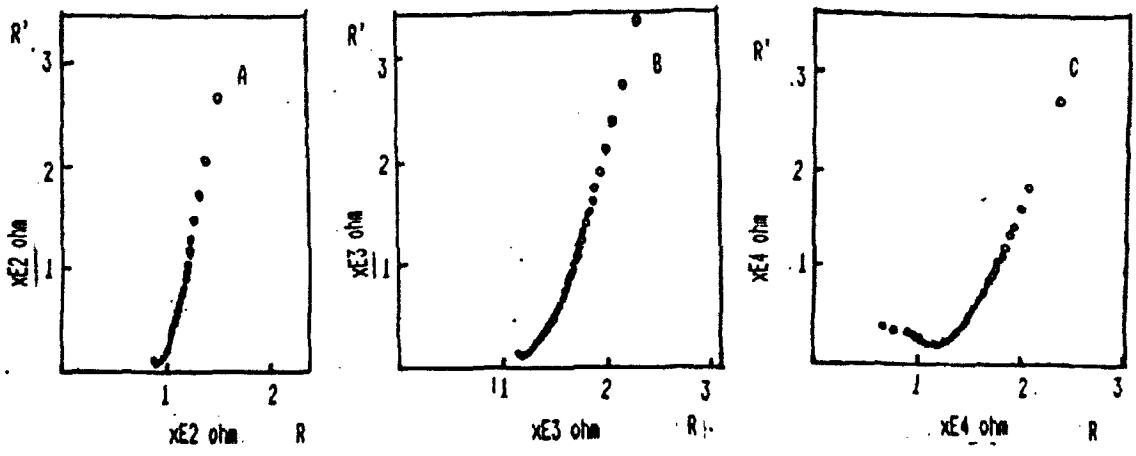

Fig.1 Impedance of Ni/mont. Systems

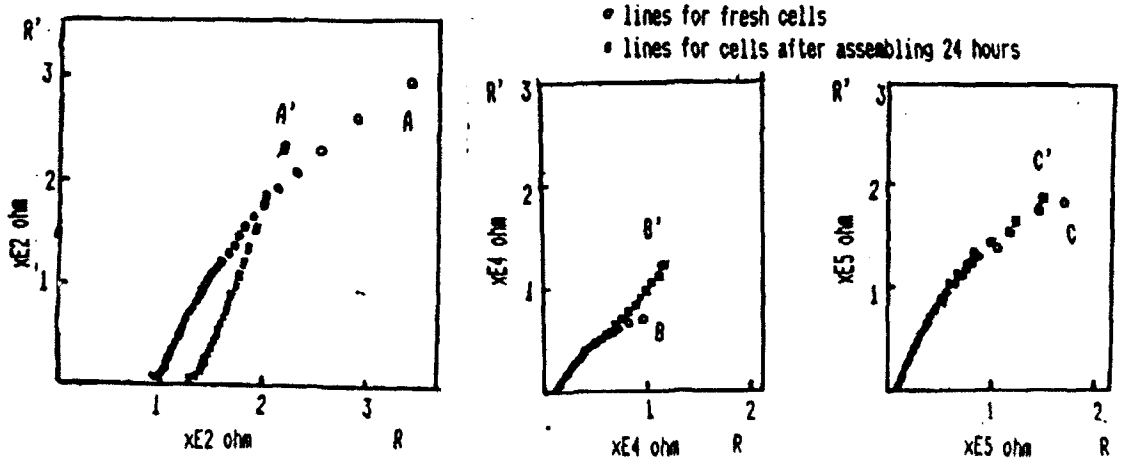

Fig. 2 Impedance of Zn/mont. systems

IMPEDANCE OF POTASSIUM BETA"ALUMINA CERAMIC AT HIGH TEMPERATURE

R. M. Williams, B. Jeffries-Nakamura, M. L. Underwood, M. A. Ryan, D. O'Connor, and S. Kikkert
Jet Propulsion Laboratory, California Institute of Technology
4800 Oak Grove Drive, Pasadena, CA 91109

The conductivity of potassium beta" alumina solid electrolyte (K-BASE ceramic) presents an interesting problem because of the great disparity between the conductivities of the ceramic and single crystal at lower temperatures.(1-3) We have recently reported that the conductivity of K-BASE ceramic is close to that of sodium beta"alumina solid electrolyte at temperatures on the order of 1000K and above, and discussed impedance measurements briefly.(4) The lower temperature conductivities of our ceramics were in agreement with the results of Crosbie and Tennenhouse, who performed the first preparation of a good quality K-BASE ceramic and reported some of its electrical and mechanical properties.(1) There has been additional recent interest in this material, and recent studies have raised additional questions about the transport and thermodynamic properties of this ceramic. Two difficulties are that ceramic samples are almost invariably neither phase-pure nor 100% dense, and the transport and electrochemical properties will reflect variations from an ideal phase pure, completely dense ceramic, as well as more acceptable variation in grain size and morphology. The effort at JPL on this material is oriented toward preparation of good quality, dense ceramics; characterization of the conduction process in the ceramic and its electrochemistry with a refractory porous metal electrode in potassium vapor; and characterization of its thermodynamic and mechanical properties. The ultimate goal of these investigations is the feasibility analysis of potassium based alkali metal thermal to electric converter (AMTEC) devices for power generation. This paper will deal principally with the conductivity and electrochemical studies, which have been carried out with the use of impedance spectroscopy and other electrical and electrochemical methods.

High temperature measurements were carried out either in an evacuated chamber containing potassium vapor, or under argon. Also, effective blocking electrodes cannot be used under these conditions. Conductivity measurements were carried out using a four probe configuration to eliminate faradaic and lead resistance effects. Investigations of the faradaic response of porous metals on K-BASE in potassium vapor used a two probe configuration with thin magnetron sputter-deposited molybdenum electrodes. Electrical and thermocouple feedthroughs were protected by high purity alpha alumina insulators from the "hot zone" to room temperature connections outside the test environment.

Samples studied have included both K-BASE ceramics prepared from commercial Na-BASE ceramics (Cerametec) by a slight modification of the ion exchange method of Crosbie and Tennenhouse, as well as potassium aluminate samples, nominally $KAlO_2$, prepared by reaction of KOH and finely divided gamma/alpha Al_2O_3 at temperatures ranging from 1625 to 1775 K. K-BASE samples were also prepared by annealing pressed pellets of homogeneous precursor materials prepared by a variety of methods.

Four probe ac impedance data and dc conductivity data were obtained with a Solartron model 1250 frequency analyzer and 1286 electrochemical interface, with an IBM PC-AT controller. Some data including dc two and four probe current-voltage curves were also obtained using a PAR 173 potentiostat and 175 signal generator, or with the Solartron 1286 and a digital voltmeter. Software commercially available as well as software written in our laboratory were used in instrument control, data analysis, and simulation of or fitting to experimental data.

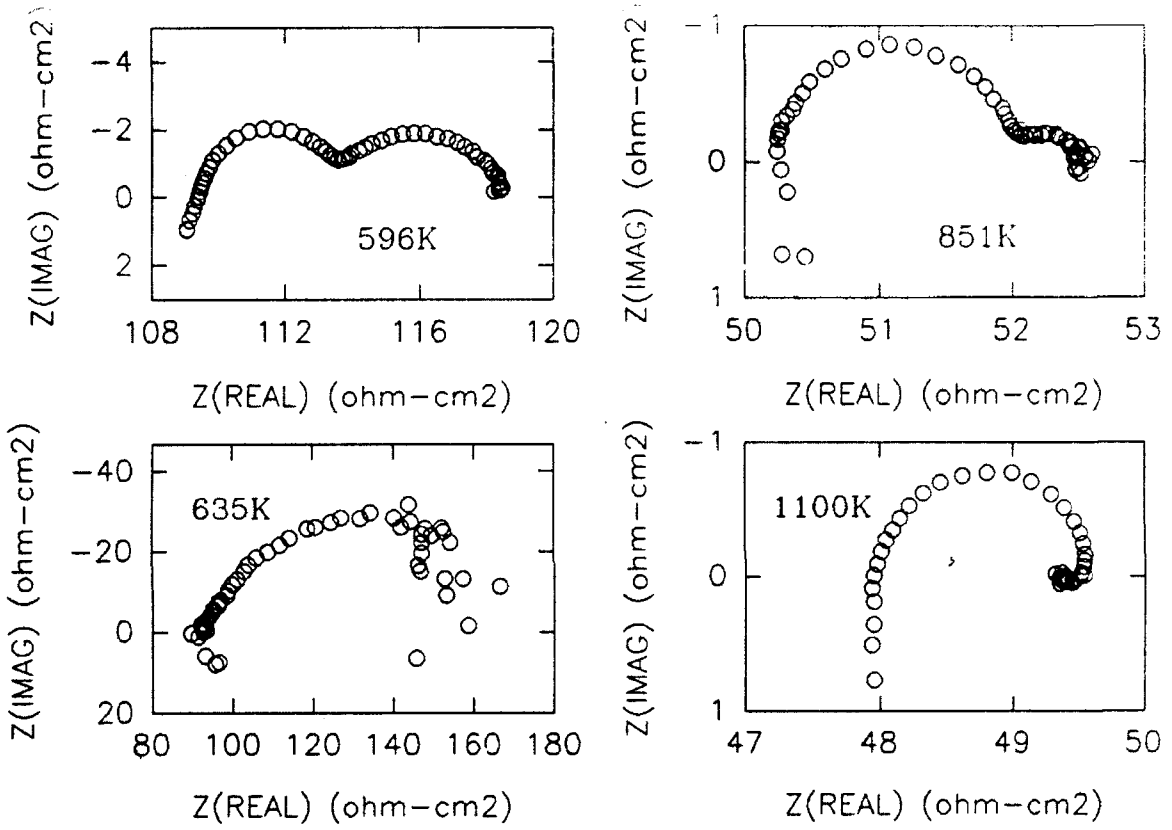

Figure 1. Complex plane impedance plots of grain boundary contribution to K-BASE ceramic conductivity at several temperatures. Frequency range is .1Hz to 64kHz, except for 635K data which begins at .02Hz.

The variation in the four probe ac impedance spectrum of K-BASE is shown as at several temperatures in Figure 1. The high frequency intercept is taken to be the contribution to the overall conductivity of the bulk conductivity of the beta" alumina phase as well as the conductivity of any conducting intergranular material, while the observed arcs are associated primarily with interfacial phenomena. The justification for this assumption will be explained below, but may be concisely ascribed to the very short RC time constants associated with conductivity in potassium beta" alumina single crystals and polycrystalline anhydrous potassium aluminate above 700K. The four probe results for bulk conductivity and interfacial contributions to conductivity of K^+ BASE ceramic as well the conductivities of potassium beta"alumina single crystals, from referenced sources, and polycrystalline $KAlO_2$ are collected in Figure 2.

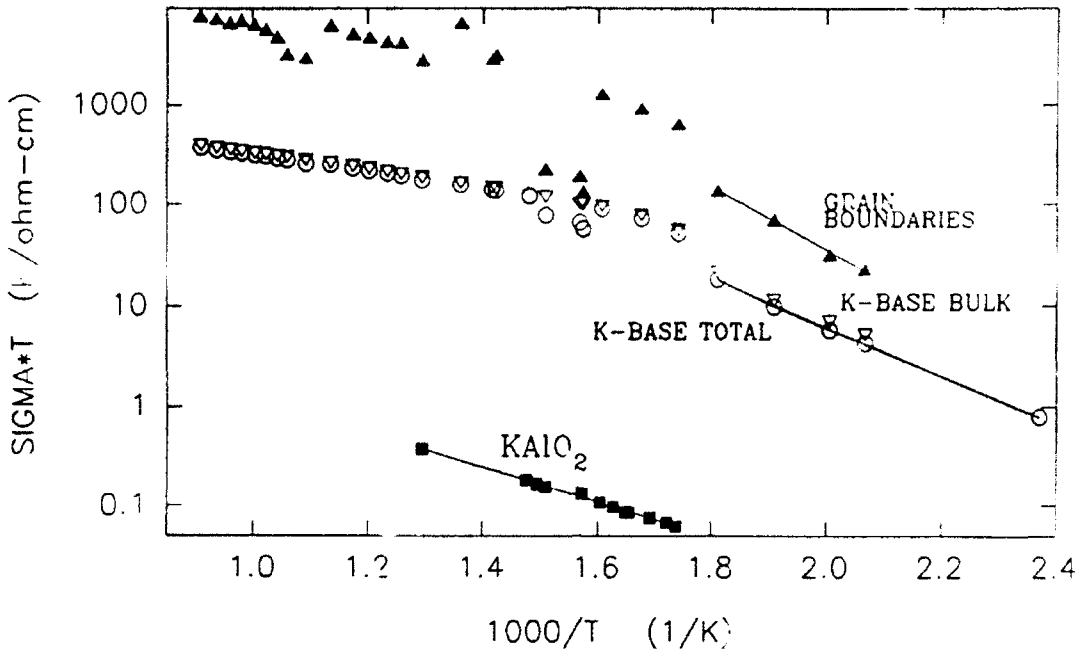

Figure 2. Conductivity Data for K-BASE and $KAlO_2$.

The activation energy for conductivity of bulk K-BASE at lower temperatures is less than that for the grain boundary contribution, but greater than the activation for ionic conduction in $KAlO_2$, the most likely minor phase in the ceramic. Only at temperatures < 600K, is the time constant for $KAlO_2$ conduction is low enough to contribute to the impedance features observed in K-BASE ceramic impedance spectra. At higher temperatures, impedance measurements on $KAlO_2$ reveal only the low frequency limit including a small arc probably due to grain boundaries in the $KAlO_2$ sintered pellet. It is likely that the poor conductivity of $KAlO_2$ is one factor in the poor conductivity of K-BASE ceramic at temperatures less than 700K, but purely interfacial processes with a larger activation energy are also involved.

The research described in this paper was performed by the Jet Propulsion Laboratory, California Institute of Technology, and was supported by the President's Fund of the California Institute of Technology. We acknowledge very helpful discussions with Prof. B. Dunn, and Drs. J. T. Kummer, N. Weber, and J. Rasmussen.

1. G. Crosbie and G. Tennenhouse, J. Amer. Ceram. Soc., 65, 187 (1982)

2. J. Briant and G. Farrington, J. Solid State Chem., 33, 385 (1980)

3. H. Engstrom, J. Bates, W. Brundage, J. Wang, Solid State Ionics, 2, 265 (1981)

4. R. Williams, B. Jeffries-Nakamura, M. Underwood, M. Ryan, D. O'Connor, S Kikkert, Solid State Ionics, in press.

A KINETIC MODEL FOR THE DISSOLUTION MECHANISM OF COPPER IN ACIDIC SULFATE SOLUTIONS

Danny K.Y.Wong
School of Chemistry, Macquarie University
Sydney, New South Wales 2109, Australia

Bruce A.W.Coller and Douglas R.MacFarlane
Department of Chemistry, Monash University
Clayton, Victoria 3168, Australia

Abstract

Steady-state polarization curves and impedance data have been obtained for the electrochemical dissolution of copper in 1.0 M Na_2SO_4 solutions at pH 1, 2, 3, 4 and 5. The steady-state polarization curves display only active dissolution in the potential range investigated (from the open circuit potential up to +100 mV vs saturated calomel electrode) and exhibit a Tafel range of 54.8 mV to 55.6 mV. Two time constants, over a wide spectrum of frequencies (10^{-3} to 10^{4} Hz), have been observed in all complex impedance plots. The experimental results have been quantitatively fitted, using a matrix approach, by the reaction model shown below which provides an excellent fit to the steady state data and is in qualitative agreement with the impedance data.

$$Cu + Cu(II)_{ad} \xrightarrow{k_1} Cu(II)_{ad} + Cu(II)_{sol} + 2e^-$$

$$k_{-2} \uparrow\downarrow k_2$$

$$Cu \underset{k_{-1}}{\overset{k_1}{\rightleftharpoons}} Cu(I)_{ad}$$

$$k_{-3} \uparrow\downarrow k_3$$

$$Cu(I)^{*}_{ad}$$

$$\downarrow \text{diff}$$

$$Cu(I)_{sol}$$

In this model, the reaction step (1/-1) represents the electrochemical conversion of copper metal to an adsorbed Cu(I) species on the electrode surface. The latter is further oxidised to Cu(II), also adsorbed on the electrode surface. The reaction step relating to k_4 is a self-catalytic process and no consumption of $Cu(II)_{ad}$ takes place. Alternatively, Cu(I) may also be transformed, through step (3/-3), into another adsorbed species, $Cu(I)^{*}$, probably anion-associated, which can then be desorbed and diffuse into the bulk of the solution.

References

1. E.Mattsson and J.O'M.Bockris, *Trans.Faraday Soc.*, **55**, 1586 (1959).
2. J.O'M.Bockris and M.Enyo, *Trans.Faraday Soc.*, **58**, 1187 (1962).
3. J.O'M.Bockris and H.Kita, *J.Electrochem.Soc.*, **109**, 928 (1962).
4. O.R.Brown and H.R.Thirsk, *Electrochim.Acta*, **10**, 383 (1965).
5. Q.J.M.Slaiman and W.J.Lorenz, *Electrochim.Acta*, **19**, 791 (1974).
6. Z.D.Stankovic, *Electrochim.Acta*, **28**, 109 (1983).
7. K.Balakrishnan and V.K.Venkatesan, *Transactions of the SAEST*, **12** 221 (1977).
8. S.A.Awad, Kh.M.Kamel, Z.Abd EL-Hadi and H.A.Bayumi *J.Electroanal.Chem.*, **199**, 341 (1986).
9. D.K.Y.Wong, B.A.W.Coller and D.R.MacFarlane, *Proc. of the 7th Australian Electrochemistry Conference*, February 1988, Sydney, Australia, page 154.
10. D.R.MacFarlane, D.K.Y.Wong and B.A.W.Coller, *Bull.of Electrochemistry*, **6**, 893 (1990).

AN IMPEDANCE STUDY OF POLYPYRROLE FILMS DOPED WITH TETRATHIOMOLYBDATE ANION

Siyu Ye, François Girard, and Daniel Bélanger
Département de Chimie, Université du Québec à Montréal,
C.P. 8888, Succ. A, Montréal, Québec, Canada, H3C 3P8

Electrochemical impedance spectroscopy (EIS) has proved to be a useful method for studying the behavior of Polypyrrole (PPy) film electrode in contact with solution.[1-3] In this work we have focused on the application of EIS to characterize the performance of the PPy films doped with tetrathiomolybdate anions, which were prepared in order to enhance the conductivity of a cathode material in secondary lithium battery, a- MoS_3.[4] An equivalent circuit (Fig. 1) which is based on an adatom model,[5-7] and describes the behavior of the polymer electrode both in its neutral and oxidized states is proposed.

The $Pt/PPy^+(1/2MoS_4^{2-})$/electrolyte system is characterized by a reversible electrochemical oxidation-reduction process for the polymer coating, assisted by an electrostastic insertion/repulsion of electrolyte cation, K^+, to and from the polymer chains.[4] This process can be described as:

$$PPy^+(1/2MoS_4^{2-}) + K^+ + e^- \underset{\text{oxidation}}{\overset{\text{reduction}}{\rightleftharpoons}} PPy\text{-}(1/2MoS_4^{2-})\text{-}K^+ \qquad (1)$$

This process is similar to the electrochemical intercalation of atoms into solid hosts.[5] In order to show their feature in the course of the electrochemical process represented by the cyclic voltammogram, schematic sketches of the data in the Nyquist representation are depicted in Fig. 2. The impedance data were analysed for different d.c. potentials from 0.4 to -1.0V and resulted in modelling the electrode impedance by an equivalent circuit based on the adatom mechanism[6,7] as shown in Fig.1. The cell impedance is represented by the solution resistance (R_S) in series with a ladder-type circuit composed of the charge transfer resistance (R_{ct}) which represents the formation of an adatom, or more correctly described as partially charged adion, the diffusion impedance (Z_D) which describes the diffusion of the fully desolvated ion in the polymer film, a resistance R_a which represents the resistance of the adion to cross the electrode/electrolyte interface and its incorporation into the lattice, and two constant elements $Z_{CPE,dl}$ and $Z_{CPE,a}$. $Z_{CPE,dl}$ and $Z_{CPE,a}$ are used instead of the double layer capacitance of the polymer/electrolyte interface (C_{dl}) and a pseudo-capacitance (C_a) respectively, due to the fractal nature of the surface of the polymer electrode, where C_a represents the capacitance of the adion across the electrode/electrolyte interface, and depends on the surface concentration of the adions. As shown in Fig. 2, at d.c. potentials more positive than -0.3V, the impedance plots are characterized by one semicircle at high frequencies and the linear branch(es) at lower frequencies. As the d.c. potentials are more negative than -0.60V, the Nyquist plots indicate the existence of two semicircles. Instead of the diffusion impedance, the adions transport across the polymer/solution interface becomes important in the low-frequencies at more negative potentials.

By analysizing the impedance data obtained from the fit to the adatom model, we can get the following results: (1) The values of C_{lf} are in the order of magnitude of $mFcm^{-2}$, which are one order of magnitude lower than those for PPy films doped with small anions.[1] The low C_{lf} values correspond to a relative low conductivity for $PPy^+(MoS_4)^{2-}$ film in comparison with that for PPy doped with small anions. The values of C_{lf} decrease as the potential is varied from 0.4 to -1V. (2) The values of D_f are in the order of magnitude from

10^{-13} to 10^{-12} cm^2s^{-1}. These values are lower than those reported for various PPy films in the literature.[1] The difference must be in relation with the kinetics of electrochemical processes occuring within PPy films and at PPy/electrolyte interface which depend on the film thickness, the procedures used to synthesize the film, the nature of the contacting electrolyte phase, and, perhaps the most important, the film composition. The values of D_f show a minimum value at -0.1V. (3) The thickness of PPy film has great influence on its impedance behavior. The most dramatic change is the values of the diffusion coefficients in the finite diffusion region D_f. As the film thickness increases from 0.029 to 11.9 μm, D_f increases from $1.4x10^{-13}$ to $1.8x10^{-7}$ cm^2s^{-1}. The variation of the D_f values with film thickness may be in relation with the change of the film morphorlogy and composituon.

In conclusion, the interpretation of the impedance behaviour with the adatom model gives satisfactory results, and the mechanism for the reaction at the polymer / electrolyte interface based on this model is reasonable.

(1) N. Mermilliod, J. Tanguy, and F. Petiot, *J. electrochem. Soc.* **133**, 1073 (1986).
(2) A.M. Waller and R.G. Compton, *J. Chem. Soc., Faraday Trans. I* **85**, 977 (1989).
(3) J. Tanguy, *Synth. Met.* **41-43**, 2991 (1991).
(4) F. Girard, S. Ye, G. Laperrière, and D. Bélanger, *J. electroanal. Chem.* in press.
(5) J.O'.M. Bockris and G.A. Razumney, *Fundamental aspects of electrocrystallisation*, Plenum Press, (1967).
(6) S. Ye, *Ph. D. Thesis*, Xiamen University, Xiamen (1988).
(7) P.G. Bruce and M.Y. Saidi, *J. electroanal. Chem.* **322**, 93 (1992).

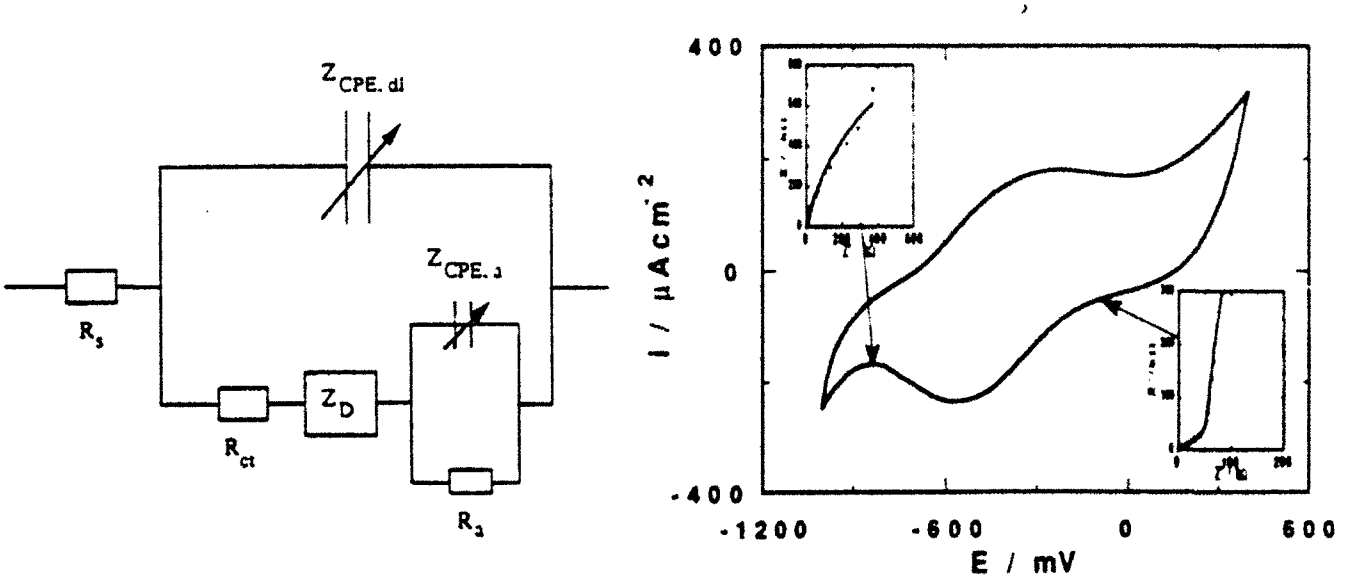

Fig. 1 Equivalent circuit based on the adatom model. .

Fig. 2 Shapes of the Nyquist plots for Pt/$PPy^+(1/2MoS_4^{2-})$ film electrode at d.c. potentials corresponding to the cyclic voltammetric response in 0.1M KCl. (▫) experimental. (—) CNLS fit to the circuit shown in Fig. 2. The potential scan rate: 100 mVs^{-1}; film thickness: 0.029 μm.

Studies on Anodic Film formed on Copper Electrodes by Cyclic Voltammetry, AC-Impedance Spectroscopy and IR-Reflection Spectroscopy

Qiguang Yin, Rulin Zhao, Jiujun Zhang
Chemistry Department, Huazhong Normal University
Wuhan 430070, P.R.China

The structure and composition of surface film formed on copper electrode have been widely studied by electrochemical methods[1,2], ellipsometry[3], Raman spectroscopy[4], visible reflection spectroscopy[5], and IR reflection spectroscopy[6]. Majority of the reported studies put attention on the oxide film anodically formed in basic solutions. We have maintained continuing interest in understanding the structure and composition of the film anodically formed in CN^-, SCN^-, $Fe(CN)_6^{3-/4-}$, and oxalate containing aqueous solutions[6-8].

In this paper, we present a study on the structure and composition of copper surface formed in oxalic/oxalate solution by cyclic voltammetry, impedance spectroscopy, and IR reflection spectroscopy.

Cyclic voltammetry: Fig.1 shows the cyclic voltammograms of Cu electrode in 0.1M oxalic/oxalate aqueous solutions at various pH. At pH 1.3, at potentials more positive than 0.0v, a totally irreversible anodic wave was observed. From the IR spectra which will be discussed below, it is clear that this anodic wave is due to the formation of copper oxalate film on the copper surface. At pH 7.0, a similar anodic wave was also observed. However, the significant difference is that the copper oxalate film can be reduced (cathodic wave) rather than totally irreversible at pH1.3. In correlation to the results of far-IR reflection spectral data obtained for the same electrode, it is concluded that the film formed at pH7.0 contains a certain portion of copper oxides, while that formed at pH 1.3 contains no measurable copper oxides. Furthermore, increase in pH of the solution resulted in a gradual increase in the quantity of copper oxides in the film. At pH 12, the formation of copper oxides on the surface starts from potential of -0.6v (dashed line), while the appearance of copper oxalate component begins at 1.0v, which also can be indicated by following IR spectra.

The cyclic voltammetric data showed that there are at least two processes occurring on the surface[1,2,7], which are:

(1) $Cu + C_2O_4^{2-} \text{--------} > CuC_2O_4 + 2e^-$

(2)
$$\begin{cases} 2Cu + H_2O\ (\text{or } OH^-) \text{-----} > Cu_2O + 2e^- \\ Cu + H_2O\ (\text{or } OH^-) \text{-----} > CuO + 2e^- \end{cases}$$

Impedance spectroscopy: At pH 1.3, in the potential region of copper oxalate film formation (more positive than 0.0v), the semi-circle spectra were observed, from which the solution resistance Rs, Faradic impedance Rt, and double layer capacitance Cd can be calculated[10]. The reciprocal of Faradic impedance Rt corresponds to the rate of reaction (1) mentioned above. The radius of the semi-circles decrease with increase in potential, which indicates that the rate of reaction (1) is accelarated by positively shifting the electrode potential. At high pH (Fig.2B), the complex plan diagram with two semi-circles were obtained, which may imply that there

are two processes occurring on the surface during the polarization. It is possible that the first semi-circle is due to reaction (1), and the second one is attributed to reaction (2) which represents the formation of copper oxides. The process can be described by the equivalent circuits shown in Fig.2. At low pH, no copper oxides exist on the surface, which suggest the R(2)=0 in Fig.2A, and the equivalent circuit can be expressed as what shown in Fig.3B.

IR reflection spectroscopy: In this study more attention were drawn to study the structure of copper oxalate film. Unfortunately, no direct evidences about the details of the film structure can be obtained by either cyclic voltammetry or impedance spectroscopy. Due to the strong IR absorption of oxalate in IR region, IR reflection spectroscopic technique can be employed to probe the surface structure. Fig.3 shows the IR reflection spectra of copper surface films formed in oxalic/oxalate solutions at various pH. It can be seen from Fig.3 that the IR spectra of surface films formed at different pH and potentials have different spectral features. IR bands near 3400-3600 cm^{-1}, 1650-1730 cm^{-1}, 1362 cm^{-1}, 1318 cm^{-1}, and 850 cm^{-1} were observed, which are very similar to the standard spectra of copper oxalate[11]. From the differences of the spectra obtained at different pH, the spectra can be explained in terms of the differences of anodic films formed at different solution pH by comparing them to the standard spectra of copper oxalates. At low pH, the dominate structure of copper oxalate film is the bidentate chelate, that is, the oxalate anion coordinates to a copper ion as a bidentate ligand.
The film contains both unidentate and bidentate chelate structures at high pH..

On the other hand, at high pH, the first layer on the surface is copper oxides, then with increasing the potential the copper oxalate layer is formed gradually on top of the copper oxide layer.

IR spectra also show that for films containing copper oxides and copper oxalate, no significant quantity of $Cu(OH)_2$ were observed.

REFERENCE

[1] U.Beitocci, and D.R. Turner, in *Encyclopedia of Electrochemistry of the Elements*, edited by A.J. Bard, vol.2, Chap. 6(1974).

[2] J.G. Becerra, R.C. Salvarezza, and A.J. Arvia, *Electrochim. Acta*, 5, 613(1988).

[3] J.L. Ord, D.J. Desmet, and Z.Q. Huang, *J. Electrochem. Soc.*, 134(4), 826(1987).

[4] J.C. Hamilton, J.C. Farmer, and R.J. Anderson, *ibid*, 133(4), 739(1986).

[5] C.H. Pyun, and S.M. Park, *ibid*, 133(10), 2024(1986).

[6] J.J. Zhang, J.T. Lu, C.S. Cha, and Z.G. Feng, *Chinese J. Inorg. Chem.*, 6(3), 319(1990)

[7] R.L.Zhao, Q.G. Yin, and J.J. Zhang, *J. Central China Normal Univ.(Nat. Sci.)*, 24(4), 442(1990).

[8] J.J. Zhang, J.T. Lu, Z.G. Feng, and C.S. Cha, *Chinese Bull. Chem. Anal.*, 8(6), 33(1989).

[9] J.J. Zhang, H.Z. Wong, J.L. Song, and J.L. Li, *J. Central China Normal Univ.(Nat. Sci.)*, monog.1, 37(1988).

[10] D.D. MacDonald, *Transient Techniques in Electrochemistry*, plenum, New york, (1981).

[11] K. Nakamoto, *Infrared and Raman Spectra of Inorganic and Coordination Compounds(fourth edition)*, John Wiley & Sons, New York, (1986)

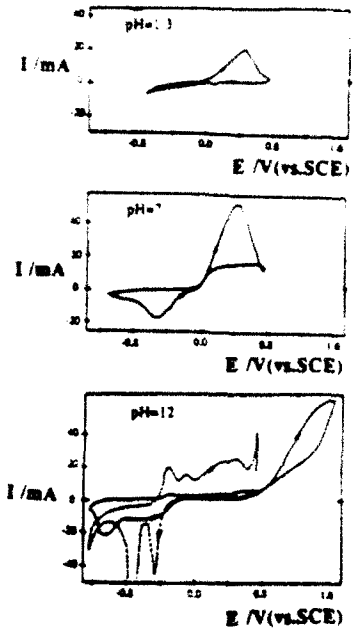

Fig.1 Cyclic voltammetry of copper electrodes in 0.1M oxalic/oxalate aqueous solutions at various pH. Potential scan rate: 0.05 vs^{-1}

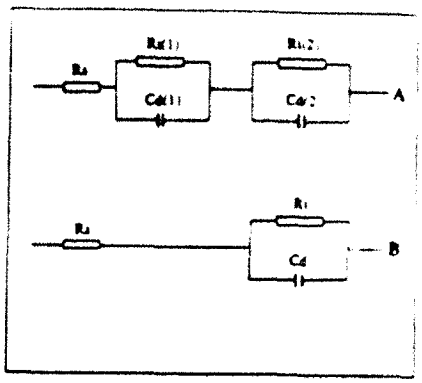

Fig.2 The equivalent circuits for surface films formed on copper electrodes in 0.1M oxalic/oxalate aqueous solutions

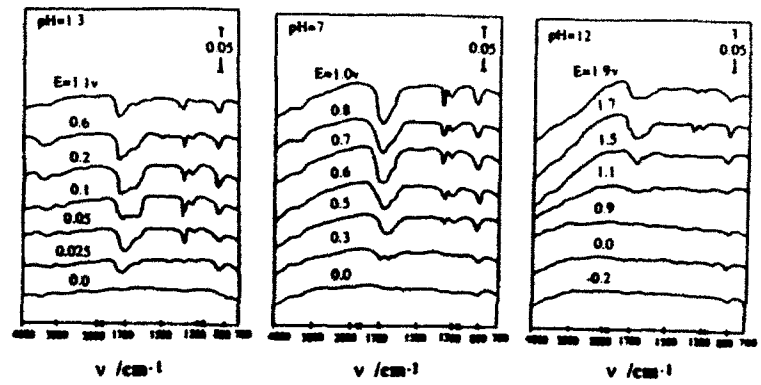

Fig.3 IR reflection spectra of copper electrode surface films formed in 0.1M oxalic/oxalate aqueous solutions.

STUDY ON SnO_2-Fe_2O_3 GAS SENSING SYSTEM BY AC COMPLEX IMPEDANCE TECHNIQUE

Liu X-Q Chen Ch-H Xu W-D Shen Y-Sh Meng G-Y
(Dept. Mater. Sci & Engi., Univ. Sci. & Tech. of China, Hefei, Anhui 230026, P.R. China)

AC complex impedance technique has been used to obtain a better understanding of gas sensing SnO_2-Fe_2O_3 system. Previously, most work on its electrical property were done by direct current (DC) method.

EXPERIMENTAL Tin oxide (SnO_2) and iron oxide (Fe_2O_3) were prepared by hydrolysis of $SnCl_4$ $5H_2O$ and $FeSO_4$ $7H_2O$. Several compositions: x wt% SnO_2 + (100-x) wt% Fe_2O_3 (x= 0,20,40,60, 80,100, written as $S_{x/10}F_{(100-x)/10}$) were selected to make the gas sensing elements of thick film type. Little amount of Sb2O3 was doped to decrease the resistance. A GenRad 1689 precision digibridge was used to measure their frequency response in air, 1000ppm liquid petrol gas (LPG) and 1000ppm acetylene C_2H_2).

RESULTS AND DISCUSSIONS Fig.1 shows some typical obtained impedance plots. To unmixed samples (fig.1a-e), a simple equivalent circuit (fig.2) is put forward to describe them. Rg stands for the grains resistance while Rgb for the grains boundaries resistance. Cgb is the grain boundaries capacitance. It can be seen that both grains and grain boundaries contribute to the gas sensitivity of SnO_2 and Fe_2O_3. Fig.1c looks like a result of a pure resistor which suggest a possible operation mechanism in C_2H_2 different from in LPG. Maybe more active acetylene would react with chemiadsorbed oxygen and produce some conductive species, such as acetic acid that can decrease Rgb and Cgb. Another phenomeno is that the semicircle in LPG is less depressed than in air. We don't know the real reason for it. The plots of Fe_2O_3 (fig.1d,e) have not given complete senicircles because of its very large grain boundaries resistance. Their characteristic frequency (1/RC) is beyond the scope of our instrument. SnO_2-Fe_2O_3 mixed system displays the impedance spectra with an almost complete semicircle typically shown in fig.1f,g,h. Obviously, the grain boundaries are greatly dominant in total resistance. And the gas sensitivity must be chiefly ascribed to the change of adsorption in grain boundaries.

CONCLUSION AC impedance measurement can tell the contributions of grains and grain boundaries to the gas sensitivity. In SnO_2 and Fe_2O_3, Both Rg and Rgb are important.But in their mixed system, the role of grain boundaries is highly dominant.

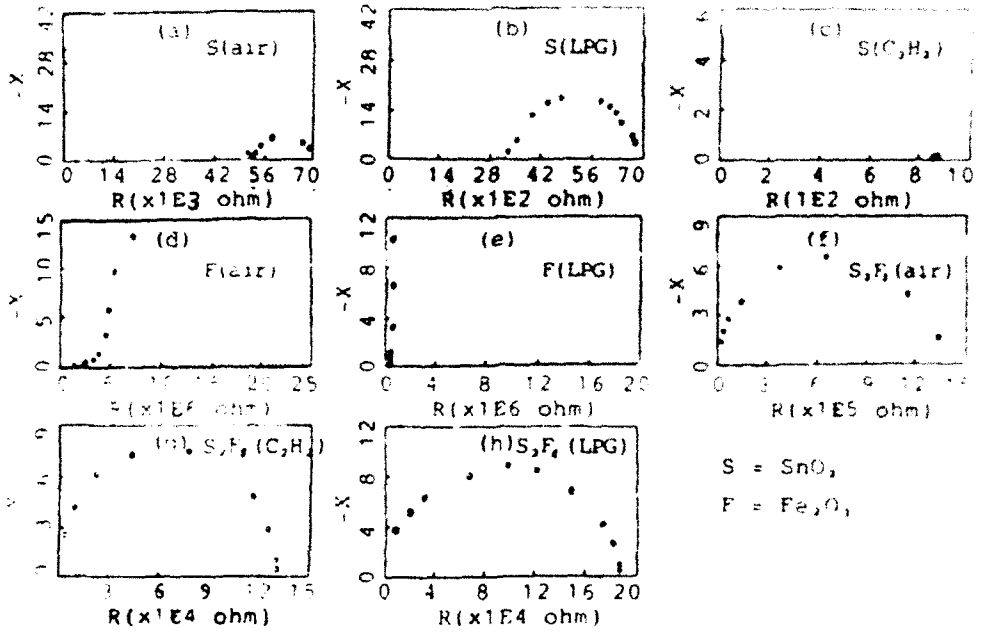

fig.1 Complex impedance plots

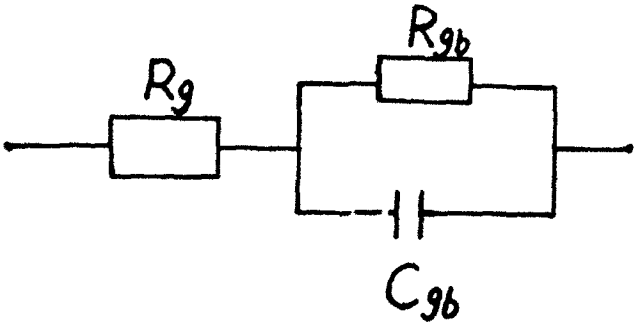

fig.2 Equivalent Circuit

THE CAPACITY OF MONOCRYSTALLINE NICKEL ELECTRODE IN POTASSIUM HYDROXIDE SOLUTION AT LOW HYDROGEN OVERPOTENTIALS

P. Zoltowski
Institute of Physical Chemistry of the Polish Academy of Sciences, ul. Kasprzaka 44/52, 01-224 Warsaw, Poland.

DC current (i) and the two components of ac admittance (ωc_p and $1/R_p$) at two frequencies (63.2 and 632 Hz) were measured for monocrystalline nickel electrodes [(111), (100), (110) and (210)], used as hanging meniscus electrodes (10 mm in diameter), in 0.1M KOH aqueous solution, being only deoxygenated or saturated by hydrogen, at room temperature, under conditions of slow potential sweeps (1 or 10 mV/s) between -0.45 and +0.55 V of hydrogen overpotential.

The values of the potential (E) are given in the RHE scale. The values of the extensive quantities (i, c_p etc.) are normalized to unit geometric area of the electrode.

At high negative potentials, a short Tafel straight line section on i vs E dependencies were observed. The values of Tafel parameters were similar to those noted earlier in the literature [1].

At positive potentials, a maximum on i vs E up-curves (increasing potential) was observed. The potential of the maximum (E_1^{max}) changed from ~+0.2 V to ~+0.3 V with the succession of (100)<(110)<(210)<(111) plane electrodes. These E_1^{max} values are lower and the succession of crystallographic planes is different than it was noticed earlier [1].

In Figure 1 an example of the c_p vs E dependencies is presented. For the up-curves, three sections can be distinguished: a shoulder or a maximum at ~-0.2 V, a plateau at ~+0.1 V, and a maximum or a minimum in the vicinity of E_1^{max}, at the frequency 63.2 or 632 Hz, respectively. For these three sections, three surface processes are probably responsible: adsorption of hydrogen, adsorption of $(OH)^-$ ions, and $Ni(OH)_2$ formation, respectively (earlier the hydrogen adsorption was noted at the potential -0.1 V [1]). Only the last process seems to be sensitive to the crystallographic structure of the electrode.

It should be noticed that c_p at frequency 632 Hz had values equal to or lower than estimates for the double layer capacity [2]. This suggests that in this case the parallel 2-elements RC circuit is not a good approximation. The values of c_s, computed from admittance data and presented in Figure 2, are more acceptable. This gives some information on the kinetics of the surface processes [3,4].

References

1. J.L. Weininger and M.W. Breiter, J. Electrochem. Soc. **110**, 484 (1963); ibid **111**, 707 (1964).
2. A. Lasia and A. Rami, J. Electroanal. Chem. **294**, 123 (1990).
3. M. Sluyters-Rehbach and J.H. Sluyters in "Comprehensive Treatise of Electrochemistry" Vol. 9, Plenum Publ., New York (1984), Ch. 4.
4. P. Zoltowski, J. Electroanal. Chem. **240**, 53 (1988).

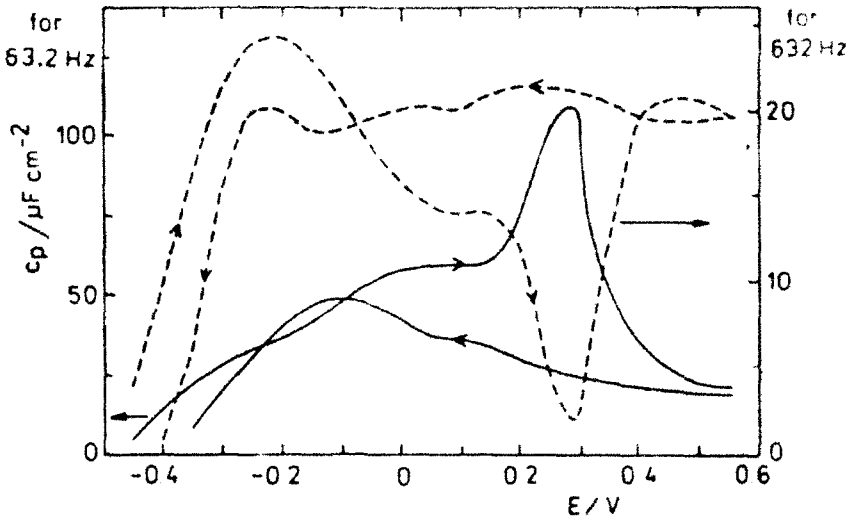

Fig. 1. c_p vs potential curves, at frequencies 63.2 (full line) and 632 Hz (dashed line), for the (111) plane electrode in hydrogen-saturated solution.

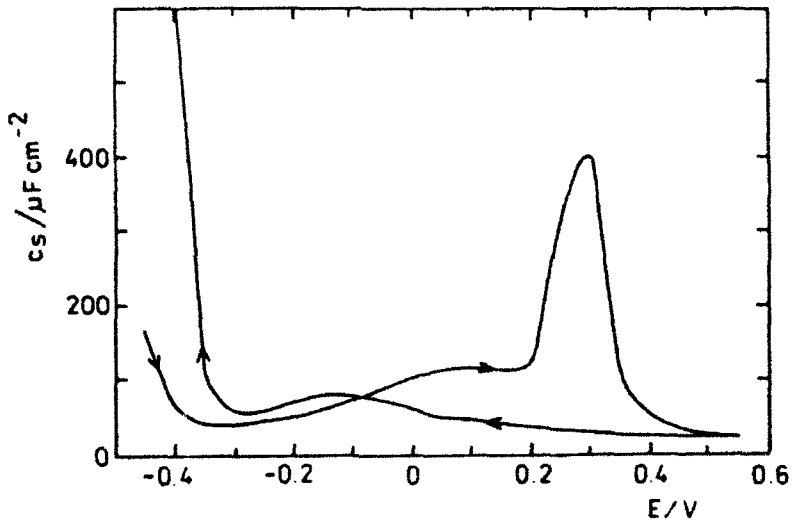

Fig. 2. c_s vs potential curve for the (111) plane electrode at frequency 632 Hz, computed from the admittance data.